EVALUATION OF PATIENT DOSE AND IMAGE RECEPTOR PERFORMANCE IN INTERVENTIONAL CARDIOLOGY

Evelien Bogaert ■ 2008

cover: Balloon dilatation of a pulmonary valve of a child (Figure 7, chapter 1.2).

EVALUATION OF PATIENT DOSE AND IMAGE RECEPTOR PERFORMANCE IN INTERVENTIONAL CARDIOLOGY

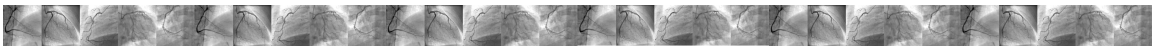

EVALUATIE VAN PATIËNTDOSIS EN BEELDRECEPTOR KARAKTERISTIEKEN IN INTERVENTIONELE CARDIOLOGIE

Evelien Bogaert ■ 2008

University Ghent
Faculty of Medicine and Health Sciences
Department of Basic Medical Sciences
Promotor: Prof. Dr. H. Thierens
Thesis submitted in fulfilment of the requirements for
the degree of Doctor in Medical Sciences

Promotor

Prof. Dr. H. Thierens	Universiteit Gent

Doctoral guidance committee

Prof. Dr. D. De Wolf	Universiteit Gent
Prof. Dr. Y. Taeymans	Universiteit Gent
Dr. M. Monsieurs	Universiteit Gent

President of the examination committee

Prof. Dr. Ir. C. De Wagter	Universiteit Gent

Examination committee

Prof. Dr. Ir. H. Bosmans	UZ Leuven
Prof. Dr. Ir. C. De Wagter	Universiteit Gent
Prof. Dr. D. De Wolf	Universiteit Gent
Prof. Dr. R. Padovani	Osp. S Maria della Misericordia Udine (Italy)
Prof. Dr. Y. Taeymans	Universiteit Gent
Prof. Dr. K. Verstraete	Universiteit Gent
Dr. J. Zoetelief	Technische Universiteit Delft (Nederland)

Dean of the Faculty of Medicine and Health Sciences

Prof. Dr. J.-L. Pannier

Woord vooraf

Heel wat mensen hebben bijgedragen tot dit werk en ik wil hen daarvoor speciaal bedanken. Zonder hun hulp zou dit doctoraatsproefschrift niet geworden zijn tot wat het nu is.

Vooreerst bedank ik mijn promotor Prof. Dr. Thierens. De mogelijkheid die ik kreeg mijn thesis onder zijn hoede te maken apprecieer ik ten zeerste. Bedankt voor alle nuttige aanwijzingen, leerrijke discussies en het vertrouwen.

Dr. M. Carlier (Hôpital St. Joseph, Gilly), Prof. Dr. W. Desmet (Universitair Ziekenhuis Gasthuisberg, Leuven), Dr. X. De Wagter (Algemeen Ziekenhuis Maria Middelares – St. Jozef, Gent), Dr. D. Djian (Centre Hospitalier Namur, Namur), Prof. Dr. C. Hanet (Cliniques Universitaires St. Luc, Bruxelles), Dr. G. Heyndrickx (Onze Lieve Vrouwziekenhuis, Aalst), Prof. Dr. V. Legrand (Centre Hospitalier Universitaire, Liège) en Prof. Dr. Y. Taeyamans (Universitair Ziekenhuis, Gent) draag ik een warm hart toe voor de gastvrijheid in de catheterisatiezalen van hun ziekenhuis en hun interesse in het onderzoek dat ik verrichte.

ALLE cardiologen bij wie ik procedures mocht mee volgen, bedank ik voor hun toelichting, jovialiteit en interesse.

ALLE verplegend personeel bedank ik voor hun vriendelijkheid, hartelijkheid en praktische, vlotte en aangename samenwerking. In het bijzonder gaat mijn dank uit naar Tonny en Pieter (AZ Maria Middelares – St. Jozef, Gent). Ik was er steeds welkom op beide catheterisatiezalen voor verschillende metingen tijdens mijn onderzoek. Bij hen kon ik terecht voor alle praktische regelingen. Ik kon er steeds rekenen op een bereidwillige, enthousiaste en vlotte medewerking!

Martin Acket en Sophie Verschuere (St. Jan ziekenhuis Brugge) bedank ik voor de praktische hulp tijdens metingen te Brugge.

J. Dermaut, M. Terriere en I. Van Driessche (Siemens, Medical Solutions Belgium) worden bedankt voor de technische ondersteuning.

Mijn collega's bedank ik voor de aangename werksfeer. Klaus in het bijzonder voor de interessante discussies en praktische samenwerking. Kim voor alle hulp bij het praktische meetwerk. Nick voor suggesties tijdens de kalibraties. Barbara voor het uitlenen van statistiek boeken. An en Liesbeth voor het scoren van de beelden. Nele, voor het oplossen van alle computerproblemen. Frederik voor de introductie in '*R-Project*'. Virginie en Isabelle voor de antwoorden op alle vragen over sleutels, CD-ROMs, kopies, en verjaardagsetentjes… An, met wie ik mijn bureau deelde, bedankt voor de aangename sfeer. Alle collega's wiens naam hier niet expliciet vermeld staat: bedankt voor het vriendelijk woord en de glimlach die ik steeds van jullie mocht ontvangen. Het was voor mij een groot plezier met jullie samen te werken!

Roland, Philippe en George draag ik een warm hart toe voor de immer opgewekte '*goeiedag*' en de grapjes 'en passant'. Bedankt voor het uitfrezen van de TLD-doosjes en het meermaals vervangen van de N_2-fles in het TLD-lokaal.

Mme Eva Malchair et sa famille sont cordialement remerciées pour leur gentillesse, amicalité, hospitalité et petits-déjeuners savoureux pendant mon séjour à Liège.

Ouders, grootouders en schoonouders, broer en schoonbroers, hartelijk dank voor jullie begrip en onvoorwaardelijke steun in drukke tijden. De laatste loodjes wegen niet alleen spreekwoordelijk het zwaarst.

Johan en Reinhild, jullie zijn mama's grootste motivatie.

Iedereen die bijgedragen heeft tot dit werk draag ik een warm hart toe. Bedankt.

Evelien
juni 2008

Table of contents

List of abbreviations

ABC: Automatic Brightness Control

Al: Aluminium

ALARA: As Low As Reasonably Achievable

AMFPI: Active-Matrix Flat-Panel Imagers

ANOVA: Analysis of Variance

AP: Anterior Posterior

ASD: Atrial Septal Defect

a-Se: Amorphous Selenium

a-Si: Amorphous Silicon

BMI: Body Mass Index

CAD: Coronary Artery Disease

CAUD: Caudal

CCD: Charge Coupled Device

CD: Contrast-Detail

CF: Conversion Factor

CHD: Congenital Heart Disease

CMRA: Coronary Magnetic Resonance Angiography

CNR: Contrast-to-Noise Ratio

CRAN: Cranial

CT: Computed Tomography

Cu: Copper

DDREF: Dose and Dose Rate Effectiveness Factor

DICOM: Digital Imaging and Communications in Medicine

DQE: Detective Quantum Efficiency

E: Effective Dose

ESC: European Society of Cardiology

ESD: Entrance Skin (or Surface) Dose

FDA: Food and Drug Administration

Gy: Gray

IAEA: International Atomic Energy Agency

IC: Interventional Cardiology

ICRP: International Commission on Radiological Protection

ICRU: International Commission on Radiation Units and Measurements

IQFinv: Inverse Image Quality Figure

IR: Image Receptor

LAO: Left Anterior Oblique

LCA: Left Coronary Artery

LSS: Life Span Study

MRI: Magnetic Resonance Imaging

MSCT: Multi-Slice Computed Tomography

MTF: Modulation Transfer Function

NPS: Noise Power Spectrum

PMMA: Polymethylmethacrylate

RAO: Right Anterior Oblique

RCA: Right Coronary Artery

RL-CA: Right-Left Catheterization

ROC: Receiver Operating Characteristics

SID: Source to Image Receptor Distance

SNR: Signal-to-Noise Ratio

Sv: Sievert

TEE: Trans-Esophageal Echocardiography

TFT: Thin-film Transistor

TLD: Thermoluminescent dosemeter

Summary

Catheterization of coronary arteries, shortly denoted by Interventional Cardiology (IC) in medicine, is highly appreciated for its non-invasive character in comparison to surgery. Both adults and children can benefit of the technique, most frequently for diagnosis and/or treatment of Coronary Artery Disease (CAD) and Congenital Heart Disease (CHD) respectively. Annual numbers of 4 diagnostic Coronary Angiography (CA) procedures and 1.5 Percutaneous Transluminal Coronary Angioplasty (PTCA) interventions per thousand inhabitants in Europe (2004) are still increasing.

As investigation of the coronary arteries is performed through dynamic x-ray imaging the radiation burden to the patient can be important. The procedures belong to those involving 'high doses' to patients and the effects of these possibly high doses were classified by the International Commission on Radiation Protection (ICRP) into deterministic (short-term) and stochastic (long-term). Regarding short–term effects, the skin is the tissue at greatest risk, and skin dose thresholds as low as 2 Gy have been stated by ICRP in its report 85 for onset of transient erythema. For long-term effects, it is mostly the youngest generation i.e. the paediatric population that is of highest risk. Due to their higher radiosensitivity and the longer post-exposure life-time expectance, possible radiation induced sequelae are more likely to occur.

The first part (publication 1) of this dissertation deals with skin doses during IC of an adult population in a multicentre setting by a grid of Thermo-Luminescent Dosimeters (TLD) covering the entire skin dose distribution. In 3% of the procedures, the Maximum Skin Dose (MSD) exceeded the threshold dose of 2 Gy in one single procedure. Action levels in terms of Dose-Area Product (DAP), indicating an important probability that MSD has the threshold levels of skin exposure, were proposed. National Dose Reference Levels (DRL) were put forward for diagnostic and therapeutic procedures and serve for comparison of specific hospital data with respect to radiation burden to the patient.

Publications 2 and 3, on the other hand, deal with stochastic effects for the considered adult population, submitted to IC. Effective dose (E) was

calculated from exposure and geometric parameters, using Monte Carlo simulation software (PCXMC). The predicting value of DAP in terms of E, was translated into Conversion Factors (CF) that provide a fast and straightforward way of E-assessment. The influence of additional copper (Cu) filtration was studied and was found to favourably influence DAP and E towards lower values. Fluoroscopy contributions to DAP and risk factors for cancer induction were derived.

Publication 4 studied the radiation burden related to IC on a paediatric population, with ages < 10 year. The large variety in body mass and length according to age of the population required an individual calculation of E using Monte Carlo simulations (MCNP). Risk for cancer induction was obtained using the age-dependent life-time risk factors from ICRP publication 60 and is demonstrated to be increased with a factor of ten compared to the risk for the adult population. Skin doses, on the other hand, are a factor hundred smaller, putting the issue of skin injuries at a less probabilistic level. Additional Cu filtration with a thickness of 0.2 mm for implementation of low-dose fluoroscopy lowered E with 18%. Also within this study, DAP values and fluoroscopy contributions to DAP were considered.

The last part of this dissertation (publication 5) comprises a comparative study between a conventional Image Intensifier (II) and the recent technology of Flat Detectors (FD) for image capture in IC. Both contrast - detail (CD) measurements for assessment of image quality (IQ) and patient dose measurements were performed. Distinction was made between fluoroscopy and cinegraphy mode, for analysis of IQ-dose relation. FD presented with better and more efficient imaging performance in cinegraphy mode for the same entrance exposure rate. With respect to fluoroscopy mode no significant difference was noted. No dose reduction was found in daily practice, when using this new imaging technology.

Samenvatting

Catheterisatie van de kransslagaders wordt als discipline in de geneeskunde omschreven als Interventionele Cardiologie (IC) en kent een grote appreciatie omwille van zijn niet invasief karakter in vergelijking met chirurgische alternatieven. Zowel volwassenen als kinderen kunnen genieten van de voordelen van deze techniek, voor de diagnose en/of behandeling van 'kransslagader lijden' (CAD) en 'congenitaal hartlijden' (CHD). Statistieken geven een aantal van 4 diagnostische procedures (Coronaire Angiografie) (CA) en 1.5 therapeutische procedures (Percutane Transluminale Coronaire Angioplastie (PTCA)) per duizend inwoners in Europa (2004), per jaar. Deze aantallen nemen nog steeds toe.

Aangezien onderzoek van de kransslagaders gebeurt onder dynamische röntgenstralen beeldvorming, kan de stralingsbelasting van de patiënt betrekkelijk oplopen. IC procedures worden geclassificeerd als 'hoge dosis onderzoeken' en de effecten van deze mogelijk hoge dosissen onderscheiden zich volgens de 'Internationale Commissie voor Stralingsbescherming' (International Commission on Radiation Proctection (ICRP)) in deterministische (korte termijn) en stochastische (lange termijn) effecten. Met betrekking tot de korte termijn effecten loopt de huid het hoogste risico. In rapport 85 stelt de ICRP drempelwaarden voor de huiddosis voorop vanaf 2 Gy voor optreden van voorbijgaand erytheem. Wat betreft de lange termijn effecten, loopt vnl. de jongste generatie het hoogste risico. Door de hogere stralingsgevoeligheid en de grotere levensverwachting na de blootstelling aan röntgenstralen, is de kans op stralingsgeïnduceerde gevolgen bij deze populatie groter.

Het eerste deel (publicatie 1) van dit doctoraatsproefschrift onderzoekt in verschillende catheterisatie afdelingen de dosis op de huid van volwassen patiënten. Hiervoor beslaat een rooster Thermo-Luminescente Detectoren (TLDs) de volledige huiddosis distributie. In 3% van de procedures overschreed de Maximale Huid Dosis (MSD) de 2 Gy drempelwaarde in een enkel onderzoek. Actieniveaus in termen van Dosis Oppervlakte Product (DAP) werden vooropgesteld bij een belangrijke waarschijnlijkheid voor overschrijden van de drempelwaarden. In deze studie was afleiding van

Nationale Dosis Referentie Niveaus (DRL) voor diagnostische en therapeutische procedures mogelijk. Gegevens uit specifieke ziekenhuizen met betrekking tot de stralingsbelasting van de patiënt kunnen hiermee worden vergeleken.

Publicaties 2 en 3, nemen voor de beschouwde volwassen populatie de lange termijn effecten gerelateerd aan IC onder de loep. Berekening van de Effectieve Dosis (E) uit de parameters die de blootstelling en de geometrie beschrijven, gebeurde aan de hand van Monte Carlo simulatie software (PCXMC). De voorspellende waarde van DAP met betrekking tot E liet distillatie van Conversie Factoren (CF) voor snelle en gemakkelijke afschatting van deze waarde toe. Onderzoek naar de invloed van extra koper filtratie toonde een gunstige verlaging van DAP en E aan. Relatieve bijdragen van fluoroscopie tot de totale DAP en risicofactoren voor kankerinductie werden beschouwd.

Publicatie 4 bestudeert de stralingsbelasting van kinderen jonger dan 10 jaar, die een IC procedure ondergaan. De grote variatie in lichaamsgewicht en lengte per leeftijd in deze populatie vereist een geïndividualiseerde aanpak voor E berekening aan de hand van Monte Carlo simulaties (MCNP). Risicoschatting voor kankerinductie, gebaseerd op de leeftijdsafhankelijke risicofactoren uit ICRP rapport 60, resulteerde in een toename met factor 10, vergeleken met de volwassen populatie. De huiddosis waarden zijn voor de pediatrische groep echter een factor honderd kleiner, zodat hier de problematiek van stralingsgeïnduceerde huidletsels naar de achtergrond verschuift. Een extra filtratie uit koper met een dikte van 0.2 mm verlaagde E in een lage-dosis-fluoroscopie toepassing met 18 %. Ook in deze studie werden DAP waarden en fluoroscopie bijdragen tot DAP beschouwd.

Het laatste deel van deze verhandeling (publicatie 5) houdt een vergelijkende studie in tussen een conventioneel beeldversterker (II) systeem en een systeem met vlakke detector (FD), de recente ontwikkeling voor beeldvorming in IC. Zowel contrast-detail (CD) metingen voor bepaling van beeldkwaliteit (IQ) als patiëntdosis metingen werden uitgevoerd. Bij de analyse van de IQ-versus-dosis relatie werd een onderscheid gemaakt tussen fluoroscopie en cinegrafie mode. In deze laatste mode oversteeg de recente FD technologie de conventionele met een betere en meer efficiënte beeldvorming voor een zelfde intrede dosistempo. In fluoroscopie mode echter werd geen significant verschil vastgesteld. Een reductie van de patiëntdosis bij klinisch gebruik van deze nieuwe techniek kon niet worden waargenomen.

Chapter 1

Introduction

1.1 Interventional Cardiology (IC)

Before the discovery of x-rays by Wilhelm Röntgen in 1895, the only source of radiation that human beings were exposed to, was natural radiation. Rapidly scientists became aware of the promising applications of x-rays in terms of medical imaging. From then on – and still up to now - medical applications of x-rays expanded enormously and became the main contribution to human's radiation burden. In 2006, medical applications represented 48% of the sources of ionizing radiation for inhabitants of Dutch-speaking Belgium (Flanders), being responsible for a dose of 1.92 mSv per head [1]. In Belgium, an average of 1.2 x-ray examinations is performed per person, per year [1]. Both benefit and risks of the new techniques became clear. Appreciation of the new world to diagnose went hand in hand with a growing concern about the hazardous side effects of radiation. Very soon, optimisation of the dose versus diagnostic benefit relation became important.

One of the medical applications involving x-rays and being the research domain of this thesis is *interventional cardiology* (IC). Imaging and/or treatment of the coronary arteries is performed by means of catheterization under x-ray guidance. In 1977 Andreas Gruentzig [2] dared to perform the first angioplasty (Percutaneous Transluminal Coronary Angioplasty (PTCA)) on a human being (stenosis of the Left Anterior Descending (LAD) artery (Figure 1)). After the first excellent results achieved for this patient (and subsequent ones) belief grew and rapid development of new catheterization tools occurred.

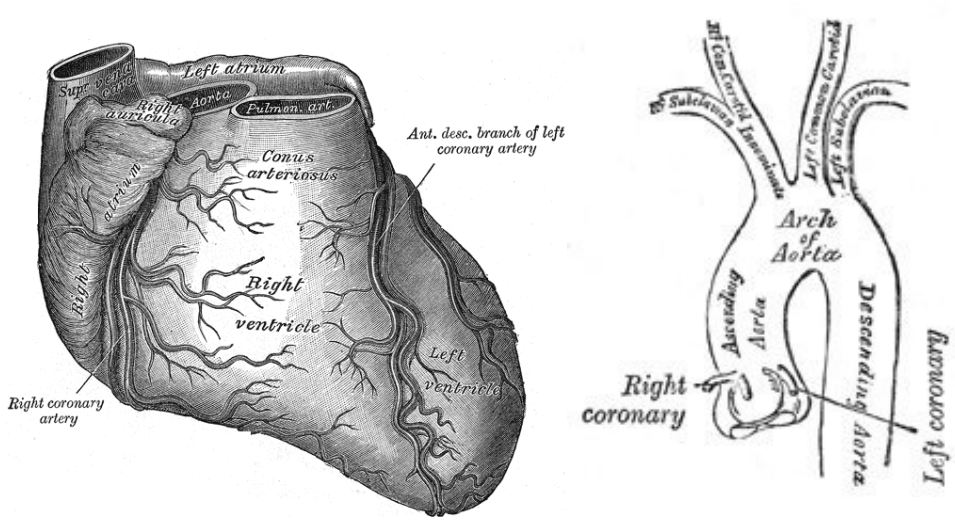

Figure 1. Left: Sternocostal surface of heart. Right: Plan of the branches. The only branches of the ascending aorta are the two coronary arteries, which supply the heart; they arise near the commencement of the aorta immediately above the attached margins of the semilunar valves. (figures 492 and 506 [3]).

The importance of medical applications involving x-rays and especially interventional cardiovascular procedures, is reflected by the number and time-evolution of the occurrence per inhabitant of a certain population (per country or region). Many (governmental) societies keep up with statistics about medical procedures. An overview for Europe and Belgium is given below.

The European Society of Cardiology (ESC) notices in its publication of 1999, describing IC in Europe in 1995, an incidence of 1937 coronary angiographies (CA) per million inhabitants [4]. The newest data by ECS (2004), however, report a total number of 3928 (CA) per million inhabitants, revealing a 3.2-fold increase since 1992 [5]. With its 4.06 CA's and 1.09 PTCA's per 1000 inhabitants, a third place for Belgium in the European classification was reserved (1995). A rate of 0.27 PTCA's per CA was reported (1995) [4]. A number of 1553 PTCA's per million inhabitants in 2004 constitutes an almost 6-fold increase compared to 1992 in Europe [5]. 1350 stents per million inhabitants were placed in 2004, being a 22% increase compared to 2003. The European Society of Cardiology (ECS) reports 2.6 cardiac catheterization facilities per million inhabitants in Europe in 2004 [5]. Time-evolution of the number of procedures is given in Figure 2.

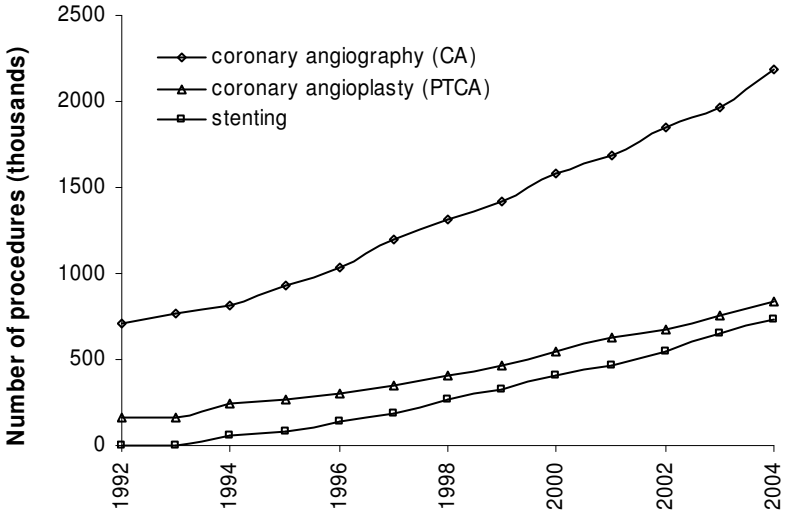

Figure 2. Number of IC procedures (CA, PTCA and Stenting) in Europe from 1992 till 2004 (data from ESC-report 2007 [5].

Recent data and specific for Belgium are presented in the MIRA-T report about ionising radiation (Vlaamse Milieumaatschappij) [1]. Figure 3 shows the evolution of the annual figures from 1997 until 2006 of cardiovascular imaging procedures in Belgium. Mean numbers of about 2.5 to 9 procedures per 1000 inhabitants (therapeutic and diagnostic respectively) can be read from the graph. Latest statistics show a number of more than three therapeutic procedures per thousand inhabitants. Data was provided by the RIZIV Belgium (Rijksinstituut voor Ziekte- en Invaliditeitsverzekering). In comparison with the ESC publications, lower values were reported. A worldwide gradual increase for both diagnostic and therapeutic procedures is the consequence of many advantages of this technique. Mainly the non-invasive character of the intervention leading to short recovery time, a short stay in the hospital and a reduced risk for the patient during treatment of narrowed coronaries make it very popular, against the alternative of surgery. Indeed, ESC concludes from its data that procedures are performed safer now. This is reflected by an unchanged mortality rate of 0.5% since 1992 and a slightly decreased need for emergency coronary artery bypass grafting (CABG) of 0.2%. Specifically for Belgium, diagnostic procedures show a regression in the year 2006. This is explained by the MIRA-report by an increased use of non-radiation imaging techniques as echography and Magnetic Resonance Imaging (MRI). However, this finding was not reported

by ECS, on the contrary. An increased performance of cardiac-CT procedures needs also to be mentioned. The statistics of the next years will show whether this trend will be continued.

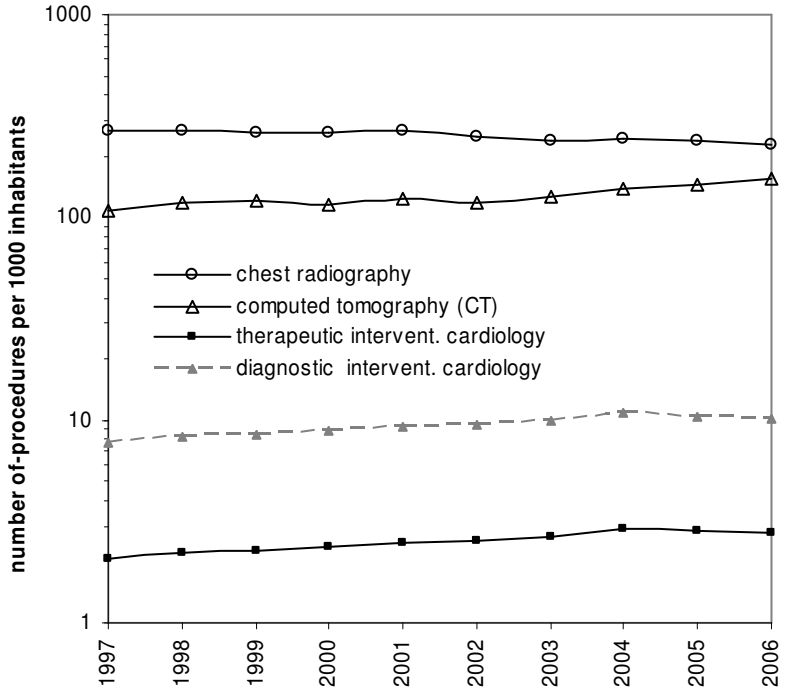

Figure 3. Evolution of relative numbers of procedures using x-rays, performed in Belgium. Data are taken from MIRA-T report (2007) [1] and form S. Dieltiens [6].

However, within a larger medical context, the number of IC procedures is not that high. For comparison, Figure 3 also includes the relative number of chest radiography and (computed tomography) CT examinations in Belgium. A 10-fold larger occurrence for CT and a 20-fold larger occurrence for chest radiography are apparent. The importance of taking a closer look at the IC procedures lies in the fact that they are known as 'high dose procedures' [7-10]. The guidance of the catheters in fluoroscopy mode and image acquisition in cinegraphy mode generates literally thousands of images, combined together to video-fragments during one procedure. This way of viewing, diagnosing and treating is inherent to the dynamic character of anatomical structures as the heart with its coronaries.

1.2 Imaging of the coronary arteries, great vessels and heart chambers

During cardiac catheterization, viewing of the coronary arteries, great vessels and heart chambers is performed through x-ray imaging of a radiocontrast, injected at the locations of interest. Occlusion, stenosis, restenosis, thrombosis or aneurysmal enlargement of the coronary artery lumens can be visualised. Heart chamber size; heart muscle contraction performance; perfusion problems e.g. through septal defects and some aspects of heart valve function can be recognized during the test. Several internal heart and lung blood pressures, not measurable from outside the body, can be accurately measured. Most frequently, the main focus of heart catheterization with adults is visualization and treatment of atherosclerosis (paragraph 1.3). To a lesser extend, valvular, heart muscle, or arrhythmia issues are of primary interest. With children, treatment of Congenital Heart Diseases (CHD) is the major goal (paragraph 1.3).

The use of catheters became practically feasibly when Dr. Sven-Ivar Seldinger introduced in 1953 a new technique to access hollow organs in a safe way [11]. First, a sharp needle is introduced in the artery, mostly arteria femoralis or arteria brachialis for IC. Following, a round-tipped guidewire passes through the needle. After withdrawal of the needle, a "sheath" or blunt cannula is passed over the guidewire into the vessel. Finally a catheter of typically ~2.0 mm (6-French) in diameter with a new guidewire inside (different shape at the top end) accesses the artery through the sheath. A next step in an IC procedure consists in moving guidewire and catheter up to the aorta and the right and left coronary arteries for injection of radiocontrast. Differences in attenuation characteristics of tissue, radiocontrast and used devices make visualization by x-rays possible.

Two modes of x-ray imaging, named fluoroscopy and cinegraphy, are used during IC. Guiding of guidewires and catheters to the desired location and confirmation of their position is performed under fluoroscopy. Normally brief looks provide the practitioner with sufficient information. As no images in this mode are stored nor are of purpose to diagnose, a lower dose and correspondingly lower image quality are allowed. X-ray tube current in this mode ranges from 50 to 150 mA for adult patients and from 4 to 18 mA for paediatric patients. Pulse rates of 12.5 frames/s are mostly used.

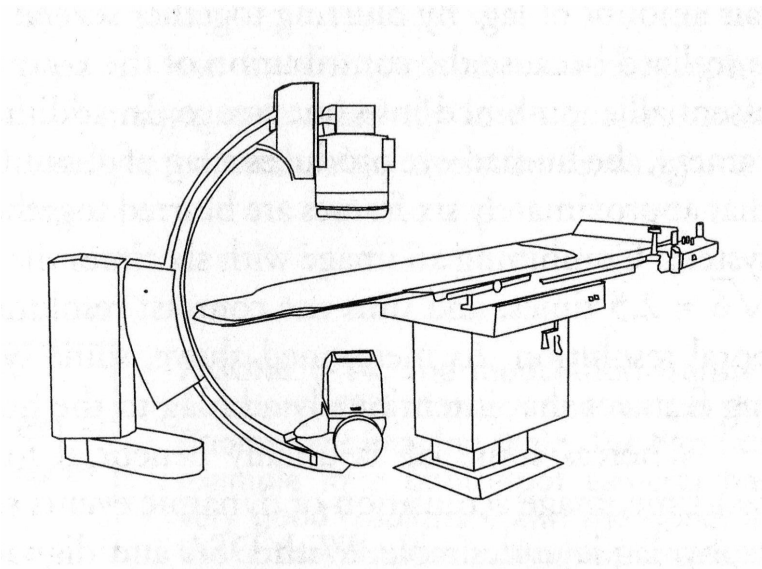

Figure 4. Monoplane x-ray system for IC. The x-ray source is mounted at the bottom, the IR is located at the top [12].

In contrary with fluoroscopy mode, cinegraphy mode is used for a diagnosis to be made. Injection of blood compatible radiocontrast (typically 3-8 cc) visualizes the coronaries, heart chambers or great vessels for 3-5 seconds, before it is washed away into (coronary) capillaries. Details of internal coronary structure or the heart chambers (by examination of the blood flow) are discernible. Video fragments at a higher dose rate with higher image quality are saved in patient's record. Typical pulse rate numbers for adult catheterisation are 12.5 to 30 frames per second, combined with tube current values of 200 till 900 mA. During paediatric catheterisation, up to 50 frames per second are necessary due to higher heart rates. Tube current values vary around 300 mA.

The setup in the cardiac catheterization laboratory consists of a rotational C-arm system where the x-ray tube is mounted in an under-couch configuration (Figure 4). The other end of the configuration contains the image receptor (IR), i.e. a conventional image intensifier (II) or a flat detector (FD). Sometimes two C-arm systems are installed together in 'perpendicular' configuration in order to have two different views with one injection of radiocontrast. This configuration is called biplane; the former is called monoplane. The center of the photon beam coincides with the center of the IR. The point round which the configuration rotates is called the isocentre of the system. The heart is considered as being located in the isocentre of the system.

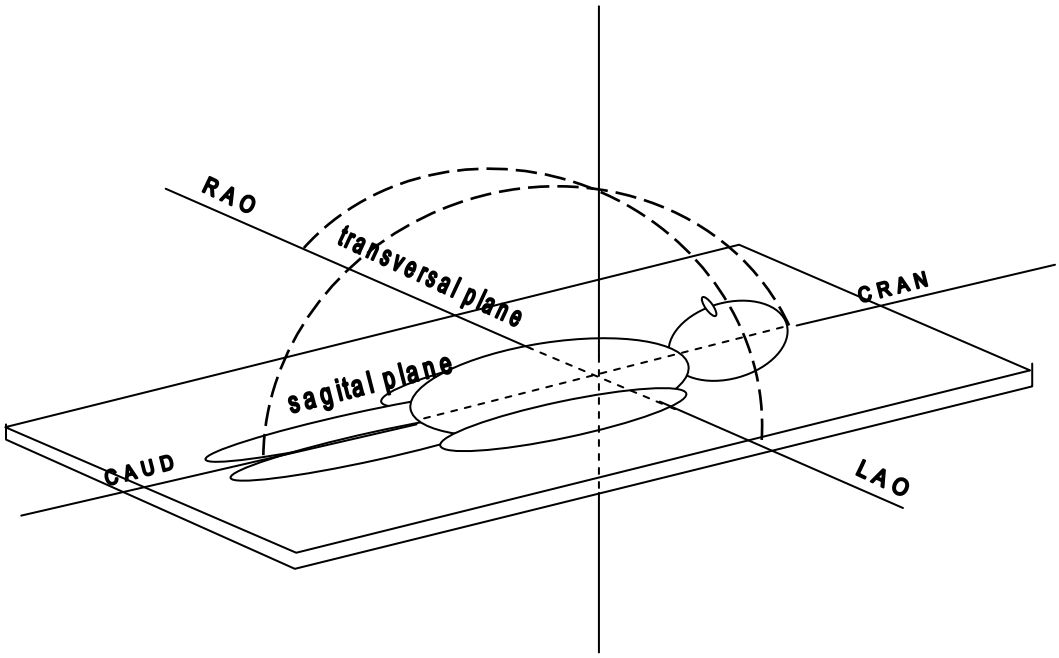

Figure 5. Geometrical indications in IC: caudal and cranial angles in saggital plane and RAO and LAO angles in transverse plane.

Geometry of the tube and IR relative to the patient during an intervention is described by angles in two planes through the patient. The sagital plane includes the length-axis of the patient and the transverse plane is perpendicular to the length-axis of the patient (Figure 5). The angles indicate the position of the IR relative to the patient. The reference system is considered as fixed to the patient with the origin in the heart. The number of degrees that the IR inclines right or left in the coronal plane is indicated respectively by RAO or LAO (Richt/Left Anterior Oblique), whereas the number of degrees that de IR inclines in the sagital plane towards head or feet of the patient is indicated respectively with cranial (CRAN) or caudal (CAUD). Two frequent used projections receive special names. RAO0-CRAN0 is the anterior-posterior (AP) projection and LAO90-CRAN0 is the lateral (LAT) projection.

As so far, diagnostic procedures as coronary angiography (CA) (Figure 6) with or without additive ventriculography or investigation of the great vessels and heart chambers due to CHD are described. However, by changing the diagnostic catheter into a guiding catheter, a variety of instruments can be moved up to a lesion in a vessel. In this way, endoluminal, therapeutic procedures such as angioplasty (reshaping of a vessel) or closing of an Atrial Septal Defect (ASD) (see paragraph 1.3) can be performed.

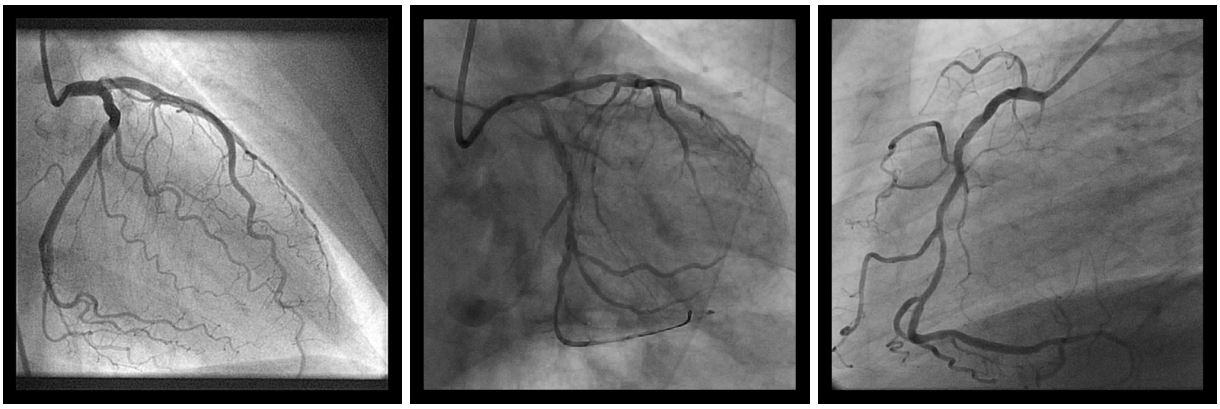

Figure 6 a, b and c. x-ray images of adult coronary arteries, taken during coronary catheterization. Parts 6a. and 6b. represent the left coronary artery (LCA) with the circumflex. The tube geometry for 6a was RAO 0, CRAN 10. Geometry for 6b. was RAO 0; CAUD 20 . 6c represents the right coronary artery with side branches (geometry LAO 90, CAUD 0).

The most commonly performed procedure is balloon dilatation. A balloon of specific length is folded around the tip of a catheter and brought as such through a luminal or valvular stenotic area. Expansion of the balloon, due to radiocontrast filling, widens the narrowed passage. The hydraulic pressure applied within the balloon may extend to as high as 2500 kPa. (For comparison: normal coronary artery pressures are within the 27 kPa range = 200 mmHg). The expanding process is followed under fluoroscopy and as much hydraulic pressure and duration of the inflation is applied as judged needed. With children, the size of the devices needs to be much smaller. When a large balloon is needed for a child (e.g. for opening a pulmonary valve), 2 balloon devices will be introduced. Whilst one will take the arterial way, the other will pass through the venous way to meet at the pulmonary valve (figure 7).

Additionally, several other devices can be introduced into the artery via a guiding catheter. These include stent catheters, IVUS (Intravascular Ultrasound) catheters, Doppler catheter, pressure or temperature measurement catheter and various grinding devices. Of all these devices, stents are the most popular ones. These are specially manufactured expandable stainless steel mesh tubes, mounted on a balloon catheter. By inflation of the balloon, the stent is expanded, widening and stiffening the coronary. Recent developments resulted in drug eluting stents, allowing a protracted delivery of drugs in order to avoid early restenosis. Different especially designed occluder devices similar to stents exist for treatment of CHD (e.g. ASD) in paediatric patients (paragraph 1.3).

Figure 7. Balloon dilatation of a pulmonary valve of a child. Use was made of two balloons. A notch is still visible corresponding to the stenotic area of the valve. The balloon had to be inflated further to widen the narrowing.

Whereas for adults the main points of interest are the coronary arteries, these are the heart chambers and the great vessels with children. This makes that proportionally more contrast is needed in children (mean: 3.4 ml/kg, range: 3 to 6 ml/kg) than in adults (mean 2.4 ml/kg, max: 4 ml/kg). Moreover, higher heart beats with children result in the contrast medium washing away faster than with adults. Mean values of 185 ml for the amount of contrast used, and of 78 kg for weight were obtained for the adult population followed in this work (irrespective whether the procedure is diagnostic or therapeutic). Values of 40 ml and 11.7 kg were obtained for the paediatric population. With respect allergic reactions, the amount of contrast used is a very important and defining parameter.

1.3 Patient population and indication for IC

Within IC, the patient population consists mainly of two groups according to age and with different indications: children and adults. Although this partition is a broad notion, the difference in age is very pronounced especially as it pertains to *young* children (mean age around 4y [13-15]) and *elderly* people (mean age 63 y [16-18]). Indications for IC in these two groups are very different. IC in adults mainly comprises treatment of *Coronary Artery Disease* (CAD), whereas for children treatment of *Congenital Heart Diseases* (CHD) dominates.

CAD is the narrowing or blockage of the coronaries, with reduced blood flow and thus preventing oxygen and nutrients to reach the heart. As the heart is a continuously working muscle, these elements are of capital need.

Decrease in supply, mainly of oxygen, will cause the muscle to cramp. This situation is called "*ischemia*" and mostly occurs during exertion (activity), eating, excitement or stress, entailing extra oxygen for the heart. Ischemia – usually noticed by the patient as chest pain – can be relieved in less than 10 minutes with rest or medications but CAD can progress to a point where ischemia lasts, even at rest.

Typically, CAD occurs when the elastic lining inside a coronary artery develops *atherosclerosis*. Fatty deposits and inflammatory cells form an atheromatous plaque that hardens and narrows the artery's lining. The plaques initially expand into the walls of the arteries, but with progression they expand into the lumen of the vessel, affecting the flow of blood through the arteries.

In an advanced stage of CAD, *Acute Myocardial Infarction* (AMI or MI), more commonly known as a heart attack, can occur. If oxygen shortage is left untreated for a sufficient period, damage and/or death of the heart tissue can result. Chest pain (eventually extended to the left arm and throat), shortness of breath, palpitations, sweating, nausea, vomiting and anxiety are typical symptoms of MI. The most common triggering event is the disruption of an atherosclerotic plaque in an epicardial coronary artery, leading to obstruction or sometimes-total occlusion of an artery. Myocardial infarction is the leading cause of death for both men and women all over the world [19].

There are many risk factors which are associated with (but are not all causes of) various forms of cardiovascular disease. These include:

- Genetic factors/Family history of cardiovascular disease
- Age (CAD incidence increase with age)
- Gender (men present a higher incidence of CAD than women) [20]
- Smoking
- Excessive alcohol consumption
- High LDL (low-density lipoprotein, "bad cholesterol") and low HDL (high density lipoprotein, "good cholesterol"),
- Insulin resistance & Diabetes mellitus
- High blood pressure
- Obesity
- Chronic high stress levels
- Elevated heart rate [21]
- Physical inactivity
- Medication nonadherence, that is, neglecting or refusing to take prescribed drugs [22]

If pre-test likelihood for CAD is considerable, a diagnostic coronary angiography (CA) on the IC-department can be advised, with immediate treatment of the culprit lesion if necessary. As was described in paragraph 1.2, different devices are used for treatment. The most common are dilatation balloons for PTCA (percutaneous transluminal coronary angioplasty) and stents for ad-hoc stenting or stenting after PTCA (Figure 8).

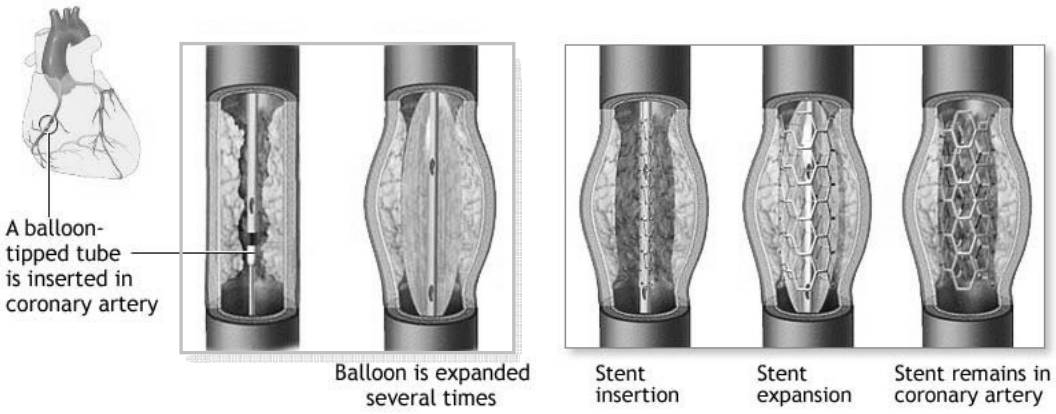

Figure 8. Shematic representation of balloon dilatation and stenting of coronary artery. [http://www.georgetownuniversityhospital.org]

Percutaneous treatment of other diseases as narrowed cardiac valves, arrhythmias, CHD (e.g. Atrial Septal Defect (ASD)) in adults or removal of thrombus (blood clot) is possible. Respectively valvuloplasty, electrophysiology, ASD-occlusion by Amplatzer Septal occluder and coronary thrombectomy are not described here. Information about percutaneous treatment of many other heart and/or coronary diseases can be found in specialised literature.

When considering the paediatric patient population, CHD is the most frequent indication for IC. CHD occurs when the heart or blood vessels next to the heart are not developed properly before birth, or when the necessary structural changes in blood flow immediately after birth do not take place. These structural defects lead to arrhythmias and malfunction of the heart muscles. CHD is mostly detected in newborns; however, sometimes this is eventually noticed in adulthood. Stenosis or obstruction of heart-related vessels or a defect in atrial or ventricular septum cause abnormal and suboptimal conditions for the heart making it work harder and/or beat faster.

Two specific forms of CHD, namely Atrial Septal Defect (ASD) and Patent Ductus Arteriosus (PDA) are described briefly here.

Atrial Septal Defect (ASD) is a specification of CHD related to a hole (foramen ovale) in the septum, i.e. the division between right and left atria. With septum deficiency, blood may flow from the left side of the heart to the right side, or vice versa, resulting in the mixing of arterial and venous blood. During development of the foetus, the foramen ovale remains open, to allow blood from the venous system to bypass the lungs (oxygenation is provided through the placenta) and enter directly in the circulatory system. When the septum does not entirely seal after birth, the foramen ovale is considered as *patent foramen ovale*. If necessary, percutaneous closure of ASD or patent foramen is possible. Numerous closure devices are available. The most popular for ASD closure is the Amplatzer Septal Occluder consisting of two self-expandable round discs connected to each other with a 4-mm waist, made of a wire mesh filled with Dacron fabric (Figure 9). Percutaneous closure is the preferred method of treatment, if the anatomy of the defect is suitable, due to minimal invasiveness of the method [23, 24]. The alternative treatment is surgical closure and involves opening up at least one atrium and closing the defect with a patch under direct visualization during cardiac bypass.

Patent ductus arteriosus (PDA) is another type of CHD wherein a child's ductus arteriosus fails to close after birth. This opening connects pulmonary artery and aortic arch of the developing foetus, to protect the right ventricle to pump against the foetus' fluid-filled compressed lungs. Normally, within 12-24 hours after birth, the ductus arteriosus is closed, with complete sealing after 3 weeks. Symptoms in the first year of life include difficult breathing and poor weight gain. If left uncorrected a patent ductus can lead to congestive heart failure in later childhood or adulthood.

Figure 9. Amplatzer Septal Occluder for closure of Atrial Septal Defect. [http://www.stronghealth.com]

PDA can be treated with both surgical and non-surgical methods. PDA devices, specially designed , yield satisfactory results [24].

A number of other CHD-types can be treated percutaneously. Aortic coarctation, stenosis of pulmonary artery branches, pulmonary and aortic valve stenosis are few of them. Isolated diagnostic procedures become rather rare in paediatric patients, as other tools as echocardiography and magnetic resonance provide sufficient data for complete diagnosis of most CHD.

1.4 Assessment of patient dose and image quality

Several quantities describing patient dose from radiation exposures have been defined by the International Commission on Radiation Protection (ICRP), in its report 60 [8] and by the International Commission on Radiation Units and Measurements (ICRU), in its report 33 [25], and more recently (2005) in its Report 74 [9]. The fundamental quantities (Report 33) are based on measures of the energy deposited in organs and tissues of the human body. Often, these variables are not directly measurable and therefore operational quantities are used for the assessment of "dose". Two main quantities will be described here shortly.

Absorbed dose is the basic quantity used in different radiation related medical fields as radiation biology, radiotherapy, radiology, and nuclear medicine. It is defined as the quotient of mean energy imparted by ionising radiation in a volume element and the mass of matter in this volume. Its unit is Gray (Gy). With respect to skin and underlying dermis, the absorbed dose is related with the direct pathological effects of radiation. Thus, if short-term effects are considered to be a possibility, the absorbed dose to the more heavily radiated regions at the surface of the body is the radiation quantity of interest.

Effective dose E is a quantity designed to describe the 'amount' of exposure quantitatively related to the probability of late radiation induced effects in human bodies. This probability is assumed to be related to the average absorbed dose in an organ and strongly depends on the type of organ or tissue and the type of radiation. Thus, the detriment of lethal cancer induction is assumed the summed products of weighted organ doses $D_{R,T}$ (weighting factors: w_R and w_T). The tissue weighting factors w_T represent the relative contribution of that specific organ or tissue to the total detriment due to radiation effects resulting from uniform irradiation of the whole body. This implies that the sum of the tissue weighting factors is normalized to unity. Detailed description of the tissue weighting factors w_T can be found

in paragraph 1.5.1. The radiation weighting factors w_R represent the relative biological effectiveness of the radiation. The unit of E is Sievert (Sv).

$$E = \sum_T w_T \sum_R w_R D_{T,R}$$

A practical quantity for measurement of the output of an x-ray tube, giving an indication of the absorbed dose is *dose-area product (DAP)*. It is the product of dose to air (air kerma) and the area of the x-ray beam, in units of Gycm^2. A flat large-area ionization chamber is mounted at the exit window of the x-ray tube and intercepts the entire useful beam (irrespective of collimation). The use of a DAP-meter provides a complete measurement of the total exposure of the patient and hence to be closely related to the radiation risk. The reasoning is that this risk is considered as depending both on the extent of the irradiated volume within the patient and the exposure at the centre of the x-ray beam (point-measurement with small ionisation chamber). A practical advantage regarding positioning of this measurement instrument is inherent at the concept of DAP (Figure 10). The product of both quantities is approximately invariable for all planes perpendicular to the beam axis between collimators and the patient.

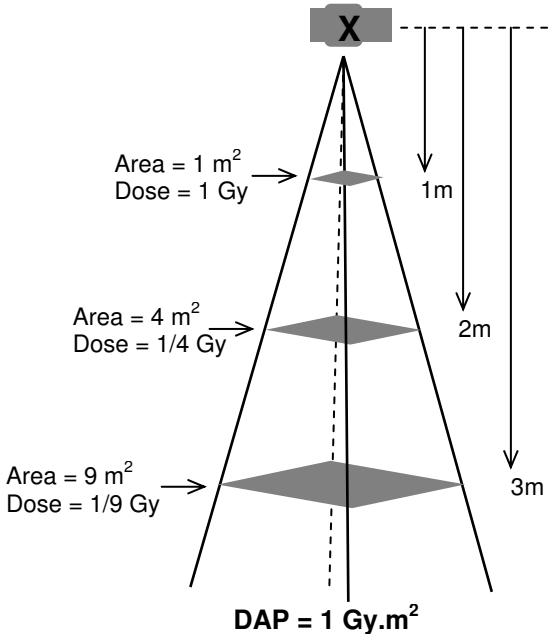

Figure 10. Schematic overview of the principle of DAP. Due to relative proportionality and inverse proportionality of the squared distance for area and dose, the product remains constant.

If properly calibrated against a reference or standard dosimeter, the DAP-meter can serve as a monitor of imparted energy in the patient. In combination with procedure parameters, dose values from phantom measurements or computer simulations, its value can lead to different useful and practical radiation and risk related quantities.

To this end, Monte Carlo simulation code can be used. Monte Carlo codes enable researchers to calculate organ doses normalized to easily measurable quantities such as DAP. Different examples of radiation transport codes are PCXMC [26] and MCNP [27], both used in this work for E calculation.

Registration of the absorbed dose to the skin and more specifically the *Maximum Skin Dose* (MSD) in IC, can only be guaranteed by entire coverage of the whole patient's thorax by a suitable dosimeters (Figure 11). Three-dimensional rotation of the C-arm equipment result in a dose, spread over almost the entire thorax of the patient. Appropriate measuring devices are radiographic film and Thermo Luminescence Dosimeters (TLDs), both calibrated to the right dose conversion. Due to their characteristics, they do not appear on clinical images. Positioning of film under patient's back implies missing of the radiation field at the lateral side. Therefore, a grid of TLDs attached equidistantly at patient's thorax, provides reconstruction of the complete skin dose distribution and is thus a better solution. Unfortunately, this implies a high workload. Some alternatives have been stated, combining film and TLDs with predicting methods for the location where the highest dose might be located [28, 29]. However, this is a rather speculative method especially for individual patient measurements. Anatomical structures and location of the lesion influence largely the irradiation geometry during each individual procedure.

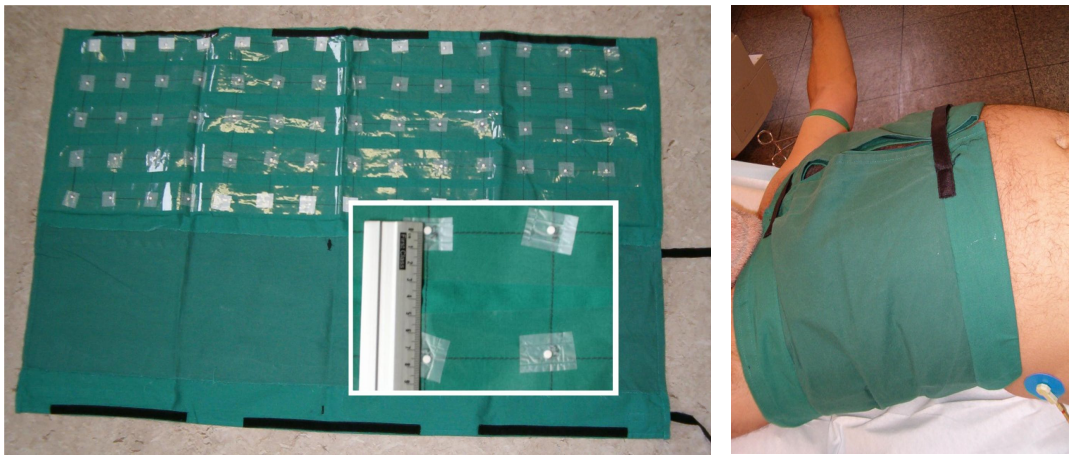

Figure 11. Wrap-around (paragraph 3.1) with grid for TLDs (a) and the positioning of the wrap-arounds (b) to cover entire skin dose distribution.

Image quality and dose are directly related quantities in x-ray imaging, since both are influenced by combinations of tube voltage, filtration and tube current. Assessment of IQ is a complex issue, because the quality of a medical x-ray image is assumed to be task dependent. This means that an image should be judged satisfactory to accomplish the clinical task. The next step is to consider whether the dose to the subject can be reduced, preserving the same or optimal 'task dependent IQ'.

There are a number of ways quantifying the quality of x-ray images, all with their specific advantages and emphasises. The most mathematical way of analysing an image is the determination of *physical parameters* such as Modulation Transfer Function (MTF), Contrast to Noise Ration (CNR), Noise Power Spectrum (NPS) describing spatial resolution, contrast and noise. These parameters are required for any objective determination of system performance, but they are largely 'task independent'. They do not provide any definitive way of ranking systems but they serve as the basic means of system IQ specification. Detective Quantum Efficiency (DQE) describes mathematically the efficiency by which an imaging system transfers absorbed x-ray energy into useful information.

$$DQE = \frac{SNR_{out}^2}{SNR_{in}^2}$$

DQE combines Signal to Noise Ratio (SNR) at input and output of the system and is plotted as a function of spatial frequency. It depends on x-ray spectrum, radiation dose and the detector medium. It is regarded as the most covering indicator for imaging performance but measurement is unfortunately rather unpractical and sensitive to setup [12, 30-32].

Besides determination of physical parameters, a *psychophysical approach* can be considered. These subjective methods – 'subjective' meaning involvement of human observers – have the advantage that clinical utility can be assessed more directly. Receiver Operating Characteristic (ROC) methods and Multiple Alternative Forced Choice (MAFC) methods are examples. In ROC, images from actual clinical cases, phantoms or computer simulations are presented with or without a known target. The observer is asked to grade on a predefined scale his/her degree of certainty that the target is present. The graded response methodology approaches clinical practice where a radiologist also scores lesions as apparent by a certain level of confidence. MAFC methods use phantom images with a certain signal located at one of M alternative positions with equal probability of occupation. The other M-1 locations only contain noise. The observer is asked to score the location of the signal. Forced choice methods are often combined with contrast-detail

(CD) methods. CD diagrams depict the borders of detectability represented by the minimum detectable contrast of an image signal as a function of its diameter.

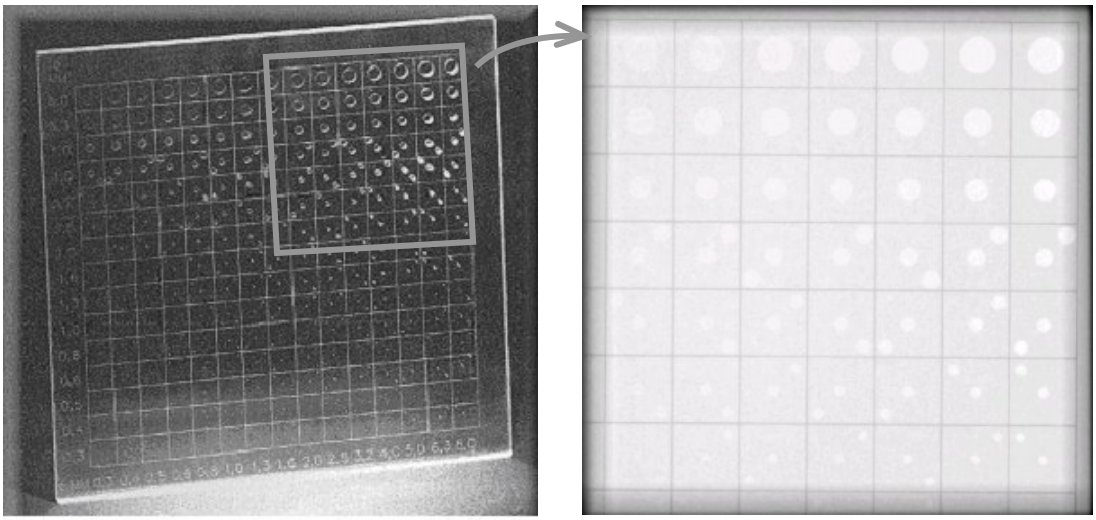

Figure 12. Digital Acquisition (right) of the CDRAD 2.0 phantom (left). The CDRAD 2.0 phantom consists of a PMMA plate (265 x 265x10 mm) with an array (15x15) of 225 square cell regions in which circular holes are drilled. For each column the and for each row diameter and respectively depth vary logarithmically from 8.0 to 0.3. For a diameter < 4.0 mm 4AFC method is to be applied [33].

MAFC CD studies allow assessment of the imaging chain as a whole, with image formation (through data acquisition), image processing and display integrated. This relatively fast technique lends itself to take images in busy clinical departments, demanding minimum clinical downtime. Due to the known target position of the phantom and the correction scheme after scoring, 4AFC provides a more objective IQ measure. The involvement of human observers, however, demands a sufficient number of them for averaging purposes [34]. In this work the preferred method for IQ assessment was 4AFC method with the CDRAD 2.0 CD phantom (Figure 12) [33].

The third and last method for image quality assessment is the use of clinical patient data. Although scoring of these images best approaches clinical practice, huge databases for optimal statistics and ethical considerations (Can I image the same patient on two different modalities, without clinical indication or relevance of the second imaging procedure?) are necessary making this method very time consuming and difficult in practice.

1.5 Radiation risks related to IC

Biologic effects of radiation exposure can be classified as either *stochastic* or *deterministic*. For stochastic effects, the probability, not the severity, increases with dose. Both radiation-induced cancer and heritable effects are included in stochastic effects. In case of higher exposure, deterministic effects may occur, resulting mainly from killing many cells in the exposed tissue, such that the tissue function is decreased. A threshold dose below no effect is seen exists and from there on, incidence and severity of the injury increases with dose. Skin lesions, erythema, fibrosis and haematopoietic damage are typical deterministic effects.

1.5.1 Stochastic Effects

Cancer induction is the most important effect of radiation to consider at dose levels below 1 Gy. It results as chemical changes at the atomic and molecular level of e.g. a biological macromolecule as DNA. Most of the available experimental and epidemiological data support the assumption that the induction of tumors is a probabilistic (therefore stochastic) function of radiation dose [8, 35, 36]. An increase in the dose is assumed to increase the probability of the effect but to have little or no influence on its severity. No threshold is assumed for cancer induction and even a small dose of radiation is assumed to increase the risk of radiation-induced cancers.

Table 1. Estimates of Mean Latent periods for various tumors following external radiation [38].

Tumor type	Mean Latent Period (y)
Thyroid	20
Breast	22
Lung	25
Stomach	14
Colon	26
Bone	10-15
Leukaemia	7-10
Skin	24

Between exposure to radiation and clinical appearance of a cancer there is a certain time span. The mean *latent period* for solid tumors is approximately 20 to 30 years (Table 1). Data are available from epidemiological studies and

long-term follow-up of atomic bomb survivors. UNSCEAR (1994) recommends that 'for risk assessment purposes, most solid tumors should be assumed to have a latent period of at least 10 year, since risks, if any, before that time are extremely small' [37].

Within risk calculation for radiological protection, E is developed to be a quantity, describing possible stochastic effects in the public. The concept of E, associated with a given exposure, involves weighting of individual organs and tissues of interest by the relative detriments for these parts of the body. Derivation of the organs at interest themselves, and more specifically their radiation detriment is complex, and is mainly based on incidence and mortality data for cancers from the studies of the Japanese atomic bomb survivors (LSS-study). Table 2 represents the outcome of these nominal risk and detriment calculations, as performed in report 103 of the ICRP. The sum of the tissue detriments at the bottom of the third column represents the total detriment due to radiation and is estimated to be 5.7 10^{-2}/Sv. In the former report 60 of the ICRP, this value was estimated to be 7.3 10^{-2}/Sv. The difference is explained by novel understanding in incidence and risks for heritable effects.

Table 2. Summary of sex-averaged nominal risk and detriment for the whole population. Taken from ICRP publication 103 [39].

Tissue	**Nominal Risk Coeff.** (cases per 10 000 Persons per Sv)	**Detriment** (relating to column 1)	**Relative Detriment**
Oesophagus	15	13.1	0.023
Stomach	79	67.7	0.118
Colon	65	47.9	0.083
Liver	30	26.6	0.046
Lung	114	90.3	0.157
Bone	7	5.1	0.009
Skin	1000	4.0	0.007
Breast	112	79.8	0.139
Ovary	11	9.9	0.017
Bladder	43	16.7	0.029
Thyroid	33	12.7	0.022
Bone Marrow	42	61.5	0.107
Other Solid	144	113.5	0.198
Gonads (heritable)	20	25.4	0.044
Total	**1715**	**574**	**1.000**

Total radiation detriments for cancer induction, heritable effects and the total of these two in comparison of the two ICRP reports 60 (1990) and 103 (2007) can be found in Table 3. The most significant change from ICRP 60 is the 6-8 fold reduction in the total detriment (nominal risk coefficients) for heritable effects. However, given the uncertainties, the ICRP considers the small difference in the estimate of nominal risk since 1990 of no practical significance. The approximated overall fatal risk coefficient of 5% per Sievert on which current international radiation safety standards are based, continues to be appropriate for the purposes of radiological protection.

Table 3. Detriment-adjusted nominal risk coefficients (10^{-2} Sv^{-1}) for stochastic effects after exposure to radiation at low dose. Taken from ICRP 103 [39].

Exposed population	Cancer		Heritable effects		Total	
	ICRP103	*ICRP60*	*ICRP103*	*ICRP60*	*ICRP103*	*ICRP60*
Whole	5.5	6.0	0.2	1.3	5.7	7.3
Adult	4.1	4.8	0.1	0.8	4.2	5.6

Now, for derivation of the tissue weighting factors w_T, the relative detriment (last column, Table 2) is considered. Due to inherent uncertainties associated with their estimation, the relative radiation detriments are grouped into four categories and the relative detriment is translated into rounded weighted factors. Table 4 represents these four groups with their assigned weighted factors. Changes between the ICRP reports 60 and 103 are clear. New information of the LSS study (follow-up until 1998) (Preston *et al.* 2007) [40] and a revised approach in calculation of radiation detriment associated with both cancer and heritable effects (gonads) explains adaptation of the factors. The current estimate (ICRP 103) is based on lethality/life-impairment-weighted data on cancer incidence, with adjustment for relative life lost. The tissue weighting factors are sex-averaged and are for the assessment of E for workers as well as members of the public, including children.

The most important differences with ICRP 60 comprise the following:

- The detriments for heritable effects and cancer following gonadal irradiation were aggregated to give a w_T of 0.08, which is only 40% of the estimated value in ICRP 60. This is due to the fact that genetic damage sustained by germ cells of individuals who are beyond the reproductive period, or who are not procreating for any reason, poses no risk.

Table 4. ICRP Recommendations for tissue weighting factors in Publication 60 (1990) [8] and Publication 103 (2007) [39].

ICRP Publication 60 (1990)		ICRP Publication 103 (2007)	
Tissue	**Tissue weighting factor, w_T**	**Tissue**	**Tissue weighting factor, w_T**
Lung Stomach Colon Bone Marrow	0.12	Lung Stomach Colon Bone Marrow **Breast** **Remainder**	0.12
Gonads	**0.20**	Gonads	**0.08**
Thyroid Oesophagus Bladder Liver **Breast** **Remainder**	**0.05**	Thyroid Oesophagus Bladder Liver	**0.04**
Bone surface Skin	0.01	Bone surface Skin **Brain** **Salivary Glands**	0.01

- w_T for breast tissue changed from 0.05 to 0.12 due to raised risk estimates for breast cancer in incidence analysis of the extended data in the LSS study. Those exposed as juveniles in the LSS cohort now make a larger contribution to the overall breast cancer risk. This implies that E for women that have been submitted to an IC procedure, will now be remarkably higher. An increase of 5% to 20% was estimated by Einstein *et al.* [41].

- The 'remainder tissue'-group previously comprising 10 tissues (adrenals, brain, upper large intestine, small intestine, kidneys, muscle, pancreas, spleen, thymus, uterus) includes now 14 tissues ((13 in each sex): adrenals, extrathoracic tissue (ET), gall bladder, heart, kidneys, lymphatic nodes, muscle, oral mucosa, pancreas, prostate (♂), small intestine (SI), spleen, thymus, uterus/cervix (♀)). The weighting factor is increased from 0.05 to 0.12. The reason again is the extended data from different studies and exclusion of mass-weighting of the tissues in the remainder fraction. (In Publication 60, w_T for the

remainder was divided among the five remainder tissues which receive the highest dose, implying a non-additive system).

- Salivary glands and brain are considered separately and weighting factors of 0.01 are assigned. Their cancer risk is now judged to be greater than that of other tissues in the remainder fraction.

Thus, from Table 4 one roughly derives that the relative contribution of bone marrow to the total detriment resulting from a uniform irradiation of the whole body is estimated to be 12%, reflecting the relative high radiosensitivity of this tissue. This is also the case for colon, stomach, lung and breast.

With respect to age dependency of total radiation risk, Figure 13 shows the attributable life–time risk in % per Sievert versus the age at time of exposure as derived in the 1990 Recommendations of the ICRP 60 [8].

A gender dependency is clear from this figure. Females have been considered more likely to develop radiation-induced cancers than males, for all cancers except for leukaemia and especially for breast and thyroid cancers. The sex difference may be due to interactions between other factors such as hormone dependent promoting factors rather than a difference in radiation sensitivity [39].

A more explicit dependency exists with respect to age. Paediatric patients are more susceptible to radiation-induced cancers than adults are. This is explained by the fact that radiation sensitivity is related to the rate of cell division, in accordance with the law of Bergonié and Tribondeau (1906). During their research on cells and their characteristics affecting radiosensitivity, they formulated their law. *"Radiosensitivity is greatest for those cells that (a) have a high mitotic rate, (b) have a long mitotic future, and (c) are undifferentiated."* In other words, actively proliferating cells with a high turnover rate and long mitotic periods but that are poorly differentiated (e.g. stem cells in red bone marrow) are very radiosensitive [12, 38]. Children have a wider and increased cellular distribution of red bone marrow, that is far most located at the upper part of the body [42-44]. A second reason is that the post-exposure life expectance for children is larger than for adults, as they have their entire lives in front of them.

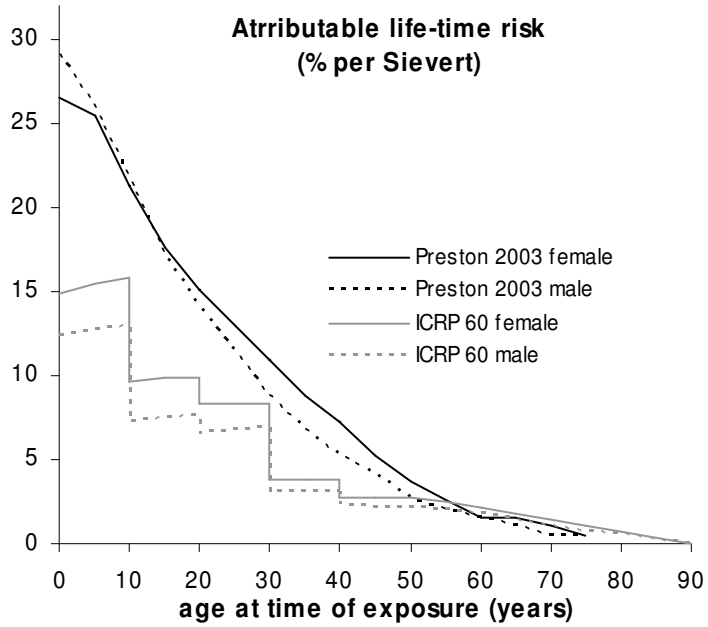

Figure 13. Comparison of attributable life-time risk versus age data form ICRP 60 [8] and the findings published by Preston *et al.* [45]. The curves reported by Preston *et al.* represent estimates for LSS (Life Span Study) life-time solid cancer mortality risk for a 1 Sv exposure. Note that life-time mortality risk for leukaemia, other haematopoietic tumors or hereditary effects is not included, contrary to the ICRP 60 data. For derivation of the ICRP60-curve, a DDREF of 2 was applied.

Figure 13 also documents on the estimates arising from recent data from the A-bomb survivors (1950-1997 Preston *et al.* [45]). It has to be stressed that the radiation related solid cancer mortality risk in the latter study was determined from people exposed to acute doses of about 200 mSv or more. However, in radiation protection, mostly risks from continuous exposures or fractionated exposures with acute fractions of a few mSv or less are involved. Experimental investigations tend to show that fractionation or protraction of dose is associated with reduced risk. Thus, to obtain values applicable for low doses and low dose rates from dose specific estimates based on high-dose, acute exposure data (as that form A-bomb survivors), ICRP suggests division by a DDREF (Dose and Dose Rate Effectiveness Factor). The magnitude of DDREF is assumed to be 2, as a broad whole number judgement for practical purposes of radiological protection and comprising elements of uncertainty. With respect to Figure 13, application of a DDREF of 2 to the data from Preston *et al.* yields the curve used in ICRP 60.

When considering IC, paediatric procedures may even last longer than interventions on adults. Higher heart rates, smaller cardiovascular structures and smaller body size are specific additional difficulties related to

paediatric IC, requiring higher frame rates and magnification modes to be used. A wider variety of unusual anatomic variants implies the potential need for relatively lengthy and complex procedures. Some of the tissues sensitive to radiation (the eyes, the gonads and the thyroid) are significantly closer to the heart in young children than in adults. This places them closer to scattered rays and to the primary beam [46]. Moreover, due the increased survival of children with complex heart-anatomy, frequent catheterizations within the first few years for treatment of chronic cardiac disease are needed [47].

Compared to children, radiosensitivity and post-exposure life-time expectance for adults is lower. Based on these two most important facts, possible induction of radiation induced injuries e.g. for a population with mean age of 65 years (paragraph 3.1, ***publication 1***) is relatively low. However, even with adults care should be taken in view of the high doses of IC, especially when they are relatively young (age 30-40 years).

The UNSCEAR 2000 report [36] indicates an average value of 7.3 mSv for E for interventional procedures in health care level I countries. Multi-slice spiral computed tomography of the chest and the abdomen/pelvis induces similar doses of 5.7 mSv and 14.4 mSv respectively [48]. UNSCEAR reported an average dose for a diagnostic CT-exam (data 1991-1996) of 8.8 mSv [49]. The average E for a PTCA intervention reported in the UNSCEAR 2000 report is 22 mSv, while individual patient data range from 7.5 up to 57 mSv in the study of Neofotistou [50]. Because of this, coronary angiography is among the medical applications of diagnostic x-rays with a high patient radiation burden.

1.5.2 Deterministic Effects

For all deterministic effects, cell killing is the central issue. The main direct effects to the skin result through damage to proliferating cells at the basal layer of the epidermis. The epidermis is the upper layer of the skin and serves as the first barrier of the human body against the environment. The underlying layer is called the dermis. Renewal of the skin by migration of new cells from basal layer to the top of the epidermis, takes about 14 days to 1 month. The time course of expression of radiation injury to the skin and restoration of tissue components generally depends on this normal rate of renewal, and is dose dependent at low doses but not at high doses. The upper part of the dermis – itself consisting of two layers: superficial papillary dermis and deeper thicker reticular dermis- is highly vascularised.

Approximately 90% of the blood flow is concerned with temperature regulation. Nutritional aspects of blood flow are also important. Hair follicles are embedded in the lower part of the dermis [38, 51, 52].

The response of the skin to high levels of ionizing radiation follows a typical pattern. The severity and the time-course may vary depending on the dose, the treatment characteristics and patient condition. Distinct phases are listed below [51, 53-55]:

1. *Transient early erythema*. This effect occurs within a few hours after a single dose in excess of about 2 Gy and represents an early phase of inflammation, with dilatation of capillary vessels, often referred to as radiodermatitis. The area is well defined and matches the entrance site of the beam (mostly at the back or under the right armpit of the patient in case of IC). The reaction - often faint and similar to sunburn - peaks at about 24 hours and vanishes after 48 hours.

2. *Main erythema*. After about 10 days (and after a dose of about 6 Gy) a second reddening of the skin occurs, explained by an inflammatory reaction to damage of the epidermal basal cell population. Either a dry or moist desquamation response may be seen after 3-6 weeks (dose: 14-18 Gy). Temporary or permanent epilation may occur within 3 weeks, for a dose >3 Gy. When skin desquamation is severe, dehydration and infection can easily complicate healing and increase the risk for second ulceration of the healed fragile skin.

3. *Late erythema, dermal ischemia and necrosis.* Between 8 to 10 weeks, mauve skin discoloration becomes apparent (dose > 15 Gy). Microvascular damage occurs and overall reduction in capillary density leads to progressive vascular insufficiency of the dermis. The probability of the development of ischemic necrosis increases with increasing dose after a threshold dose of ~18 Gy. Radiation ulcers recur and require – in a progressed stage – surgical excision and grafting [56-59].

4. *Late skin damage.* This is the result of damage to deeper layers of the skin, mainly the dermis. This last phase is characterised by dermal atrophy, a thinning of dermal tissue, telangiectasia (atypical dilatation of superficial dermal capillaries) and necrosis (> 52 weeks).

Table 5. Radiation induced skin injuries: effects with dose and onset. NR = not reported [53].

Effect	Dose (Gy)	onset
Early transient erythema	2	hours
Main erythema	6	~ 10 days
Temporary epilation	3	~ 3 wk
Permanent epilation	7	~ 3 wk
Dry desquamation	14	~ 4 wk
Moist desquamation	18	~ 4 wk
Secondary ulceration	24	> 6 wk
Late erythema	15	~ 8-10 wk
Ischemic dermal necrosis	18	> 10 wk
Dermal atrophy (1st phase)	10	> 12 wk
Dermal atrophy (2nd phase)	10	> 1 y
Invasive fibrosis	10	NR
Telangiectasia	10	> 1 y
Late dermal necrosis	>12 ?	> 1 y
Skin cancer	-	> 5 y

Skin tolerance to radiation depends significantly on the volume of tissue irradiated. As the volume of skin irradiated becomes smaller, the dose required to produce necrosis increases. For example, the skin threshold dose for a circular field of 150 cm^2 (diameter = 14 cm) is approximately 15 Gy in a single dose, whereas for a circular field of 50 cm^2 (diameter = 4 cm) the threshold dose is almost 20 Gy [38, 60]. In most tissues, responses are greater when irradiated volumes are larger. With early skin reactions, the volume effect is due largely to the decreasing ability to heal large areas mainly because of limited cell migration from the margins [39]. Moreover, different regions of the skin also show a different radiosensitivity; chest, abdomen, thigh, back and face are progressively more radiosensitive. The neck skin tissue, by contrast, is very resistant to radiodermatitis [58, 61].

For low-dose-rate application, sublethal cell injuries can be repaired and killed cells replaced during the entire process of dose accumulation [51] Fractionation of the total dose, as seen in patients undergoing several procedures separated by days or weeks, increases overall tissue tolerance, but tolerance for each subsequent individual session may decrease. This is the case for patients, in need of different subsequent catheterizations. It is clear that the effect of decrease of skin tolerance overrules the effect of skin recover, with fractionation. This is emphasized by the fact that almost all medical files of patients presenting with radiodermatitis document on multiple catheterizations [53, 57-59, 62].

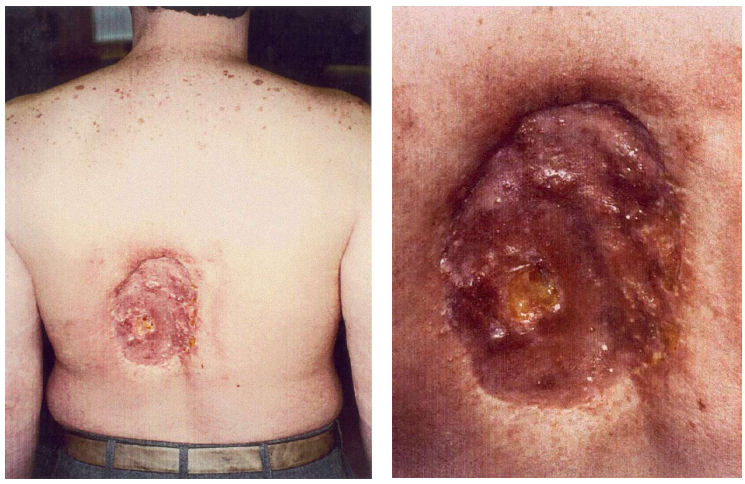

Figure 14. Photograph of the back of a 40-year old man, approximately 18-21 months after multiple coronary angiography and angioplasty procedures (all performed on one same intervention – 1990). Skin dose was unknown, but probably exceeded 20 Gy. Skin grafting was necessary for treatment of tissue necrosis [63].

Treatment and healing of skin injuries diagnosed as radiation dermatitis is not straightforward. Depending on the severity of the damage to the epidermis, dermis and subcutaneous tissues, the evolution of the lesion towards healing seems to be 'all or nothing'. If depopulation of clonogenic cells in the epidermis, and/or of matrix cells of the hair follicle is not that severe, erythema, ulceration and hair loss may cure. A repopulation of the basal cells either by surviving clonogenic cells within the irradiated area or through migration of cells from the surrounding borders will occur. Wound care by silver sulfadiazine 1% cream and sterile dressings twice daily were reported by Nahass *et al.* [61] to result in gradual reepithelialization within 3 weeks of a tender erythematous rectangular plaque (7x14 cm) with several ulcers. However, most reported cases involving necrosis do not respond to good wound care. Oral or intralesional administration of corticosteroids, oral antibiotic agents, absorbent silicone-coated foam dressings, cream and hydrocolloid dressings all appeared to be insufficient in terms of wound healing and were unable to relief persistent pain [56, 58, 59]. Conversely, the lesion becomes worse and evolution from erythema to a deep wound may take one to several years. Wound exploration under general anesthesia and final excision of the diseased tissue and skin grafting seemed to be the only solution [52, 56, 58, 59].

More than 70 injuries, related to fluoroscopically guided procedures have been reported in literature up to the beginning of the 21 century [53, 55] and

even more cases were described in recent literature [56, 58, 59] (Figure 14). As already stated above, a serious injury may require a prolonged course of intense care that sometimes lasts for years. Often, Interventionalists are unaware of the exact magnitude of the radiation dose to the skin, due to large intervariability of the individual procedures and lack of a direct skin-dose-indicator at the x-ray equipment. It is not within expectations that such injuries would occur with modern and new equipment; unfortunately, the opposite is true. Complexity of the procedures, multiple cine-runs and prolonged use of fluoroscopy are the main reasons for overexposures [7, 53, 57, 62, 64, 65]. In addition, due to delay of the onset of these injuries, physicians frequently do not recognize skin lesions as being related to the procedure, since they cannot investigate their patients immediately after the intervention.

Within IC, deterministic effects are mainly an issue for adult patients. Due to the smaller body size and tissue material thickness for passage of the x-ray beam, the difference between input and output intensity of the beam is smaller in children than with adults. Skin dose values for IC procedures on paediatric procedures are well below threshold values for skin injuries [13, 14].

1.6 Specific equipment

Examination of dynamical anatomical structures (as the heart) requires real-time imaging with high temporal resolution. Before 1950, real-time imaging was possible by viewing the faint shine of a patient, produced on a thick fluorescent screen. It implied a huge step for medical world, but for the radiologists this posed a problem with respect to radiation protection [12]. After 1950, a second generation of fluoroscopy systems coupled an image intensifier (II) - being new technological development at that time - to a video-circuit [66, 67]. With time course, better image quality and indirectly digitised images by use of Charged Coupled Device (CCD) cameras became available [68, 69]. The latest evolution in x-ray digital imaging represents introduction of flat-panel detectors (FD), also known as Active-Matrix Flat-Panel Imagers (AMFPI) [70, 71]. In the mid nineties, this new type of IR became fully integrated in x-ray systems for static examinations. However, it was only till 2003 that FD's became operational for dynamic imaging [72].

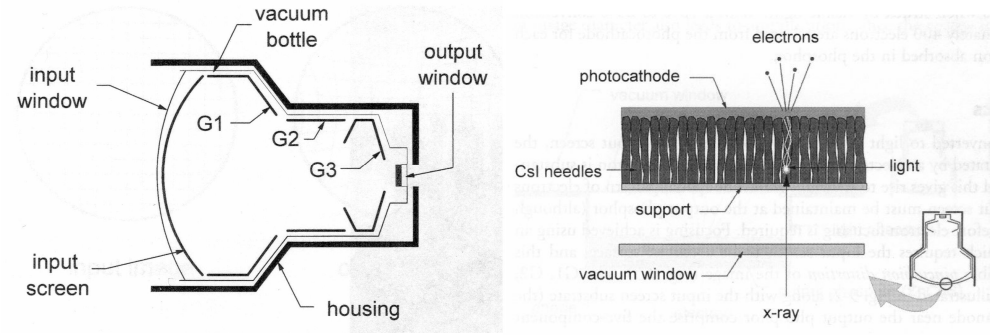

Figure 15. Structure and principle of image intensifier. Left: G1, G2 and G3 are the focussing electrodes. Right: detail of the input layer. Four layers are discernable : housing of vacuum chamber, carrier, CsI phosphor layer and photocathode [12].

The structure and principle of an *image intensifier* is schematically represented in Figure 15. An II consists of a vacuum housing, an input layer that converts x-ray photons into an electrical signal, a system of dynodes to focus and multiply electrons and an output phosphor, converting electrons into a light signal. The input layer itself consists of four layers. The first is part of the vacuum housing and the second serves as extra support: both are of aluminium (Al) in order to resist high pressures preserving the vacuum inside. On top of the additional Al support, a phosphor layer consisting of CsI crystal needles converts incoming x-rays into visible light. The needles behave like light pipes, minimizing lateral diffusion of light. Therefore, a relatively thick layer is produced for an optimal photon to light conversion. The fourth layer is a photocathode layer and converts the light into electrons.

An electric field is applied between photocathode and first dynode. Each dynode is more positively charged than its predecessor is. Secondary emission occurs at the surface of each dynode. Such an arrangement is able to amplify the small current emitted by the photocathode. Multiplication is proportional to the energy of the incoming photons. Light with a wavelength characteristic for the output layer (green (~530 nm) for ZnCdS:Ag) is emitted. This output layer is preferentially as thin as possible with view of low spatial spreading.

Transmittance of the image at the phosphor layer to a television screen first was possible through video capitation. Now, (from 1986 on) CCD cameras are used for direct digitisation of the image [69]. A photosensitive silicon (Si) layer serves as carrier for discrete pixel-electronics. Light, falling onto this layer of pixels is converted into an electrical signal, proportional to the intensity of the light [12, 68, 69]. Read out of the exposed CCD yields a

digital image. Pixel size and number (e.g. 1024 x 1024 for a surface of 2.5 cm^2 x 2.5 cm^2) determines resolution of the camera. For applications in fluoroscopy, the intensified light form the II is focused by means of lenses and fibre-optics to the small CCD surface.

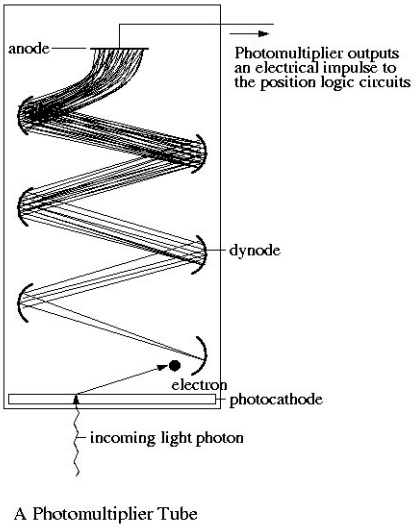

Figure 16. Multiplication of electrons by the dynodes of an image intensifier [12].

The advantages of digital images are numerous. Processing, storing, transporting, multiple viewing, duplicating becomes very easy, given high computer capacity and extended hospital network.

Different magnification modes are possible by changing the electrical fields between the dynodes. As the magnification factor increases, a smaller area on the input of the II is visualised. In order to obtain the same signal to the output phosphor a higher input dose is necessary, increasing the dose to the patient. Switching from a field of view of 23 cm to one of 18 cm increases the exposure rate by a factor of $(23/18)^2 = 1.6$. Switching from the largest to the smallest field (e.g. 13 cm) increases exposure rate with a factor 3.1. This holds true if only the tube current is increased when going to a magnified mode. With changes in tube potential, the actual increase in dose is less, than described above. Nonetheless, an increased dose is certain.

The newest generation of IRs: *flat panel detectors* are classified into two groups: those that are based on direct conversion of x-rays into electrical signal and those based on indirect conversion. (However, II-systems coupled to CCD are also often seen as indirect conversion digital systems [73].) Direct conversion detectors use amorphous Selenium (a-Se) as x-ray photoconductor. Indirect type (AMFPI) detectors use amorphous Silicon (a-Si) in a two-step process for electrical signal generation. Both a-Se and a-Si

detectors send electrical charges to an array of Thin Film Transistors (TFTs). Readout of the TFTs and Analog-to-Digital Conversion (ADC) yields a digital image. In general, the structure of a FD (both for direct or indirect conversion type) consists sandwich-like of following layers: first a layer sensitive to x-rays (eventually combined with a light- sensitive layer), secondly a TFT array with read-out electronics and thirdly a supporting layer. Putting everything into a housing and connecting it to the computer, yields the FD.

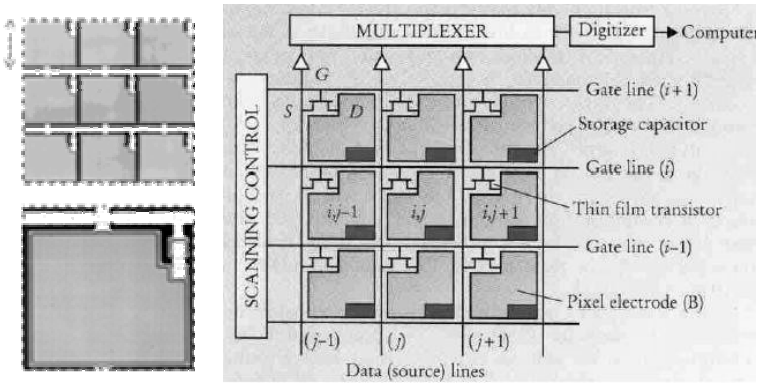

Figure 17. Left Top : a-Si:H photodiode layer on TFT array. The arrow indicates a distance of 143 μm. Left bottom : Detail of 1 TFT element (pixel) [http://www.trixell.com]. Right: Part of a TFT-array consisting of 3 by 3 pixels, seen through an optical microscope. The scheme shows the read-out mechanism. Indices *i* and *j* denominate rows and columns. S, D, and G denominate Source, Drain and Gate of the transistor [74].

The support layer of TFTs consists of a glass substrate, upon which read-out electronics and charge collecting arrays are etched at different levels. Typically, electronics are packed together in the corner of each pixel (Figure 17) to occupy smallest place possible. The reason is that this place is inactive in collecting charge, thus reducing fill factor. Electronics comprise a capacitor to hold the charge, built up during exposure. After exposure, TFT are read-out one by one or combined ('binning' of detector elements) and are reset afterwards. Current TFTs are capable of readout an entire image in 1/30 of second, sufficient to perform fluoroscopy.

The principle of direct and indirect AMFPIs will be described here shortly [71, 73, 75, 76].

Detectors of the *direct conversion* type use an a-Se photo-conducting layer turning x-rays directly into electrical charge. An electrical field is applied across the material to conduct the electrons directly to the capturing TFT-array, resulting in very low spatial spreading, and thus high spatial

resolution On the other hand, Se has less favourable x-ray absorption characteristics (compared to Cesium (Cs) or gadolinium (Gd)) at diagnostic energies > 40 keV. A thicker Se layer will compensate for this.

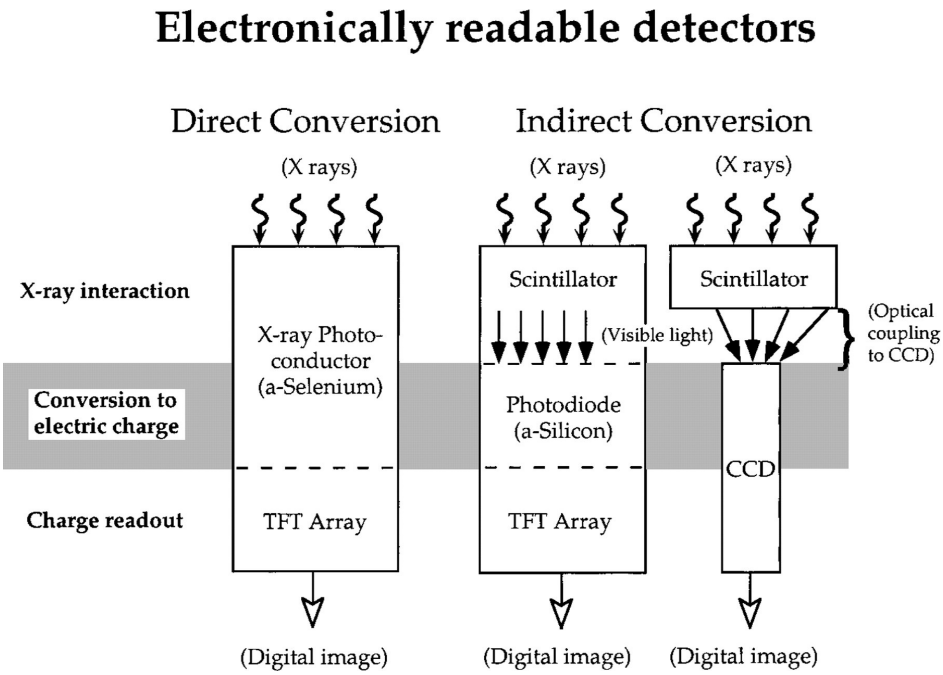

Figure 18. Illustration of the principle of direct (a-Se) conversion and indirect (a-Si and coupling with CCD) conversion digital x-ray detectors [73].

With *indirect systems*, a scintillator and an a-Si photodiode replace the a-Se photoconductor layer. The scintillator emits light proportionally with the energy of incoming x-rays and the a-Si photodiode converts the light into electrical charge. Captured by the TFT-array and passing ADC-electronics, the digital image is generated. As in IIs, the scintillation material used is CsI, grown in crystal-like needles that avoid lateral diffusion of the light. Both high DQE and high spatial resolution can be obtained.

Figure 18 schematically represents principles of direct and indirect conversion for x-ray detectors.

Both II and FD imaging techniques have their specific characteristics and plus-points. In comparison with conventional II, FDs have shown convincing advantages of better ergonomics with better patient access, lack of geometric distortion, little or no veiling glare, no vignetting, insensitivity to magnetic fields and wider dynamic range [77-80]. However, questions regarding the capabilities of FD have not been answered completely,

particularly as it pertains to IQ at low exposure levels. In IC, real–time viewing of vascularisation of the heart and tiny devices such as stents and guidewires impose stringent requirements on the imaging techniques used. Up to now, IIs achieve essentially 'noiseless' gain at low exposure rates, due to their characteristics of high electronic brightness gain and minification gain [79]. For FDs, on the other hand, system noise becomes a limiting factor in determining system performance at low exposure rates [81-83].

Chapter 2

Objectives and outline of the thesis

2.1 Objectives and outline

Within respect to deterministic effects of ionising radiation, skin dose is of major concern in IC ([8, 53, 63]), as fluoroscopy guided procedures with cinegraphy – in general - are recognised as involving high-doses to patients [7]. Moreover, due to their advantages upon surgical alternatives, the number of procedures per year increases [1, 4, 5]. Several recommendations for physicians working extensively with x-rays in IC have been published in order to reduce patient doses and to avoid radiation induced injuries [7, 84-87]. Dose thresholds as low as 2 Gy for maximum skin dose have been stated by the ICRP in its report 85 [10] for onset of transient erythema. Therefore, the Commission recommends assessment of MSD and of location of most exposed skin site. The purpose of the first study in the framework of this PhD dissertation was to derive and propose action levels for skin exposure in terms of DAP. These levels indicate a reasonable probability that MSD has exceeded the acceptable level of skin exposure. Medical follow-up of the patients can be advised, based upon the proposed levels. The concept of trigger levels was proposed by Vaño *et al*. [62]. However, never MSD was measured earlier with this extensive number of TLDs in order to reconstruct the entire skin dose distribution. It is also the first study in Belgium for dose inventarisation in IC.

Besides the recommendations regarding MSD, The ICRP also imposed the use of Diagnostic Reference Levels (DRLs). These values serve as first criterion to decide whether in routine conditions, the levels of patient dose from a specified imaging procedure are unusually high (or low). Mostly the 75^{th} percentile point of the distribution of a certain dose indicator is used [8, 85]. DRLs should be reviewed at intervals at regional, national or even international scale. The second purpose of the first study was to derive and

propose dose reference levels for diagnostic and therapeutic examinations in IC in Belgium.

The results of this study are presented in ***Publication 1: A large-scale multicenter study of patient skin doses in interventional cardiology: Dose-Area Product action levels and Dose Reference Levels. (p 39)***

A second study deals with the stochastic effects of ionising radiation exposure, for an adult patient population involved in IC. As E is the general quantity for long-term risks [8, 39], calculation by a Monte Carlo simulation code PCXMC was performed [26]. In addition, doses to organs most at risk were investigated separately. Risk factors were determined using the life-time risk coefficients proposed by the ICRP in report 60 [8]. However, this is the first study that translates individual IC procedures in terms of standard geometries of a clinical protocol and combining detailed DAP contributions for calculation of E. It is the first study for calculation of E and risk assessment for IC procedures in Belgium. The same patient population of the multicentre study of publication 1 was considered. Differences between hospitals were highlighted and measures to lower patient dose were proposed. Results were reported in ***Publication 2: A large-scale multicentre study in Belgium of Dose-Area Product values and effective doses in interventional cardiology using contemporary x-ray equipment. (p 61)***

A practical approach to obtain E was worked out in the third study. Specific conversion factors (CF) for E based on recorded DAP values were proposed. The influence of additional Cu filtration was taken into account. The effect of irradiation geometries on CF was studied. Details can be found in ***Publication 3: Interventional cardiovascular procedures in Belgium: effective dose and conversion factors. (p 85)***

As children are more radiosensitive than adults, due to a higher fraction of actively proliferating cells and high post-exposure life expectancies [40, 45, 47], special attention has to be paid to the doses administered. A paediatric population, with ages < 10 year, receiving diagnostic or therapeutic procedures in IC was followed and the risk for late effects, by means of individual E calculations was assessed [27]. The impact of additional Cu filtration was studied. Findings were reported in ***Publication 4: Patient-Specific dose and radiation risk estimation in paediatric cardiac catheterization. (p 95)***

New technologies in IC, mainly with respect to image capture have been settled well in clinical practice now [79, 88]. At the moment, Flat Detectors (FD) are preferred above conventional Image Intensifiers (II), but their response and image quality at low dose rates is still unclear. In a

comparative study between II and FD, both CD measurements for assessment of image quality and patient dose measurements were performed. Distinction was made between fluoroscopy mode and cinegraphy mode. It was our aim to investigate the dose versus image quality relation in clinical practice for conventional II and recent flat panel technologies. Results were reported in ***Publication 5: Does digital flat detector technology tip the scale towards better image quality or reduced patient dose in interventional cardiology? (p 113)***

Chapter 3

Original research: results

3.1 Part I

A large scale multicenter study of patient skin doses in interventional cardiology: Dose-Area Product action levels and Dose Reference Levels

E. Bogaert[1] – K. Bacher[1] – K. Lemmens[1] – M. Carlier[2] – W. Desmet[3] – X. De Wagter[4] – D. Djian[5] – C. Hanet[6] – G. Heyndrickx[7] – V. Legrand[8] – Y. Taeymans[9] – H. Thierens[1]

[1]*Department of Medical Physics and Radiation Protection, Ghent University, Proeftuinstraat 86, Gent B-9000, Belgium.*

[2]*Hôpital St Joseph, Gilly, Belgium*

[3]*Universitair Ziekenhuis Gasthuisberg, Leuven, Belgium*

[4]*Algemeen Ziekenhuis Maria Middelares – St Jozef, Gent, Belgium*

[5]*Centre Hospitalier Namur, Namur, Belgium*

[6]*Cliniques Universitaires Saint Luc, Bruxelles, Belgium*

[7]*Onze Lieve Vrouwziekenhuis, Aalst, Belgium*

[8]*Centre Hospitalier Universitaire, Liège, Belgium*

[9]*Universitair Ziekenhuis, Gent, Belgium*

Accepted for publication in British Journal of Radiology, May 22, 2008

Abstract

For 318 patients in eight different Belgian hospitals the entire skin-dose distribution was mapped using a grid of 70 Thermoluminescence Dosemeters (TLDs) per patient, allowing an accurate determination of MSD. Dose-Area Product (DAP) values, exposure parameters, geometry, procedure-, patient- and cardiologist-characteristics were also registered. Procedures were divided into two groups: diagnostic procedures (Conorary Angiography CA) and therapeutic procedures (dilatation, stent, combined procedures (e.g. CA+dilatation+stent)). The mean value of MSD was 0.310 Gy for diagnostic and 0.699 Gy for therapeutic procedures. The most critical projection for receiving the MSD is the LAO90 (Left Anterior Oblique) geometry. In 3% of the cases MSD exceeded the 2 Gy dose threshold for deterministic effects. Action levels in terms of DAP values as the basis for a strategy for the follow-up of patients for deterministic radiation skin effects were derived from measured Maximum Skin Dose (MSD) and cumulative Dose-Area Product (DAP) values. Two DAP action levels are proposed. A first DAP action level of 125 Gy.cm^2 corresponding to the dose threshold of 2 Gy would imply an optional radiopathological follow-up depending on the cardiologist's decision. A second DAP action level of 250 Gy.cm^2 corresponding to the 3 Gy skin dose would imply a systematic follow-up.
Dose Reference Levels (DRLs): 71.3 Gy.cm^2 for diagnostic and 106.0 Gy.cm^2 for therapeutic procedures were derived from the 75 percentile of the DAP-distributions.
As a conclusion, we propose that total DAP is registered in patient's record file as it can serve to improve the follow-up of patients for radiation induced skin injuries.

Introduction

The extensive exposure to X-rays during fluoroscopy guided procedures often involves high radiation doses to patient's skin. Several observed radiation induced skin injuries have been reported in the nineties [1, 2] . By late 1994, the Food and Drug Administration (FDA) called attention to this problem with an advisory that later appeared on its website [3]. The review paper of Koenig *et al.* describes more than 70 skin injuries [4]. These injuries varied from erythema, moist desquamation, and ulceration to necrosis. The overview of the reported cases shows that the vast majority of the overexposures took place in the catheterization room during coronary angiography and interventions [5]. This is not unexpected as the number of cardiac interventions annually performed exceeds the other interventional radiological procedures by an order of magnitude [5].

Several recommendations for physicians working extensively with X-rays in interventional cardiology have been published in order to reduce patient doses and to avoid radiation induced injuries [6, 7]. However, due to complexity of procedures, still radiation induced skin injuries in patients occur, even with contemporary state of the art dose-reducing X-ray systems and appropriate training of physicians.

As stated by the ICRP (International Commission on Radiological Protection), the risk of skin injuries has to be estimated in the individual patient in order to provide adequate follow-up and treatment of these

injuries [8]. Dose thresholds of 2 Gy (onset of transient erythema) and 3 Gy for maximum skin dose or even as low as 1 Gy have been proposed [8]. Therefore procedures to estimate and monitor patient skin dose in daily practice have to be worked out.

Several studies report skin doses in interventional cardiology mostly measured using film or using only a very limited number of TLDs [9-11]. However due to the complexity of the irradiation geometries involving often two X-ray tubes in a C-arm type setting at different angles, it is not clear in advance which location on patient's skin is going to be most critical. This implies that to measure the maximum received skin dose, the total skin dose distribution has to be mapped. Similar dose distributions were measured by Suzuki *et al.* [12] using colour-changing radiosensitive indicators, but for a restricted number of patients in only one catheterization room.

Dose-Area Product (DAP) action levels are defined as alarm levels indicating a situation in terms of skin exposure necessitating medical follow-up for possible radiation injuries. Whereas DAP action levels do not provide a guideline for optimisation of the dose versus medical benefit relation, Dose Reference Levels (DRLs) do. Initial national values can be derived from the 75th percentile of the overall DAP distribution of the patients undergoing a particular procedure. This method of calculation of DRLs is indicated when a low number of rooms is participating in the study [13]. A comparison of the local mean values with national proposed DRLs, gives an idea about the ranking of the current practice in a hospital, with respect to patient dose.

In present study, action levels derived from cumulative DAP values are proposed as indicator for skin dose. This was possible by the measurement of the entire skin dose distribution using a grid of Thermoluminescence Dosemeters (TLDs), ensuring the determination of the Maximum Skin Dose (MSD)-value. In addition, initial values for national Belgian DRLs of the diagnostic and therapeutic DAP distribution are also proposed.

Methods

Patients

The patient group comprised 318 adult patients (221 male, 97 female, age between 29 and 89 years) who underwent cardiac catheterization in 8 Belgian hospitals in a period of two years (July 2003 – July 2005). The hospitals were selected to be representative for the current Belgian situation. As well university hospitals as private hospitals, geographically chosen to

cover the Belgian territory and with contemporary x-ray equipment participated in present study. Demographic patient data are indicated in Table 1. In each hospital about 40 patients in one catheterization room were included in this study. The cardiac interventional procedures were divided into two groups. The first group comprises diagnostic coronary angiography possibly combined with Pulmonary Capillary Wedge Pressure measurements. The second group consists of therapeutic procedures: single or multiple percutaneous transluminal coronary angioplasty (PTCA) with or without single or multiple consecutive stenting, single or plural direct stenting and combined (diagnostic plus therapeutic) procedures. The procedures were performed by experienced cardiologists or medical doctors being in training for interventional cardiology, all using their own protocols. A total of 200 diagnostic and 118 therapeutic procedures were included in this study.

Table 1. Demographic patient data and measured and calculated radiation dose parameters for diagnostic and therapeutic procedures.

	Diagnostic procedures		*Therapeutic procedures*	
	Mean (range)	Median	Mean (range)	Median
Demographic patient data				
N° male (avg weight (kg))	130 (81)		91 (82)	
N° female (avg weight (kg))	70 (71)		27 (71)	
Age (years)	67 (29 - 86)		65 (31 - 89)	
BMI (kg/m^2)	27 (19 - 49)		28 (20 - 47)	
Measured and calculated radiation dose parameters				
MSD (Gy)	0.31 (0.03 – 2.62)	0.20	0.70 (0.06 – 4.50)	0.46
DAP (Gy.cm^2)	55.7 (2.71 - 265)	43.8	81.5 (10.3 - 404)	65.4
% contribution of fluoro to DAP	33 (8 - 90)		50 (9 – 91)	
% contribution of cine to DAP	67 (8 -90)		50 (9 - 91)	

Table 2. Details about the X-ray equipment used

Hos-pital	X-ray system	Mono/ biplane	Fluoroscopy (p/s) and Cinegraphy (f/s)	Image Field (cm)	Image Recep-tion	Manu-factu-ring date	Filtra-tion	Fluoroscopy (mmAl / mmCu)	Cineradiography (mmAl / mmCu)
1	Philips Integris BH 5000	bi	12.5 - 25	23, 17, 14	II	1999	fixed	(1.5 / 0 - 0.3 - 0.5)	(0 / 0)
2	Siemens Coroskop	mono	12.5 - 25	23, 17, 13	II	1998	variable	(0 / 0.2)	(0 / 0.2 - 0)
3	Phillips BH 3000	bi	12.5 - 25	23, 18, 14	II	1996	fixed	(1.5 / 0.1- 0.2 - 0.4)	(0 / 0)
4	Philips Allura FD	mono	12.5 - 25	25, 20, 15	FD	2004	variable	(1.5 / 0.1 - 0.4 - 0.9)	(0 / 0)
5	Siemens Axiom Artis	bi	15 - 30	25, 20, 16	FD	2004	variable	(0 / 0 - 0.1 - 0.2 - 0.3 - 0.6)	(0 / 0 - 0.1 - 0.2 - 0.3 - 0.6)
6	Philips Integris HM 3000	mono	12.5 - 25	23, 17, 14	II	1997	fixed	(1.5 / 0.1- 0.2 - 0.4)	(0 / 0)
7	Siemens Coroskop	mono	12.5 - 25	23, 17, 13	II	1996	variable	(0 / 0.2)	0 / 0.2 - 0)
8	Siemens Axiom Artis	mono	15 - 30	25, 20, 16	FD	2004	variable	(0 / 0 - 0.1 - 0.2 - 0.3 - 0.6)	0 / 0 - 0.1 - 0.2 - 0.3 - 0.6)

II, Image Intensifier; FD, flat detector

X-ray equipment and Dose-Area Product meter

The measurements were performed on different contemporary cardiac X-ray systems (Table 2). All tubes had an inherent filtration of 2.5 mm Al. Distinction was made between two types of filtration insertion for X-ray equipments. X-ray equipment was either provided with 'fixed filtration'-insertion or with 'variable filtration'-insertion. A system with variable filtration adapts filtration thickness and material (Al or Cu) according to patient's thickness, without the cardiologist's involvement. Fixed filtration refers to a manual filtration function of the X-ray equipment by which the cardiologist has to choose one filtration-setting out of a limited number of possible filtration settings. All possible filtration settings for the different hospitals in either fluoroscopy or cinegraphy mode for variable or fixed filtration systems are given in Table 2. Generally a combination of an Al filtration of a particular thickness and one or more Cu filters of different thickness are used.

All X-ray tubes operated in a pulsed mode and controlled tube voltage and anode current with automatic brightness control. All tubes were equipped with a PTW DAP meter integrated in the system. The DAP meters were calibrated in situ for different tube voltages, filtrations and modes (fluoroscopy or cinegraphy) with a 60cc ionisation chamber (Radcal,10X5-60, Dutoit medical) and 33x41-cm Kodak X-Omat V films (Eastman Kodak) for field size determination.

Acquisition of exposure and procedure parameters

Each irradiation geometry was determined by a set of two angles per tube, using the radiological convention for geometry setting: cranial and caudal rotations in the sagittal plane of the patient and left anterior oblique (LAO) and right anterior oblique (RAO) for rotations in the transverse plane of the patient.

For each projection used in the cardiovascular intervention, geometry, tube potential, filtration settings per mode, number of frames, source to image detector distance, image detector field size, number of frames per second, tube current, pulse duration, and mode (fluoroscopy or cinegraphy) were registered. Cumulative DAP and DAP rate as a function of time during the procedure were registered online (Figure 1) by the PTW DAP meter connected to a Diamentor M4 readout unit and a laptop. This allowed us to measure DAP contribution for each mode and projection.

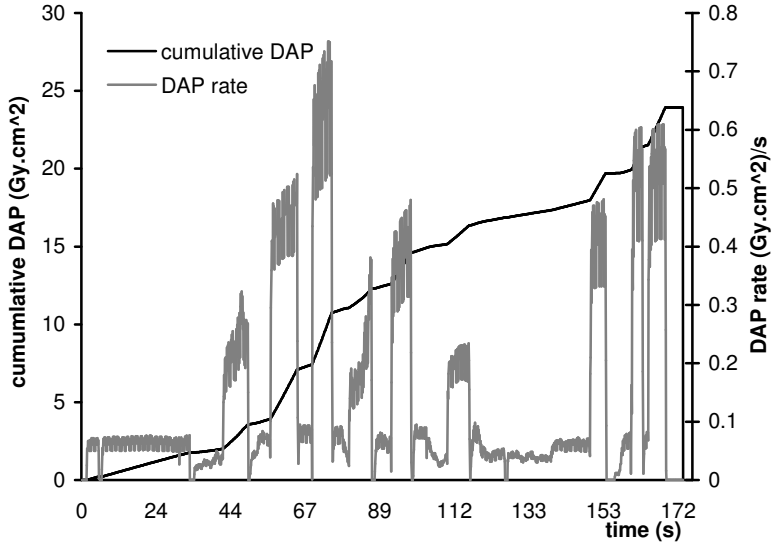

Figure 1. Typical output of DAP registration program: cumulated DAP (dark line) and DAP rate (light line) as function of time. This example shows nine cinegraphy-runs and fluoroscopy in between.

After each intervention the following information was recorded : complexity of the intervention (subjective score 1 to 3 according to 'easy', 'normal' and 'difficult') , amount of contrast used, cardiologist's experience (doctor or trainee) and standard protocol used for the intervention and patient's data (gender, age, weight, length and chest circumference). The three point scale for the complexity score was based on the duration of the procedures with respect to an equivalent procedure under normal circumstances, the number of lesions, the accessibility of the coronary arteries and the number of frames in one fixed position.

Skin Dose Measurements

A two-dimensional array of 70 TLDs (MTS-N type, Poland) covering the patient's chest was used, measuring the skin dose distributions of 318 patients in 8 cardiologic centres. In order to attach the TLDs to patient's skin, a 'wrap-around' was used, provided with a grid of 30cm by 97.5cm divided in squares of 7.5cm by 7.5cm. TLDs were wrapped in a plastic protection, labelled together with their positions, in order to be able to reconstruct the patient skin dose distribution. Patient's chest was covered completely with a wrap-around, with the middle centred at the spine and the upper end at the height corresponding to the sternum. All patients were asked to keep their arms upwards with their hands behind the neck during the procedure. The wrap-around with the TLDs did not affect image quality as their material (cotton for the wrap-around and LiF:Mg,Ti for the TLDs)

are not radio-opaque. Neither the wrap-around nor the individual TLDs were visible on the radiographic cardiovascular images.

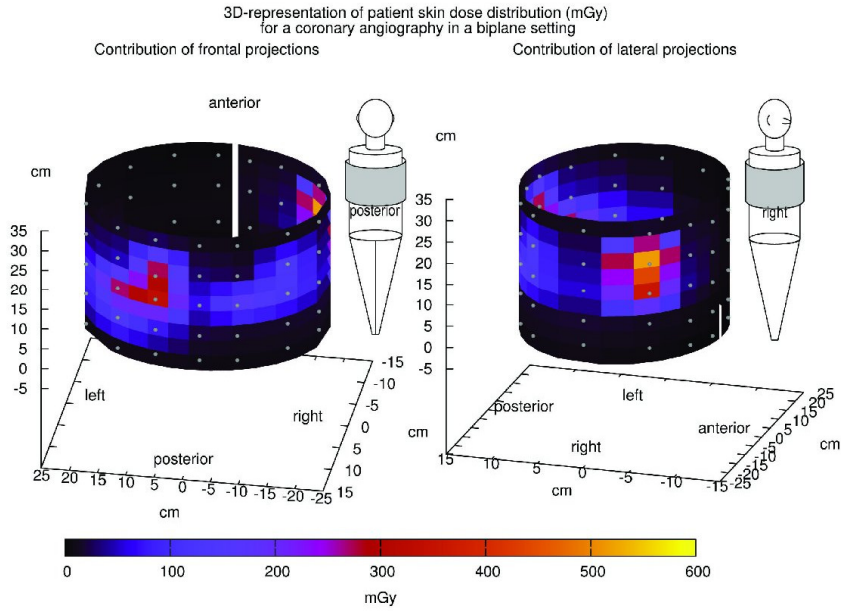

Figure 2. Three-dimensional representation of patient skin dose distribution (mGy) for a coronary angiography in a biplane setting. TLD positions are indicated. Left: viuw from the back of the patient. Right: view of the right side of the patient.

All TLDs were calibrated at the Standard Dosimetry Laboratory in Ghent (Belgium) at the beginning and at the end of the study at the same beam quality that was used in situ. Read-out was performed with a Harshaw 3500 reader (Thermo Electron Corp). For the study TLDs were selected with a calibration factor within 5 %. The maximum difference between the calibration factors at the beginning and the end of the study was less than 10%, the overall uncertainty on the measured MSD.

A graphical representation of the three-dimensional skin dose distribution was achieved by plotting TLD data on a mathematical cylindrical phantom representing the patient taking into account the circumference of the wrap-around around patient's chest as is shown in Figure 2. TLD positions are indicated.

DAP was calculated from the measured TLD skin dose and compared with measured DAP, multiplied by a factor that takes into account the backscatter

of the patient [14]. A very good correlation (r = 0.95) with a conversion factor of 1.03 was obtained which confirms the reliability of the DAP and TLD measurement sets.

Statistical analysis

As multiple factors may influence radiation dose measurements and calculations, a multifactor analysis of variance (ANOVA) was set up. Factors in the ANOVA design included the differences between hospitals, the difficulty of the procedure, system of beam filtration insertion and type of equipment (bi/monoplane, digital flat panel or conventional image intensifier). Levene's test was used to test the homogeneity of the variances between groups. A non-significant result of the Levene's test assured a correct application of the ANOVA analysis. Pillai's trace was used as a robust indicator of significance in the ANOVA analysis [15].

In cases where only two groups had to be compared, a non-parametric two-tailed Mann-Whitney test was performed. Correlations between groups were calculated by means of the non-parametric Spearman's rank correlation coefficient (r). To calculate the regression coefficients in the relation between two quantities, linear regression analysis was performed using the Levenberg-Marquardt algorithm. Fitting of data in figure 6 was performed by Weighted Least Squares method, using heteroscedasticity for determination of weighting factors. Fitting and p-values in figure 6 were calculated using 'the R-project' [16].

In all statistical calculations a confidence interval of 95% was applied. Hence, a p-value < 0.05 was considered as significant. All calculations were performed by means of the SPSS 12.0 software (SPSS, Chicago, Ill).

Results

Maximal Skin Dose

The results of the radiation dose measurements are summarized in Table 1. The mean value of MSD was 0.31 Gy and 0.70 Gy for diagnostic and therapeutic procedures respectively. The difference between these mean values was significant at a level of p= 0.001. The median values amounted to 0.20 Gy and 0.46 Gy for diagnostic and therapeutic procedures respectively. Figure 3 represents the histograms (interval of 0.25 Gy) of MSD values for

both diagnostic and therapeutic procedures with their mean values represented by a dotted line. A multifactor ANOVA analysis was performed to check whether other factors than the type of procedure (diagnostic or therapeutic) affect the MSD. Both flat panel equipment and the use of biplane configurations did not contribute to a significant lowering in MSD ($p=0.828$ and $p=0.626$ respectively). On the other hand, the lowest MSD values were found with systems equipped with variable filtration settings ($p=0.033$). The MSD depends also significantly on the difficulty level of the procedures ($p<0.001$). In the 3-point difficulty scale used in this study, level 2 and 3 resulted in significantly higher MSD values compared to first level procedures.

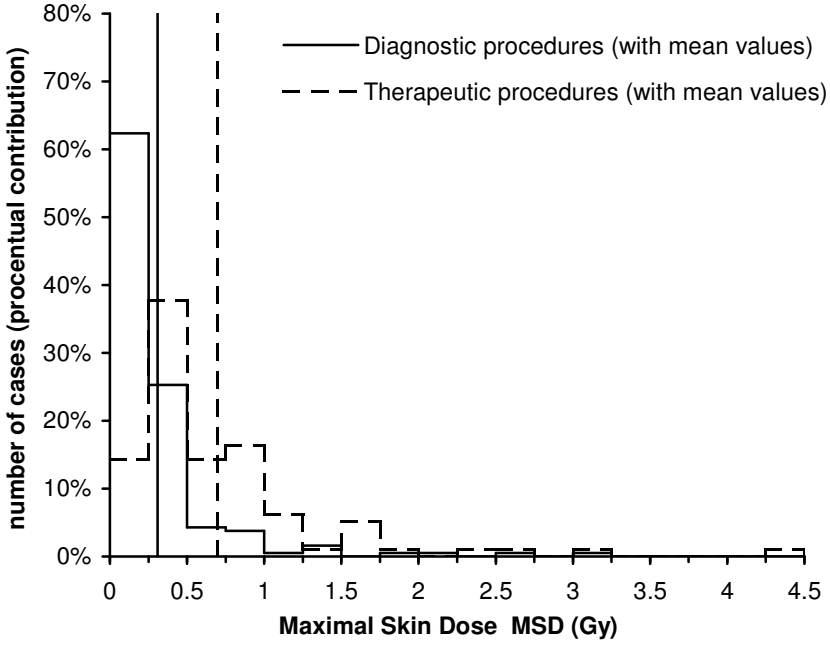

Figure 3. Histogram of maximal skin dose (Gy) for diagnostic (full line) and therapeutic (dashed line) procedures. Mean values are indicated by a vertical line.

ANOVA analysis could not reveal significant differences in MSD due to the hospital-factor ($p= 0.171$), partly due to the large variations in the dataset of the MSD. However, some clear trends were observed between hospitals. In some hospitals higher mean values could be explained by a continuous use of the fluoroscopy 'high' mode for fluoroscopy filtration setting. This mode uses least beam filtration during exposure. In other hospitals, the explanation for high doses could be found in the fact that in the period of the dose measurements, different medical doctors were trained in PTCA and stenting. Low mean values are related to 'good practice' in terms of the amount of radiation used on a monoplane system or by the local cardiology clinical practice, where a coronary angiography does not precede directly

the therapeutic intervention but is performed a few days earlier, and therefore, is not taken into account in the skin dose distribution.

The angle of the projections under which the MSD was received by the patient could be deduced from the TLD measurements. These angles, measured in a transverse plane through the patient are plotted as a histogram (interval 30 degrees) in Figure 4. The sagittal angulations of the X-ray beam were not taken into account in this figure. The most sensitive projection for receiving the MSD is the pure left lateral geometry of X-ray equipment (LAO90), in agreement with Kuon *et al.* [17]. For this projection, there is a closer positioning of the tube to patient's skin and an increase in exposure is induced by the larger patient size in the lateral dimension. The probability for the location of the MSD decreases steadily from lateral right to the centre of the back with a second prominent peak at the back left to the spine from the RAO30 projection. The angular distribution of the MSD indicates the necessity to use a large TLD set covering the whole chest for MSD determination in interventional cardiology.

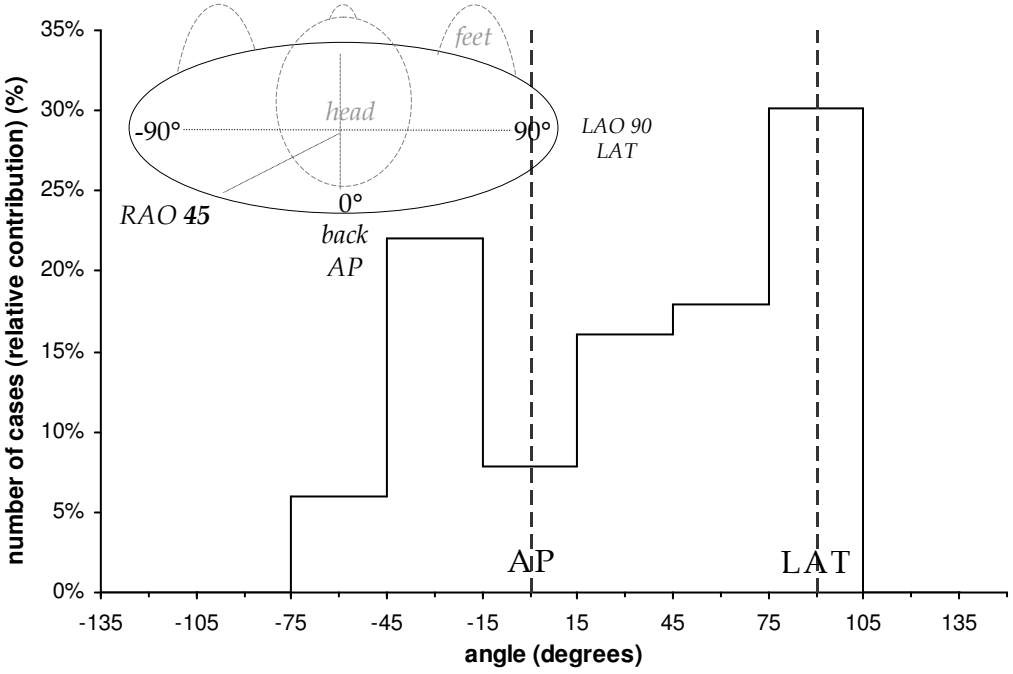

Figure 4. Distribution of the angles under which maximal skin dose was received by the patient. The coordinate system is centred at the centre of the mathematical cylindrical patient. 0 degrees means anterior-posterior projection and 90 degrees means left lateral projection.

For therapeutic procedures, the highest measured MSD was 4.50 Gy, whereas for diagnostic procedures this value was 2.62 Gy. 1% of the

diagnostic procedures (n=2) and 6 % of the therapeutic procedures (n=7) exceeded the threshold of 2 Gy for deterministic skin effects. An overview of these cases is given in Table 3. The therapeutic procedures were all 'combined procedures' which means that a diagnostic examination preceded a therapeutic intervention, except for case 2, where the procedure was a merely therapeutic intervention. In 3 out of the 9 cases a trainee was involved.

Table 3. Summary of the cases for which the maximum skin dose exceeded 2 Gy

N°	Proce-dure	MSD (Gy)	Angle MSD (°)	gender	Cardio-logist	DAP (Gy.cm²)	contribution of fluoro to MSD (%)	contribution of cine to MSD (%)
1	D	2.1	100	F	Tr.+Doc.	194	57	43
2	T	2.5	-44	M	Tr.	298	30	70
3	T	2.4	66	M	Doc	154	77	23
4	T	3.1	-47	M	Doc.	153	40	30
5	T	2.3	-15	M	Doc.	131	27	73
6	T	3.2	14	F	Tr.+Doc.	404	95	5
7	T	3.4	45	M	Doc.	315	98	2
8	T	4.5	95	M	Doc	257	89	11
9	D	2.6	94	F	Doc.	191	79	21

(D = Diagnostic, T = Therapeutic; Tr = Trainee, Doc. = Doctor-Cardiologist)

The contributions of fluoroscopy and cinegraphy in terms of percentage to the DAP that was registered for the geometry that caused the MSD exceeding 2 Gy, show that for 5 of the 9 cases a long fluoroscopy projection was obviously responsible for the highly measured peak in skin dose (contribution > 75 %). Investigation of these exposures in detail shows that the main explanation is the complexity level of the examinations necessitating automatically more X-rays for guidance of the catheter and imaging ($p<0.001$). All patients with skin peak doses of 2 Gy and higher belong to the high difficulty level. According to our study, important procedural aspects that lead to high skin doses are large patient weight, prolonged use of one and the same projection (both in cinegraphy as in fluoroscopy) and a relatively large distance between patient and image receptor, reducing the distance between X-ray source and patient in a C-arm setting.

Dose-Area Product

The mean value of DAP for diagnostic procedures was 55.7 Gy.cm^2 and differed significantly ($p<0.001$) from that for therapeutic procedures (81.5 Gy.cm^2). The corresponding 75th percentile values were 71.3 Gy.cm^2 and 106.6 Gy.cm^2 for diagnostic and therapeutic procedures respectively. Table 4 gives an overview of mean DAP values for the different hospitals considered in the study, for comparison with the proposed DRLs. DAP values differ significantly among the hospitals where the procedures were performed ($p<0.001$). Significant differences were also found between monoplane and biplane systems with lower values for monoplane systems ($p= 0.026$) (mean DAP values of 59.6 Gycm^2 versus mean DAP values of 74.6 Gycm^2). When a variable filtration setting was available, lower DAP numbers were recorded (mean DAP values of 49.2 Gycm^2 versus mean DAP values of 91.4 Gycm^2, $p<0.001$).

Table 4. Mean values for dose-area product values (Gycm^2)

	Diagnostic procedures	*Therapeutic procedures*
Hospital	**Mean DAP (Gycm^2)**	**Mean DAP (Gycm^2)**
1	76.9	120.3
2	31.2	57.0
3	74.2	90.8
4	50.6	75.8
5	46.2	78.0
6	83.1	137.7
7	18.6	41.5
8	54.9	70.0
DRL derived from this study	71.3	106.0

The installation of a digital flat panel detector generally resulted in lower DAP values, as compared to image intensifier systems (mean DAP values of 57.4 Gycm^2 versus 70.0 Gycm^2 respectively). However, this finding did not reach statistical significance ($p= 0.068$). Apart from the factors just mentioned the higher DAP values recorded in some hospitals are also due to cardiologists in training performing the procedures during the study, a continuous use of the fluoroscopy high contrast mode (least possible filtration).

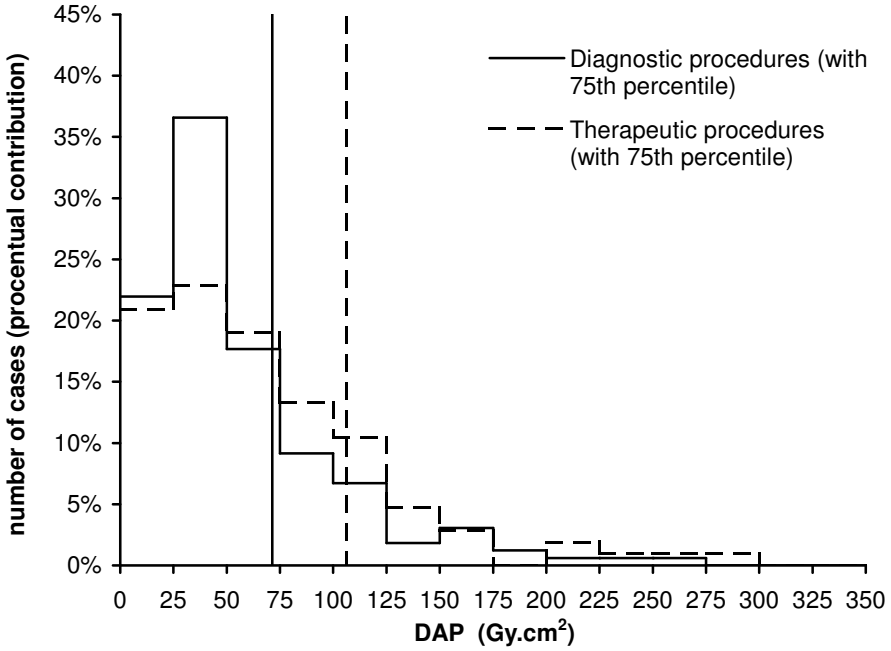

Figure 5. Histogram of Dose-Area Product (Gycm²) for diagnostic (full line) and therapeutic (dashed line) procedures. The third quartile is presented by a dashed line and represents Belgian Dose Reference Levels.

The mean contribution of fluoroscopy to DAP in diagnostic procedures was 33%, whereas this contribution was 50% in therapeutic procedures (p=0.002). In general, contributions of fluoroscopy and cine to the total DAP values varied significantly depending on the hospital (p=0.017). The level of procedure difficulty also had a significant influence (p<0.001) with an enhancement of the fluoroscopy contribution for difficult procedures. For diagnostic procedures, hospitals with biplane systems have a statistically significant (p=0.001) larger contribution of cinegraphy than hospitals with a monoplane system (p=0.001). This means that the possibility of acquiring two cinegraphy runs simultaneously at two different projections in a biplane system is not fully exploited but rather leads to an overuse due to the ease and speed of the technique. For therapeutic procedures, these trends are not so prominent.

Figure 5 represents the histograms (intervals of 25 Gycm²) of DAP values for diagnostic and therapeutic procedures. The distributions are strongly skewed and the 75th percentile values are indicated by vertical lines. In the scope of establishment of diagnostic reference levels (DRLs) these values can be proposed as initial national Belgian DRLs, taking into account the number of catheterization rooms that were considered.

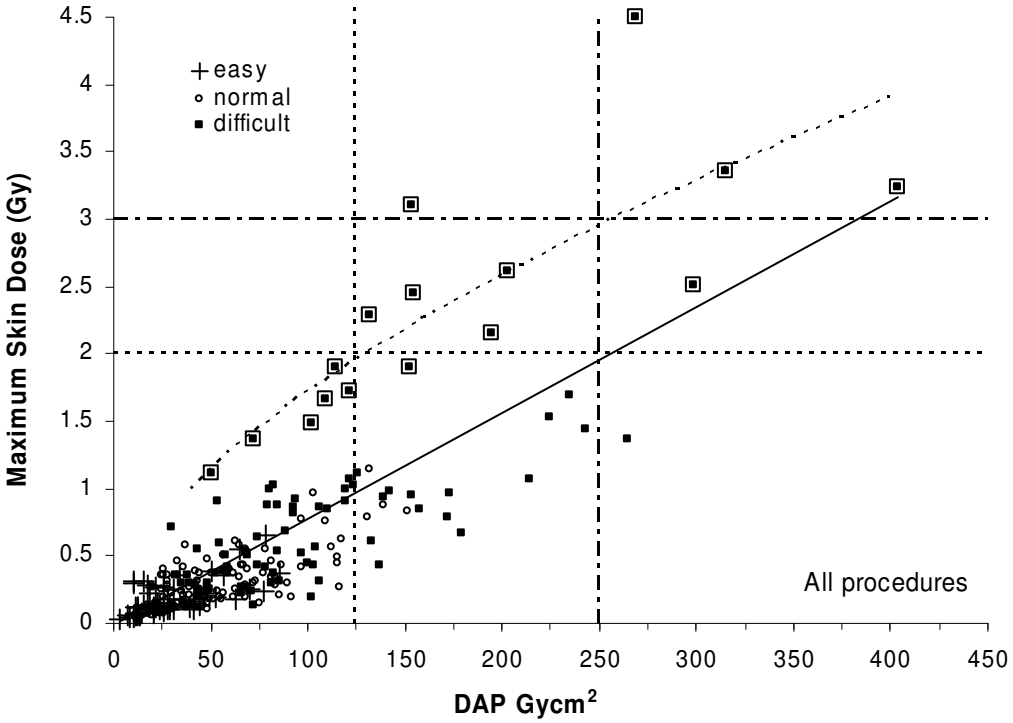

Figure 6. Maximal Skin Dose (Gy) versus Dose-Area Product (Gycm^2) for all procedures. DAP level of 125 Gycm^2 and 250 Gycm^2 are indicated corresponding to action levels for skin doses of respectively 2 Gy and 3 Gy. The different symbols refer to the complexity level of the procedure. Outlying points are squared.

Maximal Skin Dose versus Dose Area Product

The relation between cumulative DAP and MSD was investigated for both diagnostic and therapeutic interventions based on all hospital data. These data are presented graphically in Figure 6. Different symbols are used to highlight the impact of the difficulty of the procedures. The regression line for bulk data and a trend line for outlying points are indicated. For bulk data, a linear relationship was considered as first approximation and yielded a $p < 0.001$. The mathematical function (c.DAP d) chosen for the outlying points was based on their DAP dependence and to fulfil criteria of physical relevance (passing through origin and continuously increasing function). p-values for parameters c (0.113) and d (0.591) were 0.064 (p slightly > 0.05) and lower than 0.001. The fit served as guiding tool for derivation of DAP action levels. DAP values of 125 Gycm^2 and 250 Gycm^2 corresponding to 2 and 3 Gy MSD-levels can be deduced from these data.

Discussion

Maximal Skin Dose and Dose-Area Product

Results of present study for mean MSD, 0.31 Gy for diagnostic and 0.70 Gy for therapeutic procedures, confirm the high values for the MSD reported in papers published previously but now at a larger scale: 0.270 Gy [18, 19] for diagnostic procedures and 0.760 Gy [20] and 0.980 Gy [19] for therapeutic procedures. On the other hand, mean values for MSD as low as 0.113 Gy [21] and 0.217 Gy [22] for diagnostic procedures and 0.391 Gy [22] for therapeutic procedures have also been reported, but these were measured with only a limited number of TLDs, which explains the difference with the values of present work. In 9 patients, being 3% of all patients investigated, the dose threshold for deterministic effects to the skin, 2 Gy, was exceeded. This percentage can be considered to be representative for contemporary clinical practice in Belgium.

Mean and median values for cumulative DAP distributions over all patients undergoing diagnostic and therapeutic procedures, as reported in this study, are in the range of the data reported in the literature. A comparison with literature data can be found in table 5 ([18, 21, 23, 24]).

DAP action levels

Interpretation of figure 6 shows that cumulative DAP can serve as online monitor for the interventionist in terms of action levels for MSD. The trend line through the data points of outliers results in DAP action levels of 125 Gy.cm^2 and 250 Gy.cm^2 for 2 Gy and 3 Gy MSD levels respectively. The trend line is based on the behaviour of outlying MSD values, representing the highest skin doses obtained in present study. It serves as a guiding tool for derivation of DAP action levels. The function is not applicable as such for low DAP values, nor values in extend to the measured data. It does not represent a general relationship between MSD and DAP since it was only based on outlying points. According to the data set of present study the cumulative probability for MSD exceeding the 2 Gy level, amounts to 30% when the DAP exceeds the action level of 125 Gy.cm^2. Analogously, the cumulative probability for MSD exceeding the 3 Gy level is 60%, when the DAP exceeds 250 Gy.cm^2. As these DAP readings can be considered as DAP action levels for both diagnostic and therapeutic procedures, systematic registration of the DAP-value at the end of the procedure in patient's record is indicated.

In case DAP exceeds 125 Gy.cm², registration in patient's record of the entry site of the beam being responsible for the highest skin dose, according to the cardiologist on a body map (together with the DAP value) is indicated. The cardiologist can also decide that the patient has to be followed up for radiation skin effects based on the difficulty of the procedure and the total fluoroscopy time especially in single projection directions. This decision has to be based on a comparison with the local reference procedure.

Table 5. Mean and median Dose-Area Product (DAP) values for diagnostic and therapeutic procedures in interventional cardiology and literature data

Reference	procedure	Mean DAP (Gycm²)	Median DAP (Gycm²)	procedure	Mean DAP (Gycm²)	Median DAP (Gycm²)
Zorzetto *et al.* [17]	39 CA[a]	55.9	52.5	19 PTCA	91.8	82.6
Vaño *et al.* [20]	288 CA	66.5	45.7	45 PTCA	87.5	66.7
Padovani *et al.* [22]	76 CA-LV[b]	55.9		54 PTCA	101.9	
Karambatsakidou [23]	20 CA	49		40 PTCA	40	
Present work	200 CA	55.7	43.7	118 therap[c]	81.5	65.4

[a] CA = Coronary Angiography
[b] CA-LV = Left catheterism + Coronary Angiography + left ventriculography + 1-2 other acquisitions
[c] therap = therapeutic procedures as defined in present work.

At the 3 Gy action level (250 Gy.cm²), the patient and his personal physician should be informed on the possible radiation effects. Of course, in view of the higher probability of skin-overexposures in therapeutic interventions, this action level is indicated for therapeutic interventions. In our multicentre study four interventions (all were therapeutic) resulted in skin doses exceeding 3 Gy, being 1% of all procedures or 3% of the therapeutic interventions. In our study one patient with a DAP value of 153 Gy.cm² and a skin dose of 3.1 Gy can be considered as a false negative. The DAP action level resulting from our study, 250 Gy.cm², is somewhat lower than the level resulting from the European DIMOND III project, 300 Gy.cm² [25].

According to ICRP publication 85 [8], an additional level of 1 Gy for procedures, likely to be repeated should be considered. This is applicable to patients undergoing PTCA, since a significant number of them need a repeat PTCA or additional coronary procedures later on. According to us, a 1 Gy action level is not relevant as this is only half of the threshold dose and the skin site with the MSD can only be estimated by the cardiologist. A 1 Gy action level would be applicable to a larger fraction of the treated patients: in

our study 25% of the therapeutic procedures. Also, a difference in action level between diagnostic and therapeutic procedures, as stated by the ICRP, is not relevant as in some hospitals a diagnostic procedure precedes a therapeutic intervention a few days earlier.

Dose Reference Levels

At the end of the EC DIMOND II project in 1999 the following DRLs were proposed: 67 Gy.cm^2 for coronary angiography and 110 Gy.cm^2 for PTCA [26]. The 75th percentile data obtained in present study, 71.3 Gy.cm^2 and 106.0 Gy.cm^2 for respectively diagnostic and therapeutic procedures, as shown in Figure 5, support these DRLs. When applying these reference levels to the mean DAP values of the Belgian hospitals five of the cardiologic centres pass for diagnostic interventions and six for therapeutic interventions. However, the following EC project (DIMOND III, 2003) proposed new DRLs based on the 75th percentiles: 45 Gy.cm^2 for coronary angiography and 75 Gy.cm^2 for PTCA [25]. When applying these more stringent DRLs, only three of the Belgian cardiologic centres in our study would pass for diagnostic interventions and four for therapeutic interventions.

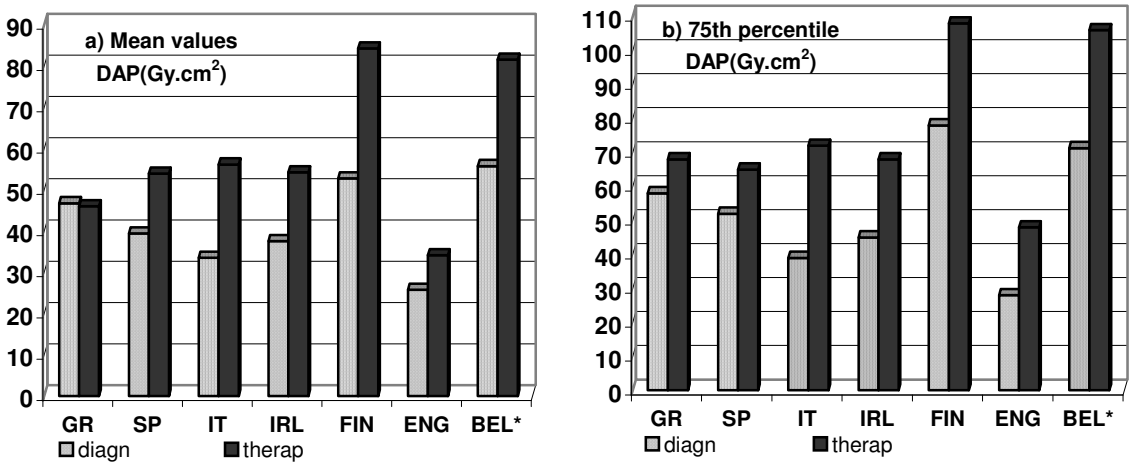

Figure 7. a) Comparison of the mean values for Dose-Area Product (Gycm^2) for diagnostic and therapeutic procedures for Belgium (* = this work) and other EU countries [25]. b) Comparison of the third quartile values for dose-area product (Gycm^2) for diagnostic and therapeutic procedures for Belgium (* = this work) and other EU countries [25].

In Figure 7 a and b, the mean and the 75th percentile values for the DAP for diagnostic and therapeutic cardiac interventions obtained in present work for Belgium are compared to the data reported by Neofotistou *et al.* [25] for

different European countries as a result of the European DIMOND III project. From this figure it is apparent that DAP values in Belgium are relatively high in comparison with DAP values obtained in other European countries as well for CA as for therapeutic interventions.

Training Programs and Quality Control

The lower reference values of DIMOND III compared to the previously proposed ones were explained by the continued education and training of personnel involved in interventional cardiology procedures and the increase of constancy checks of the X-ray systems. The skin dose distribution data obtained in present study support practical training programs dedicated to patient skin dose reduction in interventional cardiology. Besides the emphasis on dose reduction techniques (such as use of pulsed fluoroscopy at low frame rate, last image hold, beam collimation, variable filtration, use of 'store-fluoro' mode, use of the largest image intensifier field size and variable C-arm orientation), these programs should also focus on the relevance of DAP values as guideline in optimisation of procedure protocols in terms of radiation protection and in prediction of radiation induced skin injuries. Furthermore, an annual quality control of the X-ray equipment should be performed. The systematic registration of DAP for interventional procedures imposed by present Belgian legislation will allow a comparison of hospital DAP values with the DRLs proposed in this paper and lead towards optimization in terms of radiation exposure. The impact of training programs and quality control on patient dose will emerge from the follow up of the database of patient DAP values. This will allow an update of the DRLs, very probably lower than the values presented now and closer to the DRLs proposed in DIMOND III.

It must be kept in mind that DAP action levels and DRLs are not a dose constraint nor a dose limit. It is a kind of investigation tool to identify unusually high levels of radiation that call for investigation if substantially exceeded [27].

Conclusion

Cumulative DAP can serve as online monitor to provide the interventionist with an immediately readable dose display representative for the MSD. Therefore, systematic registration of this DAP at the end of the procedure in patient's record is necessary. In case DAP exceeds 125 Gy.cm^2

(corresponding to a MSD of 2 Gy), registration in patient's record of the entry site of the beam being responsible for the highest skin dose is indicated. A possible follow up of the patient for radiation skin effects is to the cardiologist's decision. In case DAP exceeds 250 Gy.cm^2 (corresponding to a MSD of 3 Gy) the patient and his personal physician should be informed on the possible radiation effects. A systematic follow-up should be performed.

In present study, 71.3 Gy.cm^2 and 106.0 Gy.cm^2 are proposed as national DRLs for diagnostic and therapeutic procedures respectively in Belgium. Local mean values should be compared to these values in view of optimisation in terms of patient dose.

Present study supports practical training programs in interventional cardiology. Beside the emphasis on dose reduction techniques (such as use of pulsed fluoroscopy at low frame rate, last image hold, beam collimation, variable filtration, use of 'store-fluoro' mode, use of the largest image intensifier field size and variable C-arm orientation), these programs should also focus on the relevance of DAP as guideline in optimisation of procedure protocols with respect to radiation protection and in prediction of radiation induced skin injuries.

Acknowledgment

The Federal Agency for Nuclear Control is acknowledged for the financial support and the follow up of the project.

The authors wish to thank the nurses, the technical personnel and the medical staff of the catheterization departments of all hospitals involved in this study for their participation and help with patient skin dose measurements.
N. Reynaert of the Standard Dosimetry Laboratory in Ghent is acknowledged for the practical help with TLD calibration.
Special thanks are expressed to V. de Gelder, A. De Hauwere, J. Lauwaert, B. Vanderstraeten for their help, their practical support in the measurements and in data analysis.

References

1. Shope TB. Radiation-induced skin injuries from fluoroscopy. Radiographics 1996;16(5):1195-1199.
2. Wagner LK, Eifel PJ, Geise RA. Potential biological effects following high X-ray dose interventional procedures. J. Vasc. Interv. Radiol. 1994;5(1):71-84.
3. FDA Public Health Advisory: Avoidance of serious X-ray-induced skin injuries to patients during fluoroscopically-guided procedures. . http://www.fda.gov/cdrh/fluor.html 1994.
4. Koenig TR, Wolff D, Mettler FA, Wagner LK. Skin injuries from fluoroscopically guided procedures: part I, Characteristics of radiation injury. Am. J. Roentgenol. 2001;177(1):3-11.
5. Koenig TR, Mettler FA, Wagner LK. Skin injuries from fluoroscopically guided procedures: part 2, Review of 73 cases and recommendations for minimizing dose delivered to patient. Am. J. Roentgenol. 2001;177(1):13-20.
6. Kuon E, Glaser C, Dahm JB. Effective techniques for reduction of radiation dosage to patients undergoing invasive cardiac procedures. Br. J. Radiol. 2003;76(906):406-413.
7. Hirshfeld JW, Balter SD, Brinker JA, Kern MJ, Klein LW, Lindsay BD, *et al.* ACCF/AHA/HRS/SCAI clinical competence statement on physician knowledge to optimize patient safety and image quality in fluoroscopically guided invasive cardiovascular procedures - A report of the American College of Cardiology Foundation/American Heart Association/American College of Physicians Task Force on Clinical Competence and Training. Circulation 2005;111(4):511-532.
8. ICRP. Recommendations of the International Commission on Radiological Protection. Publication 85: Avoidance of radiation injuries from medical interventional procedures. Ann. ICRP, Oxford, UK: Pergamon Press 2000;30(2).
9. Vaño E, Gonzalez L, Ten JI, Fernandez JM, Guibelalde E, Macaya C. Skin dose and dose-area product values for interventional cardiology procedures. Br. J. Radiol. 2001;74(877):48-55.
10. Neofotistou V, Karoussou A, Lobotesi H, Hourdakis K. Patient dosimetry during interventional cardiology procedures. Radiat. Prot. Dosim. 1998;80(1-3):151-154.
11. Betsou S, Efstathopoulos EP, Katritsis D, Faulkner K, Panayiotakis G. Patient radiation doses during cardiac catheterization procedures. Br. J. Radiol. 1998;71(846):634-639.
12. Suzuki S, Furui S, Kohtake H, Yokoyama N, Kozuma K, Yamamoto Y, *et al.* Radiation exposure to patient's skin during percutaneous coronary intervention for various lesions, including chronic total occlusion. Circ. J. 2006;70(1):44-48.
13. Marshall NW, Chapple CL, Kotre CJ. Diagnostic reference levels in interventional radiology. Phys. Med. Biol. 2000;45(12):3833-3846.
14. Grosswendt B. Conversion coefficients for calibrating individual photon dosimeters in terms of dose equivalents defined in an ICRU tissue cube and PMMA slabs. Radiat. Prot. Dosim. 1990;32(4):219-231.
15. Olson CL. Comparative robustness of 6 tests in multivariate-analysis of variance. J. Am. Stat. Assoc. 1974;69(348):894-908.
16. R Development Core Team. R: A language and environment for statistical computing. R Foundation for Statistical Computing, Vienna, Austria. ISBN 3-900051-07-0, URL http://www.R-project.org. 2008.

17. Kuon E, Dahm JB, Empen K, Robinson DM, Reuter G, Wucherer M. Identification of less-irradiating tube angulations in invasive cardiology. J. Am. Coll. Cardiol. 2004;44(7):1420-1428.

18. Zorzetto M, Bernardi G, Morocutti G, Fontanelli A. Radiation exposure to patients and operators during diagnostic catheterization and coronary angioplasty. Catheter. Cardiovasc. Diagn. 1997;40(4):348-351.

19. Hansson B, Karambatsakidou A. Relationships between entrance skin dose, effective dose and dose area product for patients in diagnostic and interventional cardiac procedures. Radiat. Prot. Dosim. 2000;90(1-2):141-144.

20. van de Putte S, Verhaegen F, Taeymans Y, Thierens H. Correlation of patient skin doses in cardiac interventional radiology with dose-area product. Br. J. Radiol. 2000;73(869):504-513.

21. Vaño E, Gonzalez L, Fernandez JM, Guibelalde E. Patient dose values in interventional radiology. Br. J. Radiol. 1995;68(815):1215-1220.

22. Vaño E, Goicolea J, Galvan C, Gonzalez L, Meiggs L, Ten JI, *et al.* Skin radiation injuries in patients following repeated coronary angioplasty procedures. Br. J. Radiol. 2001;74(887):1023-1031.

23. Padovani R, Novario R, Bernardi G. Optimisation in coronary angiography and percutaneous transluminal coronary angioplasty. Radiat. Prot. Dosim. 1998;80(1-3):303-306.

24. Karambatsakidou A, Tornvall P, Saleh N, Chouliaras T, Lofberg P, Fransson A. Skin dose alarm levels in cardiac angiography procedures: is a single DAP value sufficient? Br. J. Radiol. 2005;78(933):803-809.

25. Neofotistou V, Vaño E, Padovani R, Kotre J, Dowling A, Toivonen M, *et al.* Preliminary reference levels in interventional cardiology. Eur. Radiol. 2003;13(10):2259-2263.

26. Lobotessi H, Karoussou A, Neofotistou V, Louisi A, Tsapaki V. Effective dose to a patient undergoing coronary angiography. Radiat. Prot. Dosim. 2001;94(1-2):173-176.

27. European Commission Council Directive of 30 June 1997 (97/43/Euratom) on Health Protection of Individuals against the Dangers of Ionising Radiation in relation to Medical Exposure. Official J Eur Commun 1997;180:22-27.

3.2 Part II

A large-scale multicentre study in Belgium of dose area product values and effective doses in interventional cardiology using contemporary X-ray equipment

E. Bogaert[1] – K. Bacher[1] – H. Thierens[1]

[1]*Department of Medical Physics and Radiation Protection, Ghent University, Proeftuinstraat 86, Gent B-9000, Belgium.*

Reprint from Radiation Protection Dosimetry 2008; 128: 312–323
Advanced Published August 6, 2007, doi:10.1093/rpd/ncm379

Abstract

In this paper, a large-scale multicentre patient dose study performed in eight Belgian interventional cardiology departments is presented. Effective dose (E) was calculated based on a detailed dose–area product (DAP)-registration during each procedure and by using conversion coefficients generated by the Monte Carlo-based computer program PCXMC. Conversion coefficients were found to be 0.177 mSv $Gy^{-1}cm^{-2}$ for systems that do not use any additional copper filtration in cineradiography and 0.207 mSv $Gy^{-1}cm^{-2}$ for systems that use additional copper filtration in cineradiography. Mean E values of 9.6 and 15.3 mSv for diagnostic and therapeutic procedures, respectively, were obtained. DAP distributions were investigated in order to derive dose reference levels: 71 and 106 $Gycm^2$ for diagnostic and therapeutic procedures, respectively, are proposed. Significant differences were observed in DAP distributions taking into account whether additional copper filtration was used in the cineradiography mode. Apart from the skin, the organs most at risk are lungs and heart. The probability of fatal cancer for the studied population amounted to 1.1×10^{-4} and 2.1×10^{-4} for diagnostic and therapeutic procedures, respectively, for the age distribution of the patients considered in this multicentre study.

Introduction

Effective dose (*E*), introduced by the International Commission on Radiological Protection (ICRP) in publication 60[(1)], represents the risk of late radiation-induced effects such as malignancies and genetic effects.

During cardiac procedures in the catheterization laboratory carried out under fluoroscopic control, such as coronary angiography (CA) and percutaneous transluminal coronary angioplasty (PTCA), the radiation doses received by the patient can be high[(2-5)]. The hazards associated by the use of X-rays must therefore be justified by the procedure's benefits. Adaptation of the clinical protocols and knowledge of *E* or other dose

related quantities such as dose-area product (DAP) of a procedure can lead to optimisation of patient safety and image quality in fluoroscopically guided invasive cardiovascular procedures[6].

In order to determine *E* for a certain X-ray examination, knowledge of specific organ doses is essential. Unfortunately, specific organ doses cannot be measured directly during the procedure. Therefore Monte Carlo-based computer simulation codes are available, providing organ doses as a function of DAP or entrance surface dose (ESD) for certain irradiation geometries, X-ray spectra and clinical examination parameters. Thus, the problem of determination of organ doses in order to find effective dose has shifted towards the calculation of accurate DAP to *E* conversion factors.

The National Radiological Protection Board (NRPB) has published conversion factors for E, referring to both DAP and ESD measurements for 68 common radiographic projections and 9 complete X-ray examinations[7]. Tapiovaara *et al.*[8], of the Finnish Centre for Radiation and Nuclear Safety (STUK), developed a Monte Carlo-based computer program PCXMC in order to define specific *E* conversion factors in freely adjustable X-ray projections and other examination conditions used in projection radiography and fluoroscopy.

For a number of types of interventional procedures, used in cardiology, conversion coefficients can be found in literature. Reported values are mainly restricted to a total conversion coefficient for *E* owing to a complete procedure. For instance, for PTCA values of 0.18[9] and 0.27 mSv $Gy^{-1}cm^{-2}$ [10] were reported for conversion of DAP to *E*.

This study was undertaken in catheterization rooms in eight different Belgian hospitals, covering 318 patients of which 200 underwent a diagnostic procedure and 118 underwent a therapeutic procedure. Equivalent organ doses and effective dose were calculated based on DAP values recorded during the whole procedure. The goal of this study was to determine DAP/E conversion coefficients using the Monte Carlo code PCXMC, and the information gathered in the catheterization rooms. Dependency of conversion factors of additional copper (Cu) filtration used in cineradiography was examined. DAP distributions were interpreted in terms of dose reference levels (DRLs) and mean values of each hospital specific distribution were compared with the proposed DRLs.

Materials and Methods

Population and interventional procedures

E was calculated for a total number of 318 patients (221 male, 97 female, age between 29 and 89) who underwent cardiac catheterization over a period of 2 y (July 2003 – July 2005) in eight hospitals in Belgium, selected to be representative for the whole territory. Mean BMI was found to be 27.5 kg m^{-2}, ranging from 19 to 49 kg m^{-2}. In each hospital about 40 patients in one catheterization room were included in this study. Patients were asked to keep their arms behind their neck during the procedure.

The cardiac interventional procedures were divided into two groups. The first group comprises diagnostic CA possibly combined with Pulmonary Capillary Wedge Pressure measurements. The second group consists of therapeutic procedures: single or multiple PTCA with or without single or multiple consecutive stenting, single or plural direct stenting and combined (diagnostic plus therapeutic) procedures. The procedures were performed by experienced cardiologists or medical doctors being in training for interventional cardiology. A total of 200 diagnostic and 118 therapeutic procedures were included in this study.

X-ray equipment and DAP-meters

The measurements were performed on different contemporary cardiac X-ray systems. Table 1 gives detailed information about the systems and describes the possible filtration combinations used in fluoroscopy and cineradiography mode.

Most frequently a combination of an aluminium (Al) filtration of a particular thickness and one or more Cu filters of different thickness are used in addition to an inherent filtration of 2.5 mm Al. If we look into detail at the filtration for the two modes, we see, as indicated in Table 1, that systems 2, 5, 7 and 8 have additional Cu filtration available for cineradiography mode and that for systems 1, 3, 4 and 6 this is not the case. For the fluoroscopy mode, all systems have the possibility to use extra Cu filtration. All X-ray tubes operated in a pulsed mode and controlled tube voltage and anode current with automatic brightness control.

As calculation of *E* was based on the DAP values of the different projections used in the procedure, all X-ray tubes are equipped with a DAP meter. These DAP meters (PTW, Freiburg), were all integrated in the system and

were calibrated *in situ* for different tube voltages, filtrations and modes (fluoroscopy or cineradiography) with a 60cc ionisation chamber (Radcal,10X5-60, Dutoit medical) and 33x41-cm Kodak X-Omat V films (Eastman Kodak) for field size determination.

Image quality was checked for all systems, at normal clinical conditions using a Leeds FG18 phantom to comply with the minimum criteria, defined in Radiation Protection 91 report of the European Commission (RP91)[11]. According to this report, the contrast threshold under automatic brightness control should be ≤ 4%. With respect to resolution, the requirements to be met for field sizes of 23 – 25 cm are 1.0 lp mm^{-1} and 1.4 lp mm^{-1} for field sizes of 15 – 18 cm.

Acquisition of data and exposure parameters

Each projection used in a clinical protocol, can be characterised by a set of two angles per tube, using the radiological convention for geometry setting: cranial and caudal rotations in the sagittal plane of the patient and left anterior oblique (LAO) and right anterior oblique (RAO) for rotations in the transverse plane of the patient. For each projection used in the cardiovascular intervention, geometry, tube potential, filtration settings per mode, source to image detector distance, image detector field size, number of frames per second and the mode (fluoroscopy or cineradiography) were registered. Cumulative DAP and DAP rate as a function of time during the procedure were registered online by the PTW DAP meter connected to a Diamentor M4 readout unit and a laptop. An in-house written software made the measuremenof the DAP contribution for each mode and projection possible, based on the large difference in DAP rate ($cGycm^2\ s^{-1}$)[12]. After each intervention, the following information was also recorded: complexity of the intervention (score 1 to 3), cardiologist's experience (doctor or trainee) and patient's data (gender, age, weight and length).

Calculation of equivalent organ doses and effective dose

Using the recorded data, equivalent organ doses and *E* were calculated. Values for *E* were derived using two different methods for determination of conversion coefficients ($mSv\ Gy^{-1}cm^{-2}$), converting DAP into *E.* The first method used the Monte Carlo-based computer simulation program PCXMC, developed at the Medical Radiation Laboratory of the Finnish Radiation and Nuclear Safety Authority[8]. The user defines, via a graphical interface, beam

parameters such as focus to skin distance, rotation geometry in transverse and sagittal plane, skin entry point and field size at this position. According to the practical set-up of this study, the arms were left out of the hermaphrodite phantom of the program.

The second method used the tables of conversion factors, published by the NRPB[7]. These factors were derived for certain filtrations and irradiation geometries for radiological examinations of different organs. The calculation of the coefficients in the NRPB-report was based on the Monte Carlo technique as described by Jones and Wall[13]. Specific factors for examinations of the heart are listed for four specific irradiation geometries.

The calculation of *E* with PCXMC was practically performed taking into account a set of standard projections describing the irradiation geometry. These standard projections are adapted to the local clinical protocol used for diagnostic procedures and are specific for each hospital. For therapeutic procedures, the cardiologist selects a projection used in the diagnostic procedure where the lesion is most clearly visible. As a consequence, the standard projections used for diagnostic procedures can also be used to describe the geometry for therapeutic procedures. Practically, each standard projection can be characterized by two angles (θ and φ). Each projection in the cardiac intervention of a patient was decoded in the same way by θ′ and φ′ . A study of the differences between θ and θ′ and between φ and φ′ allowed to determine the standard projection closest to each patients projection. The data on the geometry for the standard protocols of each hospital are summarized in Table 2. These standard projections include geometries for frontal and lateral tubes in case of biplane systems.

Contrary to cineradiography where the projections are fixed during imaging, fluoroscopy implies rotation of the tube resulting in multiple projections for guidance of the catheter. However, a very logical assumption about the irradiation geometry for fluoroscopy can be made taking into account the fact that fluoroscopy always precedes cineradiography in order to have the optimal view of the heart and the catheter during the following cineradiography run. Therefore, the different fluoroscopy projections were reduced to one covering projection chosen to be the same as that used in the following cineradiography run.

Table 1. Details about the X-ray equipment

Hos-pital	X-ray system	Mono/ biplane	Fluoroscopy (p/s) and Cineradiography (f/s)	Image Field (cm)	Image Recep-tion	Manufactu-ring date	Fluoroscopy (mmAl / mmCu)	Cineradiography (mmAl / mmCu)
1	Philips Integris BH 5000	bi	12.5 - 25	23, 17, 14	II	1999	(1.5 / 0 - 0.3 - 0.5)	(0 / 0)
2	Siemens Coroskop	mono	12.5 - 25	23, 17, 13	II	1998	(0 / 0.2)	(0 / 0.2 - 0)
3	Phillips BH 3000	bi	12.5 - 25	23, 18, 14	II	1996	(1.5 / 0.1- 0.2 - 0.4)	(0 / 0)
4	Philips Allura FD	mono	12.5 - 25	25, 20, 15	FD	2004	(1.5 / 0.1 - 0.4 - 0.9)	(0 / 0)
5	Siemens Axiom Artis	bi	15 - 30	25, 20, 16	FD	2004	(0 / 0 - 0.1 - 0.2 - 0.3 - 0.6)	(0 / 0 - 0.1 - 0.2 - 0.3 - 0.6)
6	Philips Integris HM 3000	mono	12.5 - 25	23, 17, 14	II	1997	(1.5 / 0.1- 0.2 - 0.4)	(0 / 0)
7	Siemens Coroskop	mono	12.5 - 25	23, 17, 13	II	1996	(0 / 0.2)	0 / 0.2 - 0)
8	Siemens Axiom Artis	mono	15 - 30	25, 20, 16	FD	2004	(0 / 0 - 0.1 - 0.2 - 0.3 - 0.6)	0 / 0 - 0.1 - 0.2 - 0.3 - 0.6)

II, Image Intensifier; FD, flat detector

Beside irradiation geometry represented in the standard projections, other parameters such as field size, filtration and tube voltage, specific for a hospital's equipment and/or clinical protocol have to be taken into account. The source to image receptor distance (SID) was kept systematically 98 cm for monoplane systems and 105 cm for biplane systems with a distance from patient's skin to image intensifier of 10 cm. For projections with an angle in the cranial direction that was larger than or equal to 40° the SID was increased with 5 cm and the distance from patients skin to image intensifier with 10 cm. It is necessary to simulate the real clinical situation for this kind of projections.

Table 2. Standard projections for each hospital

	Hospital 1 (bipl.)	Hospital 2 (monopl.)	Hospital 3 (bipl.)	Hospital 4 (monopl.)
1	LAO 10 CRAN 10	LAO 10 CRAN 10	RAO 0 CAUD 0	RAO 30 CAUD 0
2	RAO 30 CAUD 30	RAO 30 CAUD 0	RAO 30 CAUD 0	RAO 20 CAUD 20
3	RAO 30 CRAN 30	RAO 30 CRAN 20	RAO 30 CAUD 30	RAO 10 CRAN 40
4	RAO 0 CRAN 40	RAO 30 CAUD 20	RAO 20 CRAN 30	LAO 50 CRAN 20
5	RAO 45 CRAN 25	LAO 50 CRAN 10	RAO 15 CRAN 40	LAO 90 CAUD 0
6	RAO 30 CAUD 0	LAO 40 CRAN 30	RAO 0 CAUD 35	LAO 20 CRAN 20
7	LAO 90 CAUD 0	LAO 90 CAUD 0	RAO 30 CRAN 20	LAO 0 CRAN 0
8	LAO 50 CRAN 20	LAO 70 CAUD 20	LAO 90 CAUD 0	LAO 40 CAUD 0
9	LAO 50 CAUD 30	LAO 40 CAUD 30	LAO 60 CAUD 0	
10	LAO 90 CRAN 10	LAO 45 CAUD 0	LAO 50 CRAN 20	
11	LAO 45 CRAN 25	RAO 45 CAUD 0	LAO 50 CAUD 20	
12	LAO 45 CAUD 0		LAO 60 CRAN 20	
	Hospital 5 (bipl.)	Hospital 6 (monopl.)	Hospital 7 (monopl.)	Hospital 8 (monopl.)
1	RAO 30 CAUD 0	RAO 30 CAUD 30	RAO 30 CAUD 20	RAO 30 CAUD 0
2	RAO 30 CAUD 20	RAO 30 CAUD 0	RAO 30 CRAN 20	RAO 25 CAUD 25
3	RAO 30 CRAN 20	RAO 30 CRAN 30	RAO 5 CRAN 20	RAO 10 CRAN 40
4	RAO 0 CRAN 25	LAO 40 CRAN 30	RAO 5 CAUD 20	LAO 45 CRAN 25
5	RAO 0 CAUD 25	LAO 45 CAUD 0	LAO 40 CRAN 20	LAO 90 CAUD 0
6	RAO 0 CRAN 15	LAO 45 CAUD 30	LAO 40 CAUD 0	LAO 35 CAUD 15
7	RAO 45 CAUD 0	LAO 90 CAUD 0	LAO 40 CAUD 20	LAO 10 CRAN 30
8	LAO 50 CRAN 10	LAO 0 CAUD 30	RAO 30 CAUD 0	LAO 60 CAUD 0
9	LAO 90 CAUD 0	LAO 0 CAUD 0		
10	LAO 70 CAUD 20	LAO 30 CAUD 0		
11	LAO 45 CAUD 0			

monopl., monoplane system; bipl., biplane system.

Factors were calculated for the three different image receptor field sizes possible for each hospital (e.g. 23cm, 17cm and 13 cm) and the different filtrations used in each hospital were taken into account.

For a certain standard projection with appropriate geometry, field size and filtration, conversion factors were calculated using PCXMC for tube voltages between 50kV and 120 kV in steps of 10kV. This implied calculation of a total of 5328 conversion factors. For tube voltages in-between, interpolation of the conversion factors was applied.

Figure 1 gives an example of the kV dependence of the DAP to *E* conversion factors for a standard projection of hospital 1 characterised by LAO 10 CRAN 10 and a field size of 17 cm.

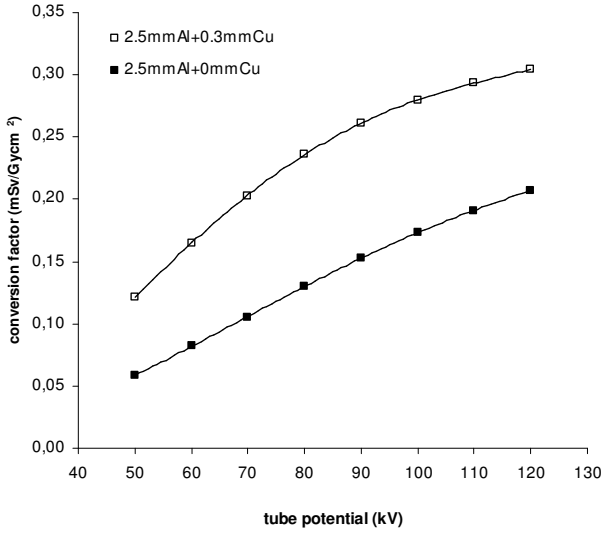

Figure 1. Conversion factor for effective dose from Dose-Area Product-values (mSv $Gy^{-1}cm^{-2}$) for field size of 17 cm and for projection LAO10 CRAN10 (hospital 1).

DAP values of the individual patients were used together with the conversion factors calculated for an adult hermaphrodite phantom with reference dimensions which is essentially based on the phantom of Cristy[14]. As the program only allows a scaling in height and weight of the phantom including its organs, without adding any additional layers of adipose tissue, this would lead to a simulation that is not realistic. As a consequence, the dimensions of the individual patients were not used as input in the program. Moreover, as a very large number of patients was considered in present study (318) the average dimensions of the patient group approached the reference dimensions. Therefore, no size correction[15] was applied.

Summarising, calculation of effective dose for each patient using PCXMC implies multiplication of the correct conversion factor defined by field size,

filtration, tube potential and geometry with the DAP contribution for each consecutive mode (fluoroscopy, cineradiography) in the procedure of that patient. This results in an effective dose contribution for each projection used in the cardiac intervention. Summing these effective dose contributions gives the effective dose for a specific patient.

Athough, for the procedure of dose calculation with PCXMC, a set of standard projections was derived from the clinical protocol for each hospital, only four standard projections are available in the NRPB-tables, implying a reduction of the number of conversion coefficients. The coefficients are given for spectra with peak potential ranging from 50 to 120 kV and total beam filtrations of 2 to 5 mm Al. Cu is not considered as filtration material in the tables. For the dose calculations based on the NRPB tables, each projection during a catheterization procedure of a patient was reduced to one of the four available standard projections. The same method for assessment of the fluoroscopy projection as explained for *E* calculation with PCXMC was applied here. Interpolation was performed for tube voltages when necessary.

Recent X-ray tubes for interventional cardiology are equipped with Al and Cu filtration, while the NRPB tables only consider Al filtration. In case of the procedures with Cu filtration the maximum value of Al filtration of the tables, 5 mm, is used. The standard focus-to-skin distance (FSD) applied in the NRPB-tables is 45 cm. Calculated from the SID, the FSD used for the PCXMC calculations ranged from 63 to 75 cm, taking into account projections with angulations larger than or equal to CRAN 40.

Equivalent organ doses were be calculated using PCXMC. The simulation resulted in conversion factors for DAP to equivalent dose (mSv $Gy^{-1}cm^{-2}$) for different organs together with the DAP to *E* conversion factors for the different standard projections, field-size, filtration and tube voltage as described above. Equivalent organ doses were considered for diagnostic and therapeutic procedures separately.

Effect of patient support table

The effect of the patient support table being in the beam at frontal projections had to be considered when calculating effective dose, both with the PCXMC program and NRPB-tables. Patient support table induces beam hardening but influences to a greater extend the photon fluence in the beam. Beam hardening implies an increase in effective dose contribution for frontal projections whereas a decrease of photon fluence implies a decrease in

effective dose contributions. Both effects will only partially compensate, resulting in a decrease in effective dose contribution for frontal projections. Beam hardening effect was simulated by PCXMC and the decrease in fluence, due to presence of patient support table, was measured. We found all patient support tables, except for the patient support table in hospital 7, to have an equivalent of 0.8 mm Al, which caused an increase of effective dose contribution for frontal projections of 11.5 %. The patient support table of hospital 7 had an equivalent of 0.5 mm Al, causing and increase of 7.4% in effective dose contribution for frontal projections. Decrease in photon fluence was measured to be 32.6 % for all hospitals except for hospital 7 where the decrease in photon fluence was 19.4%. The resulting factor for the decrease of effective dose contribution for projections with patient support table in the beam was 0.751 for all hospitals, except for hospital 7 where the factor was 0.866. For all frontal and inclined projections for which the patient support table was located in the beam, these factors were applied.

Statistical Analysis

Because multiple factors may influence radiation dose measurements and calculations, a multifactor analysis of variance (ANOVA) was set up. Factors in the ANOVA design included the differences between hospitals, the difficulty of the procedure, system of beam filtration insertion and type of equipment (bi/monoplane, digital flat panel or conventional image intensifier). Levene's test was used to test the homogeneity of the variances between groups. A non-significant result of the Levene's test assured a correct application of the ANOVA analysis. Pillai's trace was used as a robust indicator of significance in the ANOVA analysis[16].

In cases where only two groups had to be compared, a non-parametric two-tailed Mann-Whitney test was performed. Correlations between groups were calculated by means of the non-parametric Spearman's rank correlation coefficient (r). To calculate the regression coefficients in the relation between two quantities, linear regression analysis was performed using the Levenberg-Marquardt algorithm. The difference between regression lines was calculated using the general linear model.

In all statistical calculations, a confidence interval of 95% was applied. Hence, a p-value <0.05 was considered as significant. All calculations were performed by means of the SPSS 12.0 software (SPSS, Chicago, IL, USA).

Results

Mean values of DAP and *E* for diagnostic and therapeutic interventions in the different hospitals of present study are listed in Table 3 . Mean DAP values were found to be 56 and 82 Gycm² for diagnostic and therapeutic procedures, respectively. Overall distributions of diagnostic and therapeutic procedures resulted in DRL values (75 percentile) for DAP of 71 and 106 Gycm² respectively. Overall mean values for *E* are 9.6 mSv for diagnostic procedures and 15.3 mSv for therapeutic procedures.

Figures 2 and 3 represent the histograms of DAP values for diagnostic and therapeutic procedures respectively, taking together the hospitals that use additional Cu filtration in cineradiography mode in their cardiac X-ray equipment, and hospitals that do not. A striking reduction in the mean value, indicated by the vertical lines, is observed as well in diagnostic as in therapeutic procedures, when additional Cu filtration is used in cineradiography. A mean value of 38 Gycm² (60 Gycm²) was observed for systems that use additional Cu filtration in cineradiography mode and 71 Gycm² (108 Gycm²) for systems that did not have that option, for diagnostic (and therapeutic) procedures.

Figures 4 and 5 compare the mean values of the DAP distribution of each hospital (full line) with the proposed DRLs (dashed line) for diagnostic and therapeutic procedures, respectively (71 and 106 Gycm²). The histograms and the ANOVA statistical analysis performed, show that DAP depends significantly on the hospital ($p < 0.001$).

Table 3. Mean effective dose values calculated with the Monte Carlo simulation program PCXMC and dose-area-product values, both for diagnostic and therapeutic procedures.

	Diagnostic procedures		Therapeutic procedures	
	E (mSv)	DAP (Gycm²)	E (mSv)	DAP (Gycm²)
1	13.4	76.9	21.7	120.3
2	6.5	31.2	12.9	57.0
3	11.2	74.2	13.9	90.8
4	8.3	50.6	13.2	75.8
5	8.4	46.2	15.2	78.0
6	14.0	83.1	24.9	137.7
7	4.3	18.6	9.8	41.5
8	9.1	54.9	13.1	70.0

Figure 6 shows the correlation between total DAP values and calculated *E*. An excellent overall correlation between the effective dose and DAP was found, resulting in a conversion factor of 0.185 mSv $Gy^{-1}cm^{-2}$ (dashed line) [r = 0.966, p < 0.001, 95% confidence interval for the slope (0.182 - 0.188)]. When analysing diagnostic and therapeutic procedures separately, similar correlations and regression lines were found (slope 0.179 mSv $Gy^{-1}cm^{-2}$, r = 0.968, p < 0.001 and slope 0.190 mSv $Gy^{-1}cm^{-2}$, r = 0.974, p < 0.001 respectively). The difference in slope of the regression lines did not reach statistical significance (p = 0.723). However, a significantly lower conversion factor for the systems that do not have extra Cu filtration implemented in cineradiography was found compared to the systems that do have this option. The resulting conversion factor was 0.177 mSv $Gy^{-1}cm^{-2}$ (r = 0.976, p < 0.001) for systems that do not use any extra Cu filtration in cineradiography versus a conversion factor of 0.207 mSv $Gy^{-1}cm^{-2}$ (r = 0.979, p < 0.001) for other systems. The p-value for the distinction of the slope of both regression lines was smaller than 0.001.

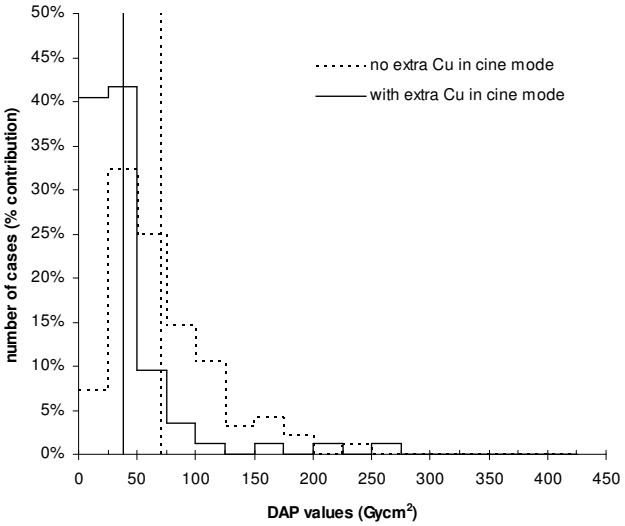

Figure 2. Comparison of histograms of dose-area product values for diagnostic procedures, taking into account the availability of additional copper filtration in cineradiography mode.

Relative contributions of fluoroscopy and cineradiography to *E* were calculated. Fluoroscopy contributions for both diagnostic and therapeutic procedures are represented in Figure 7. Mean values were 39% for diagnostic and 56% for therapeutic procedures. Of all hospitals, hospital 6 has a very large contribution of fluoroscopy to *E* for both types of

procedures. This is due to the continuous use of high fluoroscopy mode, with the lowest filtration in the X-ray beam in this hospital.

Besides the use of the Monte Carlo simulation program PCXMC, *E* was also calculated using the NRPB tables and the measured DAP values. *E* calculated based on the NRPB tables is, in general, 12% lower.

Equivalent doses for all organs defined in ICRP 60[1] are calculated with PCXMC. Organs that received the highest dose are listed in Table 4. As can be expected, the lungs and the heart are exposed to the highest level and receive mean equivalent doses in the range of 40 and 60 mSv for diagnostic and therapeutic procedures respectively. Doses for liver, breasts, pancreas and muscle were calculated to be below 15 mSv for both diagnostic and therapeutic procedures. Stomach, thyroid, kidneys, spleen and gall bladder received doses lower than 5 mSv while ovaries, testes, intestine, urinary bladder, brain and uterus receive a low dose level (< 0.5 mSv).

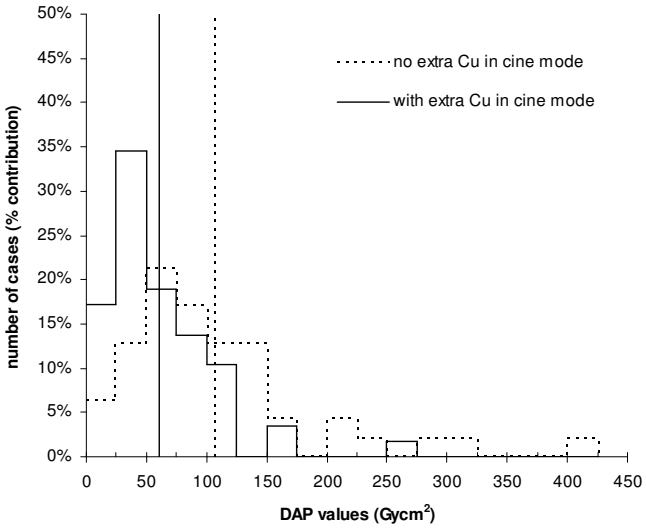

Figure 3. Comparison of histograms of dose-area product values for therapeutic procedures, taking into account the availability of additional Cu filtration in cineradiography mode.

Imaging performance tests were carried out for all X-ray systems and were checked to comply with RP91[11]. Concerning contrast visibility, all systems fulfilled the criteria (contrast threshold under automatic brightness control ≤ 4%). Average values for contrast threshold at normal operation mode are 2.4 % (10% variation in terms of percentage) for fluoroscopy and 1.5% (8% variation in terms of percentage) for cineradiography. This difference is statistically significant ($p < 0.001$). With respect to resolution, all systems except for two fulfilled the requirements of RP 91 (for field sizes of 23 – 25 cm resolution should be at least 1.0 lp mm^{-1} and for field sizes of 15 – 18 cm at least 1.4 lp mm^{-1}). The elder image intensifiers of hospitals 3 and 6 did not

comply with the criteria for magnification (smallest fields). Average values for resolution for fluoroscopy and cineradiography at normal operation mode are 2.00 lp mm^{-1} (18% variation in terms of percentage) and 2.16 lp mm^{-1} (18% variation in terms of percentage) respectively. This difference is not significant (p =0 .236).

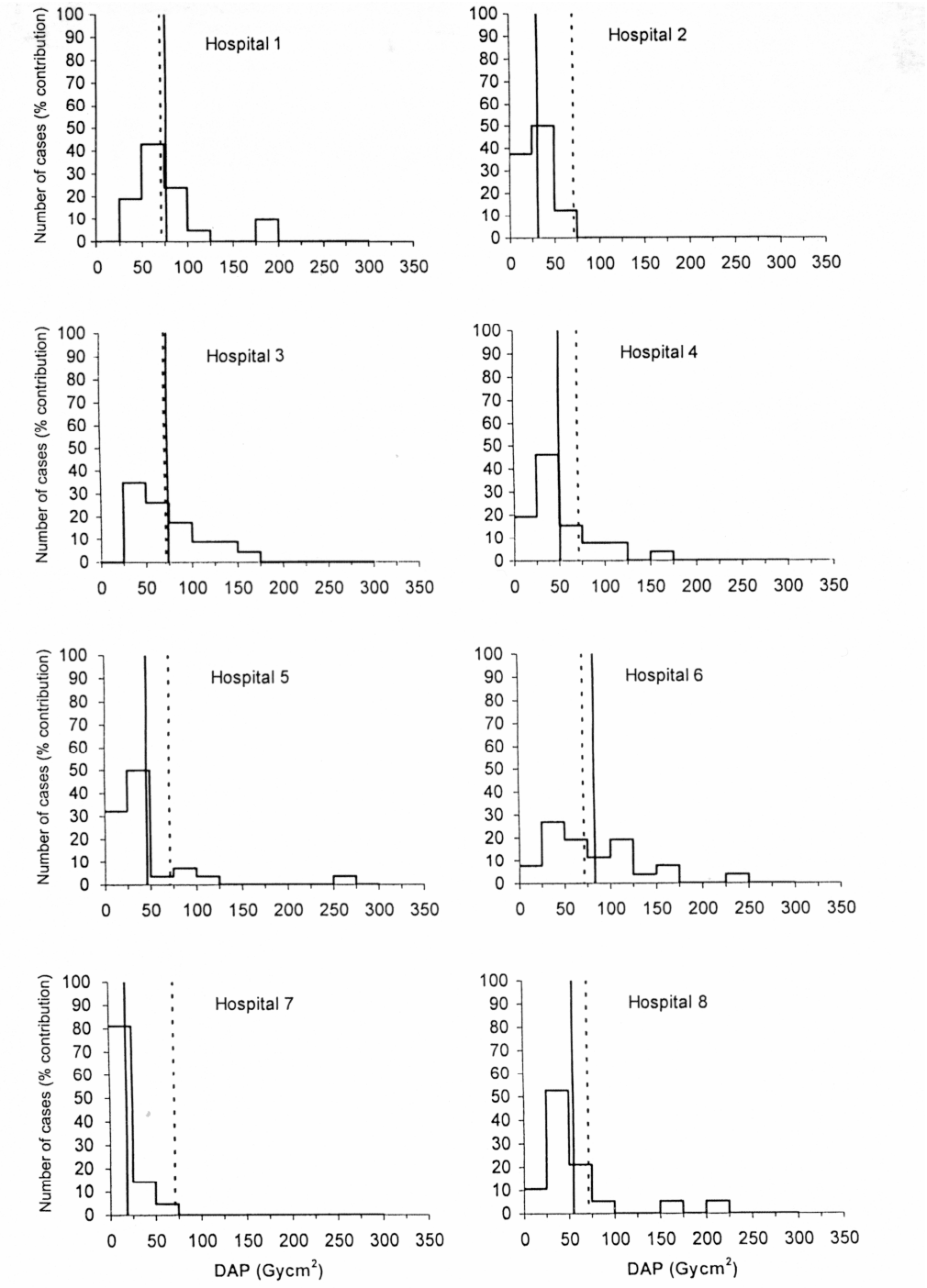

Figure 4. Comparison of histograms of DAP values for diagnostic procedures for the different hospitals. The general third quartile, is indicated by a dashed line. The local mean values and the local distribution are indicated by a full line.

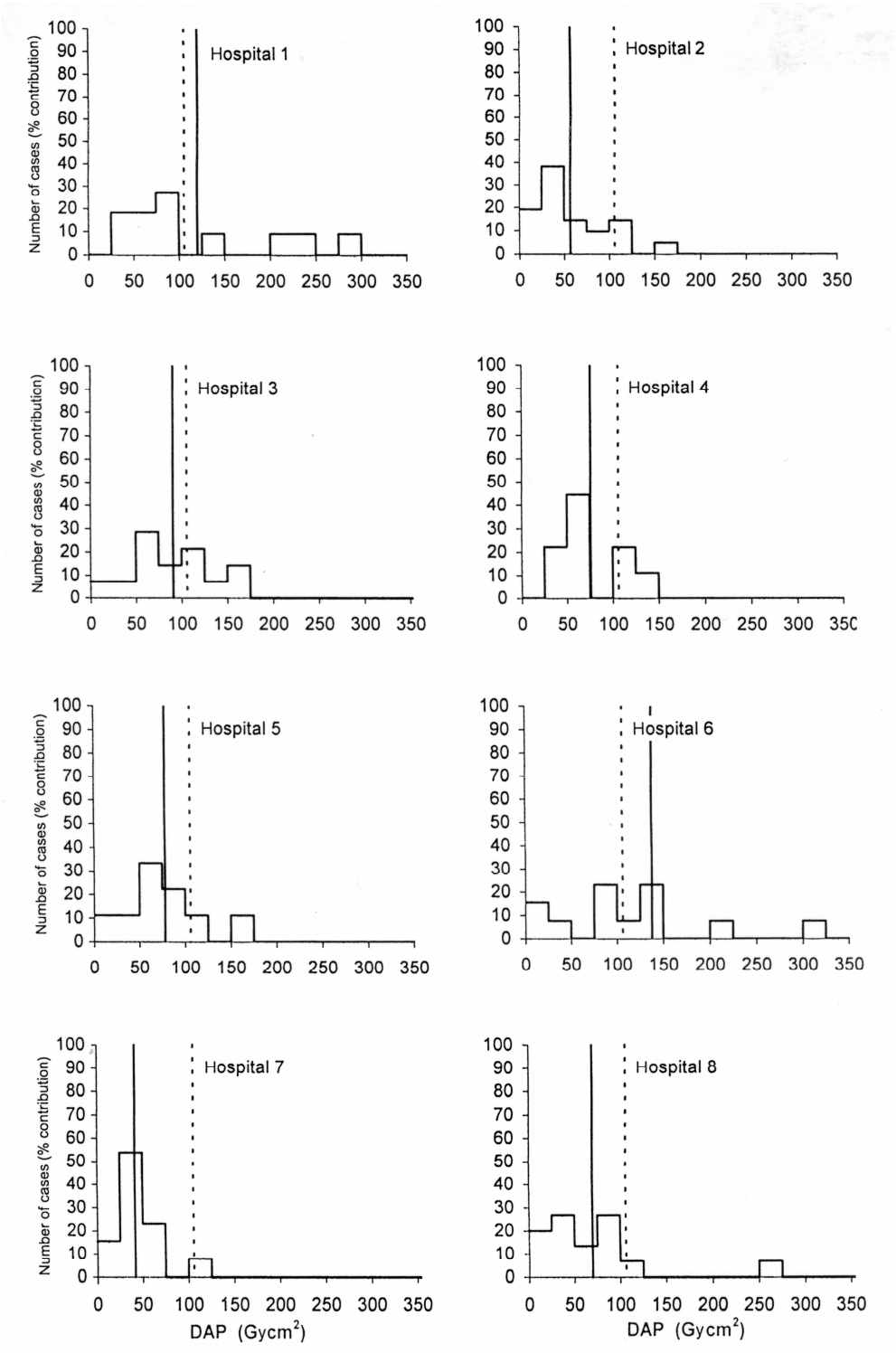

Figure 5. Comparison of histograms of DAP values for therapeutic procedures for the different hospitals. The general third quartile, is indicated by a dashed line. The local mean values and the local distribution are indicated by a full line.

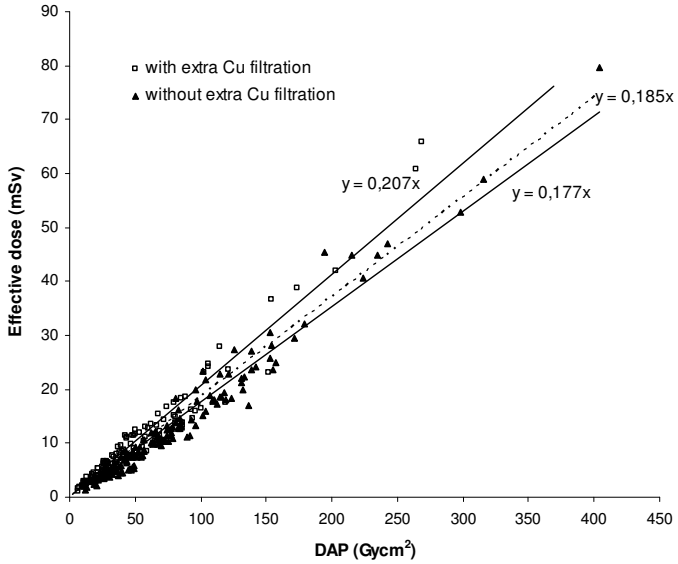

Figure 6. Correlation between DAP values (Gycm²) and effective dose (mSv) for the studied patient population. Distinction is made for the hospitals where additional copper filtration was available in cineradiography mode and for hospitals where this was not the case.

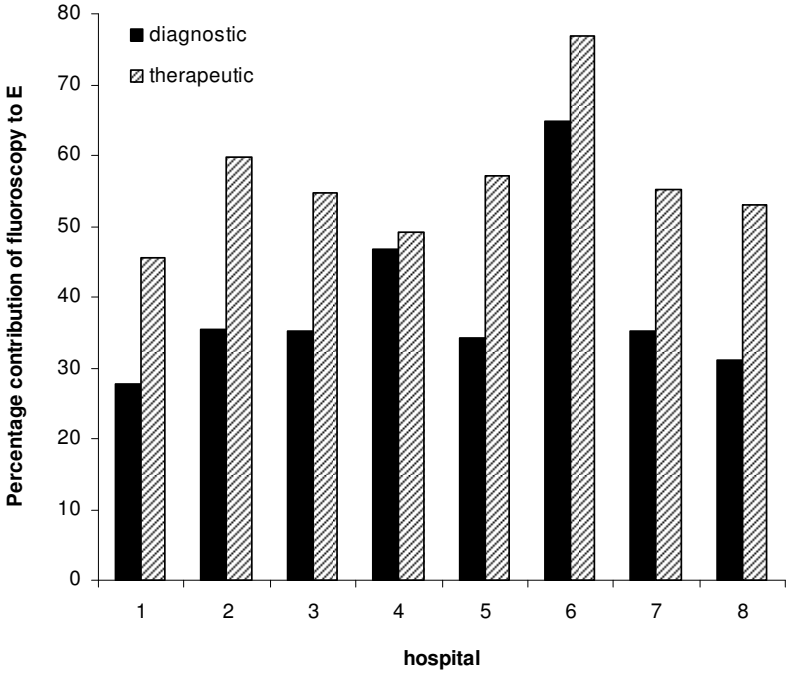

Figure 7. Contribution in terms of percentage to effective dose due to fluoroscopy for diagnostic and therapeutic procedures.

Table 4. Mean equivalent doses (mSv) for the organs mostly exposed during diagnostic and therapeutic procedures.

	Mean equivalent organ doses (mSv)	
	Diagnostic procedures	Therapeutic procedures
Active Bone marrow	9.7	16.8
Skeleton	18.1	29.5
Lungs	43.3	67.2
Oesophagus	25.5	48.1
Adrenals	13.0	16.2
Thymus	14.4	22.9
Heart	35.9	64.5

Discussion and Conclusion

In this study, detailed DAP registration made determination of overall DAP distributions possible. Third quartile values led to national DRLs for interventional cardiovascular diagnostic and therapeutic procedures. The proposed values are 71 and 106 Gycm^2 for diagnostic and therapeutic procedures respectively.

These correlate well with DRLs proposed in Refs. (17) and (18) as a result of the DIMOND II and the DIMOND III project: 67 and 57 Gycm^2, respectively for diagnostic procedures and 110 and 94 Gycm^2 respectively for therapeutic procedures. DRL values of 122, 84 and 67 Gycm^2 were derived by Aroua *et al.*[19] for cardiac catheterization, stent insertion and PTCA, respectively, in a national survey in Switzerland. They attribute the large difference with the literature in DRL for diagnostic procedures (CA) to the variability in techniques used, particularly in the case of complex examinations. The lower values found bij Aroua *et al.* for stent insertion and PTCA in comparison with the present work can be explained by the fact that 'therapeutic' procedures, as defined in this study, also contain combined procedures where a therapeutic intervention immediately follows a diagnostic examination.

Figures 2 and 3 show a significant difference in DAP distribution depending on the availability of additional Cu filtration. Lower DAP values can be attributed at least partly to higher filtration of the X-ray equipment in

cineradiography mode, and might be lowered even more by dose conscious action or training of the cardiologists. The data support that additional Cu filtration is a very helpful tool for dose reduction if correctly installed or upgraded and implemented in clinical practice. Dose saving tools such as additional Cu filtration can be implemented on an existing X-ray system to lower mean values of a local distribution in order to comply with established DRLs. Additional filtration will lower not only DAP values but also skin doses and *E*.

A good correlation was found between *E* and DAP, providing an overall conversion factor between these two quantities of 0.185 mSv $Gy^{-1}cm^{-2}$. Statistical significance was not observed for the difference in DAP/E conversion factors between diagnostic and therapeutic procedures.

Table 5. Comparison of the different conversion factors from dose-area product to effective dose (mSv/Gycm^2) for the different systems in the hospitals corresponding to whether extra copper filtration was available in cineradiography mode or not.

	Conversion factor (mSv $Gy^{-1}cm^{-2}$)
All systems	0.185
Systems with Cu[a]	0.207
Systems without extra Cu[b]	0.177

[a]Systems that use extra Cu filtration in cineradiography mode
[b]Systems that do not use any extra Cu filtration in cineradiography mode

However, distinction based on filtration used in cineradiography mode in terms of the availability of extra Cu material in the beam does make sense. A conversion factor of 0.207 mSv $Gy^{-1}cm^{-2}$ for systems that use extra Cu filtration in cineradiography was found, whereas the conversion factor amounts to 0.177 mSv $Gy^{-1}cm^{-2}$ for the other systems. The beam hardening as a consequence of the additional Cu filtration leads to a higher mean E-value for the same DAP value.

Although conversion factors were calculated for each hospital individually, taking into account the X-ray set up and the clinical protocol, as stated by Schultz and Zoetelief[20], geometry related factors did not result in significant differences in conversion factor. The standard projections derived from the clinical protocol and presented in Table 2 show that more geometries are used in biplane than in monoplane systems and that different hospitals

indeed use different projections. The lateral projection LAO 90 CAUD 0, for instance, is not included in the standard clinical protocol of hospital 7. Instead of influencing E, this fact affects mostly maximum skin dose, as highest values for this dose quantity can be found under this projection, as shown in a complementary study in the same 8 hospitals[21]. Considering the different standard projections of the hospitals, we see that only hospitals 3, 4 and 6 use the pure frontal (AP) projection (LAO 0 CAUD 0) to make a cineradiography run, whereas the other hospitals use this projection only during fluoroscopy at the beginning of the procedure for guidance of the catheter.

Effective doses were calculated for 318 cardiovascular procedures taking into account the X-ray set up and the clinical protocol in each participating hospital using the Monte Carlo Code PCXMC and also using conversion coefficients of the NRPB-tables. As a result of the PCXMC calculations, a mean value of 9.6 mSv was obtained for effective dose of diagnostic procedures but with individual outliers up to 60.7 mSv. The UNSCEAR 2000 report indicates as mean value for health care level I countries 7.3 mSv. With this effective dose, CA is among the medical applications of diagnostic X-rays with a high patient radiation burden. Computed tomography of the thorax and the abdomen induces similar doses of 9.7 mSv and 12.0 mSv respectively [22].

For patients undergoing therapeutic interventions the mean effective dose of our study was 15.3 mSv with outliers up to 79.8 mSv. For comparison, the mean effective dose for a PTCA intervention reported in the UNSCEAR 2000 report is 22 mSv. In the study of Neofotistou *et al*. [23] individual patient data range from 7.5 up to 57 mSv. Dose values of 5.6 mSv for diagnostic procedures and of 13.0 mSv for therapeutic procedures were reported by Betsou *et al*.[9].

Dose ranges of 4.6 – 15.8[23] and 2.7 – 8.8 mSv[24] for diagnostic procedures and of 5.4 – 41.0[23] and 5.7 – 15.3 mSv[24] for therapeutic procedures were reported before. Both dose values and dose ranges present slightly lower mean *E* values than observed in our study. It should be mentioned that Betsou *et al.*[9] based *E* determination on phantom (RANDO) measurements, that Neofotistou *et al.*[23] based their *E* determination on effective dose conversion factors published by NRPB and that only Stisova[19] based *E* determination on PCXMC calculations.

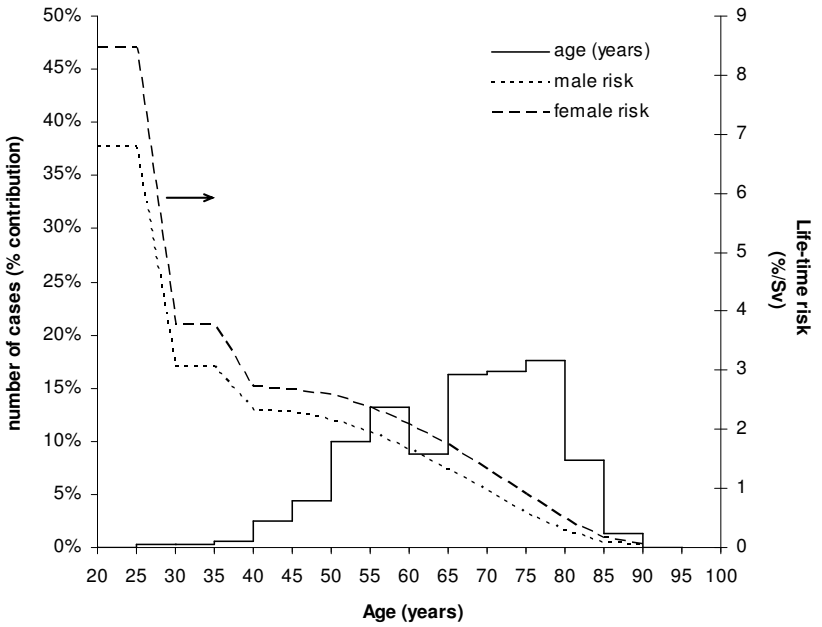

Figure 8. Age distribution of the patients included in this study and age dependency of the life-time risk for males and females in per cent per Sv[1].

In this study, Comparing the *E* determined using the NRPB tables with *E* calculated by means of PCXMC revealed a systematically lower value (12%). This can be explained by the fact that NRPB only provides conversion factors for beam filtration in millimeters of Al, which cannot always be applied in contemporary equipment for interventional cardiology. Cu filters are often inserted into the beam as skin-dose saving tool. A higher filtration implies beam-hardening and thus a higher *E* value to be expected.

When we look at the organs at risk, certainly the skin is the most important tissue. However, in contrast with maximal skin dose, mean skin doses are of no interest. The skin is only partially exposed and only hot spots of high doses can relatively easy pass the threshold for deterministic effects: 2 Gy[1]. With respect to the skin, PCXMC is able only to calculate mean doses. If one wants to know what the maximal skin doses amounts to we should perform *in situ* measurements using thermoluminescent dosimeters. This was performed in a complementary study in the same 8 hospitals[21]. Organs directly in the beam apart from the skin that receive highest equivalent dose are the lungs and the heart.

The risk for late effects is strongly dependent on patient's age and is different for males and females. In Figure 8, the age dependence of the attributable life-time risk in per cent per Sievert according to the ICRP publication 60[1] following the multiplicative model is depicted graphically

for males and females. On the same figure the age distribution of the patients considered in our multicenter study is presented. Using these data together with the effective doses of the patient population, the average risk for late effects for a diagnostic cardiologic intervention amounts to 1.1×10^{-4} for both males and females and 2.1×10^{-4} for a therapeutic cardiologic intervention also for both genders, for the age distribution of the patients considered in this multicenter study. In view of these values all measures have to be taken to reduce cumulative DAP value and consequently also the effective dose leading to a reduced risk for late effects especially when treating relatively young patients.

In conclusion, From this study national DRLs for Belgium for diagnostic and therapeutic cardiovascular interventional procedures could be derived for DAP values. Proposed conversion factors for *E* differed significantly for systems that used additional Cu filtration in cineradiography mode and systems that did not.

Additional Cu filtration is a very effective dose saving tool on X-ray systems used for fluoroscopy-guided procedures and has its influence on the dose registered to the patient through lower DAP and *E* values. Therefore, comparison of local mean values with DRLs, together with specific practical training for cardiologists leading towards dose conscious action and towards practical use of dose saving tools in X-ray equipment, make dose reduction possible.

Acknowledgements

The authors wish to thank Drs M. Carlier, W. Desmet, X. De Wagter, D. Djian, C. Hanet, G. Heyndrickx, V. Legrand and Y. Taeymans, together with the nursing staff and the technical personnel of the catheterization departments of all hospitals involved in this study for their participation and help with the dose measurements. The Federal Agency for Nuclear Control is acknowledged for the financial support and the follow up of the project.

References

1. ICRP. Recommendations of the International Commission on Radiological protection. ICRP Publication 60. Ann ICRP 21, (1-3) (Oxford, UK: Pergamon Press) (1991)
2. Faulkner K, Love H.G, Sweeney JK, Bardsley RA. Radiation doses and somatic risk to patients during cardiac radiological procedures. Br J Radiol. 59, 359-363 (1986)
3. Pattee PL, Johns PC, Chambers RJ. Radiation risk tot patients from percutaneous transluminal coronary angioplasty. J Am Coll Cardiol 22 (4), 1044-1051 (1993)
4. Karpinnen J, Parvianen T, Servomaa A, Komppa T. Radiation risk and exposure of radiologists and patients during coronary angiography and percutaneous transluminal coronary angioplasty (PTCA). Radiat Prot Dosim. 57, 481-485 (1995)
5. Vaño E, Gonzalez L, Fernandez JM, Guibelalde E. Patient dose values in interventional radiology. Br J Radiol. 68, 1215-1220 (1995)
6. Hirshfeld Jr *et al.* ACCF/AHA/HRS/SCAI Clinical Competence statement of physician knowledge to optimise patient safety and image quality in fluoroscopically guided invasive cardiovascular procedures. J Am Coll Card. 44 (11) 2259-82 (2004)
7. Hart D, Jones DG, Wall BF. Estimation of effective dose in diagnostic radiology from entrance surface dose and dose-area product measurements. Report NRPB – R262. (London : HMSO) (1994)
8. Tapiovaara M, Lakkisto M, Servomaa A. PCXMC – A PC-based Monte Carlo program for calculating patient doses in Medical x-ray examinations. (Helsinki, Finland: Finnish Centre for radiation and Nuclear Safety (STUK)) (1997).
9. Betsou S, Efstathopoulos E P, Katritsis D, Faulkner K, Panayiotakis G. Patient radiation doses during cardiac catheterisation procedures. Br J Radiol. 71, 634-639 (1998)
10. Delichas M G, Psarrakos K, Molyvda-Athanassopoulou E, Giannoglou G, Hatziioannou K, Papanastassiou, E. Radiation doses to patients undergoing coronary angiography and percutaneous transluminal coronary angioplasty. Radiat Prot Dosim. 103 (2) 149-154 (2003).
11. European Commission. Criteria for acceptability of radiological (including radiotherapy) and nuclear medicine installations. Radiation Protection No 91. (Luxembourg: Office for official publications of the European Communities) (1997).
12. Bacher K., Bogaert E., Lapere R., De wolf D., Thierens H. Patient-specific dose and radiation risk estimation in pediatric cardiac catheterisation. Circulation 111, 83-89 (2005)
13. Jones DG, Wall BF. Organ doses from medical X-ray examinations calculated using Monte Carlo techniques. NRPB-R186, Chilton (London: HMSO) (1985).
14. Cristy M. Mathematical phantoms representing children of various ages for use in estimates of internal dose. NUREG/CR-1159, ORNL/NUREG/TM-367, Springfield. (Oak Ridge National Laboratory) (1980)
15. Chapple *et al.* A phantom based method for deriving typical patient doses from measurements of dose-area product on populations of patients. Br J Radiol. 68, 1083-1086 (1995)
16. Olson CL. Comparative robustness of six tests in multivariate analysis of variance. J. Am. Stat. Assoc. 69, 894-908 (1974)
17. Neofotistou V. Review of patient dosimetrie in cardiology. Radiat Prot Dosim. 94, 1-2: 177-182. (2001)

18. Neofotistou V., Vaño E., Padovani R., Kotre J., Dowling A., Toivonen M. *et al.* Preliminary reference levels in interventional cardiology. Eur Radiol 13, 2259 – 2263 (2003)

19. Aroua A., Besancon A., Buchillier-Decka I., Trueb P., Vallery J.-F., Verdun F. R. *et al.* Adult reference levels in diagnostic and interventional radiology for temporary use in Switzerland. Radiat Prot Dosim. 111 (3), 289-295 (2004)

20. Schultz F W, Zoetelief J. Dose conversion coefficients for interventional procedures. Radiat Prot Dosim. 117 (1-3), 225-230 (2005)

21. Bogaert E, Bacher K, Thierens H. Multicentre study on skin doses of patients, treated with prolonged cardiological interventions. Report of a study performed for the Federal Agency for Nuclear Control. (2005)

22. Hiles PA, Scott SA, Brennen SE, Davies JH. All Wales CT dose and technique survey. Report by the Medical Imaging Sub-Committee of the Welsh Scientific Advisory Committee (Cardiff: Welsh Office) (1996)

23. Neofotistou V, Karoussou A, Lobotesi H. Hourdakis K, Patient dosimetry during interventional cardiology procedures. Radiat Prot Dosim. 80 (1-3), 151-154 (1998)

24. Stisova V. Effective dose to patient during cardiac interventional procedures (Prague workplaces). Radiat Prot Dosim. 111 (3), 271-274 (2004)

3.3 Part III

Interventional cardiovascular procedures in Belgium: effective dose and conversion factors

E. Bogaert[1] – K. Bacher[1] – H. Thierens[1]

[1]*Department of Medical Physics and Radiation Protection, Ghent University, Proeftuinstraat 86, Gent B-9000, Belgium.*

Reprint from Radiation Protection Dosimetry,
Advanced published April 2, 2008, doi:10.1093/rpd/ncn021

Abstract

Effective dose (E), representing the risk of late radiation-induced effects can be estimated by the use of conversion factors (CF), converting direct measurable quantities such as Dose-Area-Product (DAP) into *E*. Eight Belgian hospitals participated in the study with a total number of 318 procedures. *E*-values, calculated with PCXMC, were compared for the different hospitals for diagnostic and therapeutic procedures separately. *E* varied significantly depending on the hospital where the procedure was performed ($p < 0.001$), on filtration insertion ($p < 0.001$), on whether a centre is a training centre or not, the dose conscious action of the cardiologists and the complexity of the procedure ($p < 0.001$). Hospital specific CF were calculated. An average CF of 0.185 mSv $Gy^{-1}cm^{-2}$ was obtained with a satisfactory correlation ($r = 0.966$, $p < 0.001$). The differences in CF between hospitals were due to a large extent to the availability of additional filtration in cinegraphy mode ($p < 0.001$) and not to differences in irradiation geometries in the clinical protocol of the interventional procedures.

Introduction

As stated in the draft recommendations of the ICRP (2007)(1), *Effective Dose (E) can be of value for comparing the use of similar technologies and procedures in different hospitals and countries as well as the use of different technologies for the same medical examination, provided the patient population is similar with regard to age and sex*. Determination of *E* is very important for high dose examinations as cardiovascular procedures carried out under fluoroscopic control. Moreover, in recent years the number of fluoroscopy-guided procedures in interventional cardiology has increased substantially. Typical annual figures for Percutaneous Transluminal Coronary Angioplasty (PTCA) in developed countries are 500-1000 per million inhabitants(2) . Comparing literature data, *E*-values range from 5 to 9 mSv for Coronary Angiography (CA) and from 6 to 15 mSv for PTCA (3-6).

Yet, determination of *E* being defined in ICRP 60[7] as the sum of the weighted equivalent doses in twelve critical organs is quite complex since direct organ dose measurements are not possible in patients undergoing a cardiovascular procedure. Therefore, several indirect methods have been proposed to allow for a practical estimation of *E*. Based on the use of Monte Carlo modelling of radiological exposures, these methods only require the measurement of the incident radiation, e.g. Dose Area Product (DAP), to estimate patient E[8] .

The goal of this study was to calculate E based on detailed DAP registration during the procedures and by the use of specific conversion factors (CF), for eight catheterization rooms in Belgian hospitals representing the situation of the Belgian territory. Differences in mean E-values were analysed in terms of protocol- or equipment-related parameters. Hospital specific conversion factors converting DAP into E, generated by the Monte Carlo simulation code PCXMC [9], were compared to each other. The influence of different factors on the CF such as clinical protocol (orientation of the fluoroscopy and cine views), equipment (filtration) and procedure (diagnostic or therapeutic) was investigated.

Materials and Methods

Eight Belgian hospitals participated in this study, providing a population of 221 male and 97 female patients, between 29 and 89 years of age. An average of 40 patients per catherisation room was followed for both diagnostic CA and therapeutic procedures. Therapeutic procedures comprised both single or multiple balloon or stent dilatation as combined procedures. In the latter the therapeutic part follows immediately the diagnostic part (CA) of the procedure. A total number of 200 diagnostic and 118 therapeutic procedures were included in this study.

The X-ray equipment in the participating hospitals, all manufactured by either Philips or Siemens, consisted of three biplane and five monoplane systems. Three of the systems had flat detectors for image capture. The others used conventional image intensifiers. All X-ray systems can be considered as contemporary state of the art equipment with pulsed mode for X-ray generation. All systems inserted aluminium (Al) and copper (Cu) filtration into the beam in fluoroscopy mode, but only for four of them additional Cu filtration was available in cinegraphy mode. All systems were provided with a build-in DAP-meter that was calibrated *in situ*, using a 60cc ionisation chamber (Radcal Corporation, Monrovia, USA) and a

radiographic film (Eastman Kodak) for field size determination. Online computer registration of cumulative DAP and DAP rate made interpretation in terms of fluoroscopy and cinegraphy mode possible.

During a cardiovascular procedure, following parameters were recorded: field size, tube potential, filtration, mode (fluoroscopy or cinegraphy), irradiation geometry, number of frames per second, complexity score of the procedure according to the cardiologist and patient characteristics (gender, age, height and weight). A three-point scale for the complexity score was based on the duration of the procedures with respect to an equivalent procedure under normal circumstances, the number of lesions, the accessibility of the coronary arteries and the number of frames in one fixed orientation.

For calculation of *E* and CF, the Monte Carlo-based computer program PCXMC[9] was used. For each hospital the irradiation geometry of the clinical protocol was described in 'standard projections'. For calculation of *E*, the irradiation geometry of each procedure was described in terms of the standard projections. Field size, filtration and tube voltage recorded during the procedure and a fixed source to image receptor distance (SID) were used as input in the program. SID was 98 cm for monoplane systems and 105 for biplane systems. The distance from patient's skin to the image receptor (PID) was 10 cm. For geometries with an angle in cranial direction larger than 40 degrees, SID was increased with 5 cm and PID with 10 cm, according to the realistic clinical situation.

Statistical analysis was based on a multifactor ANOVA. In cases were only two groups had to be compared, a non-parametric two-tailed Mann-Whitney test was performed. A p-value < 0.05 was considered as significant.

Results and Discussion

Effective Dose values

E was calculated for each procedure taking into account the CF for the hospital where the procedure was performed. Overall histograms of *E* are represented for diagnostic and therapeutic procedures separately in Figure 1. The vertical lines represent the median values of these distributions and amount to 7.3 mSv for diagnostic procedures and 11.6 mSv for therapeutic procedures. Both distributions are strongly skewed, with *E* values reaching up to 79.8 mSv for therapeutic interventions. Overall mean values for *E* are 9.6 mSv for diagnostic procedures and 15.3 mSv for therapeutic procedures.

E distributions were also calculated for the different hospitals, for diagnostic and therapeutic procedures respectively and are represented in Figures 2 and 3. The median values of the overall distribution for diagnostic and therapeutic procedures respectively are taken as a guidance for comparison of local median *E* values. In figures 2 and 3, the local distributions and their median values are indicated by a full line and the overall median values are represented by a dashed line. Based on these histograms and on the ANOVA statistical analysis performed, we can conclude that *E* varies significantly depending on the hospital where the procedure was performed ($p < 0.001$), on filtration insertion ($p < 0.001$), on whether a centre is a training centre or not, the dose conscious action of the cardiologists and the complexity of the procedure ($p < 0.001$).

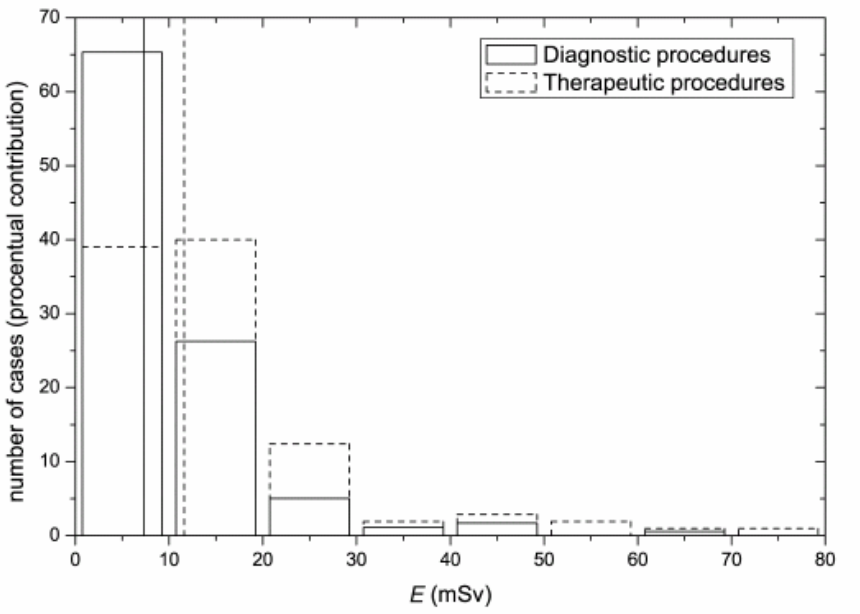

Figure 1. Histogram of effective dose *E* (mSv) for diagnostic (full line) and therapeutic (dashed line) procedures. The median values are indicated by a vertical line.

A comparison of the *E* histograms for the different hospitals revealed significant differences between the hospitals with respect to *E* for the patient ($p < 0.001$). This means that in some hospitals doses are significantly higher or lower than the average for both diagnostic and therapeutic procedures. In hospital 6, higher *E*-values and in hospitals 2 and 7, lower *E*-values are obtained.

In hospital 1 (training facility for cardiologists), we should take into account that, at the moment our measurements were carried out, different assistant cardiologists in training performed PTCA and stenting procedures. This explains the high *E*-values for therapeutic procedures related to this hospital. For both diagnostic and therapeutic procedures, mean *E* numbers

of hospital 6 were considerably higher than the overall figures. Although hospital 6 is a also training centre, the high values could mainly be attributed to the poor attention of some cardiologists with respect to radiation burden of the patient and the continuous use of the fluoroscopy 'high' mode for fluoroscopy filtration setting.

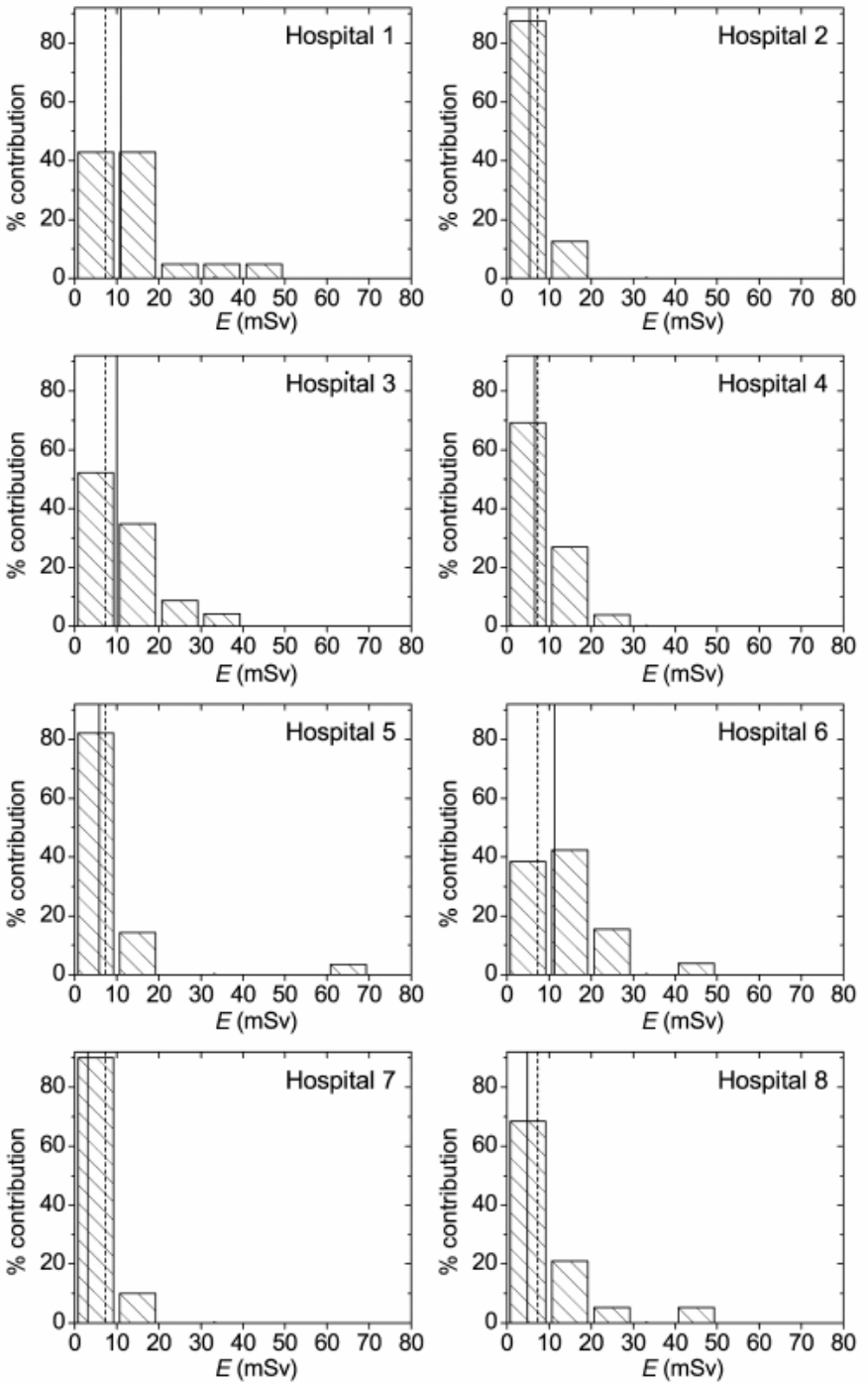

Figure 2. Comparison of histograms of effective dose for diagnostic procedures for the different hospitals. The overall median value is indicated by a dashed line. The median value of the local distribution is indicated by a full line.

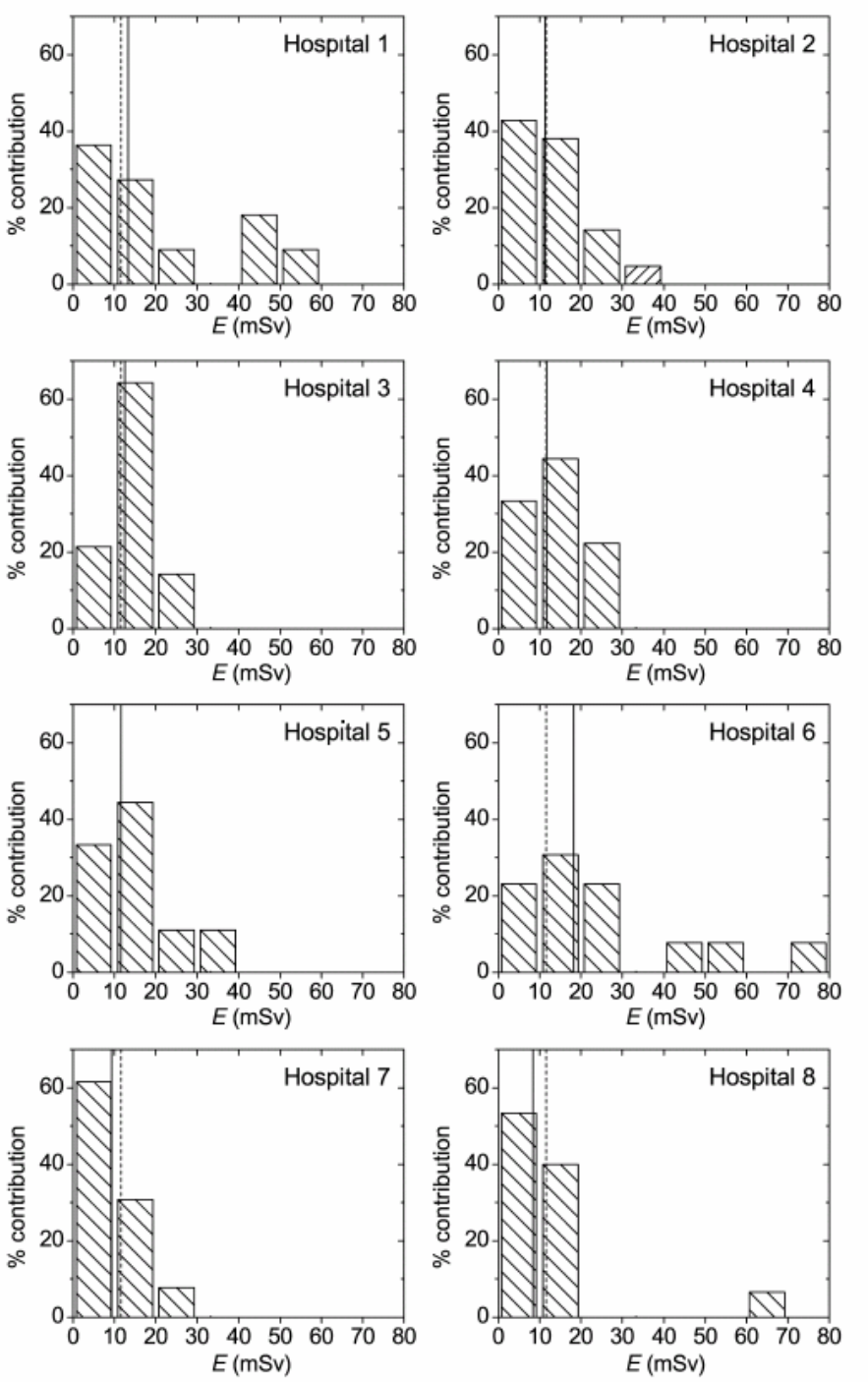

Figure 3. Comparison of histograms of effective dose for therapeutic procedures for the different hospitals. The overall median value is indicated by a dashed line. The median value of the local distribution is indicated by a full line.

In hospital 7, diagnostic and therapeutic procedures are performed with the lowest *E*, which can be explained by the very low tube-current setting in comparison to the tube currents of the other hospitals. Highest doses were recorded in hospital 1 , 3 and 6. These were the only departments where a manual filtration methodology was used. Hence, using automatic filtration insertion will generally result in lower *E*-values. It is, however, worthwhile

to mention that only very little filter variability was implemented in the systems of hospital 2 and 7. Therefore, in the latter centres, low *E*-values can be more attributed to the good practice in terms of the amount of radiation used by the cardiologist.

In conclusion, with respect to technical parameters, automated variable filtration settings result in significantly reduced effective patient doses ($p < 0.001$). This relates to hospitals 2, 4, 7 and 8.

In centers where flat-panel technology was introduced (hospitals 4, 5, 8), lower *E*-values were obtained. However, this effect did not reach significance ($p = 0.068$). A similar conclusion could be drawn for the comparison of *E*-values obtained in rooms equipped with a biplane and with a monoplane system. The use of biplane systems resulted in higher dose values.

The complexity of the procedure had a significant influence on *E* ($p < 0.001$). In the 3-point difficulty scale used in this study, level 2 and 3 resulted in significantly higher median *E*-values compared to the first level (4.1 versus 10.6 mSv).

Conversion Factors

An excellent overall correlation between *E* and DAP was found ($r = 0.966$, $p < 0.001$). When analysing diagnostic and therapeutic procedures separately, similar correlations were found ($r = 0.965$, $p < 0.001$ and $r = 0.964$, $p < 0.001$ respectively). Table 1 describes the different hospital specific CF from DAP to *E*. The average value for the CF is 0.185 mSv $Gy^{-1}cm^{-2}$. Statistical significance was not observed for the difference in CF between diagnostic (0.179 mSv $Gy^{-1}cm^{-2}$) and therapeutic (0.190 mSv $Gy^{-1}cm^{-2}$) procedures ($p = 0.723$).

However, distinction based on filtration used in cinegraphy mode in terms of the availability of additional Cu material in the beam does make sense. A CF of 0.207 mSv $Gy^{-1}cm^{-2}$ for systems that use extra Cu filtration in cinegraphy was found, whereas the CF amounts to 0.177 mSv $Gy^{-1}cm^{-2}$ for the other systems. The beam hardening as a consequence of the additional Cu filtration leads to a higher mean *E*-value for the same DAP value.

Although CF were calculated for each hospital individually, taking into account the X-ray set up and the clinical protocol, as stated by Schultz and

Zoetelief[10], geometry related factors did not result in significant differences in CF.

Table 1. Conversion Factor from DAP to E, for the different hospitals involved in this study. The last column mentions whether additional Cu filtration is available in cinegraphy mode or not.

Hospital	CF (mSv $Gy^{-1}cm^{-2}$)	Additional Cu?
1	0.184	No
2	0.225	Yes
3	0.157	No
4	0.170	No
5	0.203	Yes
6	0.183	No
7	0.235	Yes
8	0.211	Yes

For practical use of CF for calculation of *E*, the availability of additional Cu filtration can be taken into account. The CF factors derived in present work can be used for both diagnostic and therapeutic procedures.

Conclusion

Local *E*-distributions show statistical significant differences between different hospitals. This means that further dose reduction is possible for interventional cardiovascular procedures in Belgium. The importance of additional Cu filtration in clinical practice should be stressed. It is a very helpful tool that not only lowers *E* but also the Entrance Skin Dose (ESD), as shown in a complementary study in the same 8 hospitals[11]. ESD easily exceeds the threshold of 2 Gy[7] for deterministic effects in these high-dose procedures. The use of conversion factors provides a very practical methodology to calculate *E* from DAP. In present work separate CF are proposed for X-ray systems that use additional Cu filtration in cinegraphy mode and systems that do not: 0.207 versus 0.177 mSv $Gy^{-1}cm^{-2}$.

Acknowledgement

The authors wish to thank all cardiologists, nursing staff and technical personnel of the catheterization departments of all hospitals involved in this study.

Funding

The Federal Agency for Nuclear Control is acknowledged for the financial support and the follow up of the project.

References

1. ICRP. Draft Recommendations of the International Commission on Radiological Protection (February 2007) http://www.icrp.org
2. Vaño, E., Faulker, K. (2006) ICRP special radiation protection issues in interventional radiology, digital and cardiac imaging. Radiat Prot Dosim 117(1-3) 13-17
3. Padovani, R., Quai, E., (2005) Patient dosimetrie approaches in interventional cardiology and literature dose data review Radiat Prot Dosim 117(1-3) 217- 221
4. Katritsis, D., Efstathopoulos, E., Betsou, S., Korovesis, S., Faulkner, K., Panayiotakis, G. and Webb-Peploe, M.M. (2000) Radiation exposure of patients and coronary arteries in the stent era: a prospective study. Catheter Cardiovas Interv 51(3), 259-264
5. Betsou, S., Efstathopoulos, E.,Katritsis, D., Faulkner, K. and Panayiotakis, G. (1998) Patient radiation doses during cardiac catheterisation procedures. Br J Radiol 71 (846) 634-639
6. Broadhead, D.A., Chapple, D.L., Faulkner, K., Davies, M.L. and McCallum, H. (1997) The impact of cardiology on the collective effective dose in the North of England. Br J Radiol 70(833) 492-497
7. Recommendations of the International Commission on Radiological protection. ICRP Publication 60.(1991) Ann ICRP 21 (1-3) Oxford, UK: Pergamon Press
8. Theocharopolos, N., Perisinakis, K. and Damilakis J. (2002) Comparison of four methods for assessing patient effective dose from radiological examinations. Med hys Biol 29 (9) 2070-2079
9. Tapiovaara, M., Lakkisto, M., Servomaa, A. (1997) PCXMC - A PC-based Monte Carlo program for calculating patient doses in Medical x-ray examinations. Helsinki, Finland: Finnish Centre for radiation and Nuclear Safety (STUK) STUK report A139.
10. Schultz, F.W., Zoetelief, J. (2005) Dose conversion coefficients for interventional procedures. Radiat Prot Dosim. 117(1-3) 225-230
11. Bogaert, E., Bacher, K., Thierens, H. (2005) Multicentre study on skin doses of patients, treated with prolonged cardiological interventions. Report of a study performed for the Federal Agency for Nuclear Control.

3.4 Part IV

Patient –Specific Dose and Radiation Risk Estimation in Pediatric Cardiac Catheterization

K. Bacher[1] – E. Bogaert[1] – R. Lapere[1] – D. De Wolf[2] – H. Thierens[1]

[1]*Department of Medical Physics and Radiation Protection, Ghent University, Proeftuinstraat 86, Gent B-9000, Belgium.*

[2]*Department of Paediatric Cardiology, Ghent University Hospital, De Pintelaan 185, Gent B-9000, Belgium.*

Reprint from Circulation 2005; 111: 83-89

Abstract

Background—Because of the higher radiosensitivity of infants and children compared with adults, there is a need to evaluate the doses delivered to pediatric patients who undergo interventional cardiac procedures. However, knowledge of the effective dose in pediatric interventional cardiology is very limited.

Methods and Results—For an accurate risk estimation, a patient-specific Monte Carlo simulation of the effective dose was set up in 60 patients with congenital heart disease who underwent diagnostic (n=28) or therapeutic (n=32) cardiac catheterization procedures. The dose-saving effect of using extra copper filtration in the x-ray beam was also investigated. For diagnostic cardiac catheterizations, a median effective dose of 4.6 mSv was found. Therapeutic procedures resulted in a higher median effective dose of 6.0 mSv because of the prolonged use of fluoroscopy. The overall effect of inserting extra copper filtration into the x-ray beam was a total effective dose reduction of 18% with no detrimental effect on image quality. An excellent correlation between the dose-area product and effective patient dose was found (r=0.95). Hence, dose-area product is suitable for online estimation of the effective dose with good accuracy. With all procedures included, the resulting median lifetime risk for stochastic effects was 0.08%.

Conclusions—Because of the high radiation exposure, it is important to monitor patient dose by dose-area product instrumentation and to use additional beam filtration to keep the effective dose as low as possible in view of the sensitivity of the pediatric patients.

Introduction

Interventional cardiology procedures are known to give high radiation doses to patients because of prolonged use of fluoroscopy, multiple cine runs, and the complexity of the procedures [1–8]. The radiation exposure issue in cardiac catheterizations is particularly relevant for infants and children because of their higher radiosensitivity compared with adults, the large fraction of the body irradiated by the x-ray beam, and the probable need to

repeat the procedure [9,10]. In addition, cardiac catheterizations are being increasingly used for therapeutic purposes, possibly resulting in higher patient radiation doses [9–11]. When these facts are taken into account, there is a strong need to evaluate the doses delivered to pediatric patients who undergo such high-dose x-ray examinations [12].

Most of the radiation dosimetry studies performed in pediatric patients are based on measurements with thermoluminescence dosimeters (TLDs) for estimating the dose to the skin, thyroid, and gonads [12–16]. Other studies have indicated the dose-area product (DAP) [10,12,17,18,21]. However, to assess the potential risk for stochastic effects such as cancer and leukemia resulting from cardiac catheterization procedures, the effective dose should be calculated [19]. The limited published results are based mainly on phantom measurements or calculated conversion factors and do not take into account the real exposure settings and geometry [9,20,21].

Therefore, the aim of the present study was to find a patient-specific determination of the effective dose in pediatric heart catheterization procedures and to investigate whether previously reported results on risk estimates are comparable to this patient-specific dosimetry. Furthermore, radiation doses of diagnostic procedures are compared with those of common therapeutic interventions. Because dose reduction in pediatric settings is of great importance, we also investigated the dose-saving effect of using extra copper filtration in the x-ray beam.

Materials and Methods

Patients

The patient population included 60 consecutive pediatric patients with congenital heart disease (age ≤ 10 years). The study group comprised 33 male and 27 female patients with a median age of 2.0 years (range, 1 month to 10 years) and a median weight of 11.7 kg (range, 3.0 to 43 kg). Nineteen patients were < 1 year of age. Of the 60 patients, 28 underwent cardiac catheterization procedures for diagnostic purposes (Table 1). Thirty-two patients were referred for a therapeutic catheter procedure: 11 for patent ductus arteriosus occlusion, 10 for atrial septal defect (ASD) closure, and 11 for balloon dilatation. All examinations were carried out by an experienced pediatric cardiologist.

Table 1: Lesions studied in the diagnostic catheterization patient group

Lesions	Patients, n
Univentricular heart	15
Double aortic arch	1
Truncus arteriosus	1
Aortopulmonary collaterals	1
Pulmonary atresia and intact septum	2
Total anomalous pulmonary venous drainage	1
Double discordance	1
Pulmonary atresia and VSD	2
Coronary artery fistula	1
Swiss cheese VSD	1
RV aneurysma	1
AVSD	1

VSD indicates ventricular septal defect; RV, right ventricular; and AVSD, AV spetal defect

X-Ray System

All studies were performed with an Integris BH5000 biplane x-ray system (Philips) consisting of a frontal Poly Diagnost C2 and a lateral L-arc 2 U. Tube settings such as peak voltage and anode current are controlled by the automatic brightness control. Pulsed fluoroscopy (12.5 frames per second) and cineangiography (25 frames per second) were used.

For fluoroscopy, 2 x-ray beam filtrations were available. The standard setting consisted of a filtration of 1.5 mm Al, combined with 0.2 mm Cu. The low-dose fluoroscopy setting had an extra filtration of 0.2 mm Cu. The half-value layers of the x-ray tubes for both fluoroscopy settings were measured at 80 kVp with a NE2571 Farmer ionization chamber (Thermo Electron, UK). For both tubes, values of 6.2 and 7.3 mm Al were obtained for the standard and low-dose fluoroscopy settings, respectively.

For the measurement of the dose-area product (DAP) at the frontal and lateral tubes, 2 transmission ionization chambers (PTW) were attached to the tube housing of each x-ray tube and connected to a Diamentor M4 readout unit (PTW). DAP meters were calibrated *in situ* with the NE2571 Farmer ionization chamber and 33x41-cm Kodak X-Omat V films (Eastman Kodak). The calibration factor was taken as the ratio between the actual DAP, calculated as the dose in the centre of the field multiplied by the field size

measured from the film, and the DAP reading from the Diamentor M4. The calibration was performed for both beam filtration settings, with a peak potential ranging from 50 to 125 kV (Figure 1).

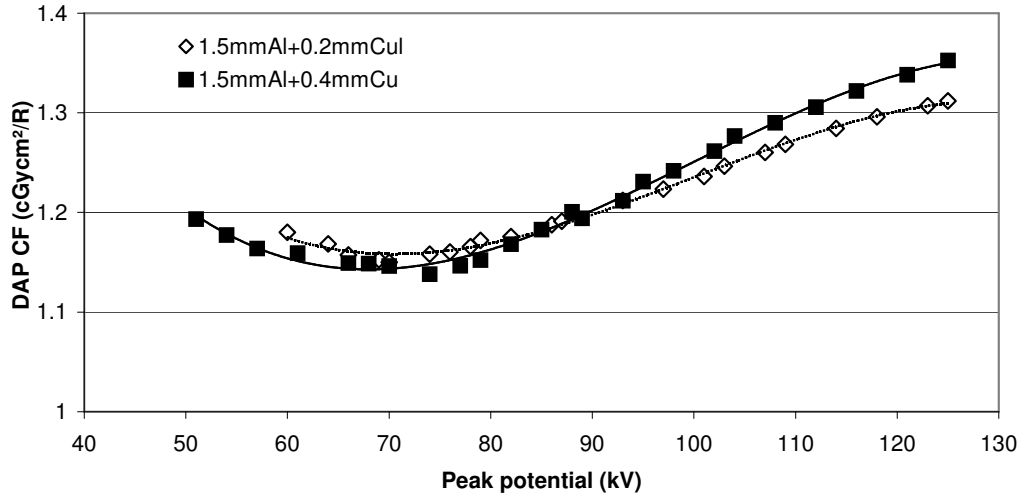

Figure 1. Calibration factor of the dose-area product monitors for the frontal X-ray tube. R represents the uncalibrated read-out of the DAP monitor.

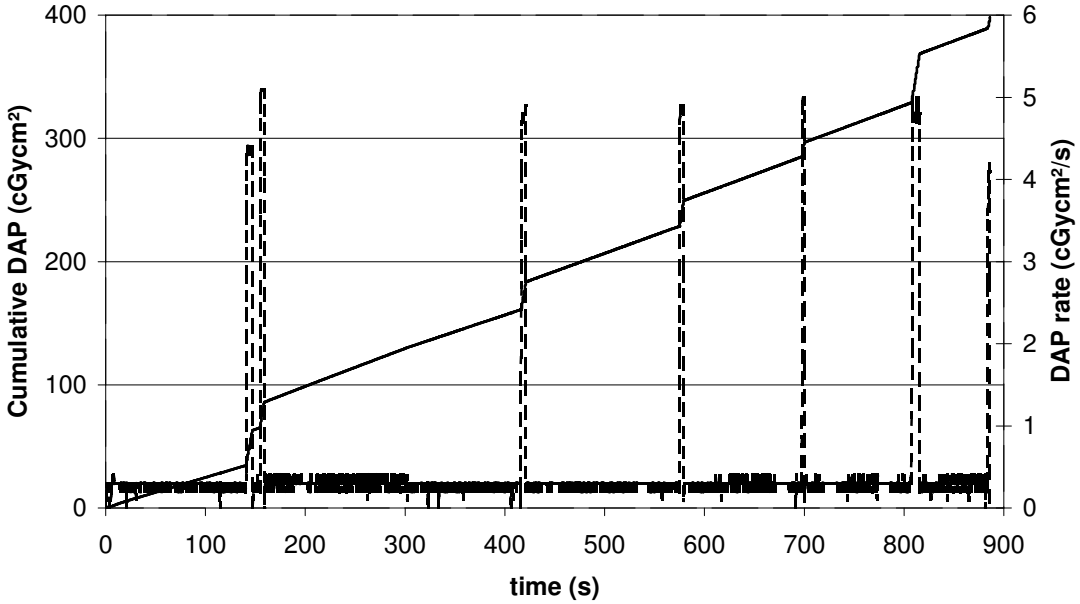

Figure 2. Typical output of the DAP registration program: the registered DAP (solid line) and DAP rate (dashed line) as a function of time. The example shows output for the frontal tube.

Effect of Extra Filtration on Image Quality and Dose

To investigate the dose reduction when an extra 0.2 mm of copper filtration (low-dose setting) was used, patients were randomized to the standard or the low-dose fluoroscopy setting. From the 28 diagnostic catheterizations, 13 were performed with low-dose fluoroscopy and 15 with standard settings. In half of the therapeutic interventions, low-dose fluoroscopy was used. Skin and effective doses were calculated in both groups as described below.

For an objective image quality analysis of the effect of the additional filtration, a CDRAD 2.0 (University of Nijmegen) contrast-detail phantom study was set up [22]. The phantom was used to assess the minimum contrast required to visualize objects of different sizes above the noise threshold.

The phantom was placed between 2 layers of 5-cm PMMA to simulate patient scatter. For both filtration settings, images were acquired in the same conditions as used for patients. All images were scored by 5 independent readers using the methodology as described by the manufacturer [22]. The results are presented in contrast-detail curves.

Acquisition of Exposure Parameters

For each projection used in the cardiac intervention, tube potential, filtration settings, fluoroscopy times, and position of the x-ray tubes were recorded for all patients. The x-ray tube position (rotation and skew), tube potential, source-to-image-intensifier distance, and image intensifier field size were registered automatically for every cine run by the system.

DAP data were gathered by connecting the Diamentor M4 readout unit to a laptop and using software written in-house. In this way, DAP values could be analyzed as a function of time. A distinction could be made between the fluoroscopy and the cine run contributions based on the large difference in DAP rate (cGycm^2/s) between fluoroscopy and cine mode (Figure 2). DAP calibration factors were applied according to the tube potential and the filtration settings of an exposure. Thus, the variation in the DAP calibration factor with beam quality was taken into account.

Skin Dose Measurements

To measure the entrance skin dose from the frontal tube, an array of 14-LiF TLD meters (Harshaw TLD-100, Thermo Electron) was attached to a 33x41 cm Kodak X-Omat V dosimeter film. Afterward, the film was placed on the table underneath the patient's back, near the frontal x-ray tube. The lateral entrance skin dose was assessed by placing 3 TLDs at the right armpit of the patient.

TLDs were analyzed by a Harshaw 3500 reader (Thermo Electron Corp). Optical density readings from the film were obtained with a digital densitometer-scanner (Vidar System Corp). All TLDs were calibrated at the same beam quality that was used in situ. The SD within the set of TLDs was minimized to 2%. The X-Omat V film dosimeter was calibrated as described elsewhere [23].

Film dosimetry was used to verify whether the maximum skin dose measured by TLD corresponded to the maximum skin dose assessed by film. If there was a good correspondence, TLD readings were preferred over film results because of their better accuracy. In addition, the measured skin dose distribution by film dosimetrie served as a verification of the results of the dose distributions obtained by Monte Carlo simulation.

Patient-Specific Effective Dose Simulation

The effective dose, introduced by the International Commission on Radiological Protection (ICRP), representative of the risk of late radiation-induced effects as malignancies, is defined by the following expression [19]:

$$E = \sum_T w_T H_T,$$

where H_T is the equivalent dose to tissue T and w_T is the weighting factor representing the relative radiation sensitivity of tissue T. Organ equivalent doses were calculated with the Monte Carlo code MCNP4b2 [24].

The simulations take into account the irradiation geometry of the x-ray tubes and the x-ray spectral distribution used for a particular projection in a patient. X-ray spectra were calculated with an analytical program [25,26]. Field size at the patient's skin level was calculated by measuring the focus-to-skin distance and by using the recorded source-to-image-intensifier distance and the image intensifier field size. The field geometry for fluoroscopy was copied from the first cine run after a series of fluoroscopy. This technique is

acceptable because most of the fluoroscopy is used to position the catheter for the next cine run, which is done with the same tube incidence.

Table 2. Demographic Patient Data and Exposure Parameters for diagnostic catheterizations

	Diagnostic Catheterizations		
	Standard Fluoroscopy (n=15)	Low-Dose Fluoroscopy (n=13)	*p*
Demographic patient data			
Age, y	2.4 (0.1-8.8)	1.3 (0.1-9.2)	0.695
BMI, kg/m²	14.6 (12.6-21.6)	14.9 (12.6-21.0)	0.945
Exposure parameters			
Peak voltage frontal tube, kV	77.0 (58.3-79.6)	76.6 (71.2-80.3)	0.818
Peak voltage lateral tube, kV	84.9 (59.5-100.0)	85.7 (74.6-102.0)	0.773
Fluoroscopy time, s	294 (30-870)	234 (96-1992)	0.316
Total DAP, cGycm²	548 (114-1461)	337 (96-1399)	0.510
Fluoroscopic DAP rate, cGycm²/s	0.61 (0.53-0.92)	0.46 (0.22-0.94)	0.042
PA cine runs, n	4.0 (1-9)	3.0 (1-7)	0.293
LAT cine runs, n	3.0 (0-9)	2.0 (0-6)	0.356

BMI indicates body mass index; PA postanterior; and LAT lateral. Values represent the median (range).

Table 3. Demographic Patient Data and Exposure Parameters for therapeutic catheterizations

	Therapeutic Catheterizations		
	Standard Fluoroscopy (n=16)	Low-Dose Fluoroscopy (n=16)	*p*
Demographic patient data			
Age, y	2.0 (0.2-10.0)	2.0 (0.3-7.8)	0.401
BMI, kg/m²	15.6 (10.1-23.7)	16.3 (13.4-30.1)	0.258
Exposure parameters			
Peak voltage frontal tube, kV	75.0 (56.0-84.8)	79.1 (77.0-91.8)	0.041
Peak voltage lateral tube, kV	83.0 (60.0-96.5)	89.7 (77.0-116)	0.024
Fluoroscopy time, s	401 (182-3612)	300 (42-2466)	0.267
Total DAP, cGycm²	472 (282-2044)	272 (41-1800)	0.079
Fluoroscopic DAP rate, cGycm²/s	0.71 (0.42-1.11)	0.55 (0.30-0.91)	0.039
PA cine runs, n	3.5 (2-7)	3.0 (2-14)	0.376
LAT cine runs, n	3.5 (0-6)	3.0 (2-13)	0.249

Abbrevitiations as in Table 2. Values represent median (range).

Because of the broad differences in body length and weight between the standard pediatric mathematical phantoms of 0, 1, 5, 10, and 15 years, [27] we developed a Visual Basic (Microsoft) program, allowing us to generate a more refined patient-specific phantom based on the gender and the length of the patient. Phantom calculation was based on the interpolation between the standard pediatric phantoms. In all cases, the arms were removed from the body phantom, simulating the normal clinical practice in which the patients have to move their arms along their head so as not to obstruct the lateral projection. The patient table was also included in the model to compensate for additional attenuation. The x-ray simulation was based on the assumption that the heart lies in the isocentre of the x-ray beams of the C arms.

The computer phantom, the geometry of the x-ray tube, and the x-ray spectrum were used as input for the Monte Carlo simulations. Then, for every tube incidence and for each exposure mode, the effective dose per unit DAP was calculated using the ICRP60 organ weighting factors [19]. For the remainder dose, the mass-weighted average of the remainder organs listed in the latter report was taken. The dose to the bone marrow was calculated with the method of Rosenstein [28] and the published kerma-to-dose conversion factors [29]. The dose to the bone surface was taken as the dose to the skeleton excluding the marrow. By multiplying the effective dose per unit DAP by the corresponding recorded DAP, we could calculate the total effective patient dose. As a verification of the Monte Carlo calculations, the dose distribution at the location of the X-Omat V film was simulated and compared with the distribution derived from the film.

Risk Estimation

The lifetime mortality risk resulting from stochastic effects such as cancer and leukemia was determined by multiplying the effective dose by the appropriate risk factor. In this study, we used the ageand gender-dependent risk factors from the multiplicative model recommended in the ICRP 60 publication: 13%/Sv for boys and 16%/Sv for girls [19] 10 years of age.

Statistical Analysis

Correlations in scatterplots were investigated by calculating the Pearson correlation (*r*). Differences between 2 independent (not normally distributed) populations were tested for significance with the 2-tailed Mann-

Whitney test (95% confidence level). All statistical calculations were performed with the SPSS 10.0.5 program.

Results

Exposure Data

Demographic patient data and exposure parameters used during the cardiac catheterization procedures are summarized in Tables 2 and 3 for the diagnostic and therapeutic interventions, respectively. The data for the 2 patient groups receiving standard and low-dose fluoroscopy are indicated separately. There was no statistical difference in age and body mass index between the patient groups; hence, no bias was introduced as a result of differences between the groups.

The median fluoroscopy time during the cardiac catheterizations was 372 seconds (range, 30 to 3612 seconds). More fluoroscopy was used in therapeutic procedures (median, 456 seconds; range, 42 to 3612 seconds) compared with diagnostic catheterizations (median, 261 seconds; range, 30 to 1992 seconds), but the difference was not statistically significant at the 95% confidence level (p=0.089).

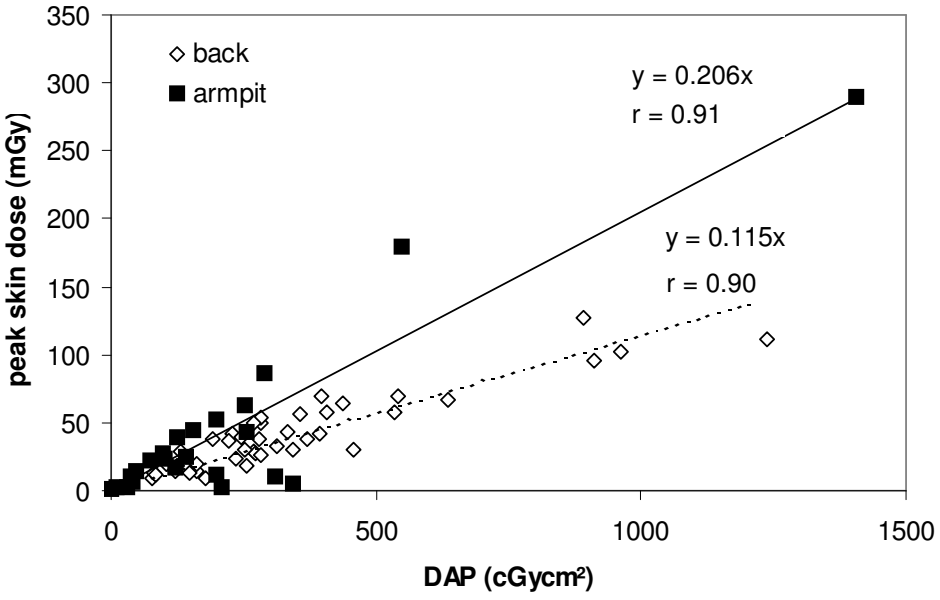

Figure 3. Correlation between maximum lateral and back skin dose, measured by TLD, and DAP. With extreme value for lateral dose taken out (hot spot > 250mGy), the correlation of lateral skin dose and DAP remains good (r = 0.78, slope = 0.203).

Use of the frontal and lateral tubes for cineangiography acquisitions was well balanced. The median measured cumulative DAP was 453 cGycm^2 (range, 41 to 2044 cGycm^2). As a result of the longer fluoroscopy times and slightly higher number of cineangiographies, the median DAP was found to be higher in therapeutic interventions (463 cGycm^2; range, 41 to 2044 cGycm^2) compared with diagnostic procedures (409 cGycm^2; range, 96 to 1461 cGycm^2). However, differences were not statistically significant (p=0.568).

The use of 0.2 mm extra copper filtration for fluoroscopy reduced the fluoroscopy DAP rate from a median of 0.71 to 0.51 cGycm^2/s. This 29% reduction was significant (p=0.041).

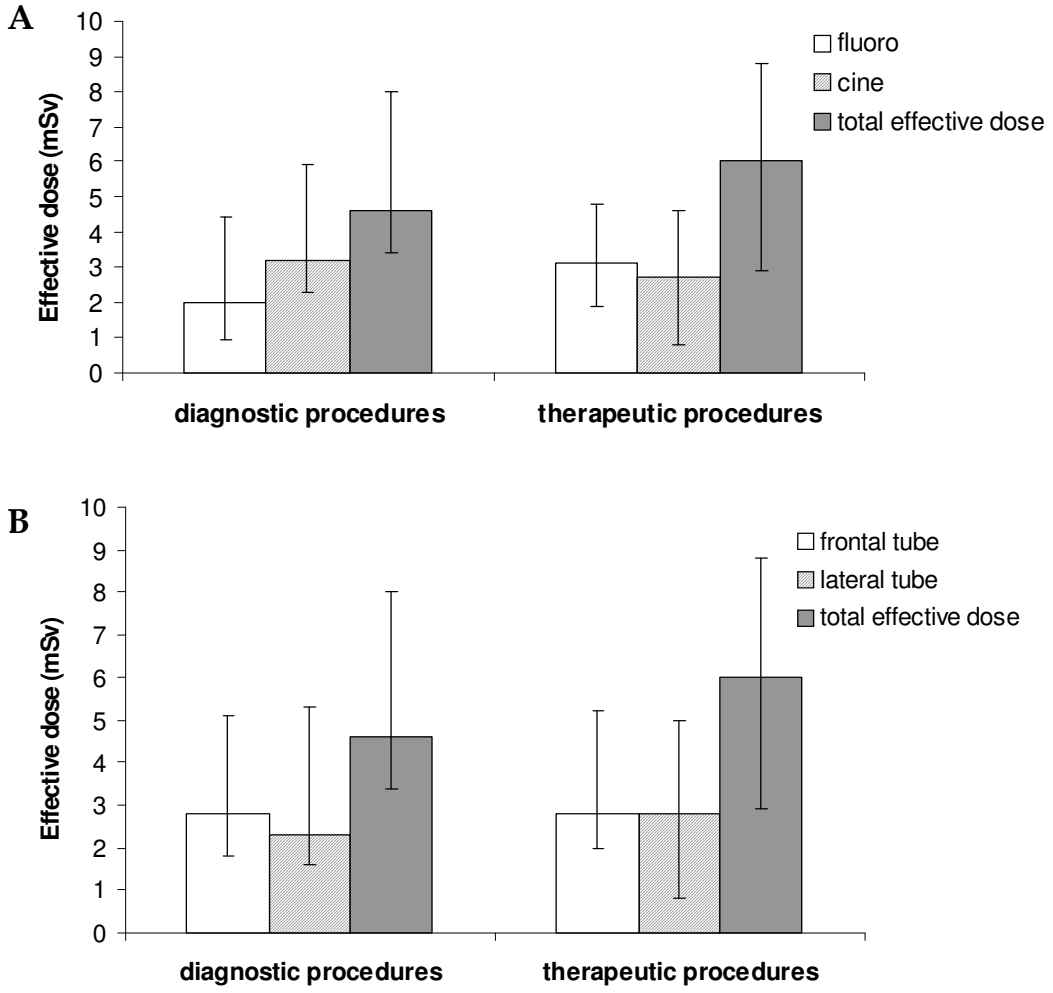

Figure 4. Median effective dose for diagnostic and therapeutic catheterizations. A, Median contributions of fluoroscopy and cineangiography in total effective dose. B, Median contribution of frontal and lateral exposure in effective dose. Error bars represent the 25% and 75% percentiles.

Skin Dose

Peak entrance skin doses measured with the TLD array on the patient's back showed very good agreement with the X-Omat film doses (r=0.98). Correspondence between the 2 measurement techniques showed that the TLD array accurately detects the maximum skin dose. The median peak skin dose at the patient's back was 34.2 mGy (range, 12.1 to 144 mGy). The median lateral peak skin dose, measured near the patient's armpit, was 23.9 mGy (range, 1.49 to 297.5 mGy).

A strong correlation was found between DAP and maximum skin dose (Figure 3). This was the case for the frontal (r=0.90) and lateral (r=0.91) skin exposure. In 4 cases, the lateral TLD dosimeters were clearly not located at the peak skin dose positions.

Effective Dose Simulation

Comparison of the dose distributions measured on film and simulated with MCNP resulted in differences of <7% in all patients.

Median effective doses for diagnostic and therapeutic cardiac interventions are shown in Figure 4. Contributions of cineangiography and fluoroscopy in the total effective dose are indicated in Figure 4A. Figure 4B illustrates the contributions of the frontal and lateral tube exposures to the effective dose.

For the diagnostic cardiac catheterization, the median effective dose was 4.6 mSv (range, 0.6 to 23.2 mSv). The cine contributed a median of 69% to the dose, and 49% of the effective dose was due to exposure of the lateral tube.

The therapeutic cardiological procedures resulted in a median effective dose of 6.0 mSv (range, 1.0 to 37.0 mSv). The cine had a median contribution of 45%, whereas 47% of the effective dose was due to the lateral exposure. ASD closure procedures were subject to a significantly lower effective dose (median, 2.8 mSv; range, 1.8 to 7.4 mSv) compared with the patent ductus arteriosus occlusions (median, 7.6 mSv; range, 2.1 to 37 mSv) and the balloon dilatations (median, 8.1 mSv; range, 2.9 to 20 mSv).

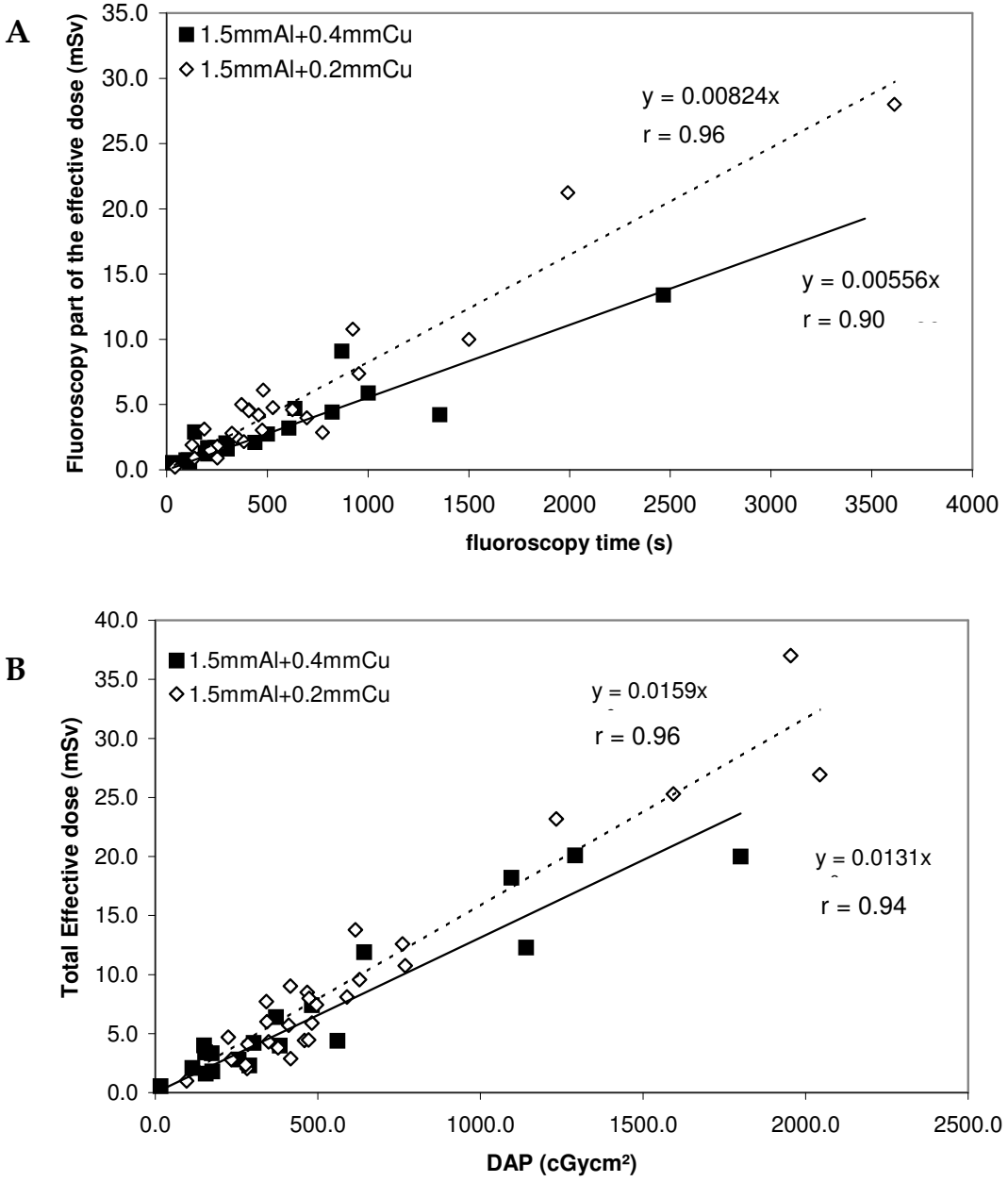

Figure 5. A, Correlation between effective dose resulting from fluoroscopy and fluoroscopy time. B, Correlation between total effective dose and DAP for 2 filtrations considered in this study.

In Figure 5A, the fluoroscopy part of the effective dose is plotted versus fluoroscopy time for standard and low-dose fluoroscopy settings. Application of low-dose fluoroscopy resulted in a mean reduction of the fluoroscopy part of the effective dose of 33%. The overall effect of inserting an extra 0.2 mm copper filtration in the x-ray beam was a total effective dose reduction of 18% (Figure 5B). An excellent correlation between the DAP and

the effective patient dose was found for both normal (r=0.96) and low-dose (r=0.94) fluoroscopy.

Image Quality of Low-Dose Fluoroscopy

The contrast-detail study showed no statistically significant difference in low-contrast performance of the standard filtration compared with the low-dose fluoroscopy settings (p=0.437). The contrast-detail curves, averaged over the 5 independent readers, are presented in Figure 6.

Risk Estimation

Including all procedures, the median lifetime risk for stochastic effects was 0.08% (range, 0.007% to 0.481%). The risk estimates for male and female patients did not differ significantly. No significant risk difference was found between therapeutic (median, 0.09%) and diagnostic (median, 0.06%) catheterizations.

The highest effective doses and corresponding risk estimates were found for the youngest patients (<1 year of age). The median lifetime risk for the latter group was 0.10% (range, 0.007% to 0.481%). For the age groups of 2 to 5 years and 6 to 10 years, the median risk was 0.08% (range, 0.016% to 0.431%) and 0.05% (range, 0.030% to 0.320%), respectively.

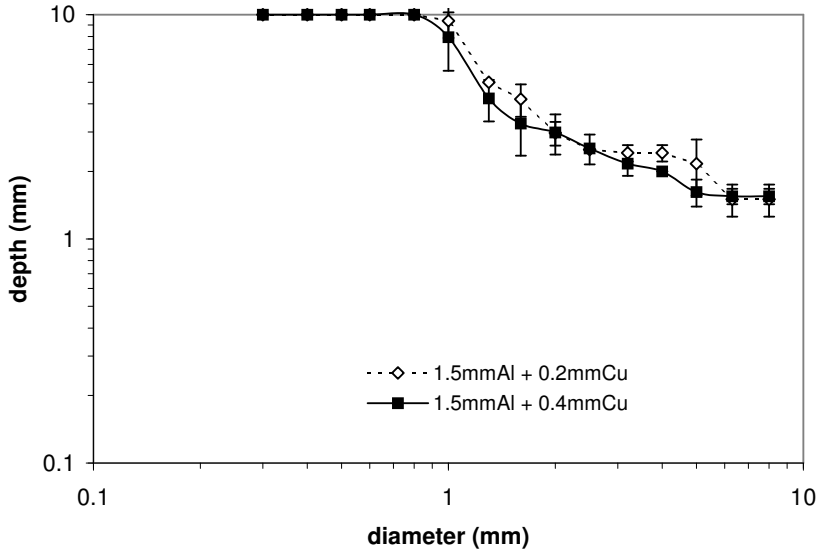

Figure 6. Contrast-detail curve for standard and low-dose filtration settings.

Discussion

Cardiac catheterizations are among the radiological x-ray procedures with the highest patient radiation dose and therefore are of great concern in pediatric settings because of the higher tissue radiosensitivity of infants and children [9–15]. Moreover, in children with congenital heart disease, there is often a need to perform multiple examinations, increasing the radiation risks [9,10]. About 7% of all cardiac angiography procedures are carried out in children 0 to 15 years of age [30].

Over the last few years, an increasing number of therapeutic catheterization procedures have been performed in children [9–11]. In general, the justification of these procedures is evident because they avoid complicated invasive surgery. However, the complexity of these procedures results in higher radiation exposures caused by the longer fluoroscopy times [9–11]. The high patient doses and the introduction of new interventional procedures stress the need for an inventory of the doses delivered to pediatric patients who undergo these high-dose x-ray examinations [9,12] .

The risk for a skin injury is related to the maximum skin dose value [7]. The maximum skin dose measured in this study (297.5 mGy) was far below the 2-Gy threshold level for transient erythema. The median peak skin dose of 34.2 and 23.9 mGy for the anterior-posterior and the lateral exposures, respectively, may be compared with previous (mean) values of 126.2 mGy [12], 149 mGy [13], and 74 mGy [14]. Only one study reported a mean entrance skin dose of 481 mGy for children <10 years of age [15]. Because of the moderate values of skin doses in pediatric catheterizations, radiation-induced skin injuries are unlikely. On the other hand, skin dose has to be monitored so that the cardiologist knows the maximum skin dose delivered during the procedure. Because the DAP correlates very well with peak skin dose (r=0.90) for the posterior-anterior and lateral exposures, DAP measurement is suitable for online skin dose estimation and may avoid radiation-induced skin injuries in any case. This finding corresponds with a similar correlation found by Boothroyd *et al.* [12].

In contrast with TLD measurements, DAP monitoring is easily performed, even for very complex procedures. As a result, DAP measurements from pediatric cardiac catheterizations were published in different studies. In our study, the overall measured DAP varied from 41 to 2044 cGycm^2, and the median value of 453 cGycm^2 is in good agreement with the results of others [10,12,17,18,21].

To assess the potential risk for stochastic effects such as cancer and leukemia, the effective dose should be calculated [19]. Unfortunately, determining the effective dose in catheterization procedures is not straightforward, mainly because of the complexity of the x-ray beam geometry (beam direction and field size variations during the catheterization procedure). Moreover, individual anatomy should be taken into account. Anatomy is very important for child dose estimations because patient weights and lengths may be subject to large variations. As a result of these dosimetric complications, data in the literature on the effective dose in pediatric interventional cardiology are scarce. The published results are based mainly on phantom measurements or a restricted number of existing conversion factors without taking into account the real exposure settings and geometry [9,20,21]. Furthermore, using only the standard pediatric mathematical phantoms of 0, 1, 5, 10, and 15 years [27] could result in errors as large as 25%. In the present study, a patient-specific Monte Carlo calculation of the effective dose was set up, taking into account the exact irradiation geometry of the x-ray tubes and x-ray exposure settings used for a particular projection in a patient. Patient anatomy was simulated by an anthropomorphic phantom that was based on the gender and length of the patient.

For diagnostic cardiac catheterizations, a median effective dose of 4.6 mSv was found. Therapeutic procedures resulted in a higher median effective dose of 6.0 mSv because of the prolonged use of fluoroscopy and the larger number of cine runs. The reported values are as high as those for a typical adult cardiac angiography [30]. In ASD closure procedures, a significantly lower effective dose (median, 2.8 mSv) was found compared with the patent ductus arteriosus occlusions (median, 7.6 mSv) and balloon dilatations (median, 8.1 mSv). This can be attributed to the higher degree of difficulty for the cardiologist in those 2 procedures [11]. Moreover, for ASD closure, the cardiologist relied more on transesophageal imaging than on cine, resulting in a low effective dose. Overall, large variations in effective doses were found for diagnostic and therapeutic procedures, mostly because of differences in the difficulty level among individual patients. In only ≈10% of the cases, the effective dose was >20 mSv. Similar variations were found by Rassow *et al.* [21] who reported effective doses varying from ≈2 mSv (25th percentile) to ≈18 mSv (90th percentile) in infants. The same authors state that at least 50% of the effective dose was due to cineangiography. Schueler *et al.* [10] calculated that cine made up 44% of the total exposure. Results from both studies are confirmed in our study, in which a median of 69% and 45% of the effective dose was attributed to cineangiography for diagnostic and therapeutic procedures, respectively. In both diagnostic and therapeutic

procedures, the lateral and frontal tube exposures each contributed ≈50% to the total effective dose. An excellent correlation between the effective dose and the DAP was found (r=0.95), indicating that using a simple conversion coefficient (mSv/cGycm^2) to estimate effective dose is an acceptable way to calculate effective doses. Even when raw DAP data (without additional corrections) are used, the correlation remains good (r=0.87). Hence, a DAP meter is suitable for online estimation of the effective dose with good accuracy.

Using the risk factors from the multiplicative model of the ICRP [19], we calculated an overall median risk of 0.08% (range, 0.007% to 0.481%). Because of the large variations in effective doses, no significant difference in risk could be shown between therapeutic and diagnostic procedures. The overall correlation between radiation risk and patient age was poor (r=0.22). However, a much higher median risk estimate was found for patients 0 to 1 year of age (0.10%) compared with patients 2 to 5 years (0.08%) and 6 to 10 years (0.05%) of age. Similar conclusions were presented by Rassow *et al.* [21], who found a significant increase in effective dose with decreasing age.

Because effective doses in pediatric cardiac catheterizations are high, dose reduction techniques should be applied to keep the dose as low as reasonably achievable and to reduce the radiation risks. Today, several techniques are available to decrease radiation exposure. Techniques that do not deteriorate image quality are of particular interest.

The introduction of pulsed fluoroscopy in the late 1980s resulted in a reduction in the radiation exposure rate of 30% to 50% [10]. In addition, the use of increased x-ray tube filtration removes lower-energy x-ray photons from the beam, thus reducing the amount of x-rays absorbed by the patient. In the present study, the dose-saving effect of an extra 0.2 mm copper beam filtration was demonstrated. With this low-dose fluoroscopy, a significant reduction in the fluoroscopy dose was measured. The overall effect was an effective dose reduction of 18%. Contrast-detail analysis showed that this dose reduction was not detrimental to image quality.

Similar results were obtained by Baldazzi *et al.* [9], who used a foil of 0.1 mm of gadolinium. In their experimental setting, a mean reduction in effective dose/frame of 14% was reported while image quality was maintained. Other attempts to reduce the radiation dose such as the use of digital zooming (acquisition zoom) also resulted in a dose reduction. However, a significant deterioration in image quality was observed with this technology [17].

In conclusion, skin doses are not problematic in pediatric interventional cardiology, but the calculated effective doses are as high as those for adult interventional cardiology, resulting in higher radiation risks. Therefore, it is important to monitor the patient dose by DAP instrumentation and to use additional beam filtration to keep the effective dose as low as possible in view of the age-related sensitivity of pediatric patients. Being a simple quantity, DAP readings can easily be included in patient records, especially those of young patients. The cumulative DAP (and hence effective dose) can be useful in decisions on the clinical management of the patient in case of follow-up examinations. Moreover, diagnostic reference levels of DAP could be useful for keeping the dose as low as possible and would be very valuable in training new interventional cardiologists.

References

1. den Boer A, de Feijter PJ, Serruys PW, *et al.* Real-time quantification and display of skin radiation during coronary angiography and intervention. Circulation. 2001;104:1779 –1784.
2. Bakalyar DM, Castellani MD, Safian RD. Radiation exposure to patients undergoing diagnostic and interventional cardiac procedures. Cathet Cardiovasc Diagn. 1997;42:121–125.
3. Lobotessi H, Karoussou A, Neofotistou V, *et al.* Effective dose to a patient undergoing coronary angiography. Radiat Prot Dosimetry. 2001; 94:173–176.
4. Vaño E, Arranz L, Sastre JM, *et al.* Dosimetric and radiation protection considerations based on some cases of patient skin injuries in interventional cardiology. Br J Radiol. 1998;71:510 –516.
5. Van de Putte S, Verhaegen F, Taeymans Y, *et al.* Correlation of patient skin doses in cardiac interventional radiology with dose-area product. Br J Radiol. 2000;73:504 –513.
6. US Food and Drug Administration. Avoidance of serious X-ray-induced skin injuries to patients during fluoroscopically-guided procedures. Med Bull. 1994;24:7–17.
7. Fletcher DW, Miller DL, Balter S, *et al.* Comparison of four techniques to estimate radiation dose to skin during angiographic and interventional radiology procedures. J Vasc Interv Radiol. 2002;13:391–397.
8. European Community Council Directive 97/43Euratom of 30 June 1997 on health protection of individuals against the dangers of ionising radiation in relation to medical exposure. Off J. 1997;L180:22–27.
9. Baldazzi G, Corazza I, Rossi PL, *et al.* In vivo effectiveness of gadolinium filter for paediatric cardiac angiography in terms of image qualityand radiation exposure. Phys Med. 2002;18:109 –113.
10. Schueler BA, Julsrud PR, Gray JE, *et al.* Radiation exposure and efficacy of exposure-reduction techniques during cardiac catheterization in children. Am J Roentgenol. 1994;162:173–177.
11. Allen HD, Driscoll DJ, Fricker FJ, *et al.* Guidelines for pediatric therapeutic cardiac catheterization: a statement for health professionals from the Committee on Congenital

Cardiac Defects of the Council on Cardiovascular Disease in the Young, the American Heart Association. Circulation. 1991;84:2248 –2258.

12. Boothroyd A, McDonald E, Moores BM, *et al.* Radiation exposure to children during cardiac catheterization. Br J Radiol. 1997;70:180 –185. 13.
13. Martin EC, Arthur MA, Olson P, *et al.* Radiation exposure to the pediatric patient during cardiac catheterization and angiocardiography: emphasis on the thyroid gland. Circulation. 1981;64:153–158.
14. Waldman JD, Rummerfield PS, Gilpin EA, *et al.* Radiation exposure to the child during cardiac catheterization. Circulation. 1981;64:158 –163. 15.
15. Li LB, Kai M, Kusama T. Radiation exposure to patients during paediatric cardiac catheterization. Radiat Prot Dosimetry. 2001;94:323–327. 16.
16. Martin EC, Olson A. Radiation exposure to the paediatric patient from cardiac catheterization and angiocardiography. Br J Radiol. 1980;53: 100–106.
17. Ross RD, Joshi V, Carravallah DJ, *et al.* Reduced radiation during cardiac catheterization of infants using acquisition zoom technology. Am J Cardiol. 1997;79:691– 693.
18. Leibovic SJ, Fellows KE. Patient radiation exposure during pediatric cardiac catheterization. Cardiovasc Intervent Radiol. 1983;6:150 –153.
19. ICRP. Recommendations of the International Commission on Radiological Protection. Oxford, UK: Pergamon Press; 1991. Publication 60. 20.
20. Axelsson B, Khalil C, Lidegran M, *et al.* Estimating the effective dose to children undergoing heart investigations: a phantom study. Br J Radiol. 1999;72:378 –383.
21. Rassow J, Schmaltz AA, Hentrich F, *et al.* Effective doses to patients from paediatric cardiac catheterization. Br J Radiol. 2000;73:172–183.
22. Thijssen MAO, Bijkerk KR, van der Burght RJM. Manual Contrast- Detail Phantom CDRAD Type 2.0: Project Quality Assurance in Radiology. St Radboud, Netherlands: Department of Radiology, University Hospital Nijmegen; 1998.
23. Vaño E, Guibelalde E, Fernández JM, *et al.* Patient dosimetry in interventional radiology using slow films. Br J Radiol. 1997;70:195–200.
24. Briesmeister JF. MCNP: A General Monte Carlo N-Particle Transport Code. Los Alamos, NM; 1997. Version 4B, LA-16252-M.
25. Verhaegen F, Nahum AE, Van de Putte S, *et al.* Monte Carlo modeling of kV x-ray units. Phys Med Biol. 1999;44:1767–1789.
26. Iles WJ. The Computation of Bremsstrahlung X-Ray Spectra Over an Energy Range 15 keV to 300 keV. London, UK: NRPB: 1987. NRPB report R204.
27. Christy M, Eckerman KF. Specific Absorbed Fractions of Energy t various Ages from Internal Photon Sources. ORNL/TM-8381, Oak Ridge, Tenn: 1987
28. Rosenstein M. Organ Doses in Diagnostic Radiology. Washington, DC: US Department of Health, Education and Welfare, Bureau of Radiological Health; 1976. BRh Tech publication DA 76–8030.
29. Kerr GD, Eckerman KF. Neutron and photon fluence-to-dose conversion factors for active marrow of the skeleton. In: Proc. of the Fifth Symposium on Neutron Dosimetry; 1985; Luxembourg. Vol I, EUR 9762 EN, CEC.
30. UNSCEAR. Sources and effects of ionizing radiation: volume I, sources: annex D, medical radiation exposure. Report to the General Assembly of the United Nations; 2000; New York, NY.

3.5 Part V

Does digital flat detector technology tip the scale towards better image quality and reduced patient dose in interventional cardiology?

E. Bogaert[1] – K. Bacher[1] - R. Lapere[1] – H. Thierens[1]

[1]*Department of Medical Physics and Radiation Protection, Ghent University, Proeftuinstraat 86, Gent B-9000, Belgium.*

Accepted for publication in European Journal of Radiology, July 28, 2008

Abstract

As dynamic flat-panel detectors (FD) are introduced in interventional cardiology (IC), the relation between patient dose and Image Quality (IQ) needs to be reconsidered for this type of image receptor. On one hand this study investigates IQ of a FD system by means of a threshold contrast detail analysis and compares it to an image intensifier (II) system on a similar X-ray setup. On the other hand patient dose for coronary angiography (CA) procedures on both systems is compared by Dose-Area Product (DAP)-registration of a patient population. The comparative IQ study was performed for a range of entrance dose rates (EDR) covering the fluoroscopy and cinegraphy working mode. In addition the IQ investigation was extended to a similar study under Automatic Brightness Control (ABC). As well the systematic study of IQ as a function of EDR as the study performed under ABC point to a better IQ for FD in cinegraphy mode and no difference between both systems in fluoroscopy mode. The patient population study resulted in mean DAP values of 31 $Gycm^2$ (II system) and 33 $Gycm^2$ (FD system) ($p=0.68$) for CA procedures. As well total DAP as contributions of fluoroscopy and cinegraphy on both systems are not significantly different.
To conclude, we could state that profit was taken from the intrinsic better performance of the FD for cinegraphy mode in producing higher quality images in this mode but without any effect on patient dose for CA procedures.

Introduction

Ever since the use of X-rays in medical applications, equipment developers have aimed for new techniques and refinement for better image quality (IQ) for both static and dynamic examinations. Nowadays, flat detectors (FD) have gained field in both radiography and fluoroscopy, replacing screen-film combinations, digital storage phosphor systems or image intensifiers (II) (1-4). In comparison with conventional II, FDs have shown convincing advantages of better ergonomics with better patient access, lack of geometric distortion, little or no veiling glare, no vignetting, insensitivity to magnetic

fields and wider dynamic range (2, 3, 5, 6). However, questions regarding the capabilities of FD have not been answered completely, particularly as it pertains to IQ at low exposure levels. In interventional cardiology, real–time viewing of vascularisation of the heart and tiny devices such as stents and guidewires impose stringent requirements on the imaging techniques used. Up to now, IIs achieve essentially 'noiseless' gain at low exposure rates, due to their characteristics of high electronic brightness gain and minification gain (5). For FDs, on the other hand, system noise becomes a limiting factor in determining system performance at low exposure rates (7-9).

Within this scope the question for dose optimisation is complex but urgently demanding clarification. Investigations whether the introduction of FD technology into the cardiac laboratory will result in an increase in clinical IQ or improved dose efficiency compared to II systems, need to be performed. Literature data report on IQ assessment under automatic brightness control (ABC) circumstances by use of the Leeds TOR 18-FG phantom placed into the X-ray beam together with a certain amount of PMMA (Polymethyl Methacrylate) (10-12). Other studies calculate modulation transfer function (MTF), point spread function (PSF), signal-to-noise ratio (SNR), contrast-to-noise ratio (CNR), noise power spectra (NPS) or Detective Quantum Efficiency (DQE) (7, 13, 14) for digital detectors for fluoroscopy, cardiac implementation or radiography. However, this is the first study comparing IQ of an II based and a FD based cardiac system, assessed by four-alternative forced-choice measurement to find the threshold contrast-detail detectability.

The goal of this study was to compare the performance of a FD based cardiac X-ray system with a contemporary X-ray II system by assessment of IQ under equal exposure circumstances and under ABC in exposure ranges of clinical practice. At the same time we investigated whether the use of a FD system resulted in a higher sensitivity for fluoroscopy and cinegraphy mode and in a reduction in patient dose in clinical practice.

Materials and Methods

Imaging Systems

The II based and the FD based cardiac systems for this study were both Siemens Axiom Artis monoplane modalities, with ABC-function and three field sizes for magnification of the image. X-ray tube configuration and filtration were identical for both systems. Details are listed in Table 1.

Although the size indications for the large, medium and small imaging fields are different for both systems (compare e.g. 23 cm with 25 cm), the dimensions of the corresponding actual radiation fields are the same. Measurement of the (diagonal) diameter of the radiation fields, as presented in Table 1 was performed using 33x41-cm Kodak X-Omat V films (Eastman Kodak) at the receptor entrance plane at reference distance (100 cm) from the focus. The explanation for the different figures for indication of the imaging fields lies in the geometry of the image receptors: circular for II and rectangular for FD. Manufacturers indicate the actual visible field diameter (diagonal) and for II, this diameter is smaller than for FD due to loss of image information at the corners of the circular field.

Table 1. Measurement of the diameter of radiation field at the entrance plane of the image intensifier and the flat detector.

	Large field	**Medium field**	**Small field**
II system	25.9	20.0	15.5
FD system	24.7	20.1	15.7

The II of the conventional system contains CCD-technology for digitalisation of the image. The FD of the more recent system is of the indirect amorphous silicon (a-Si) type, consisting of an active matrix size of 960 x 960 pixels, with a pixel size of 184 μm (Trixell, Moirans, France). Conversion of the energy of the X-ray photons into light occurs in a scintillation phosphor layer consisting of a CsI:Tl needle-shape crystalline structure. The light photons are subsequently detected by pixel photodiodes on a thin film transistor (TFT) array and stored in the form of electronic charge in the capacitors associated with each pixel. Extensive description of FD systems of the indirect (and the direct) conversion type can be found elsewhere (2, 3, 5).

In order to compare IQ in a correct way, the same magnification factor for image capture and storage is necessary. To this end a grid positioned at the isocentre of the system was used. An arbitrary distance on the grid was compared with the distance measured at the monitor in the catheterization room. A magnification factor of 2.78 and 2.73 for medium field size was obtained for the II system and the FD system respectively, which is a satisfactory result.

Test object details and images

IQ was evaluated using the commercially available CDRAD 2.0 contrast-detail phantom (Instrumentale Dienst, Nijmegen, The Netherlands (15)). This phantom is designed to perform four-alternative forced-choice measurements (4-AFC). The advantage of this method is that there is no need for the observer to set any subjective thresholds as is the case with e.g. the Leeds TOR 18-FG phantom (16). Moreover, with 4-AFC the detection errors by the observer are controlled by the correction scheme described in the manual of the test object (15). Nevertheless, as in all psychophysical measurements, variations among observers cannot be neglected (17). For averaging purposes, each image was scored by five independent readers. Based on these measurements, contrast-detail curves are obtained, reflecting the visibility limitations by the noise properties of the imaging system. A numerical value, the inverse Image Quality Figure (IQF_{inv}) can be calculated as the sum of the products of hole depth and hole diameter for the objects in the phantom at the limit of visualisation.

Scoring of the images was performed for both II and FD systems on the same monitor, a 19" TFT-LCD Avidav monitor (Jetway Computer Corporation, USA). For this scoring the freely available medical viewer software ezDICOM (18) was used, allowing dynamical presentation of all runs. Use was made of the 'Contrast Autobalance' function, meaning that readers were not allowed to change window and level of the images. Scoring was performed in a darkened room and no restrictions were implied on viewing distance or viewing time.

Image Quality measurements

The first set of measurements concerned IQ evaluation by IQF_{inv} determination of both II and FD systems for a range of EDR used in clinical practice. For this study a tube potential setting of 70 kV and a fixed filtration of 0.2 mm Cu at small focus were chosen on both imaging systems (Table 2). Image receptor EDR was gradually increased from 23 nGy/p up to 240 nGy/p (manufacturer settings). A phantom of 20 cm PMMA (with the CDRAD 2.0 phantom in the middle) was used to simulate the patient. Measurements were performed at a reference distance of 100 cm from source to image receptor entrance plane. The distance between exit of the phantom and the image receptor housing was kept 5 cm, in order to simulate clinical practice. All measurements were performed for the medium field size. All images were recorded and phantom EDR was measured with a standard

60cc ionisation chamber (Radcal Corporation, Monrovia, USA) for each radiation setting chosen.

Table 2. Exposure parameters during phantom (20 cm PMMA) measurements in cinegraphy and fluoroscopy mode at 15 f/s and large focus, under automatic brightness control for II- and FD-system.

	field size (cm)	tube potential (kV)	tube current (mA)	additional filtration (mmCu)	pulse duration (ms)	phantom entrance dose rate (mGy/min)
Cinegraphy mode						
II-system	23	65	800	0.3	6.4	60.1
	17	68	703	0.1	6.2	130.4
	13	74	800	0.1	6.4	176.3
FD-system	25	65	715	0.2	7.8	81.1
	20	68	692	0.2	7.6	102.3
	16	68	800	0.2	8.0	132.5
Fluoroscopy mode						
II-system	23	70	50	0.2	9.1	11.0
	17	68	92	0.3	13.3	16.7
	13	73	100	0.2	12.4	28.2
FD-system	25	67	158	0.6	13.5	12.2
	20	67	156	0.6	13.2	18.4
	16	69	170	0.6	13.8	20.1

A second set of measurements was performed to provide a numerical value for the IQ under ABC settings, for the three different field sizes by IQF_{inv} determination. This means that different X-ray spectra were generated according to the ABC settings of the systems. The X-ray systems were set to their default clinical values and EDR was measured. Exposure parameters are summarized in Table 3. Images of the CDRAD 2.0 phantom, positioned in between two layers of 9.5 cm PMMA (resulting in a total thickness of 20 cm PMMA) were registered and scored afterwards by the same five readers of the first set of measurements.

Table 3. Exposure parameters for imaging of CDRAD 2.0 test object for increasing phantom entrance dose rate (mGy/min) for medium field, 15 f/s, additional filtration of 0.2 mm Cu and small focus.

tube potential (kV)	tube current (mA)	pulse duration (ms)	phantom entrance dose rate (mGy/min)
II-system			
70	67	9.1	13.5
70	106	11.2	26.1
70	138	12.4	37.2
70	160	13.1	45.7
69	305	9.2	60.6
76	332	9.6	79.9
83	254	8.9	91.6
FD-system			
70	80	7.8	14.2
70	109	9.0	22.3
70	127	9.7	27.7
70	145	10.3	33.3
70	163	11.0	39.7
66	361	10.0	67.7
72	373	10.0	92.4
79	324	9.7	106.8

Patient dose measurements

Patient dose measurements consisted of real-time DAP registration during diagnostic cardiac interventions (CA) performed on both systems. In order to avoid large variations in procedure protocol, therapeutic procedures as Percutaneous Transluminal Coronary Angioplasty (PTCA) were not included in the study. The same team of cardiologists and nursing staff operated at both imaging systems, to minimize variation in clinical protocol.

Eighteen procedures were followed on the II system, while this number was 26 for the FD system. The average age of the patients was 66y (range: 35y - 86y) for the II system and 67y (range: 44y - 83y) for the FD system. Both populations had an average weight of 73 kg (II: range 55 kg – 100 kg and FD: range 55kg – 88kg). This indicates that there was no bias with respect to patient population characteristics. DAP was registered for fluoroscopy and

cinegraphy mode separately, allowing us to investigate the contributions of both modes. For each run, exposure parameters (tube potential, tube current and filtration) and tube angulations were also registered.

Statistical analysis

Statistical significance of differences between the two digital systems was assessed with the two-factor analysis of variance (ANOVA) using system-type (II or FD) and hole depth as independent variables and the observed threshold diameter as dependent variable.

For DAP patient data analysis a non-parametric two-tailed Mann-Whitney test was performed. Correlations between groups were calculated by means of the non-parametric Spearman's rank correlation coefficient (r). To calculate the regression coefficients in the relation between two quantities, linear regression analysis was performed using the Levenberg-Marquardt algorithm.

In all statistical analyses a confidence interval of 95% was applied. Hence, a p-value < 0.05 was considered as significant. All statistical tests were performed with a statistical application package (S-PLUS software – Insightful Corporation, Seattle, WA, USA).

Results

Assessment of IQ was performed by calculation of IQF_{inv}, based on the scoring of images of the CDRAD 2.0 test object. Figure 1 shows the relation between IQF_{inv} and the EDR at the 20 cm PMMA phantom, with the CDRAD 2.0 test object in the middle, resulting from the first set up of measurements. The error bars represent the standard deviations between the scores of the five independent readers. A linear regression curve was plotted for both systems. The dose rate at the entrance of the phantom ranged from 14 mGy/min to 107 mGy/min (Table 2). When we compare these values with the settings selected by the ABC system for a phantom of total thickness of 20 cm PMMA presented in Table 3, we notice that the EDR range of the data is clinically relevant both for fluoroscopy and cinegraphy mode.

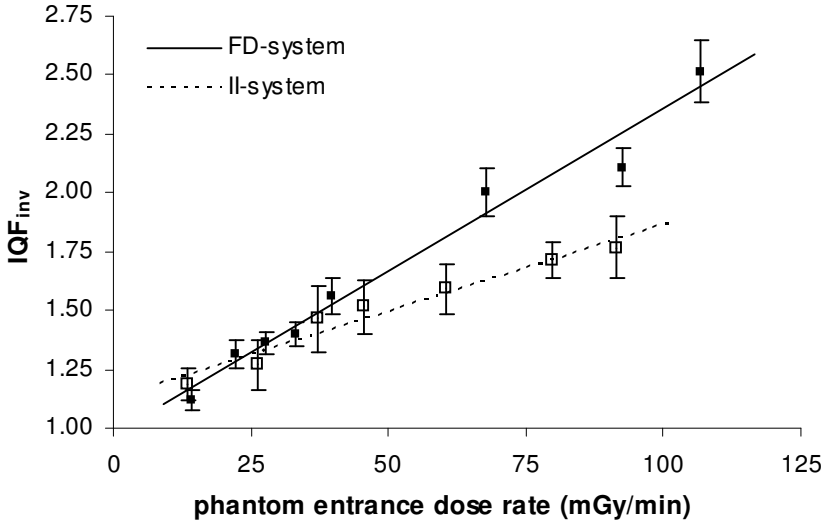

Figure 1. Image Quality Figure inverse (IQF_{inv}) versus phantom entrance dose rate (mGy/min) for medium field size at the II and the FD system, for a radiation quality of 70 kV with 0.2 mm Cu filtration.

Figures 2 and 3 compare contrast-detail curves representing phantom threshold hole diameter versus hole depth for equivalent phantom EDR used in fluoroscopy and cinegraphy mode. This type of curves is used to deduce the IQF_{inv} values represented in Figure 1. The curves were obtained at the following phantom EDR values: 37.2 mGy/min (II) and 39.7 mGy/min (FD) for fluoroscopy mode (Figure 2) and 91.6 mGy/min (II) and 92.4 mGy/min (FD) for cinegraphy mode (Figure 3). Error bars correspond again to the standard deviations between the results of the readers.

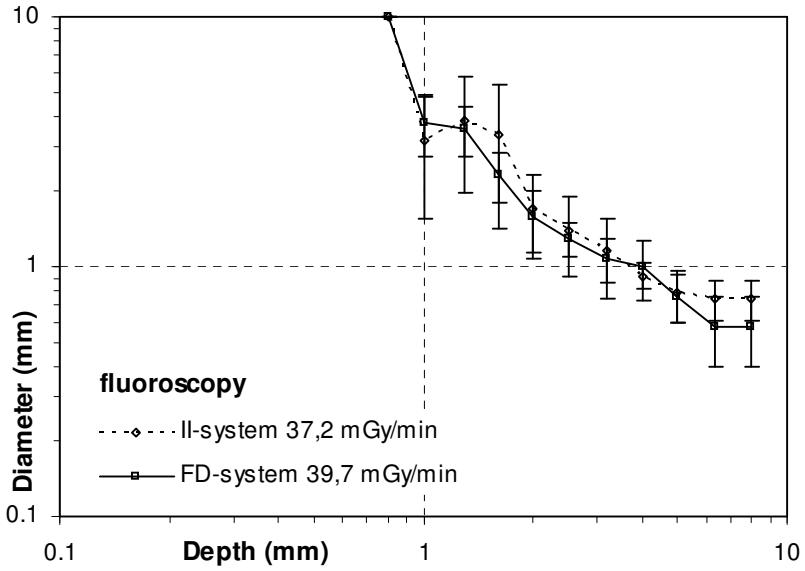

Figure 2. Contrast-detail curves for the II and FD system for equivalent phantom entrance dose rates used in fluoroscopy mode.

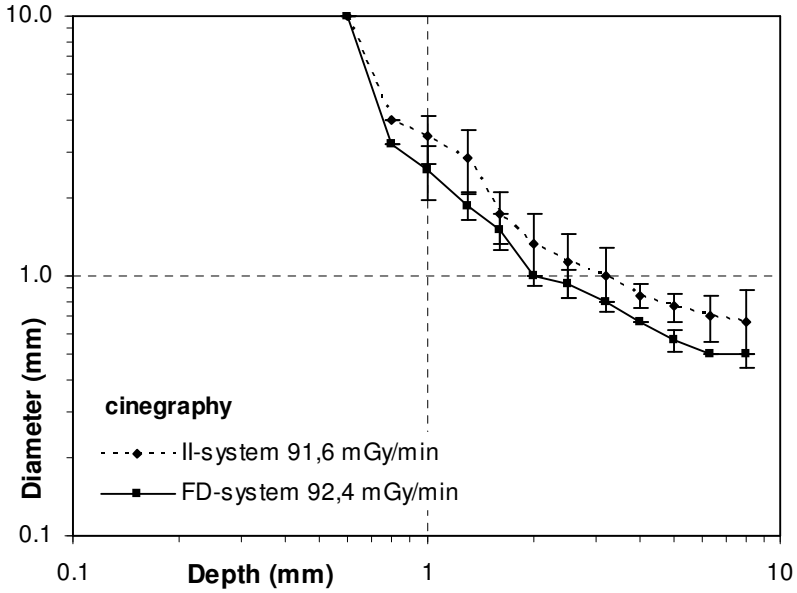

Figure 3. Contrast-detail curves for the II and FD system for equivalent phantom entrance dose rates used in cinegraphy mode.

Application of the clinically used ABC of both systems for imaging of the test object, resulted in IQF_{inv} values shown in Figure 4. Exposure conditions for these images in both fluoroscopy and cinegraphy mode can be found in Table 3. A difference in additional filtration and tube current can be attributed to differences in ABC settings of both systems. However, with respect to dose-settings, the image receptor EDR was programmed to be 170 nGy/p in cinegraphy mode for both systems. For fluoroscopy mode, the ABC settings for dose were 36 nGy/p for the FD system and 32 nGy/p for the II system. This implies other filtration, tube potential, tube current and pulse duration restrictions to produce the same (or equivalent) image receptor EDR. Figures 1-4 support a better image quality for the FD system at EDR values used in cinegraphy mode while not statistically significant differences were observed at low EDR values typical for fluoroscopy.

The DAP data obtained from the patient dose measurements are summarized in Figure 5. A comparison of DAP histograms for diagnostic procedures followed on both systems allows an assessment of image receptor influence on patient dose. For the DAP histogram reconstruction an interval op 25 $Gycm^2$ was used. Mean DAP values of 31 $Gycm^2$ and 33 $Gycm^2$ were obtained for the II and FD system respectively, resulting in no statistically significant difference in patient dose between the two systems ($p=0.68$).

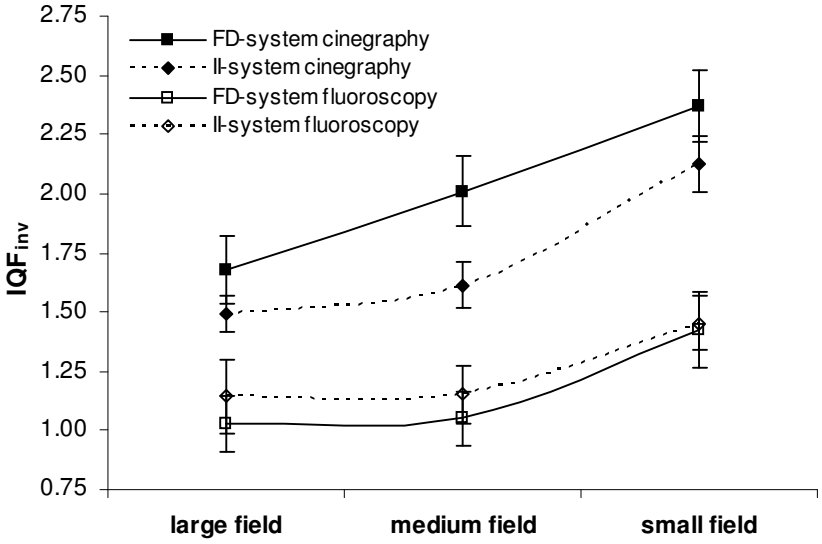

Figure 4. Image Quality Figure inverse (IQF_{inv}) versus field size for the II and the FD system, for fluoroscopy and cinegraphy mode. Images were taken under Automatic Brightness Control (ABC).

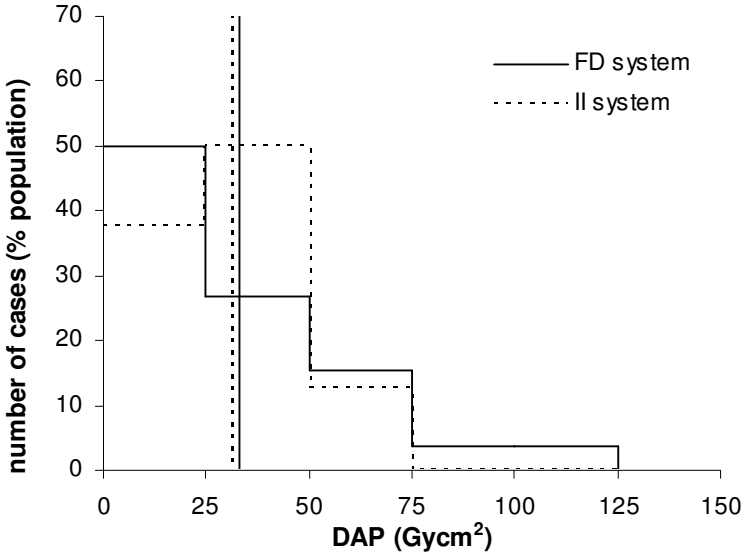

Figure 5. Distribution of patient DAP values for diagnostic coronary angiography procedures, performed with the II system (dashed line) and FD system (full line). Mean values are indicated by vertical lines.

Discussion

A first set of measurements focussed on image receptor performance as a function of increasing phantom EDR (Figure 1). The same X-ray radiation quality, tube current, field size and frame rate were used to visualize the CDRAD 2.0 test object either on II or FD. A linear relationship (r=0.99 for FD and r=0.98 for II) between EDR and IQF_{inv} was obtained for both systems, in accordance with the characteristic linear response curve for FD (4). The left-lower part of the graph with EDR ranging from 10 to 35 mGy/min, is representative for fluoroscopy mode which is supported by the EDR values obtained under ABC conditions in this study (Table 3). Similar EDR values were used in comparative studies between II and FD for fluoroscopy also on a Siemens Axiom Artis system: 22 mGy/min by Vaño *et al.* (11) and 9 mGy/min by Nickoloff *et al.* (19). The right-upper part of Figure 1, with rates ranging up to 107 mGy/min is representative for cinegraphy mode. Under ABC-conditions EDR values of 102 mGy/min and 130 mGy/min were measured for medium size field for this mode (Table 3). The higher EDR values in the ABC study can be explained by the fact that a large focus is programmed in ABC settings according to clinical protocol while a small focus is applied in service mode of the equipment used for the IQF_{inv} versus EDR study. Vaño *et al.* (11) used EDR values of 151 and 86 mGy/min in cinegraphy mode studies with Siemens Axiom Artis II and FD systems respectively, while Nickoloff *et al.* (19) applied 53 mGy/min in a similar study. Figure 1 shows very clearly that within the EDR fluoroscopy range IQF_{inv} of FD does not differ significantly from that of II. On the other hand, for the higher EDR range corresponding to cinegraphy mode the FD system shows a significantly better IQF_{inv} than the II system. As within the frame of measurements all exposure parameters were the same, the higher IQF_{inv} values reflect the intrinsic better imaging performance of FD with respect to II when higher EDR are considered (cinegraphy mode). Figures 2 and 3, representing a comparison of the contrast-detail curves of the II and FD systems for typical fluoroscopy and cinegraphy EDR values, also support these observations. Figure 2 shows overlapping curves for fluoroscopy mode resulting in a p-value of 0.56 for system dependency for an EDR of 37.2 mGy/min (II) and 39.7 mGy/min (FD). Thus, no difference in imaging performance between II or FD technology in the fluoroscopy mode is observed. On the contrary, the situation is notably different in the cinegraphy mode. The comparison of contrast-detail curves results in a p-value of 0.001 for EDR of 91.6 mGy/min (II) and 92.4 mGy/min (FD) supporting significance in technology dependency for IQ, with advantage for the FD system. From Figure 3 we can conclude that the gain in IQ for the FD system compared to the II system is due to both better contrast and

better resolution, reflected by the entire shift of the FD contrast-detail curve towards the lower left corner of the graph.

The IQ conclusions of present study based on phantom measurements are in agreement with reports regarding DQE(f) (f : spatial frequency lp/mm) (7, 14, 20). For high exposures in the cinegraphy range (80 to 400 nGy – entrance dose per pulse at image receptor), the DQE(0) is superior for the FD systems while in the fluoroscopy range (5 – 80 nGy) DQE(0) values of FD and II are overlapping. For II the DQE(0) remains almost constant over the whole exposure range covered in fluoroscopy and cinegraphy while for FD the DQE(0) increases steadily for receptor entrance doses from 1 to 100 nGy. The low DQE(0) of FD for low dose is a consequence of the low SNR of low dose images.

Based on the results obtained in the first set of measurements we could expect a better dose-IQ relationship for the FD system, in cinegraphy mode. This means that in cinegraphy mode the same IQ as for the II system could be obtained for lower dose settings, resulting in a net patient dose reduction. To investigate whether exposure parameters of the system were optimised towards dose reduction or towards better IQ we performed a contrast-detail study under ABC - settings for both modes and for different field sizes (Figure 4). From this figure, a better IQ for smaller fields and for cinegraphy compared to fluoroscopy is apparent. For the fluoroscopy mode, data do not reveal a significant difference in IQ between FD and II ($p=0.26$). On the contrary a statistically significant better IQ for the FD system is observed in the cinegraphy mode ($p=0.02$). Together with a same EDR (at image receptor) of 170 nGy/p programmed for both the II and FD system, this shows that the dose versus IQ relationship was not optimised towards dose reduction. Rather profit was taken from the intrinsic better performance of the FD for cinegraphy mode to produce images of higher quality for similar entrance doses.

Finally, DAP measurements were performed in order to investigate the influence of FD technology on patient dose in clinical practice. Mean values of 31 $Gycm^2$ (II system) and 33 $Gycm^2$ (FD system), are in agreement with previously published values for both conventional and digital technology: mean values of 31.2 $Gycm^2$ (II) and 33.4 $Gycm^2$ (FD) were reported by Trianni *et al.* (10) and median values of 30 $Gycm^2$ (II) and 31 $Gycm^2$ (FD) reported by Tsapaki *et al.* (12). The measurements (Figure 5) could not reveal a significant dose reduction by introduction of the FD system ($p=0.68$). Analysis of the DAP data according to the fluoroscopy and cinegraphy contribution did also not highlight a difference in patient dose ($p=0.15$ and 0.82). Similar findings were reported by Tasapaki *et al.* (12) and Trianni *et al.*

(10). None of them could show a significant patient dose reduction for neither FD nor II technology. Combining the patient dose results with the phantom IQ measurements we can state that for procedures performed on patients in daily practice, a better IQ is obtained with the FD system in cinegraphy mode. This better IQ is appreciated by the cardiologists but apparently does not lead towards dose reduction by e.g. a decrease in procedure exposure time. This would have become clear in reduced DAP values, which was not the case.

Whereas in cinegraphy an optimisation towards dose reduction is possible with the use of FD technology, this is not directly the case for fluoroscopy. To this end further evolution of FD technology is necessary by reducing system noise for low exposures.

Conclusions

Image Quality related to the introduction of FD in interventional cardiology, has been evaluated and compared to the IQ of an II imaging system in a similar X-ray set up. At low exposure rates used in fluoroscopy, no significant difference in IQ was found. Contrarily, at high exposure rates used in cinegraphy a remarkably (statistically significant) better IQ could be attributed to the presence of FD imaging technology. Mean DAP values, as estimates for patient dose, resulted to be the same for diagnostic (CA) procedures performed on either the FD system or the II system. No differences were noted not even when the fluoroscopy or the cinegraphy contribution was considered separately. The implementation of FD imaging technology was appreciated by the cardiologists for better IQ in cinegraphy mode, but did not involve a lowering of patient dose. Optimisation of ABC towards lower patient dose is possible in cinegraphy mode. In fluoroscopy mode further evolution of FD technology with respect to system noise at low exposure rates is necessary to improve IQ and/or reduce patient dose.

Acknowledgements

The authors wish to thank all cardiologists and nursing staff of the Maria Middelares hospital in Ghent. Mr. M. Acket and Mrs. S. Verschuere of Sint-Jan hospital in Brugge. Mr. J. Dermaut, Mr. M. Terriere and Mrs. I. Van Driessche of Siemens, Medical Solutions Belgium are acknowledged for their technical support during measurements. Ms. A. de Crop and Ms. L.Eloot are thanked for their help with scoring CDRAD 2.0 images.

References

1. Noel A, Thibault F. Digital detectors for mammography: the technical challenges. European Radiology. 2004;14(11):1990-8.
2. Holmes DR, Laskey WK, Wondrow MA, Cusma JT. Flat-panel detectors in the cardiac catheterization laboratory: Revolution or evolution - What are the issues? Catheterization and Cardiovascular Interventions. 2004;63(3):324-30.
3. Spahn M. Flat detectors and their clinical applications. European Radiology. 2005;15(9):1934-47.
4. Granfors PR, Aufrichtig R. Performance of a 41X41-cm(2) amorphous silicon flat panel x-ray detector for radiographic imaging applications. Medical Physics. 2000;27(6):1324-31.
5. Seibert JA. Flat-panel detectors: how much better are they? Pediatric Radiology. 2006;36:173-81.
6. Davies GA, Cowen AR, Kengyelics SM, Moore J, U. SM. Do flat detector cardiac X-ray systems convey advantages over image-intensifier-based systems? Study comparing X-ray dose and image quality. European Radiology. 2007;17:1787-94.
7. Antonuk LE, Jee KW, El-Mohri Y, *et al.* Strategies to improve the signal and noise performance of active matrix, flat-panel imagers for diagnostic x-ray applications. Medical Physics. 2000;27(2):289-306.
8. Maolinbay M, El-Mohri Y, Antonuk LE, *et al.* Additive noise properties of active matrix flat-panel imagers. Medical Physics. 2000;27(8):1841-54.
9. Moy JP. Recent developments in X-ray imaging detectors. Nuclear Instruments & Methods in Physics Research Section a-Accelerators Spectrometers Detectors and Associated Equipment. 2000;442(1-3):26-37.
10. [Trianni A, Bernardi G, Padovani R. Are new technologies always reducing patient doses in cardiac procedures? Radiat Prot Dosim. 2006;117(1-3):97-101.
11. Vano E, Geiger B, Schreiner A, Back C, Beissel J. Dynamic flat panel detector versus image intensifier in cardiac imaging: dose and image quality. Phys Med Biol. 2005;50(23):5731-42.
12. Tsapaki V, Kottou S, Kollaros N, *et al.* Dose performance evaluation of a charge coupled device and a flat-panel digital fluoroscopy system recently installed in an interventional cardiology laboratory. Radiat Prot Dosim. 2004;111(3):297-304.
13. Busse F, Rütten W, Sandkamp B, *et al.* Design and performance of a high-quality cardiac flat detector. Proc SPIE. 2002;4682:819-27.
14. Bruijns T, Bastiaens R, Hoornaert B, *et al.* Image Quality of a Large Area Dynamic Flat Detecor: Comparison with a sate-of-the-art II/TV system. Proc SPIE. 2002;4682:332-43.
15. Thijssen MAO, Bijkerk KR, van der Burght RJM. Manual Contrast-Detail Phantom CDRAD Type 2.0: Project Quality Assurance in Radiology (Department of Radiology, University Hospital Nijmegen, St.-Radboud, The Netherlands). 1998.
16. Tapiovaara MJ, Sandborg M. How should low-contrast detail detectability be measured in fluoroscopy? Medical Physics. 2004;31(9):2564-76.
17. Burgess AE. Comparison of receiver operating characteristic and forced-choice observer performance-measurement methods. Medical Physics. 1995;22(5):643-55.
18. ezDICOM software available at http://www.sph.sc.edu/comd/rorden/ezdicom.html.

19. Nickoloff EL, Lu ZF, Dutta A, *et al.* Influence of flat-panel fluoroscopic equipment variables on cardiac radiation doses. Cardiovascular and Interventional Radiology. 2007;30(2):169-76.

20. Granfors PR, Aufrichtig R, Possin GE, *et al.* Performance of a 41X41 cm(2) amorphous silicon flat panel x-ray detector designed for angiographic and R&F imaging applications. Medical Physics. 2003;30(10):2715-26.

Chapter 4

General discussion and conclusions

4.1 IC: Importance and population

Catheterization of coronary arteries, shortly denoted by IC in medicine, is highly appreciated for its non-invasive character in comparison to surgery and because it is fast, straightforward and safe. Both adults and children can benefit of the technique, most frequently for diagnosis and/or treatment of CAD and CHD respectively. Annual numbers (2004) of around 4000 diagnostic CA procedures per million inhabitants and around 1500 PTCA interventions per million inhabitants are still increasing [5]. Statistics regarding IC in Belgium (2005) documented in MIRA-T report show a number of two to three procedures (diagnostic and therapeutic) per 1000 inhabitants [1].

As viewing of the coronary arteries is performed through dynamic x-ray imaging the radiation burden to the patient can be important. The procedures belong to those involving 'high doses' to patients [7-9] and the effects of these possibly high doses were classified by the ICRP and the ICRU into deterministic (short-term) and stochastic (long-term). Considering deterministic effects, the skin is the most exposed tissue and in 1994, the Food and Drug Administration (FDA) called attention on the problem of radiation burden to the skin in an advisory that later appeared on its website [7]. In the year 2000, Koenig *et al.* reported more than 70 cases of skin injuries [53, 55]. With respect to late term effects, it is mostly the youngest generation i.e. the paediatric population that is of highest risk. Due to their larger radiosensitivity and the longer post-exposure life expectance, possible radiation induced sequelae are more likely to occur. Moreover, about 7% of all cardiac angiography procedures are carried out in children 0 to 15 years of age [36]. Paediatric procedures may even involve longer fluoroscopy

times than adult interventions, because of higher heart rates, smaller cardiovascular structures and smaller body size [15, 46].

4.2 Direct skin effects: discussion of nine cases with Maximum Skin Dose > 2 Gy

As reported in ***Publication 1***, MSD in nine cases exceeded 2 Gy, which is the threshold level for onset of transient erythema, appearing a few hours after irradiation [51, 53]. For two of them, the maximum measured TLD value was not the MSD, received by the patient, because of missing parts of the reconstructed peak. This means that MSD is higher than measured.

Table 6. Summary of the cases for which the maximal skin dose exceeded 2 Gy

N°	Proce-dure	MSD (Gy)	Angle MSD (°)	gender	Cardio-logist	DAP ($Gycm^2$)	contrib of fluoro to MSD (%)	Contrib of cine to MSD (%)
1	D	2.1	100	F	Ass+Doc	194	57	43
2	T	2.5	-44	M	Ass	298	30	70
3	T	2.4	66	M	Vis+Doc	154	77	23
4	T	3.1	-47	M	Doc	153	40	30
5	T	2.3	-15	M	Doc	131	27	73
6	T	3.2	14	F	Ass+Vis	404	95	5
7	T	3.4	45	M	Vis+Doc	315	98	2
8	T	4.5	95	M	Doc	257	89	11
9	D	2.6	94	F	Vis	191	79	21

(D = Diagnostic, T = Therapeutic; Ass = Doctor-Assistant, Vis. = Visitor, Doc. = Doctor-Cardiologist)

A summarised description of these cases is given in Table 6. Whether the procedure was diagnostic (D) or therapeutic (T), the MSD (Gy), the angle under which the MSD was measured (degrees), gender of the patient, the professional status of the cardiologist, DAP ($Gy.cm^2$) and contribution of cinegraphy and fluoroscopy to the contribution of DAP in the geometry that caused the MSD, are listed. The cardiologist is specified as Assistant (Ass), when he/she is in training. Visitor (Vis) represents a cardiologist who catheterises a limited amount of days a week and Doctor (Doc) is an experienced cardiologist. Therapeutic procedures were all 'combined procedures' which means that a diagnostic examination preceded a

therapeutic intervention, except for case 2, where the procedure was a merely therapeutic intervention. Mostly a supervising doctor performs the therapeutic part (especially when the case turns out to be difficult) after the diagnostic examination, performed by the assistant doctor or the visiting-doctor.

The contributions of fluoroscopy and cinegraphy in terms of percentage to the DAP that was registered for the geometry that caused the MSD, show that for 5 of the 9 cases fluoroscopy mode was obviously responsible for the highly measured peak in skin dose. A detailed description for each of the cases is given below.

Body Mass Index (BMI) was also calculated for the patients. Table 7 gives classification with respect to BMI.

Table 7. Classification of BMI index

BMI	Classification
BMI < 18.5	Underweight
18.5 < BMI< 25	Optimal body weight
BMI > 25	Overweight
BMI > 30	Obese

4.2.1 Case 1

A diagnostic procedure (coronary angiography, CA) was performed by a doctor-assistant, supervised by an experienced cardiologist on a biplane system and was classified as difficult because of the use of 3 different catheters in order to find the right coronary. The patient was a 79 years old woman of normal weight (BMI = 23). The procedure contained 10 cinegraphy-runs, simultaneous on the two x-ray tubes of the system, with an average cinegraphy radiation time (time that the doctor pushed the treadle) of 7.5 seconds and at a frame rate of 12.5 frames per second. This means that all cinegraphy-runs were taken simultaneously with frontal and lateral tube. This is equivalent to 20 cinegraphy runs on a monoplane system. For one cinegraphy-run a frame rate of 25 frames per second was taken (for both frontal and lateral tube), when a ventriculogram was registered. The pulse rate for fluoroscopy mode was 12.5 pulses per second. The II imaging field was switched between 23 and 17 cm for both frontal and lateral tube. The MSD was 2.1 Gy and was measured in lateral position due to the tube geometry of the lateral tube (LAO90, CAUD1) (Figure 17). The Source to Image Receptor Distance (SID) was rather large at that projection: 115 cm. A

rather large distance between patient's skin and II was observed, whereas the distance from the x-ray tube focus to patient's skin was rather small. The contribution of fluoroscopy to DAP, registered for the projection LAO90, CAUD1 was slightly more than the contribution of cinegraphy. Five cinegraphy-runs were taken at that projection (57% versus 43 %). With respect to the filtration used in fluoroscopy mode, fluoroscopy 'normal' filtration setting was used, which implies an additional filtration of 0.3 mm Cu (with an inherent filtration of 2.5 mm Al). This setting was selected by the cardiologist.

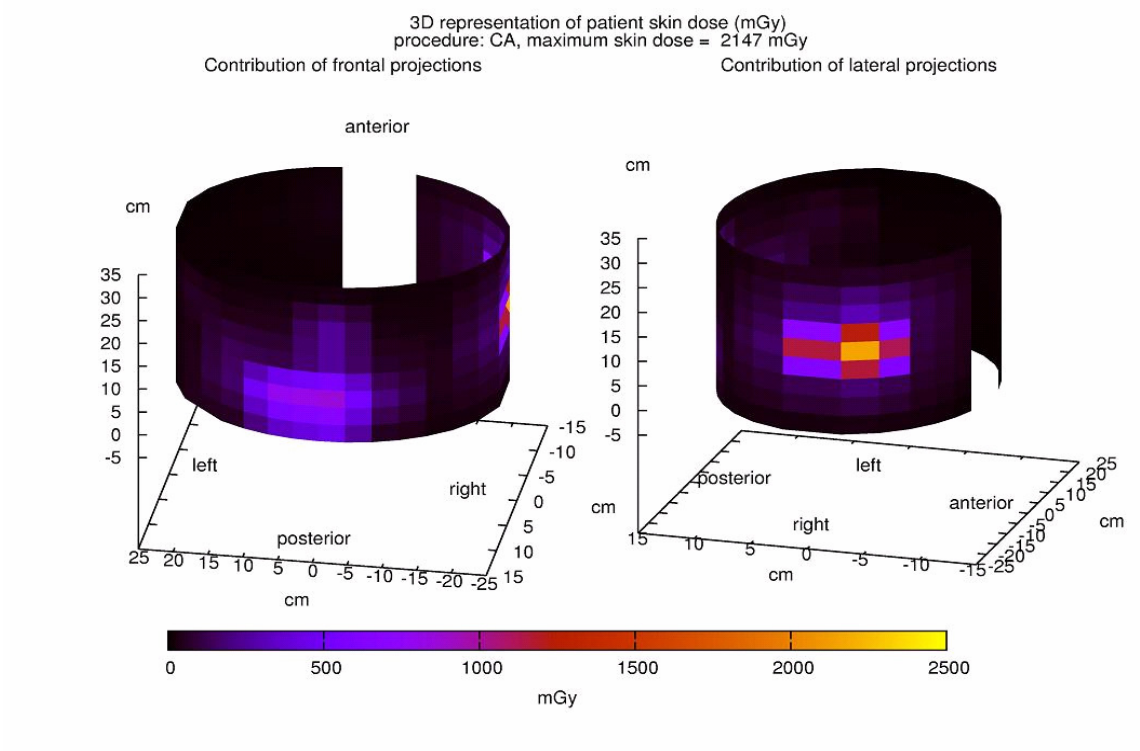

Figure 19. Three-dimensional representation of skin dose distribution for case 1.

4.2.2 Case 2

A therapeutic procedure (PTCA + direct or primary stenting) was performed by a doctor-assistant on a biplane system and was classified as difficult because of difficult positioning of balloon- and stent-catheters. The patient was a 52 years old obese man (BMI = 30). The procedure contained 14 cinegraphy-runs, simultaneous on the two x-ray tubes of the system, with an average cinegraphy radiation time (time that the doctor pushed the treadle) of 8 seconds and at a frame rate of 12.5 frames per second. This means that all cinegraphy-runs were taken simultaneously with frontal and lateral tube which is equivalent to 28 cinegraphy runs on a monoplane system. The pulse rate for fluoroscopy mode was 12.5 pulses per second. The II imaging field was kept on 17 cm for both frontal and lateral tube. Two pairs of peaks

were visible in the distribution (Figure 18). One pair could be attributed to the combined geometry of frontal and lateral tube in the following projections: RAO25, CAUD30 for the frontal tube and LAO35, CAUD30 for the lateral tube. These projections were both responsible for the 2 hot spots in patient's skin dose distribution, observed at the upper side on the wrap-around, which means near to patient's neck. This position can be explained by the highly caudal directions (CAUD30) used. Both hot spots reached the value of 2.5 Gy, representing the 9 cinegraphy-runs that were taken in the frontal projection and the 8 cinegraphy-runs in the lateral position of this biplane geometry. The reason that cinegraphy is mostly responsible for this MSD lies in the predominate contribution of cinegraphy to the DAP-values of these projections. (70% for the frontal projection and 93% for the lateral projection). The filtration for cinegraphy is 2.5 mm Al as inherent filtration without any additional filters. The filtration of fluoroscopy mode used is an additional filtration of 0.3 mm Cu with an inherent tube-filtration of 2.5 mm Al, which corresponds to fluoroscopy 'normal' filtration setting of that x-ray equipment. This setting was selected by the cardiologist. The SID was rather large at the frontal and lateral projection (114 cm and 109 cm) and a rather large distance between patient's skin and II was observed.

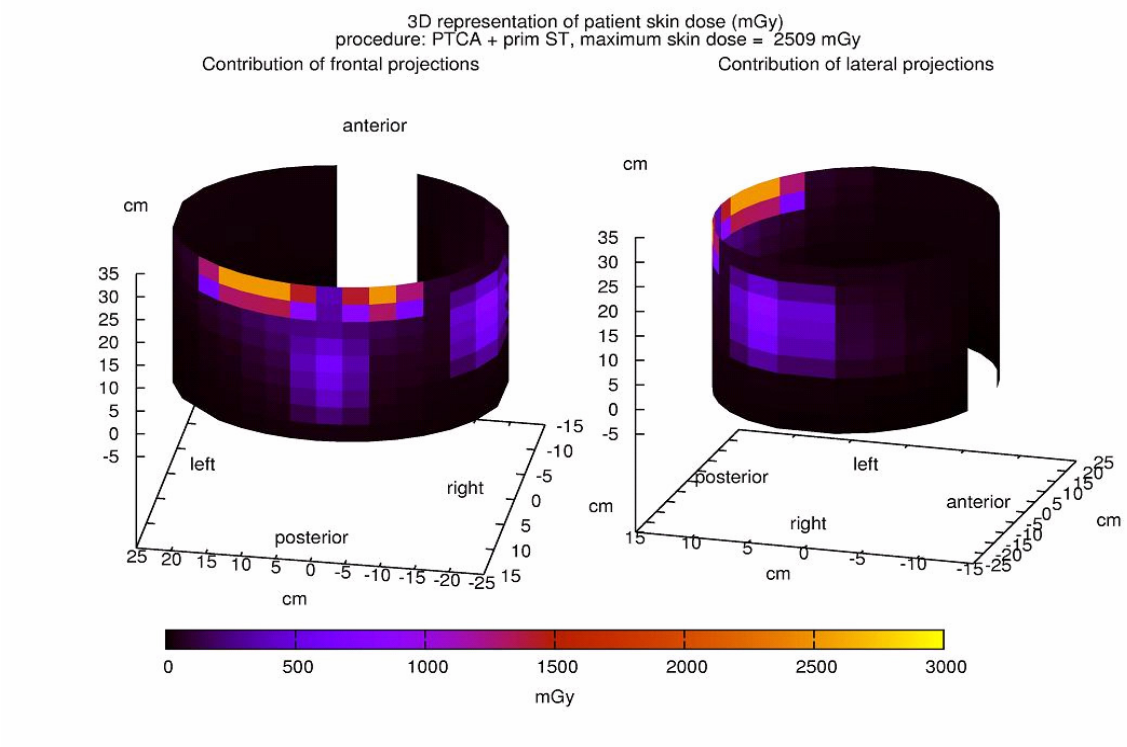

Figure 20. Three-dimensional representation of skin dose distribution for case 2.

A second pair of peaks could be attributed to the combined geometry of frontal and lateral tube in the projections RAO9, CRAN14 and LAO61, CAUD3. Here, 5 and 6 runs were taken in the frontal and respectively lateral projection of the biplane geometry. Both peak-values were measured below 1 Gy.

4.2.3 Case 3

A therapeutic procedure (RL-CA+PTCA+(PTCA-ST)) was performed by a visiting doctor and an experienced doctor on a monoplane system. A RL-CA (right-left catheterization) procedure, which is a measurement of the pressure in lung blood vessels, coronary arteries and the heart chambers, followed by a coronary catheterization, was performed by the visiting cardiologist. An experienced cardiologist did the therapeutic intervention. This procedure was classified as difficult because of difficult positioning of the balloon-catheters, trying different catheterising techniques. Two different lesions had to be treated. The patient was a 74 year old overweight man (BMI = 29). The procedure contained 34 cinegraphy-runs, a frame rate of 12.5 frames per second. No information was available on the number of frames taken per cinegraphy-run. The pulse rate for fluoroscopy mode was 12.5 pulses per second. The II field was switched between 17 for the diagnostic part (23 cm for the ventriculography) and 13 cm for the therapeutic part of the intervention. The MSD was 2.4 Gy and was measured in left anterior oblique position due to the following tube geometry LAO41, CAUD4 (Figure 19). The SID had a normal value for this projection: 100 cm. The contribution of fluoroscopy to DAP, registered for this projection was predominate (77% versus 23% for contribution of cinegraphy). Sixteen cinegraphy runs were taken at that projection. With respect to the filtration used in fluoroscopy mode, an additional filtration of 0.2 mm Cu (with an inherent filtration of 2.5 mm Al) was selected by the x-ray system. No additional filtration (Cu) and an inherent filtration of 2.5 mm Al was selected by the system for cinegraphy mode.

A second, much lower (skin dose <1 Gy) peak was measured at a projection of LAO45, CRAN19, which means at the right corner of the first, most important peak. This peak was also caused by fluoroscopy (93 % versus 7%).

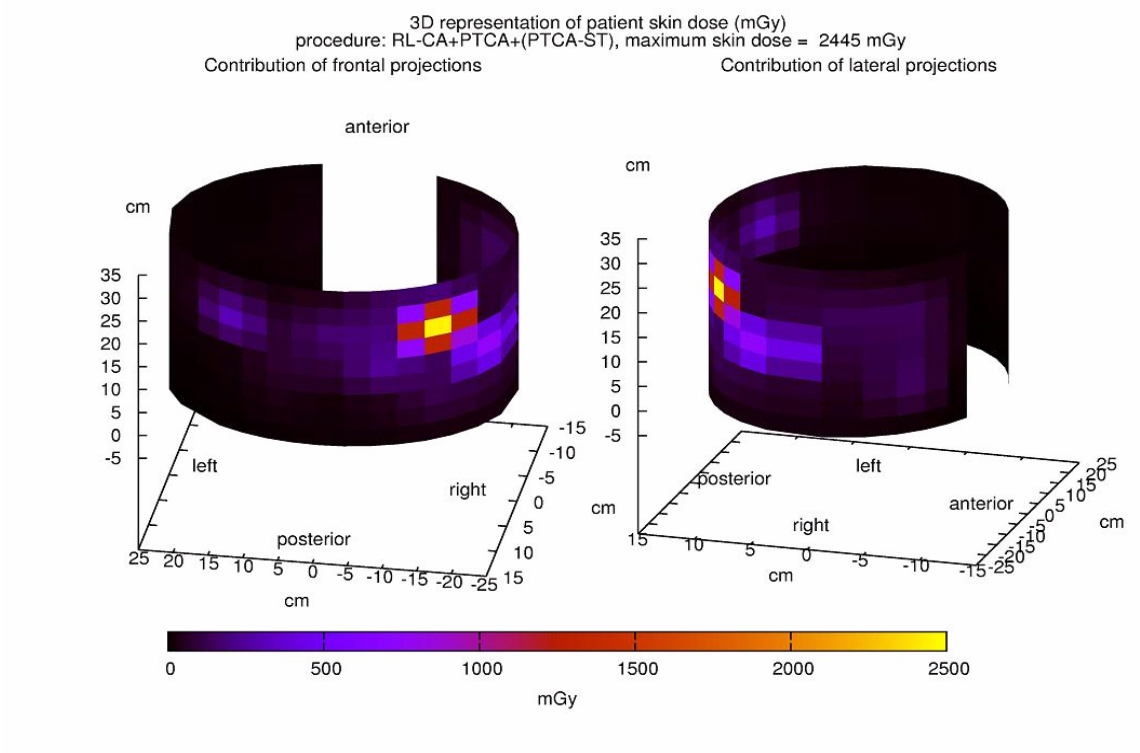

Figure 21. Three-dimensional representation of skin dose distribution for case 3.

4.2.4 Case 4

A therapeutic procedure (CA-PTCA) was performed by an experienced doctor on a monoplane system and was classified as difficult because of difficult positioning of the 3 different balloon-catheters, without any result. None of them passed the lesion. The patient was a 57 year old man of normal weight (BMI = 24). The procedure contained 26 cinegraphy-runs, with an average cinegraphy radiation time (time that the doctor pushed the treadle) of 9.1 seconds and at a frame rate of 12.5 frames per second. One cinegraphy-run had a duration of 50 sec (628 images), due to overheating of the x-ray tube. The x-ray tube switched in safety mode, which implies a restriction of the mode to cinegraphy, even when pushing the fluoroscopy treadle. The cardiologist was not aware of the consequences of the overheated x-ray tube. The median value of cinegraphy radiation time for this procedure was 6.6 seconds. The pulse rate for fluoroscopy mode was 12.5 pulses per second. The filtration used in this mode was 3.5 mm Al (of which 2.5 mm Al is inherent tube filtration) with an additional filtration of 0.4 mm Cu. This corresponds to the fluoroscopy 'low' filtration setting for this x-ray equipment. This setting was selected by the cardiologist. There was no additional filtration used in cinegraphy mode (2.5 mm Al inherent). The FD imaging field was kept on 20 cm. The MSD observed was 3.1 Gy and

was measured in right anterior oblique position due to the following tube geometry: RAO11, CAUD24 (Figure 20). Twelve cinegraphy runs were taken at this projection. The SID was of normal value at this projection: 104 cm. The contribution of cinegraphy to DAP, registered for this projection, was slightly more than the contribution of fluoroscopy (60 % versus 40 %), due to the cinegraphy in the safety mode of the x-ray equipment, meant to be fluoroscopy.

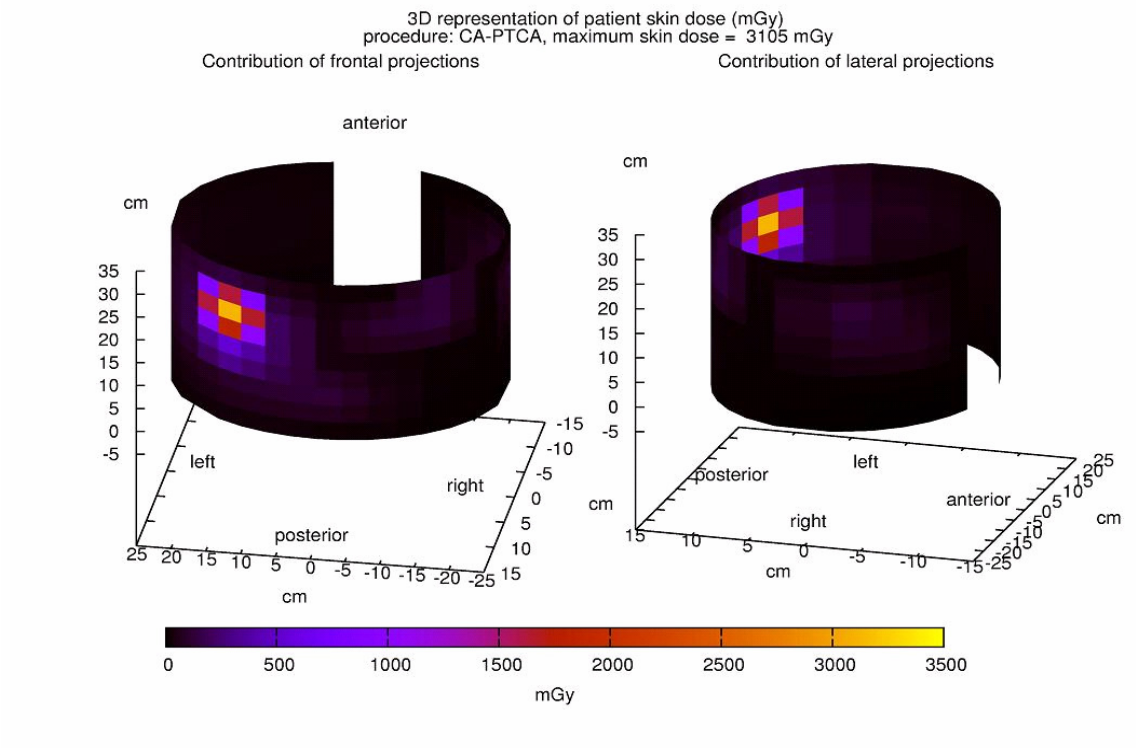

Figure 22. Three-dimensional representation of skin dose distribution for case 4.

4.2.5 Case 5

A therapeutic procedure (CA+PTCA+(PTCA-ST)) was performed by an experienced doctor on a monoplane system and was classified as difficult because of difficult positioning of the balloon-catheters at a lesion located at a bifurcation. One balloon thorn open after one inflation, and thus another had to be positioned. Secondly, a busy nurse passed by mistake a catheter of wrong shape/size to the cardiologist. The patient was a 61 year old obese man (BMI = 32). The procedure contained 31 cinegraphy-runs, with an average cinegraphy radiation time (time that the doctor pushed the treadle) of 6.8 seconds and at a frame rate of 12.5 frames per second.

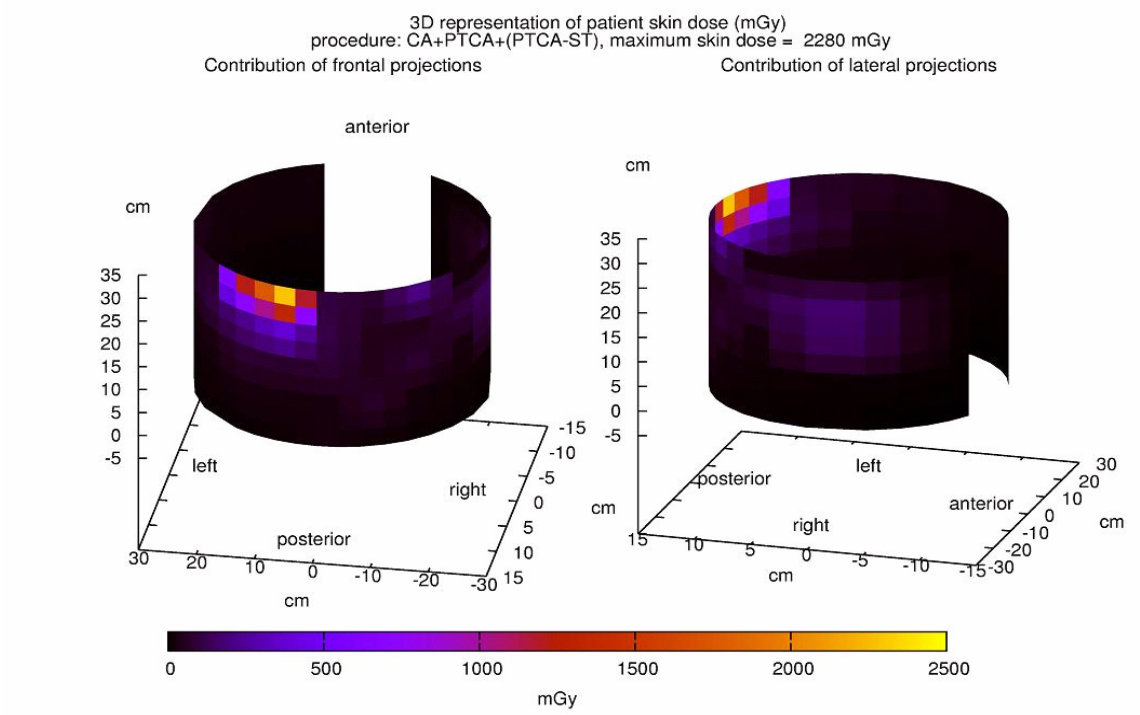

Figure 23. Three-dimensional representation of skin dose distribution for case 5.

There was a good application of the 1-frame function installed on the x-ray equipment. By selection of this setting, only one frame is taken as an image when pushing the treadle. This setting is suitable for making calibration-images for calculation of cardiac ejection fraction from ventriculography. The pulse rate for fluoroscopy mode was 12.5 pulses per second. The filtration used in this mode was 3.5 mm Al (of which 2.5 mm Al is inherent tube filtration) with an additional filtration of 0.4 mm Cu. This corresponds to the fluoroscopy 'low' filtration setting for that x-ray equipment. This setting was selected by the cardiologist. There was no additional filtration used in cinegraphy mode (2.5 mm Al inherent). The FD imaging field was kept on 25 cm for the diagnostic part of the procedure and on 20 cm for the therapeutic intervention. The MSD was 2.3 Gy and was measured in right anterior oblique position due to the following tube geometry RAO22, CAUD22 (Figure 21). This peak was marked at the upper side on the wrap-around, which means near to patient's neck. This can be explained by the rather high caudal directions (CAUD22) used. The SID was of normal value at that projection: 101 cm. The contribution of cinegraphy to DAP, registered for this projection, was predominate 73 % versus 40 % contribution of fluoroscopy to DAP for that projection. The plot of the skin dose distribution shows that the MSD-peak was not fully measured. The value of 2.3 Gy was registered on the increasing side of the peak, which means that the actual MSD can even be higher.

4.2.6 Case 6

A therapeutic procedure (CA-PTCA-ST) was performed by a doctor-assistant and a visiting doctor on a monoplane system. The CA was done by the cardiologist in training. The therapeutic intervention was done by the visiting cardiologist. This procedure was classified as difficult because of trying to position an aspirator-tool, without any result and with alternative of PTCA and stenting. The patient was a 72 year old woman suffering from obesity (BMI = 47). The procedure contained 25 cinegraphy-runs, at a frame rate of 12.5 frames per second (except 25 frames per second for the ventriculography), with an average duration of cinegraphy-runs of 4.8 seconds. The pulse rate for fluoroscopy mode was 12.5 pulses per second. The II imaging field was kept on 17 cm during the whole intervention (except for 23 cm for the ventriculography). The MSD was 3.2 Gy, with neighbouring values of 2.4 and 1.2 Gy and was measured in a vertically spread out AP position due to fluoroscopy mode (Figure 22). The SID was of normal value at this projection: 100 cm. The contribution of fluoroscopy to DAP, registered for this projection was predominate 95%). Five cinegraphy runs were taken at this projection.

With respect to the filtration used in fluoroscopy mode, no additional filtration with an inherent filtration of 2.5 mm Al was used, corresponding to the filtration setting fluoroscopy 'high'. Image Quality at this x-ray equipment was found to be insufficient at low dose fluoroscopy mode. Fluoroscopy 'high' mode was set as 'default' value for clinical practice, but could, however, be changed when judged necessary. No additional filtration (Cu) and an inherent filtration of 2.5 mm Al was used for cinegraphy mode.

A second, lower skin dose peak with value of 1.4 Gy was measured at a projection of LAO31, CAUD0. Fourteen cinegraphy runs were taken at this position, with a relative contribution of cinegraphy to DAP in this projection of 58%.

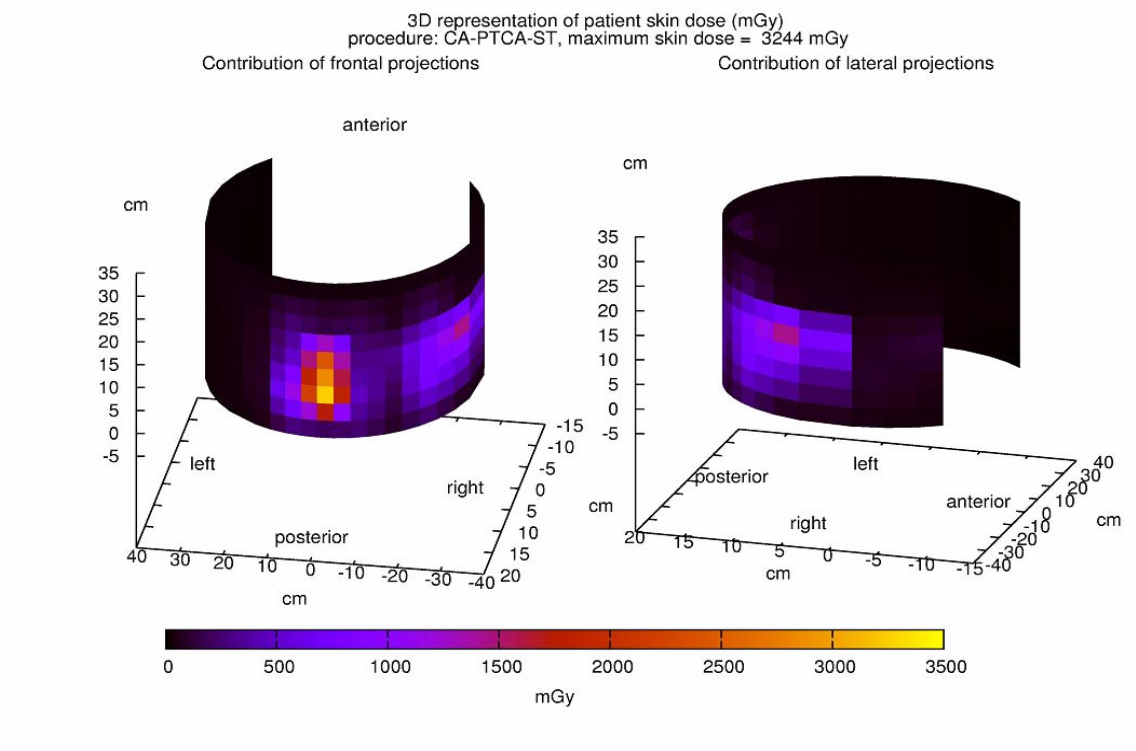

Figure 24. Three dimensional representation of skin dose distribution for case 6.

4.2.7 Case 7

A therapeutic procedure (CA-PTCA) was performed by a visiting doctor and an experienced cardiologist on a monoplane system. The CA was done by the visiting cardiologist. The therapeutic intervention was done by the experienced cardiologist. This procedure was classified as difficult because of a difficult lesion: 90% stenosis at a bifurcation. The patient was a 76 year old overweight man (BMI = 27). The procedure contained 18 cinegraphy-runs, at a frame rate of 12.5 frames per second (except 25 frames per second for the ventriculography), with an average duration of cinegraphy-runs of 3.7 seconds. The pulse rate for fluoroscopy mode was 12.5 pulses per second. The II imaging field was kept on 17 cm during the diagnostic part of the intervention (except for 23 cm for the ventriculography) and was switched between 23 cm, 17 cm and 14 cm for the therapeutic part.

The MSD was 3.4 Gy, with a long tail in a spread out AP and left anterior oblique projection in cranial direction (LAO0, CRAN30 to LAO40, CRAN30), containing values below 1 Gy, due to fluoroscopy mode (98% of fluoroscopy to DAP contribution) (Figure 23). The SID was of normal value at that projection: 100 cm. The cardiologist used collimation and used different geometries during fluoroscopy. The II was kept close to the patient.

Notwithstanding the fact that good practice was applied, high doses were measured. Five cinegraphy runs were taken at that projection. With respect to the filtration used in fluoroscopy mode, no additional filtration with an inherent filtration of 2.5 mm Al was used, corresponding to the filtration setting fluoroscopy 'high'. Image Quality at this x-ray equipment was found to be insufficient at low dose fluoroscopy mode. Fluoroscopy 'high' mode was set as 'default' value for clinical practice, but could, however, be changed when judged necessary. No additional filtration (Cu) and an inherent filtration of 2.5 mm Al was used for cinegraphy mode.

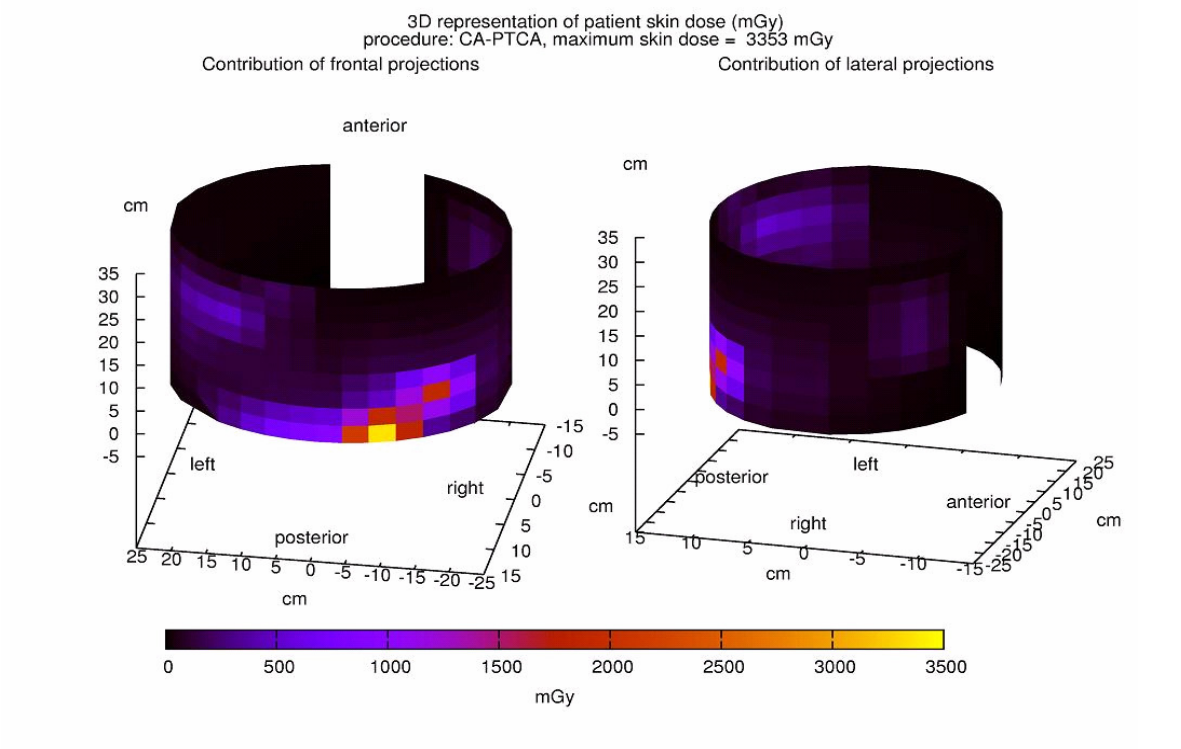

Figure 25. Three dimensional representation of skin dose distribution for case 7.

A second skin dose peak with value of 1.9 Gy was measured at a projection of LAO50, CAUD0. Three cinegraphy runs were taken at this position, with a relative contribution of cinegraphy to DAP in this projection of 78%. The plot of the skin dose distribution shows that the MSD-peak was not fully measured. The value of 3.4 Gy was registered on the increasing side of the peak, which means that the actual MSD can be assessed to be a value even higher.

4.2.8 Case 8

A therapeutic procedure (CA-2(PTCA-ST)+primST) was performed by an experienced cardiologist and on a monoplane system. This procedure was classified as difficult because of multiple difficult lesions. During PTCA and stenting, different subsequent inflations were performed. The patient was an 84 year old man of normal weight (BMI = 23). The procedure contained 45 cinegraphy-runs, at a frame rate of 15 frames per second (except 30 frames per second for the ventriculography), with an average duration of cinegraphy-runs of 2.8 seconds. The pulse rate for fluoroscopy mode was 15 pulses per second. The FD field was kept on 20 cm during the whole intervention. The MSD was 4.5 Gy, with a neighbouring value of 3.7 Gy at lateral projection (LAO90, CAUD0). The SID was of normal value at that projection: 104 cm. Twenty-four cinegraphy runs were taken at the projection corresponding to MSD of 4.5 Gy (Figure 24). With respect to the filtration used in fluoroscopy mode, the system chose filtration according to variable filtration settings: no additional Cu-filtration or an additional Cu-filtration of 0.1, 0.2, 0.3, 0.6 mm with an inherent filtration of 2.5 mm Al was used. Variable additional filtration (0, 0.1, 0.2, 0.3 mm Cu) was chosen by the system (with an inherent filtration of 2.5 mm Al) for cinegraphy mode. The contribution of fluoroscopy to DAP, registered for this projection was predominate. (89% versus 11% for contribution of cinegraphy)

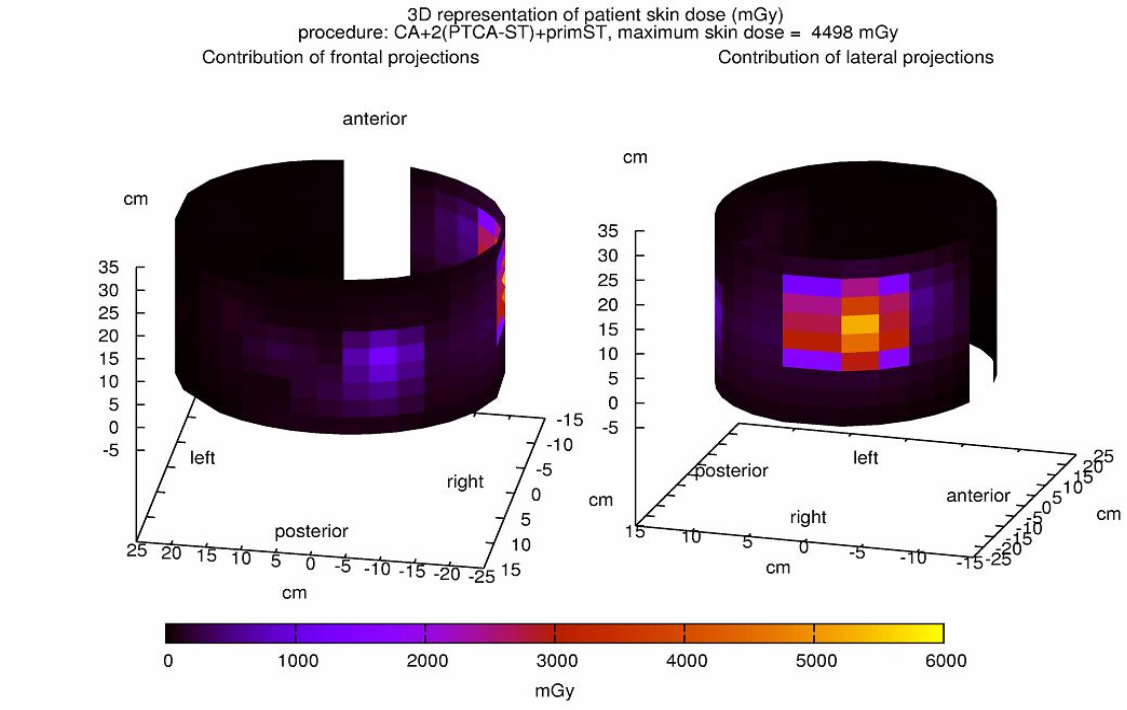

Figure 26. Three-dimensional representation of skin dose distribution for case 8.

A second spread out skin dose spot with peak value of 1.2 Gy was measured at a spread out left anterior oblique projection of LAO30-40, CRAN0-16. Twelve cinegraphy runs were taken at this position, with a relative contribution of fluoroscopy to DAP in this projection of 72%.

4.2.9 Case 9

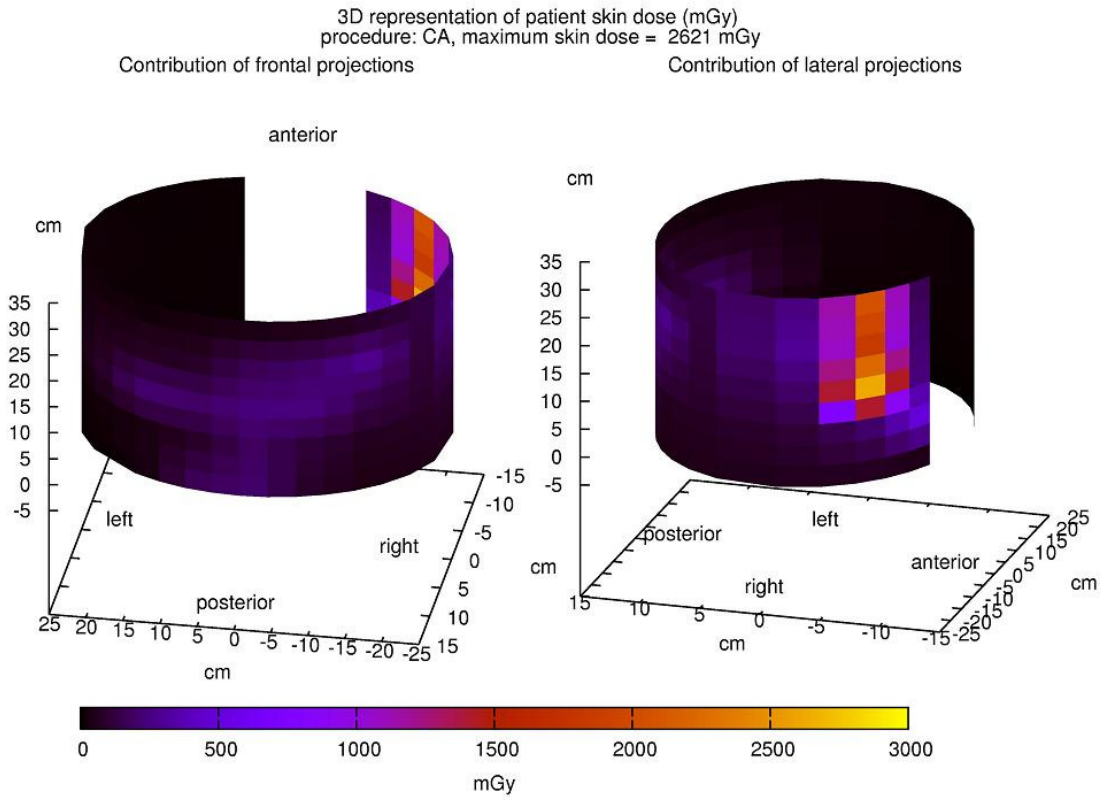

Figure 27. Three-dimensional representation of skin dose distribution for case 9.

A diagnostic procedure (CA) was performed by an experienced cardiologist and on a monoplane system. This procedure was classified as difficult because of the use of various catheters in order to find the right coronary artery. The patient was a 73 year old woman, suffering from obesity (BMI = 31). The procedure contained 21 cinegraphy-runs, at a frame rate of 15 frames per second (except 30 frames per second for the ventriculography), with an average duration of cinegraphy-runs of 5.6 seconds. The pulse rate for fluoroscopy mode was 15 pulses per second. The FD imaging field was kept on 20 cm during the whole intervention (except for the ventriculography where the II field had a size of 25 cm). The MSD was 2.6

Gy, at lateral projection (LAO90, CAUD0) (Figure 25). The SID was rather large at that projection: 111 cm. A rather large distance between patient's skin and FD was observed, whereas the distance from the x-ray tube focus to patient's skin was rather small. Twenty-one cinegraphy runs were taken at that projection. With respect to the filtration used in fluoroscopy mode, the system chose a filtration according to variable filtration settings: no additional Cu-filtration or an additional Cu-filtration of 0.1, 0.2, 0.3, 0.6 mm with an inherent filtration of 2.5 mm Al. For cinegraphy mode, variable additional filtration (0, 0.1, 0.2, 0.3 mm Cu) was also chosen by the system (with an inherent filtration of 2.5 mm Al). The contribution of fluoroscopy to DAP, registered for this projection was predominate. (79% versus 21% for contribution of cinegraphy)

4.3 Direct skin effects: General discussion

The basis of radiographic imaging is the difference in attenuation of an incident x-ray beam, by the different tissues and contrast compounds. This inevitably causes absorbed dose in patient's tissues. The first 4.5 cm of the body removes half of the beam (measured in a water phantom, for beam characteristics of 75 kVp and 3 mm Al filtration); hence most of the deterministic damage is found in the superficial tissues, with the skin as most important and sensitive one [52].

As is clear from the introduction section, procedures in IC are likely to involve high skin doses [53, 55]. In previous section, the cases in present work with skin doses exceeding 2 Gy were described. 2 Gy is considered the threshold value for onset of transient erythema (ICRP60). Parameters with the strongest effect on high MSD-values in this work are:

- overweight of the patients (6 out of 9 patients with overweight, 3 of them even suffering from obesity)
- difficulty of the procedure (all procedures were scale '3' procedures)
- prolonged use of fluoroscopy mode (5 out of 9 cases presented a fluoroscopy contribution > 75%)
- fixed geometry for both fluoroscopy and cinegraphy
- large distance between patient and entrance plane of the IR (distances between 20 and 40 cm), related to a short distance of patient's skin to the x-ray tube

From this list, only the last two determinants can be actively controlled during a procedure. Body mass index of a patient and the fact that a procedure turns out difficult are unchangeable. The latter aspect influences at least partly fluoroscopy time. An extensive list of general dose-reducing techniques is given in paragraph 4.5. The proposed measures are in favour of decreased overall tissue dose, including skin. Taking these measures and the discussion above in mind, a cardiologist can optimise its catheterization technique in order to prevent increased skin damage. Furthermore, he will recognize with more ease procedures suspected to cause MSD > 2 Gy, so that necessary follow-up can be provided.

One aspect has not been taken into account in the discussion of this work: *influence of multiple procedures*. In most of the cases with radiodermatitis reported in literature, multiple (prolonged) procedures lie at the basis of the skin injury [53, 57-59, 62]. Therefore, resulting total value of MSD is reported to be a lot higher than 2 Gy. MSD values were estimated retrospectively from clinical outcome and nature of the injury and ranged from 2 to 10 Gy [62] to values as high as 20 Gy [59, 63]. It is of major importance that DAP values, and preferably interpreted in terms of DAP action levels, are included in patient's records. Patients often do not remember how many catheterization procedures they were submitted to. They often are not aware of the radiation burden involved with the procedure and they evidently cannot be aware of the magnitude of exposure of their individual examination if they are not told so. It is advised that from a certain number of procedures on, the personal physician of the patient is informed. Actual diagnosis of skin injuries is often difficult and initially missed because the problem generally presents two to three weeks following the causative exposure. Moreover a pronounced variability in onset time, clinical features and outcome are reported [57, 59]. Therefore, both the patient and the patient's physicians mostly do not correlate the developing skin lesion to the earlier radiation exposure [57, 58]. Some indications when examining the skin of patients, sometimes presenting with a painful cutaneous ulceration can help to identify radiodermatitis, induced by IC. The lesions are typically found in the (upper) back or at the right trunk side, under the axilla. Chest side or left trunk side practically do not appear as location for skin injury, related to IC. Sometimes lesions appear on the right upper arm, when procedures were performed careless, leaving the arms in the beam or when another reason prevented the arms to be removed from the primary beam. Radiation induced skin lesions also appear to be of well-defined shape, in accordance with the shape of the entrance beam. Moreover, the occurrence of 'spontaneous' ulceration in skin regions of atrophy and scarring is highly suggestive of radiodermatitis. Moreover, when local treatment to resolve

skin lesions is not successful and when excruciating pain persists at the lesion, the possibility of a chronic radiodermatitis should strongly be considered [58].

In more moderate cases, or for patients with a single only or restricted history of IC, erythema may occur very shortly after exposure, being a matter of hours or less and peaking at about 24 hours. Afterward it fades. Therefore, and for reason of being located at a location that is difficult to be seen by oneself, early and transient erythema probably pass by unnoticed in many cases.

Mean MSD values as reported in paragraph 3.1 (***publication 1***) are 0.3 Gy and 0.7 Gy, respectively for diagnostic and therapeutic procedures. It has to be recalled that therapeutic procedures comprise single or multiple PTCA with or without single or multiple stenting, single or plural direct stenting and combined procedures (diagnostic procedures). Median values, however, amounted to 0.2 and 0.5 Gy for diagnostic and therapeutic procedures respectively and indicating the influence of the large tail of the distribution (recall figure 3, paragraph 3.1, ***publication 1***). Lower and similar mean values for skin dose have been reported in literature: 0.3 Gy [89, 90], 0.1 Gy [91], 0.2 Gy [28] for diagnostic procedures and 0.8 Gy [65], 1 Gy [90] and 0.4 Gy [62] for therapeutic procedures. It has to be mentioned that the lower values were measured only with a limited number of TLDs [62, 91].

The fact that the entire primary exposed skin was covered during measurements is of great value. By use of the grid of TLDs and the accompanied reconstruction of the skin dose distribution, we were sure to have included the maximum peak values for skin dose. In ***publication 1***, MSD was found to be significantly depending on procedure (diagnostic or therapeutic), variable filtration and difficulty of the procedure. Trends were visible according to the hospital where the procedures were performed, representing overall attention to radiation burden of the patient (catheterization methods and attitudes, equipment, …). Significance was not expressed, due to large variations in data distributions.

Skin entrance doses and peak dose values can be roughly estimated, using exposure parameters of the performed IC procedure. Research by Morell *et al.* [92] has lead towards a model for patient skin dose assessment in IC, based on data stored in DICOM headers. den Boer *et al.* described a novel modality-feature for real-time quantification and display of skin dose distribution [93]. However, these tools are not always available on x-ray equipment. Therefore, it is advised to make use of *DAP action levels*, as described in paragraph 3.1 (***publication 1***). Practically this means that if DAP

exceeds 125 Gycm^2 (assigned to a MSD value of 2 Gy), the entry site of the beam that is responsible for the highest skin dose should be included in patient's record. A possible follow-up of the patient for radiation skin effect is to the cardiologist's decision. In case DAP exceeds 250 Gycm^2, (assigned to a MSD value of 3 Gy), the patient and his personal physician should be informed on the possible radiation effects, and a systematic follow-up should be performed. This is of great concern in the patient population that needs recurrent catheterizations, with possibly the same projections as used on beforehand to visualise the lesion(s).

However DAP action levels are a very helpful tool in adult IC, the concept is not applicable in paediatric IC. As exposure geometry during paediatric IC procedures is not that variable as with adult cardiac catheterizations, one and the same skin area is more likely to be exposed. This is represented in a relative good correlation between DAP and MSD (chapter 3, Part IV, figure 3). In contradiction with adult cardiac catheterization where necessarily DAP action levels had to be derived due to a minor correlation between these two quantities, we can now simply use the MSD-DAP relation to predict on skin dose values. Doing so, a DAP value of 174 Gycm^2 would correspond with a MSD value of 2 Gy for the child's back (frontal tube). A DAP value of 97 Gycm^2 would equivalently correspond with a MSD value of 2 Gy at the armpit (lateral tube). With median cumulative DAP values of 4.5 Gycm^2 mentioned in chapter 3, Part IV, for a paediatric IC procedure, it is unlikely that the MSD threshold for transient erythema (2 Gy) is passed after one intervention. However, from the point of view of repeated procedures in young children, who receive easily four to five cardiac catheterizations in the first three years of their lives for treatment of one and the same lesion, total cumulative MSD may pass this 2 Gy threshold. Therefore it is certainly advised not only to interpret the recorded DAP values in patient's medical file in terms of long term effects but also in terms of possible deterministic skin effects. Thus, formulation of DAP action levels for a paediatric population interpretable for one single IC procedure, as is the case for adult cardiac catheterization, does not make sense. But, as said, storage and summation of cumulative DAP values over multiple procedures (preferably for frontal and lateral tubes separately) in patient's files is strongly recommended. Dermatological follow-up based on total cumulative DAP values of (rounded) 100 Gycm^2 (armpit) and/or 175 Gycm^2 (back) should be included in the clinical IC protocol.

4.4 Late effects and Dose Reference Levels (DRL)

Risks for late effects (cancer induction) are especially important for paediatric patients. As mentioned in paragraph 3.4 (***publication 4***), the risk for these effects for the paediatric population followed in the study amounts to 0.1% for the youngest patients (<1 year of age) to 0.05% for children between 6 and 10 years of age, with no significant difference between diagnostic and therapeutic examinations. The calculated risk in paragraph 3.2 (***publication 2***) amounted to 0.01 % for diagnostic and 0.02 % for therapeutic procedures for an adult population, meaning roughly a factor of 10. These estimations were based on the attributable life-time risk versus age from the ICRP report 60 [8]. The risk- values were obtained through patient-specific effective dose simulations by use of the software package MCNP. This patient-specific dose calculation is of great value, taking into account the large anatomical variations in body length and weight in young children (0-10 years in the study we performed). However, recently Smans *et al*. [94] showed that calculations for premature babies could also be performed using a downsized mathematical phantom (PCXMC).

A practical dose measure for risk estimation, which is in good correlation with E, is DAP. Paragraph 3.3 (***Publication 3***) derived CF for E calculation. There is a significant difference in CF for systems using additional Cu filtration in cinegraphy mode and systems that do not was noted. A CF of 0.207 mSv $Gy^{-1}cm^{-2}$ was derived for the first group and a factor of 0.177 mSv $Gy^{-1}cm^{-2}$ for the second group. The defining factor for this difference was not the radiation geometry of the standard clinical protocol in the different centres. The explanation was rather found in the beam hardening as a consequence of the additional filtration. This results in a higher E for the same DAP value.

Within practical interpretation of E as the multiplication of DAP and a conversion factor (CF):

$$E=CF*DAP,$$

both CF and DAP are influenced by the additional beam filtration. This additional filtration induces beam hardening but influences to a greater extend the photon fluence. Beam hardening implies an increase in conversion factor for the same DAP value, whereas a decrease of photon fluence means a direct decrease of DAP. Both effects will only partially compensate, resulting in a decrease in effective dose when additional Cu filtration is used. However, it should be stressed that the effect of additional filtration will mainly influence on ESD. Since the fractional reduction in

incident dose is greater than the fractional reduction in exit dose, when additional filtration is added, ESD will be reduced proportionally more than E.

In view of the *ALARA* principle, a constant review of mean dose values (and dose distribution) of patients who undergo high dose x-ray examinations is needed. Comparison of the local mean values with nationally proposed so-called 'reference doses', gives an idea about the ranking of the current practice in a hospital, with respect to patient dose. ICRP 73 states that '*reference doses are intended to act as investigation levels triggering a local investigation if the typical dose for a specific type of diagnostic procedures is found consistently to exceed the relevant reference level. Unless this can be justified by sound clinical judgement, appropriate corrective action should be taken to improve practice; this could involve changes in procedures or equipment to reduce doses to below the reference level without compromising the quality of the diagnostic information.*' [95]. Essentially, DRLs act as a simple test for identifying situations where patient doses are becoming unusually high and action is most urgently required. With this function in mind, we understand that they are not an 'optimum' or 'minimum achievable' level but more at a borderline between acceptable and unacceptable practice. A pragmatic way of setting this level uses the third quartile values observed in large surveys of typical doses for common procedures. Indeed, ICRP 73 recommends that '*… initial values (be chosen) as a percentile point on the observed distribution of doses to patients. The values should be selected by professional medical bodies and reviewed at intervals that represent a compromise between the necessary stability and the long-term changes in the observed dose distributions.*' Different proposals and considerations about derivation of DRLs for different procedures can be found in literature [95-98]. Specific DRLs for diagnostic and therapeutic examinations in IC, were derived in chapter 3.1 (***publication 1***). Proposed values are 71 Gycm² and 106 Gycm² respectively. It should be stressed that the availability of additional copper (Cu) filtration pulls the entire DAP distribution of a followed patient population towards lower values, with a lower mean DAP as a consequence (see paragraph 3.3) (***publication 3***). Being aware of this will contribute to an accurate comparison with DRLs.

In view of the above discussion, it is strongly advised to save dose indicators (e.g. DAP) in patient's records. An effective framework for measuring doses and saving dose values in patient's record is necessary.

The Belgian situation regarding radiation burden in cardiovascular catheterization in terms of DAP, represented in figure 7 in paragraph 3.1 (***publication 1***), shows reported values are rather high. The values for other countries than Belgium, derived in DIMONDIII project, included data from

100 examinations per country [97]. The procedures included in the DIMOND III project are CA and PTCA. The authors stated that in some interventions the diagnostic part could not be split from the therapeutic part. Therefore, the dose was considered as the value for the PTCA procedure. In paragraph 3.1 (***publication 1***), therapeutic procedures almost never consisted of a single PTCA, but were almost always made up of different therapeutic interventions, combined with a foregoing CA. This can explain the higher dose values in the Belgian study. Within the DIMOND III project, Finland also scores rather high with respect to DAP values. A possible explanation, given in the paper, is the high value of dose rate in fluoroscopy or the dose per frame. However, numbers were not given. In present study, physical technical quality control showed average entrance dose rates (20 cm PMMA) for the systems of 24 mGy/min at a distance of 1m for normal fluoroscopy settings and a medium field size. Values of 0.38 µGy/pulse at the entrance plane of the IR were measured for cinegraphy for different filtration settings, according to the ABC of the systems. Hopefully, when the recommendations for dose lowering in IC, listed below, are taken to heart, a lowering of mean and third quartile DAP values can be expected.

4.5 Recommendations for dose optimisation in IC

As described in detail in the Introduction section (paragraph 1.5) IC can involve high doses to patients (both adults and children) and may result in either deterministic or stochastic effects [36, 50]. Regarding short–term (or deterministic) effects, the skin is the tissue at greatest risk. Regarding long-term (or stochastic) effects, the youngest - and therefore most radiosensitive - population is at highest risk. Moreover, it is seen that IC procedures are by far the most frequent interventions performed in industrialised countries and with a relative high frequency of repetition on the same patient in a short period of time [36, 53, 55, 56, 58, 59]. In view of the *ALARA*-principle, dose saving handling and techniques have to be emphasized, whenever x-ray-based (and more specific interventional) techniques are used. Because of the intrinsic compromise between radiation dose and image quality, proper imaging techniques can only be described in view of these two parameters (see paragraph 1.4). It is obvious that no dose lowering at the expense of relevant diagnostic information loss, or overspill of imaging detail at the expense of an unacceptable high radiation dose, can be allowed.

The following paragraph discusses and bundles different dose saving techniques based on the recommendations formulated in several publications [10, 13, 15, 18, 47, 52, 53, 84-87, 92, 93, 95, 99-117] and on our

findings during measurements in catheterization rooms. It was my goal to give an overview of all possible techniques and to encourage application in daily practice. Therefore, I also provided a short version of this list in the appendix. Some of the techniques are specifically applicable to paediatric catheterization, while others may emphasize on skin dose. Implementation of all possible dose reduction techniques, mentioned in the following paragraph, may allow a significant dose reduction both in fluoroscopy and in cinegraphy mode.

4.5.1 Dose saving handling and techniques

1. **Decrease beam-on time! Do not apply fluoroscopy while changing the position of patient, table, tube, collimator or partial thickness shields.** The physician operating the fluoroscopy unit has the ability to significantly reduce radiation doses by reducing the exposure time [10, 47, 99-101]. As this is possibly the most efficient technique for dose reduction, it is mentioned first. During catheter changing, brief looks should be sufficient for moving it up. Most cardiologists are aware of the value of tapping the foot switch rather than standing on it. With the availability of digital cinegraphy loops, repeated as often as necessary, some shortening of cinegraphy angiograms might be possible. Modern systems have the possibility to store images taken in fluoroscopy mode or to generate 1 pulse in order to take 1 image. These options are very useful when documenting on expansion of a balloon or stent.

   Use of fluoroscopy while changing table position or when rotating the tube in a different geometry only contributes to the dose without contribution to diagnostic information. Even in overscheduled catheterization laboratories, where interventionists and nursing personnel are highly occupied and urged to hurry, this is not acceptable.

   Last but not least, when the eye is not on the screen, the foot should not be on the paddle. Do not tread the paddle when discussing.

2. **Involve the concept of personnel dose with patient dose.** The rule of thumb in this topic is '*what you give is what you receive*', meaning that the higher the patient dose is, the higher the operator dose will be [10, 99, 111]. This point of view might perhaps break through the force of habit of persisting operator, paying relatively less attention to (patient) radiation burden. Without going into detail about measurement and quantification of staff dose, the relation with personnel/operator dose is

in the right place here. Besides lowering patient dose, another number of measures to decrease staff dose can be taken. Make use of the '*inverse square law*' and step backwards when performing a cinegraphy run. Make use of the hanging acrylic shielding [115], of lead aprons, lead collars and make sure they are properly stored on hangers in order to avoid cracks. Insist on consistent wearing of dosimetry badges [116].

3. **Follow a structured training program in your department**. Information sessions, seminars, and/or topic related talks should be organised at a regular base and within a structured training program. As well cardiologists, nurses, as technicians should be involved. A culture that strives toward radiation awareness and safety being present and maintained, will easily motivate the involved personnel to adapt catheterization practice to a dose-conscious action of high medical quality.

   It is of great importance to be familiar with the equipment available in your catheterization room. All options of the equipment should be known and this is particularly important when new modalities are put into practice [99]. Discussions with the manufacturer should provide insight and training by the manufacturer's application engineer must be demanded.

   Extensive training programs for interventional cardiologists dealing with the treatment of paediatric patients are found in literature. The publication by Ruiz *et al.* touches topics as 'Principles of radiographic imaging and radiation safety', 'Diagnostic cardiac catheterization' , 'Hemodynamics', 'Cardiac catheterization laboratory pharmacology' and 'Additional core curriculum for interventional paediatric cardiology' and adds an extensive bibliography [112]. Another document resulted from The American College of Cardiology (ACC) / American Heart Association (AHA) / American College of Physicians (ACP) Task Force and describes recommendations regarding optimisation of patient safety and image quality in fluoroscopically guided invasive cardiovascular procedures [84]. Further reading regarding the IAEA's initiatives for training of interventional cardiologists can be found in Rehani *et al.* [87] and related topics are described by Beller *et al.* [113], Picano *et al.* [114] and Vañó *et al.* [117].

4. **Save dose indicating parameters, such as DAP, in patient's record**. **Compare DAP to DAP action levels (interpretation for skin dose) and to DRLs (interpretation of general practice)**. When sophisticated software that saves exposure parameters and calculates an estimate for

skin entrance doses [92, 93] is not present, use can be made of DAP action levels, as advised in paragraph 3.1 (***publication 1***). Practically this means that if DAP exceeds 125 Gycm^2 (assigned to a MSD value of 2 Gy), the entry site of the beam that is responsible for the highest skin dose should be included in patient's record. A possible follow-up of the patient for radiation skin effect is to the cardiologist's decision. In case DAP exceeds 250 Gycm^2, (assigned to a MSD value of 3 Gy), the patient and his personal physician should be informed on the possible radiation effects, and a systematic follow-up should be performed. This is of great concern in the patient population that needs recurrent catheterizations, with possibly same projections as used beforehand to visualise the lesion(s).

Secondly, in order to evaluate the current and general practice in a hospital, concerning radiation burden to the patient, a yearly comparison of the mean DAP value of an annual DAP distribution, to (inter)national DRLs should be performed [85, 95]. Specific DRLs for diagnostic and therapeutic examinations in IC in Belgium, at this moment, are 71 Gycm^2 and 106 Gycm^2 respectively.

Thus, it is strongly advised to save dose indicators (e.g. DAP, if possible estimated skin dose) in patient's record. An effective framework for measuring doses and saving dose values is necessary.

5. **Diagnostic information should be obtained primarily non-invasively**. Physical examination and e.g. echocardiogram or MRI prior to cardiac catheterization, yield a prior understanding of the cardiovascular anatomy and results in a more focused catheterization study [101]. Information already known by non-invasive studies should not be re-taken during catheterization "just because we're there". In clinical practice, this is most applicable in treatment of CHD, both in adults as in children.

6. **Plan the angiographic projections beforehand. Use the x-ray stand position memory-function.** With respect to CHD in children, rare or unusual anatomic variants are difficult to image, with trial and error-methods for best visualisation as possible consequence. Specialised textbooks contain tables, listing angiographic views for some common defects [47]. Reviewing of non-invasive prior studies can also bring some insight in geometries best chosen during catheterization.

   With respect to cardiac catheterization in adults, for diagnosis or treatment of CAD, it is advisable to define a set of standard projections

(paragraph 3.2) and describe them in terms of a clinical protocol [101]. This would be most applicable for the diagnostic part of a cardiac catheterization. The protocol should be optimised in terms of all recommendations mentioned above. Avoidance of lateral views should be encouraged. Apparently it is possible to set up a set of standard projections without the hazardous lateral geometry in terms of skin dose, as is current practice in hospital 9 (paragraph 3.2). Catheterization rooms with biplane geometry should avoid overuse of cinegraphy mode. As stated in paragraph 3.1 (***publication 1***), a significant larger contribution of cinegraphy in hospitals with biplane systems in comparison with hospitals with monoplane systems was measured. This means that the possibility of acquiring two cinegraphy runs simultaneously at two different projections with a biplane system is not fully exploited but rather leads to an overuse due to the ease and speed of the technique. A comparison of the set of projections of a certain hospital can be compared with the standard projections of the different hospitals involved in the multicentre study in ***publication 2*** (paragraph 3.2). This can give a good idea of current practice with respect to colleague-catheterization laboratories. Whenever possible LAO positions (of mage receptor, meaning a x-ray tube located at the right) should be minimized to minimize operator dose. At all time, 'x-ray stand position memory' should be used. This option allows to save the geometrical position of tube and IR (eg. RAO 30, CRAN 20) at predefined positions or at positions during the procedure. The system allows for returning to these positions fast, accurately and without use of fluoroscopy for repositioning.

7. **Use automated filter selection-function, preferably with additional copper (Cu) filtration**. Additional filtration removes the lower-energy photons that only contribute to patient's dose from the beam [18]. The patient's entrance exposure (and thus MSD) can be effectively lowered without degradation of image quality [13, 104]. Federal regulation requires a minimum of 2.5 mm of aluminium (Al) equivalent material for skin dose reduction. Increasing the filtration to an equivalent of 3.5mm of Al or even 0.1 mm of Cu can help further reduce the entrance skin dose by about 25% or more with no perceptible loss of image quality [52, 105]. Since the fractional reduction in incident dose is greater than the fractional reduction in exit dose when Cu filtration is added, entrance skin dose will be reduced proportionately more than effective dose (E).

8. **Use adapted ABC curves (paediatric patients), with optimized parameters in function of image quality**. As mentioned by Tapiovaara *et al.* [108] a remarkably increased dose efficiency for image generation

was obtained by use of a low x-ray potential combined with a high filtration and grid use for all but the smallest patients. It resulted in improved detail contrast but increased image noise. Adaptation of the ABC-curves towards these guidelines is advisable. It remains a challenge to keep SNR as high as possible with high filtration and at low tube voltages. The reason is the limited tube current, possible for the equipment. Therefore, with thicker patients, either filtration thickness should be decreased or tube potential should be increased, meaning that a less efficient x-ray spectrum in terms of dose-to-information conversion coefficient (CF) has to be chosen. Tapiovaara *et al.* mentioned possible fluoroscopic dose rate decreases of factors up to 6 in different catheterization laboratories, included in their study [108]. Considerations about SNR/dose rate and optimal tube voltages can be found in [109]. With adults, filtration values, tube potential values and tube current are differently chosen and combined, due to higher tissue material in the beam and larger vessels.

Special attention should be paid to contrast-enhancing functions that lower tube potential, sometimes less than 80 kVp (adult population). With reduction of tube potential, the x-rays become less penetrating. This requires a greater entrance dose to the patient - posing the skin at higher risk - to achieve the exit dose necessary for fluoroscopic imaging. Therefore, it is reasonable to operate an IC unit not below 80 kVp during fluoroscopy in adults, unless the beam is very heavily filtered (>0.2 mm Cu) [52]. In contrast with adults, a lower tube potential of less than 80 kVp is required for paediatric fluoroscopy.

9. **Maintain x-ray equipment in good repair and calibration, i.e. resign it to a periodically Quality Control Check.** A qualified medical specialist should periodically (yearly) check performance of the equipment, including radiation levels and image quality. In the course of time, eventual defects should be reported immediately by the users of the equipment and repaired. Ideally, each hospital should foresee in a financial programme for replacement of interventional equipment every 10 year [99]. Optimisation of exposure and image quality parameters should be performed. If necessary, a cooperation with the manufacturer has to be established. Operators should recognize that a good image contains noise to a certain extend and should not request calibration that contain excellent images containing redundant information [100, 101]. Aging image intensifiers should be replaced, as the efficiency of conversion of x-rays into light photons at the caesium iodide input phosphor decreases with time. In current practice, there is still little or no

information about the time evolution of flat detectors used for dynamic examinations, but radiation damage is very likely at the course of time.

10. **Keep the image receptor (IR) as close as possible to the patient (and the x-ray tube as far as possible) to minimize skin effects.** Moving away the IR from the patient will imply higher input doses due to signal loss in the air gap at the exit of the patient. Contrarily, the x-ray tube should be kept as far as possible to the patient [10, 86, 99]. This is most feasible in monoplane systems, with enough freedom to maintain a workable situation for operator and nursing personnel whilst moving up the table and approaching the IR towards the patient. In biplane systems the patient's heart is kept at the isocentre in order to have a correct image in both planes. A right value for SID lies between 100 and 120 cm (adults), given the fact that the IR is positioned as close as possible to the patient. Certainly with highly steep cranial projections (40 degrees) it is important to ask the patient to turn the head sideward. This allows the IR to pass patient's nose and chin to just touch the thorax. If not, this implies a distance from patient exit plane to IR of about 40 cm!

11. **Use collimators and partial thickness shields.** As collimators are extremely effective in reduction of dose to both patient and operator, they should ever be used in clinical practice to define the diagnostic important field [99, 101]. Use of collimators decreases the overall amount of irradiated tissue and minimizes scatter. Less scatter means better subject contrast in the image and also less dose to organs in proximity of the radiation field. Moreover, use of collimators and shields in radiolucent areas such as the lungs, improves the image contrast, due to increased homogeneity in the image, being in favour of accurate ABC-functioning. A rule of thumb says that collimators should always be visible within the field. No studies should be performed with the collimators wide open. Many systems are equipment with virtual markers to indicate collimator or partial thickness shield positions at the monitor. These should be used instead of verification by fluoroscopy.

12. **Remove unnecessary body parts (or instruments) from the field.** Most frequent, patient's arms are left in the beam. There is no reason to do this. It not only results in a considerable dose to the arms [53] but also to a substantial overall increase in patient's tissue dose. ABC drives up radiation dose to compensate for the additional tissue (arms) in the beam.

13. **Remove anti-scatter grid when catheterising small children**. Specifically for paediatric patients, the amount of scattered radiation,

negatively affecting image quality by elevating noise level, is less due to less tissue material in the beam [10, 86]. Within this patient group, removal of the anti-scatter grid will not seriously affect image quality and proves a significant dose reduction. Shueler *et al.* mentioned a factor of 50% dose reduction [15]. Unfortunately, not all systems are designed to easily remove the grid. Whenever installing a new system, this should be required from the manufacturer, certainly when children are to be catheterised on the new equipment.

14. **Use the lowest acceptable frame rate**. With almost all recent x-ray rotational systems, provided with pulsed fluoroscopy and cinegraphy mode, the lowest frame rate as diagnostically possible should be chosen. Only use higher frame rates (e.g. 25 f/s instead of 12.5 f/s) when necessary (e.g. for ventriculography, visualisation of rapidly moving prosthetic valve leaflets,…). It should be kept in mind that with paediatrics frame rate cannot be reduced unlimited, due to higher heart rate. Elder systems can possibly operate on continuous fluoroscopy. It has to be stressed that dose reduction with pulsed fluoroscopy is of the order of 25% [86, 102, 103] and that systems with continuous fluoroscopy mode should be replaced or upgraded [104].

15. **Use the lowest acceptable magnification mode.** A substantial dose increase is related to the use of magnification mode (paragraph 1.6) [86, 101]. Magnification means reduction in 'overview' of anatomical structures, with panning, and thus waste of radiation dose as a result Panning is moving the table to find or follow the anatomical structure of interest, during cinegraphy and should be avoided. Do not forget to select the standard field size after an angiogram has been taken in magnification mode. Even so, it is not favourable to perform the entire procedure in magnification mode.

16. **Vary the site of the radiation entrance spot**. For reduction of MSD, the radiographic position should be changed – if clinically feasible – during procedures that require long fluoroscopy times [10, 86].

17. **Perform a test injection under fluoroscopy prior to cinegraphy.** The test injection makes clear whether the catheter is correctly positioned, whether the correct magnification mode is used (prevent panning), whether the angiographic projection is as desired. A small amount of contrast and a few seconds of fluoroscopy are less costly to the patient than a wasted cinegraphy-run in terms of radiation and contrast load [47].

18. **Use roadmap and overlay features.** A good angiogram of the culprit lesion can be used as roadmap or can even be superimposed on a live fluoroscopy image (and faded out when necessary) for vessels of interest to be found with minimal trial and error [47]. Certainly when an interventional therapeutic part is needed immediately after a diagnostic catheterization, this technique is of value. Confirmation of the catheter position can be done without additional contrast injection.

19. **Take angiograms (cinegraphy-runs) only during inspiration.** During expiration, the diaphragm shows up in the beam, causing the ABC to drive up exposure. Because of inhomogeneity in the image (denser diaphragm versus lungs), the ABC will not function optimally. The vessel below the diaphragm will be 'invisible', while the part above will be 'burnt out' due to too high a dose. On full inspiration, the entire vessel is clearly seen with better contrast. An expiratory acquisition will generally have twice the radiation dose of one in full inspiration, and will be of less quality [107].

20. **Avoid use of steep LAO-projections**. In almost the entire clinical practice of cardiac catheterization, a lateral view of the heart is taken with the x-ray tube located at the patient's right side, being the operator side. The IR at that stage is located at the left side (= closest to the heart) of the patient, and at the other side of the cardiologist. This convention is derived to minimize artefactual enlargement due to magnification of the heart. However, within practice of IC (certainly with paediatric population for treatment of CHD), as much left-sided structures as right-sided structures are likely to be involved in coronary angiograms. So, rotation of the tube for 180° would have little or no impact on clinical decision making in the catheterization laboratory [47]. As the current lateral convention is far most familiarised with interventionists, a change is not likely to be introduced yet, although repercussion on operator and patient dose is considerable. Kuon *et al.* [110] and [100] state that steep LAO tube angulations (LAO views ≥ 60° with cranial or caudal angulation ≥ 20° are unjustifiable and obsolete. It is precisely those views which imply a longer SID and consequently, more radiation exposure to patients and staff [111].

21. **Center the region of interest correctly to the field.** With II, less geometric distortion is found at the centre of the image, however with FD this is not the case (paragraph 1.6.) [10, 106]. Centring allows tighter collimation, easier magnification (when necessary) without panning (moving the table to find or follow the anatomical structure of interest,

during cinegraphy) and optimal exposure, due to central location of the ABC-sensor (with II).

22. **Use last image hold-function.** Practically all new (or recent) x-ray equipment for fluoroscopically guided (cardiovascular) interventions has last image hold function. The system holds and continuously displays the last frame after radiation is turned off [86]. Only elder equipment (II with video capture and monitoring) do not include this feature.

4.6 Recent evolution in IC: flat detectors

Since its introduction in 1950, II-technology grew and has become the golden standard for image reception in dynamical fluoroscopic x-imaging. The latest step comprised coupling of the II with a CCD-camera, bringing along greater temporal stability and low electronic noise [79]. It was only recently, thanks to technological innovations, that a relatively new imaging technology started to compete with II for dynamical investigations. In the late 1990's, time resolution of flat-panel displays reached a sufficient level to be suitable as IRs for fluoroscopy guided interventions. Many of its advantages are very appreciated: direct digitization of the images, better ergonomics with better patient access, lack of geometric distortion, little or no veiling glare, no vignetting, insensitivity to magnetic fields and wider dynamic range, with an advanced image quality as a promise… [77-80]. With nowadays computer capacity and extended intra- and interhospital networking, digital data processing, storing, transporting, multiple viewing and duplicating are performed with ease and at a astonishing velocity.

However, the successful story has also its minor side and some questions remain unanswered. This pertains to the relation between image quality and patient dose and especially at low exposure rates, since system noise seems to become a limiting factor in determining system performance [81, 83]. Paragraph 3.5 (***Publication 5***) tackles this problem and compares IQ by means of threshold contrast–detail analysis of an II and a FD-system and investigates patient dose on both modalities.

From the study a difference became apparent in dose-IQ relation for the two modes used in IC practice: fluoroscopy and cinegraphy. In fluoroscopy mode an equal IQ performance was noted, whereas for cinegraphy a higher IQ performance was found for the FD system. This reflects the intrinsic better imaging performance of the FD with higher EDR values (recall figure 1, chapter 3.5, ***publication 5***).

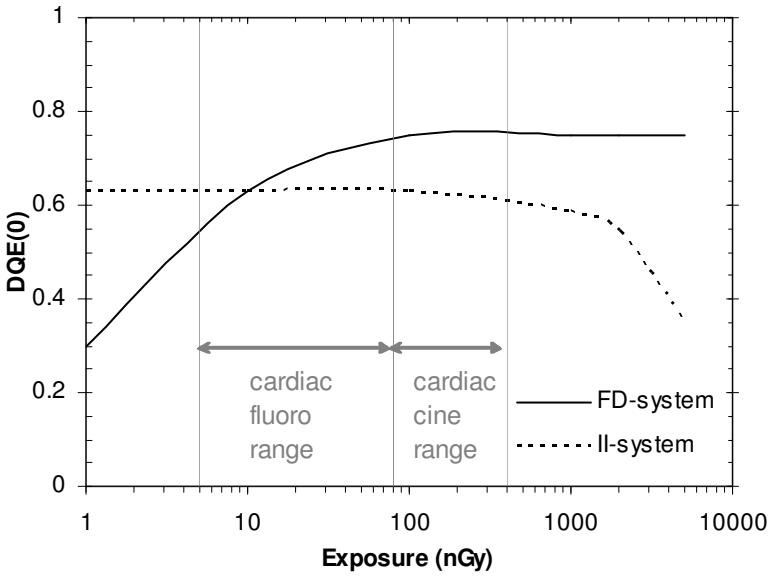

Figure 28. Comparison of DQE(0) versus exposure (nGy) for an II and a FD-system. Values and behavior were taken from Antonuk *et al.* [81], Busse *et al.* [118] and Bruijns *et al.* [119]. Entrance dose per pulse at the IR for cardiac fluoroscopy mode ranges from 5 to 80 nGy whereas for cardiac cinegraphy mode it ranges from 80-400 nGy.

Overlapping performance of II and FD for low exposure rates has also been previously reported considering DQE(f) (f = spatial frequency: lp/mm) [72, 81, 119]. A comparison between DQE(0) values for FD and II based on refs. [81, 118, 119] (Antonuk *et al.*, Busse *et al.* and Bruijns *et al.*) is represented in Figure 26. The behavior for FD is a consequence of the low SNR of low dose images. For these images not only signal amplitude but also electronic and other noise are increased in order to obtain the necessary signal level for digitisation. In contrast to FD-systems, DQE(f) for II remains constant (values equal to that of FD corresponding to entrance doses of 10 nGy) while a decrease becomes only apparent for higher entrance doses starting from 1000 nGy.

From the measurements in clinical default settings (ABC mode) any significant difference in IQ in fluoroscopy mode could be assigned. In cinegraphy mode, however, IQ did differ significantly in favor of the FD system (recall figure 4, paragraph 3.5, ***publication 5***). This means that for daily practice, profit was taken of the better IQ relation to dose of the FD for higher entrance dose rates to obtain images of better quality. Apparently the system was not tuned in terms of a possible dose reduction, with conservation of an IQ, as set with an II-system. However, optimization towards lower patient doses is preferred and evaluation of the default parameters in new equipment is strongly recommended. Technically, optimization of the exposure versus IQ relationship is possible through

adaptation of the ABC-parameters. DAP-measurements to investigate the influence of this new technology on patient dose could not reveal a lowering nor increase in exposure burden.

To conclude, FD IRs, specifically designed for fluoroscopic interventions provide a better IQ versus dose efficiency than II for the higher cinegraphy levels. Optimal benefit can be taken from this feature by a possible dose reduction, since IQ in II (being in good condition) has ever shown to fulfill clinical requirements. As with all technological innovations, there is a learning curve for implementation, optimal use and adjustment. Advantages of FD, being good uniformity, no geometric distortion, no veiling glare or vignetting and small, thin physical size for improved patient accessibility, can be an important consideration for paediatric imaging [79]. With respect to FD, the long term reliability, radiation tolerance and replacement costs are still unknown. Considering II, it is known that the conversion of incoming photons into light by the input CsI phosphor layer becomes less effective with time. However, as for all equipment, maintenance and yearly check-up is necessary and this does not diminish overall reliability [106].

4.7 Alternative techniques for IC

In Western World, myocardial infarction (MI) remains the leading cause of death for both men and women, and its prevalence is still increasing. The current gold standard for the detection of CAD is conventional CA, by means of catheterization. As already explained, this technique allows direct visualisation of the coronary lumen and its high spatial and temporal resolution are of great value. However, the procedure is invasive and drawbacks include a significant cost, a small risk of serious complications [120, 121] and the use of ionising radiation. Furthermore, in a substantial number of procedures (ranging from 10% [122], to 41% [123], no evidence of clinically important CAD is demonstrated. Thus, for patients with a low to intermediate pre-test likelihood of CAD, a non-invasive alternative for evaluation of the coronary arteries would be desirable. For high-risk patients with high pre-test likelihood, direct referral for invasive, catheter-based CA may still be preferred [124].

In following paragraphs, some alternatives for catheter-based CA will be presented. These include Rotational x-ray CA, Multi-Slice CT Coronary Angiography (MSCT-CA), Echocardiography and Coronary Magnetic Resonance Angiography (CMRA).

4.7.1 Rotational x-ray coronary angiography

During selective CA, angiograms have to be taken in multiple projections to overcome superimposition of cardiac structures and foreshortening of vessels. The intrinsic 2D character of the imaging technique imposes this. In contrast to e.g. MRI, (MS)CT and echocardiography, x-ray angiography has only recently advanced into the area of 3D reconstruction and visualisation [125]. Active rotation of the imaging system around the patient, carefully positioned in the isocentre and during angiographic injection, makes 3D reconstruction of cardiac structures possible. This method is referred to as rotational x-ray coronary angiography (rotational CA).

Several case reports and publications already mentioned the use of rotational CA in clinical practice [126-128] and comparative studies between standard and rotational CA have been performed [129, 130]. On the average four to six different projections are sufficient for visualisation of the left coronary artery (LCA) and three to four for the right coronary artery (RCA), during standard CA. The rotational protocol uses one or two rotations (e.g. of 100°) with a small tilt (e.g. 25° cranial or 30 ° caudal) for LCA acquisition and a single rotation for the RCA acquisition [128-130]. Mostly the images are taken at 25 to 30 f/s and one spin acquisition takes about 5 seconds [127]. Besides a significant reduction in contrast media utilization of 19% [129], 33% [131], and even up to 40% [130], which is in favour of patients with advanced renal insufficiency, a dose reduction of 28% [131] and 34% and 59% for left and right coronary acquisition respectively [129] was reported. Panzer *et al.* not only endorsed to this viewpoint, recalling their experience in daily clinical practice, but also reported on possible lowering of skin dose, mentioning a value of 101 mGy for cumulative skin dose [127]. Indeed, the varying entrance site of the x-ray beam lets us expect lower peak values for skin doses. This means that the probability for radiation induced short-term effects on the skin could be largely reduced in rotational x-ray CA.

All authors mentioned above, stated that rotational CA was a clinical valuable alternative for standard CA. No need for additional image acquisitions beyond the protocol acquisitions was reported with rotational CA [130], nor systematic tendency to over- or under-estimate percent stenosis with rotational CA was noted [129]. Following Kuon *et al.*, 'this method is able to exactly document multiple LCA lesions and to reliably disclose lesions at crucial regions, such as the RCA ostium and bifurcations in circumflex and obtuse marginal arteries' [128]. Moreover, with the cost of a 3D rotational CA system being comparable to a modern monoplane system, this new modality is very promising.

4.7.2 Echocardiography

For treatment of ASD, both in adults and children, an extremely precise assessment of the defect is crucial. Different techniques are available: balloon-sizing manoeuvre, Trans-Esophageal Echocardiography (TEE) and recently Intracardiac Echography. The latter technique comprises a catheter-based transducer for ultrasonic visualization, moved up through the venous system to reach the heart. Rigatelli *et al.* [132] reported a significant reduction in terms of DAP and fluoroscopy time. This could be attributed to a more adequate imaging and estimation of the defect with improved safety and accuracy of the procedure as result. In comparison with TEE, no sedation or intubation is needed, meaning good patient acceptance for a relatively prolonged period of time (time of the procedure). Drawbacks include the high cost due to disposable catheter-system, large catheter size, which limits optimal use, certain in children or babies, and significantly increased procedure time [132-134]. The technique has proven to be of potential value not only during catheter-based treatment of ASD but also during radiofrequency ablation, measurement of aortic valve area and other applications [134]. However, it does not belong to clinical routine (yet?). In view of dose reduction, echography during catheter-based treatment of CHD on a paediatric population, reduces dose considerably.

4.7.3 Multi-slice CT Coronary Angiography (MSCT-CA)

Rapid evolution of Multi Slice Computed Tomography (MSCT) (16 and 64 slice) facilitated an alternative for coronary angiography, performed by interventional methods [135-138]. Its non-invasive character makes performance of MSCT-CA attractive. Psychological burden e.g. to heart transplant patients who require yearly follow-up coronary angiogram can be relieved to a certain extend [139]. MSCT is automated, reliable, widely available and fast (certainly with nowadays 64-slice scanners, introduced in 2004) in terms of breath-hold data acquisition. Spatial resolution is high enough to visualize adequately small anatomic structures such as coronary arteries (with diameter of at least 2 mm) [140] and temporal resolution satisfactorily avoids motion artefacts with heart beats < 65 beats/min [140-142]. Disadvantages include lack of ability to image walls of arteries, or areas treated by stenting. The latter is due to artefacts in image reconstruction. High or arrhythmic heart rates hamper imaging with MSCT and there is still a need for iodinated contrast to be used [143, 144]. Yet, the highest drawback of this method is the '*consuming*' of x-rays. Remarkably higher

doses for MSCT-CA compared to conventional CA in daily practice have been reported. Higher tube currents necessary with thinner collimation and z-overscanning in helical applications are some of the reasons to fear high doses with implementation of higher number slices [145, 146].

Radiation induced injuries to the skin, in terms of direct effects, practically do not exist with MSCT. The difference between entrance dose and dose central in the patient is only 30 % (in comparison with factors 100 to 1000 in projection radiography) due to rotational acquisition. This however contrasts sharply with mounting E and risks for long term-effects.

A recent study (2006, Coles *et al.*) [147], comparing doses from diagnostic coronary angiograms obtained by use of MSCT (MSCT-CA) and by use of coronary catheterization (conventional CA), performed on the same patient population, revealed significant differences in E. Ninety-one patients both underwent conventional CA in a modern Siemens mono- or biplane system and a coronary MSCT (MSCT-CA) examination on a Siemens Sensation 16-slice scanner. The mean E for MSCT-CA (16-slice) was 15.3 mSv, compared to 5.6 mSv for the conventional CA. Hausleiter *et al.* (2006) [148] illustrated that dose reduction techniques such as ECG dependent mAs modulation and use of low kilovoltage (100 kV instead of 120 kV) are effective to lower mean E-values to 5.0 mSv and 5.4 mSv for MSCT-CA at 16 and 64 slice scanners respectively. ECG dependent mAs modulation only applies tube current during diastolic phase of the cardiac cycle, at which less time imaging artefacts occur. As this technique depends on patient's heart rate requiring a regular sinus rhythm, it is not always applicable for the whole population. However, when suitable, this technique has showed dose reduction by about 40 % [135, 149] and it is said to be 'the most significant improvement in minimizing radiation from CT technology and the only one dedicated to cardiac imaging' [150]. Abada *et al.* (2006) endorsed the viewpoint of Hausleiter *et al.* and applied low-kilovoltage protocols for slim patients together with ECG-dependent mAs modulation to obtain significant dose reduction, without image quality loss [150]. Firstly, it should be remarked, however, that tube voltage cannot be lowered infinitely as noise and contrast will increase and affect image quality at a certain point. Secondly, ECG-dependent mAs modulation is only applicable in clinical routine when heart rate is low and constant and therefore effective implementation in daily practice is difficult [145].

Within this context, it should be emphasized that the lack of information of clinicians and angiographers about the influence of different imaging protocols on radiation burden to the patient is of great concern. Practically, implementation of new modalities at the imaging site of a hospital mostly

stands for unfamiliarity with the integrated protocols. Optimization of these protocols, adaptation of the 'default' parameters and thorough training on application of the new modality are strongly advised [148].

As a scan protocol for MSCT-CA mostly consists of a topogram, a calcium scoring scan, test bolus scan (sequence of scans to determine a time delay, necessary for contrast material to arrive at the organ of interest) and the actual coronary angiogram, proposals for dose reduction of the different parts have been suggested. Lowering of mAs values from 165 mAs to 55 mAs for calcium scoring scan resulted in a dose lowering with one third with the same clinical outcome for diagnosis [151]. Omission of the test bolus scan would only yield a small reduction as it contributed for 5 % to the overall dose as shown in the study of Coles *et al.* [152].

The current debate about the appropriate use of MSCT-CA is certainly not yet closed and the topics discussed here, only raised a corner of the veil. Guidelines for inclusion novel modalities as MSCT-CA within standard diagnostic algorithms or screening programs need special attention [153]. As with overall medical practice, a clear medical justification is required in each specific case [48].

Due to higher heartbeat of children, MSCT-CA is only applicable to an adult population. Nevertheless, paediatric CT of any other part of a child's body remains hot topic with respect to radiation risk and late, long–term effects [42, 154-156].

Whenever dose saving techniques such as ECG dependent mAs modulation, and use of low kilo-voltage evolve to be applicable to the entire patient population submitted to coronaro-CT, further progress of the technique for diagnosis of CAD can be made. However, the situation becomes dangerous when intervention is needed for a patient, who was first thought to be of low risk with respect to CAD and therefore was referred to CT… With referral to the catheterization laboratory to receive the due PTCA or stenting, the following question will arise: 'Will the diagnostic part be retaken (performing conventional CA) in order to get acquainted with the lesion, imaged with a different technique?'. As this is true, the added value of the MSCT-CA and its involved dose is strongly questioned. For these cases, the benefit of an ad-hoc dilatation or stenting, immediately following a diagnostic conventional CA probably involves less radiation exposure than the 'alternative ', performing the diagnostic part by MSCT.

4.7.4 Coronary Magnetic Resonance Angiography (CMRA)

Besides cardiac catheterization and MSCT, MRI has emerged as diagnostic cardiac imaging technique. Strengths for this technique are non-invasive character, lack of exposure to ionising radiation, possibilities to image wall, lumens and plaque composition and avoidance of iodinated contrast media [143, 144]. Weaknesses include exclusion of patients with pacemakers and implanted defibrillators, long scan-time (20-25 min), 3D post-processing time (up to 45 min) and less availability of MRI-scanners.

Up to now, the technique has evolved a lot, and many studies have been published, comparing different approaches of CMRA, new software implementations, protocol optimisation or new equipment with catheter-based CA. In 2004, Danias *et al.* [157] performed a meta-analysis of all available studies, at that time, comparing CMRA and catheter-based CA. They concluded that the sensitivity of CMRA is moderately high (73%) and that the technique has satisfactory negative predictive value for excluding significant major epicardial coronary artery stenosis in patients with suspected CAD.

With this technique being in full expansion regarding imaging of the coronary arteries, it could possibly provide a diagnostic pre-test for exclusion of CAD. Kim *et al.* [123] also reported possibility for exclusion of left-main coronary artery of three-vessel disease by the technique. And Prakken *et al.* described the evolution from multiple breathhold thin slab acquisition to whole heart free-breathing balanced turbo field echo [158]. However, even within these recent developments, the diagnostic accuracy of CMRA for detection of significant stenosis in coronary arteries is still suboptimal [124, 143, 158]. This and other drawbacks, with some of them mentioned above, are still to overcome and make the procedure difficult to implement in clinical environment at the moment.

4.8 Future Prospects

As radiation risks related to IC both on adult and paediatric populations are characterized now as accurate as possible, the priority for the future is practical implementation of dose monitoring and dose reduction. Possible measures to take for reducing probability of radiation induced injuries and cancer are clearly summarized in this work. In October 2006, the Federal Agency for Nuclear Control (Belgium) enacted an advisory regarding 'Patient Dosimetry in Medicine' [159]. With respect to high-dose

examinations as IC both on adults and children, a three-yearly extended inventory of patient dose has to be performed, a calibrated DAP meter has to be installed on the system and DAP values have to be saved in patient records. Up to now, only recently installed systems, have a DAP meter incorporated. Up to now, DAP values are not always included in patients' record in a standardized way. Once a considerable data set is available, annual statistics can be performed with comparison to DRLs. Possible corrective actions can be formulated. Thus, practical implementation of all regulations and recommendations regarding dose reduction and optimization is necessary in the near future.

Innovative technologies, such as FD as image reception, are now well over their teething troubles and have shown good performance in daily practice [78, 79, 160]. However, improvement is possible, certainly in low dose rate applications, as in fluoroscopy mode. Different improvement strategies have already been proposed [81, 82], but up to now, they are not (yet) implemented in detectors for clinical daily use. A second topic related to FD is optimization towards a better IQ, taken into account the linear signal response and a wider dynamic range [161]. As became clear in chapter 3.5 (***publication 5***) fine-tuning of the ABC-function is necessary in cinegraphy mode. Thirdly, the question regarding long-term reliability, detector radiation damage and degradation of IQ and associated replacement costs remains open. In the future these aspects have to be followed up and will more clearly outline the cost-benefit of these detectors.

A recent evolution in imaging of coronary arteries, is the shift from conventional catheterization techniques towards non-invasive imaging techniques as MSCT and MRI [124, 141, 143, 162, 163]. Whereas MSCT shows a significantly higher accuracy to detect or exclude significant CAD by imaging of atherosclerosis in comparison to MRI, which of the two techniques is more likely to be implemented in the diagnostic workup of patients with suspected CAD is still a matter of debate [124]. Although MSCT has promising features as fast acquisition, sufficient spatial and temporal resolution and wide availability, the highest drawback of this method is the '*consuming*' of x-rays. The topic of patient exposure in MSCT, all or not combined with therapeutic IC catheterizations as PTCA demands further investigation. Some comparative studies were already performed between MSCT and conventional CA [147, 164] and did not show a lowering or even an equivalent in dose for MSCT. Some dose reducing techniques are possible but tend to be unusable for a considerable fraction of the patients [145, 148]. Not only for investigation of atherosclerosis but more explicitly in systematic screening of patients the use of MSCT has to be discussed in view of the high patient dose.

A very promising technology performed with the same x-ray C-arm modality as used in conventional standard CA, is rotational x-ray CA. An upgrade of the software and steering system of the modality enables 3D reconstruction of cardiac structures and vessels. Although in some studies DAP-values from conventional CA and from rotational CA have been compared, up to now actual skin dose has not been measured. Furthermore, this new application seems to get lost in the heated debate with respect to coronary CT angiography, although its remarkable advantages comprising significant dose and contrast utilization lowering [128-130].

Chapter 5

Conclusions

Present work deals predominantly with radiation burden to both adults and children who underwent IC procedures. In a multicentre study of patient skin doses on an adult population, 3% of the procedures exceeded the threshold dose for transient erythema (2Gy) in one single procedure. Given this prevalence, skin doses are likely to exceed values much larger than 2 Gy in subsequent and difficult interventions on adults with high BMI, even with state of the art equipment and by highly experienced cardiologists. Measurement of entire skin dose distributions by a grid of TLDs and analysis of exposure parameters and dose indicators such as DAP revealed the factors associated with high MSD. A method, using DAP action levels for interpreting DAP values recorded during IC procedures on adults was developed for prediction and follow-up of possible radiation induced skin injuries after IC. A value of 250 $Gycm^2$ was proposed for dermatological follow up of patients. Whereas deterministic effects related to the skin are a major radiation protection issue with adults, this is not the case for children. Median MSD values of 0.2 Gy and 0.5 Gy for diagnostic and therapeutic procedures on adults have to be compared with an overall median value of 0.03 Gy for the paediatric population, being a factor of 10 in difference. However, interpretation of registered total cumulative DAP values for multiple IC procedures on children in terms of deterministic effects is recommended. Values of 100 $Gycm^2$ (armpit) and 175 $Gycm^2$ (back) could imply that the 2 Gy threshold for transient erythema has been passed in these children.

Apart from the interpretation of DAP in terms of DAP action levels, DAP has also proven to be an operational quantity indicating differences in patient radiation burden between hospitals and correlating well with effective dose (E). Median values for diagnostic and therapeutic procedures were 44 $Gycm^2$ and 65 $Gycm^2$ for the adult population and 4.1 $Gycm^2$ and 4.6

Gycm² for the paediatric population, revealing roughly a difference by a factor of 10 between the two populations. DRLs for comparison of local mean DAP values (adult interventions) of 71 Gycm² and 106 Gycm² were obtained for diagnostic and therapeutic procedures respectively. These values are relatively high in comparison to European levels, resulting from the *DIMOND III*-project. The relative (mean) contribution of fluoroscopy to total DAP amounted to 33% and 50% for adult diagnostic and therapeutic examinations although a significant larger contribution of cinegraphy to total DAP resulted from biplane systems. The same contribution for fluoroscopy mode (31% and 55% for diagnostic and therapeutic procedures) was found for the paediatric population.

E, a representative quantity for late stochastic effects, was calculated using exposure parameters and showed a very good correlation with DAP. Values of 9.6 mSv and 15.3 mSv for the adult population and 4.1 mSv and 4.6 mSv for the paediatric population (diagnostic and therapeutic examinations) showed a difference by a factor of 2 to 3. However, risk estimation based on ICRP60 age dependent life-time risk factors, revealed a difference by a factor of 10. Values of 0.01% and 0.02% for diagnostic and therapeutic examinations for an adult population stand against risk factors of 0.1% for the very youngest generation (0-1 year) regarding cancer induction following IC procedures. The large variety in body mass, length and age of the paediatric population required an individual calculation method (MCNP), whereas adult E-values were derived by a more standardised way, using the standard projections assigned to the clinical protocol and an anthropomorphic phantom with the dimensions of an average person (PCXMC). The predicting value of DAP in terms of E, was translated into conversion factors (CF) that provide a fast and straightforward way of E-assessment.

The dose reducing effect of additional copper (Cu) filtration showed up throughout this work. A significant lowering of DAP and E was found for systems that used optimised an automated filtration insertion. Additional filtration in fluoroscopy not only has a positive effect on skin sparing, but also reduced total E by 18% for the paediatric population. Besides this technical improvement, a number of measures for radiation protection of the patient (and related staff dose) can be taken. Reduction of beam on time, fully exploitation of all dose reducing techniques on recent imaging modalities (pulsed fluoroscopy, last image hold, x-ray stand position memory,…), training and education, planning of procedure strategies and optimisation of protocols are some of them. With adult population, every measure should be taken to avoid high skin doses for critical patients with high BMI and difficult lesions. With respect to paediatric population, every

recommendation should be followed to lower E and with this the risk for cancer induction in these young children.

Together with a discussion on reliability, cost-benefit balance and possible application in different patient populations, the development of new x-ray imaging technologies brings along questions about the relationship between IQ and dose. In this work, we focussed on the recent introduction of FD in IC. In cinegraphy mode, a significantly better IQ for the same entrance dose rate was found for FD, whereas for fluoroscopy mode no difference was observed. The imaging performance of FD in cinegraphy mode was intrinsically better, in line with the higher detective quantum efficiency. However, measurements under daily working conditions (ABC) showed that the new modality was optimised rather in terms of IQ than in terms of radiation burden. Measurement of patient DAP values lacked significant difference for the two systems. With implementation of new modalities, care has to be taken that ABC setting take into account as well patient dose as IQ.

Appendix

Recommendations for dose optimisation in IC (chapter 4.5)

1. Decrease beam-on time ! Do not apply fluoroscopy while changing the position of patient, table, tube, collimator or partial thickness shields.
2. Involve the concept of personnel dose with patient dose.
3. Follow a structured training program in your department.
4. Save dose indicating parameters, such as DAP, in patient's record. Compare DAP to DAP action levels (interpretation for skin dose) and to DRLs (interpretation of general practice).
5. Diagnostic information should be obtained primarily non-invasively.
6. Plan the angiographic projections beforehand. Use the x-ray stand position memory-function.
7. Use automated filter selection-function, preferably with additional copper filtration.
8. Use adapted AEC curves (paediatric patients), with optimized parameters in function of image quality.
9. Maintain x-ray equipment in good repair and calibration, i.e. resign it to a periodically Quality Control Check.
10. Keep the image receptor (IR) as close as possible to the patient (and the x-ray tube as far as possible) to minimize skin effects.
11. Use collimators and partial thickness shields.
12. Remove unnecessary body parts (or instruments) from the field.
13. Remove anti-scatter grid when catheterising small children.
14. Use the lowest acceptable frame rate.
15. Use the lowest acceptable magnification mode.
16. Vary the site of the radiation entrance spot.
17. Perform a test injection under fluoroscopy prior to cinegraphy.
18. Use roadmap and overlay features.
19. Take angiograms (cinegraphy-runs) only during inspiration.
20. Avoid use of steep LAO-projections.
21. Center the region of interest correctly to the field.
22. Use last image hold-function.

References

1. Vanmarcke, H., H. Bosmans, G. Eggermont and J. Brouwers, *MIRA (2007) Milieurapport Vlaanderen, Achtergronddocument 2007, Ioniserende straling.* http://www.milieurappport.be. 2007: Vlaamse Milieumaatschappij.
2. Gruentzig, A.R., R.K. Myler, E.S. Hanna and M.I. Turina, *Coronary transluminal angioplasty.* Circulation, 1977. **56**(4): p. 84-84.
3. Gray, H., *Anatomy of the Human Body. 20th ed., thoroughly revised and re-edited by Warren H. Lewis.* 2000: Philadelphia: Lea & Febiger, 1918; Bartleby.com, 2000.
4. Windecker, S., W. Maier-Rudolph, T. Bonzel, G. Heyndrickx, J.M. Lablanche, M.C. Morice, et al., *Interventional cardiology in Europe 1995.* European Heart Journal, 1999. **20**(7): p. 484-495.
5. Cook, S., A. Walker, O. Hugli, M. Togni and B. Meier, *Percutaneous coronary interventions in Europe.* Clinical Research in Cardiology, 2007. **96**(6): p. 375-382.
6. Dieltiens, S., *Schatting van de patiëntdosis bij radiologische en nucleair geneeskundige ingrepen in België.* eindwerk, KUL, 2008.
7. *FDA Public Health Advisory: Avoidance of serious X-ray-induced skin injuries to patients during fluoroscopically-guided procedures.* . http://www.fda.gov/cdrh/fluor.html, 1994.
8. ICRP, *1990 Recommendations of the International Commission on Radiological Protection. Publication 60.* Ann. ICRP, Oxford, UK: Pergamon Press, 1991. **21**(1-3): p. 1-201.
9. ICRU, *International Commission on Radiation Units and Measurements. Patient Dosimetry for X-rays used in medical imaging ICRU Report 74*. 2005, Bethesda, MD: International Commission on Radiation Units and Measurements.
10. ICRP, *Avoidance of radiation injuries from medical interventional procedures. Publication 85.* Ann. ICRP, Oxford, UK: Pergamon Press, 2000. **30**(2).

11. Seldinger, S.I., *The Seldinger technique - catheter replacement of the needle in percutaneous arteriography - a new technique (reprinted).* American Journal of Roentgenology, 1984. **142**(1): p. 5-7.

12. Bushberg, J.T., J.A. Seibert, E.M. Leidholdt and J.M. Boone, *The essential Physics of Medial Imaging*. 2nd ed. 2002, Philadelphia, USA: Lippincott Williams & Wilkins.

13. Bacher, K., E. Bogaert, R. Lapere, D. De Wolf and H. Thierens, *Patient-specific dose and radiation risk estimation in pediatric cardiac catheterization.* Circulation, 2005. **111**(1): p. 83-89.

14. Martinez, L.C., E. Vaño, F. Gutierrez, C. Rodriguez, R. Gilarranz and M.J. Manzanas, *Patient doses from fluoroscopically guided cardiac procedures in pediatrics.* Physics in Medicine and Biology, 2007. **52**(16): p. 4749-4759.

15. Schueler, B.A., P.R. Julsrud, J.E. Gray, J.G. Stears and K.Y. Wu, *Radiation exposure and efficacy of exposure-reduction techniques during cardiac-catheterization in children.* American Journal of Roentgenology, 1994. **162**(1): p. 173-177.

16. Delichas, M.G., K. Psarrakos, K. Hatziioannou, G. Giannoglou, E. Molyvda-Athanasopoulou, E. Papanastassiou, *et al.*, *The dependence of patient dose on factors relating to the technique and complexity of Interventional Cardiology procedures.* Physica Medica, 2005. **21**(4): p. 153-157.

17. Lobotessi, H., A. Karoussou, V. Neofotistou, A. Louisi and V. Tsapaki, *Effective dose to a patient undergoing coronary angiography.* Radiation Protection Dosimetry, 2001. **94**(1-2): p. 173-176.

18. Bogaert, E., K. Bacher, K. Lemmens, M. Carlier, W. Desmet, X. De Wagter, *et al.*, *A large scale multicenter study of patient skin doses in interventional cardiology: Dose-Area Product action levels and Dose Reference Levels.* British Journal of Radiology, 2008.

19. WHO, *WHO World Health Organization. The World Health Report 2004 - Changing History* 2004.

20. Jousilahti, P., E. Vartiainen, J. Tuomilehto and P. Puska, *Sex, age, cardiovascular risk factors, and coronary heart disease - A prospective follow-up study of 14 786 middle-aged men and women in Finland.* Circulation, 1999. **99**(9): p. 1165-1172.

21. Cook, S., M. Togni, M.C. Schaub, P. Wenaweser and O.M. Hess, *High heart rate: a cardiovascular risk factor?* European Heart Journal, 2006. **27**(20): p. 2387-2393.

22. Munger, M.A., B.W. Van Tassell and J. LaFleur, *Medication nonadherence: an unrecognized cardiovascular risk factor.* MedGenMed, 2007. **9**(3): p. 58.

23. Bjornstad, P.G., *Is interventional closure the current treatment of choice for selected patients with deficient atrial septation?* Cardiology in the Young, 2006. **16**(1): p. 3-10.

24. Holzer, R. and Z.M. Hijazi, *Interventional approach to congenital heart disease.* Current Opinion in Cardiology, 2004. **19**(2): p. 84-90.

25. ICRU, *International Commission on Radiation Units and Measurements. Radiation Quantities and Units ICRU Report 33*. 1980: Bethesda, MD: International Commission on Radiation Units and Measurements.

26. Tapiovaara, M., M. Lakkisto and A. Servomaa, *PCXMC: A PC-based Monte Carlo program for calculating patient doses in medical X-ray examinations. STUK-A139*. 1997: STUK, Finnish Centre for Radiation and Nuclear Safety, Helsinki, Finland.

27. Briesmeister, J.F., *MCNP: A general Monte Carlo N-particle transport code. Version4B, LA-16252-M*. 1997: Los Alamos, NM.

28. Vaño, E., L. Gonzalez, J.I. Ten, J.M. Fernandez, E. Guibelalde and C. Macaya, *Skin dose and dose-area product values for interventional cardiology procedures.* British Journal of Radiology, 2001. **74**(877): p. 48-55.

29. Betsou, S., E.P. Efstathopoulos, D. Katritsis, K. Faulkner and G. Panayiotakis, *Patient radiation doses during cardiac catheterization procedures.* British Journal of Radiology, 1998. **71**(846): p. 634-639.

30. Moy, J.P., *Signal-to-noise ratio and spatial resolution in x-ray electronic imagers: Is the MTF a relevant parameter?* Medical Physics, 2000. **27**(1): p. 86-93.

31. Neitzel, U., S. Gunther-Kohfahl, G. Borasi and E. Samei, *Determination of the detective quantum efficiency of a digital X-ray detector: Comparison of three evaluations using a common image data set.* Medical Physics, 2004. **31**(8): p. 2205-2211.

32. Borasi, G., A. Nitrosi, P. Ferrari and D. Tassoni, *On site evaluation of three flat panel detectors for digital radiography.* Medical Physics, 2003. **30**(7): p. 1719-1731.

33. Thijssen, M.A.O., K.R. Bijkerk and R.J.M. van der Burght, *Manual Contrast-Detail Phantom CDRAD Type 2.0: Project Quality Assurance in Radiology (Department of Radiology, University Hospital Nijmegen, St.-Radboud, The Netherlands)*. 1998.

34. Burgess, A.E., *Comparison of receiver operating characteristic and forced-choice observer performance-measurement methods.* Medical Physics, 1995. **22**(5): p. 643-655.

35. *National Research Counsil (NRC), Committee on the Biological Effects of Ionizing Radiations (BEIR), Health risks from exposure to low levels of ionizing Radiation.BEIR VII. .* Washington, DC:NRCUSNA Press., 2006.

36. UNSCEAR, *(2000) UNSCEAR, United Nations Scientific Committee on the Effects of Atomic Radiation (UNSCEAR), Sources and effects of ionizing radiation: UNSCEAR 2000 report to the General Assembly, with scientific annexes. New York: United Nations*. 2000: New York.

37. UNSCEAR, *(1994) UNSCEAR, United Nations Scientific Committee on the Effects of Atomic Radiation (UNSCEAR), Sources and effects of ionizing radiation: UNSCEAR 1994 report to the General Assembly, with scientific annexes. New York: United Nations*. 1994.

38. Mettler, F.A. and R.D. Moseley, *Medical Effects of Ionizing Radiation, 3rd edition*. 3rd ed. 2008, Philadelphia, USA: Sauders, Elsevier.

39. ICRP, *2007 Recommendations of the International Commission on Radiological Protection: Publication 103.* Ann. ICRP, Oxford, UK: Pergamon Press, 2007. **37**(2-4): p. 1-332.

40. Preston, D.L., E. Ron, S. Tokuoka, S. Funamoto, N. Nishi, M. Soda, *et al.*, *Solid cancer incidence in atomic bomb survivors: 1958-1998.* Radiation Research, 2007. **168**(1): p. 1-64.

41. Einstein, A.J., K.W. Moser, R.C. Thompson, M.D. Cerqueira and M.J. Henzlova, *Radiation dose to patients from cardiac diagnostic imaging.* Circulation, 2007. **116**(11): p. 1290-1305.

42. Lee, C., R.J. Staton, D.E. Hintenlang, M.M. Arreola, J.L. Williams and W.E. Bolch, *Organ and effective doses in pediatric patients undergoing helical multislice computed tomography examination.* Medical Physics, 2007. **34**(5): p. 1858-1873.

43. Pierce, D.A., Y. Shimizu, D.L. Preston, M. Vaeth and K. Mabuchi, *Studies of the mortality of atomic bomb survivors. Report 12 .1. Cancer: 1950-1990.* Radiation Research, 1996. **146**(1): p. 1-27.

44. Sherwood, L., *Human Physiology. From Cells to Systems*. 5th ed. 2004, Belmont, USA: Brooks/Cole - Thomson Learning

45. Preston, D.L., Y. Shimizu, D.A. Pierce, A. Suyama and K. Mabuchi, *Studies of mortality of atomic bomb survivors. Report 13: Solid cancer and noncancer disease mortality: 1950-1997.* Radiation Research, 2003. **160**(4): p. 381-407.

46. Baldazzi, G., I. Corazza, P.L. Rossi, G. Testoni, T. Bernardi and R. Zannoli, *In vivo effectiveness of gadolinium filter for paediatric cardiac angiography in terms of image quality and radiation exposure.* Physica Medica, 2002. **18**(3): p. 109-113.

47. Justino, H., *The ALARA concept in pediatric cardiac catheterization: techniques and tactics for managing radiation dose.* Pediatric Radiology, 2006. **36**: p. 146-153.

48. Brix, G., H.D. Nagel, G. Stamm, R. Veit, U. Lechel, J. Griebel, *et al.*, *Radiation exposure in multi-slice versus single-slice spiral CT: results of a nationwide survey.* European Radiology, 2003. **13**(8): p. 1979-1991.

49. Ron, E., *Cancer risks from medical radiation.* Health Physics, 2003. **85**(1): p. 47-59.

50. Neofotistou, V., A. Karoussou, H. Lobotesi and K. Hourdakis, *Patient dosimetry during interventional cardiology procedures.* Radiation Protection Dosimetry, 1998. **80**(1-3): p. 151-154.

51. Hopewell, J.W., *The skin - its structure and response to ionizing-radiation.* International Journal of Radiation Biology, 1990. **57**(4): p. 751-773.

52. Wagner, L.K., P.J. Eifel and R.A. Geise, *Potential biological effects following high X-ray dose interventional procedures.* Journal of Vascular and Interventional Radiology, 1994. **5**(1): p. 71-84.

53. Koenig, T.R., D. Wolff, F.A. Mettler and L.K. Wagner, *Skin injuries from fluoroscopically guided procedures: part I, Characteristics of radiation injury.* American Journal of Roentgenology, 2001. **177**(1): p. 3-11.

54. ICRP, *The biological basis for dose limiation in the skin. Publication 59.* Ann. ICRP, Oxford, UK: Pergamon Press, 1991. **22**(2).

55. Koenig, T.R., F.A. Mettler and L.K. Wagner, *Skin injuries from fluoroscopically guided procedures: part 2, Review of 73 cases and recommendations for minimizing dose delivered to patient.* American Journal of Roentgenology, 2001. **177**(1): p. 13-20.

56. Lee, J., D. Hoss and T.J. Phillips, *Fluoroscopy-induced skin necrosis.* Archives of Dermatology, 2003. **139**(2): p. 140-142.

57. Dehen, L., C. Vilmer, C. Humiliere, T. Corcos, D. Pentousis, L. Ollivaud, *et al.*, *Chronic radiodermatitis following cardiac catheterisation: a report of two cases and a brief review of the literature.* Heart, 1999. **81**(3): p. 308-312.

58. Aerts, A., T. Decraene, J.J. van den Oord, J. Dens, S. Janssens, P. Guelinckx, *et al.*, *Chronic radiodermatitis following percutaneous coronary*

interventions: a report of two cases. Journal of the European Academy of Dermatology and Venereology, 2003. **17**(3): p. 340-343.

59. Frazier, T.H., J.B. Richardson, V.C. Fabre and J.P. Callen, *Fluoroscopy-induced chronic radiation skin injury - A disease perhaps often overlooked.* Archives of Dermatology, 2007. **143**(5): p. 637-640.

60. Von Essen, C.F., *Roentgen therapy of kin and lip carcinoma: Factors influencing success and failure.* American Journal of Roentgenology, 1960. **83**: p. 556-570.

61. Nahass, G.T., *Acute radiodermatitis after radiofrequency catheter ablation.* Journal of the American Academy of Dermatology, 1997. **36**(5): p. 881-884.

62. Vaño, E., J. Goicolea, C. Galvan, L. Gonzalez, L. Meiggs, J.I. Ten, *et al.*, *Skin radiation injuries in patients following repeated coronary angioplasty procedures.* British Journal of Radiology, 2001. **74**(887): p. 1023-1031.

63. Shope, T.B., *Radiation-induced skin injuries from fluoroscopy.* Radiographics, 1996. **16**(5): p. 1195-1199.

64. Mooney, R.B., *Skin dose to patients from interventional radiology and cardiology procedures with potentially long fluoroscopy times.* Radiation Protection Dosimetry, 2000. **90**(1-2): p. 123-126.

65. van de Putte, S., F. Verhaegen, Y. Taeymans and H. Thierens, *Correlation of patient skin doses in cardiac interventional radiology with dose-area product.* British Journal of Radiology, 2000. **73**(869): p. 504-513.

66. Wang, J.H. and T.J. Blackburn, *The AAPM/RSNA physics tutorial for residents - X-ray image intensifiers for fluoroscopy.* Radiographics, 2000. **20**(5): p. 1471-1477.

67. Coltman, J.W., *Fluoroscopic image brightening by electronic means.* Radiology, 1948. **51**: p. 359-367.

68. Boyle, W.S. and G.E. Smith, *Charge Coupled Semiconductor devices.* Bell System Technical Journal, 1970. **49**(4): p. 587-+.

69. Herron, J.M., W.H. Kennedy, D. Gur, S.L. Miller, W.F. Good, B.C. Good, *et al.*, *X-ray-imaging with two-dimensional charge-coupled device (CCD) arrays.* Proceedings of the Society of Photo-Optical Instrumentation Engineers, 1984. **486**: p. 141-145.

70. Zhao, W. and J.A. Rowlands, *X-ray-imaging using amorphous selenium - feasibility of a flat-panel self-scanned detector for digital radiology.* Medical Physics, 1995. **22**(10): p. 1595-1604.

71. Antonuk, L.E., J. Yorkston, W.D. Huang, J.H. Siewerdsen, J.M. Boudry, Y. Elmohri, *et al.*, *A Real-Time, Flat-Panel, Amorphous-Silicon, Digital X-Ray Imager.* Radiographics, 1995. **15**(4): p. 993-1000.

72. Granfors, P.R., R. Aufrichtig, G.E. Possin, B.W. Giambattista, Z.S. Huang, J.Q. Liu, *et al.*, *Performance of a 41X41 cm(2) amorphous silicon flat panel x-ray detector designed for angiographic and R&F imaging applications.* Medical Physics, 2003. **30**(10): p. 2715-2726.

73. Chotas, H.G., J.T. Dobbins and C.E. Ravin, *Principles of digital radiography with large-area, electronically readable detectors: A review of the basics.* Radiology, 1999. **210**(3): p. 595-599.

74. Rowlands, J. and S. Kasap, *Amorphous semiconductors usher in digital x-ray imaging.* Physics Today, 1997. **50**(11): p. 24-30.

75. Hunt, D.C., O. Tousignant and J.A. Rowlands, *Evaluation of the imaging properties of an amorphous selenium-based flat panel detector for digital fluoroscopy.* Medical Physics, 2004. **31**(5): p. 1166-1175.

76. Rowlands, J.A., W. Zhao, I.M. Blevis, D.F. Waechter and Z.S. Huang, *Flat-panel digital radiology with amorphous selenium and active-matrix readout.* Radiographics, 1997. **17**(3): p. 753-760.

77. Holmes, D.R., W.K. Laskey, M.A. Wondrow and J.T. Cusma, *Flat-panel detectors in the cardiac catheterization laboratory: Revolution or evolution - What are the issues?* Catheterization and Cardiovascular Interventions, 2004. **63**(3): p. 324-330.

78. Spahn, M., *Flat detectors and their clinical applications.* European Radiology, 2005. **15**(9): p. 1934-1947.

79. Seibert, J.A., *Flat-panel detectors: how much better are they?* Pediatric Radiology, 2006. **36**: p. 173-181.

80. Davies, G.A., A.R. Cowen, S.M. Kengyelics, J. Moore and S.M. U., *Do flat detector cardiac X-ray systems convey advantages over image-intensifier-based systems? Study comparing X-ray dose and image quality.* European Radiology, 2007. **17**: p. 1787-1794.

81. Antonuk, L.E., K.W. Jee, Y. El-Mohri, M. Maolinbay, S. Nassif, X. Rong, *et al.*, *Strategies to improve the signal and noise performance of active matrix, flat-panel imagers for diagnostic x-ray applications.* Medical Physics, 2000. **27**(2): p. 289-306.

82. Maolinbay, M., Y. El-Mohri, L.E. Antonuk, K.W. Jee, S. Nassif, X. Rong, *et al.*, *Additive noise properties of active matrix flat-panel imagers.* Medical Physics, 2000. **27**(8): p. 1841-1854.

83. Moy, J.P., *Recent developments in X-ray imaging detectors.* Nuclear Instruments & Methods in Physics Research Section a-Accelerators Spectrometers Detectors and Associated Equipment, 2000. **442**(1-3): p. 26-37.

84. Hirshfeld, J.W., S.D. Balter, J.A. Brinker, M.J. Kern, L.W. Klein, B.D. Lindsay, *et al.*, *ACCF/AHA/HRS/SCAI clinical competence statement on physician knowledge to optimize patient safety and image quality in fluoroscopically guided invasive cardiovascular procedures - A report of the American College of Cardiology Foundation/American Heart Association/American College of Physicians Task Force on Clinical Competence and Training.* Circulation, 2005. **111**(4): p. 511-532.

85. *European Commission Council Directive of 30 June 1997 (97/43/Euratom) on Health Protection of Individuals against the Dangers of Ionising Radiation in relation to Medical Exposure.* Official J Eur Commun, 1997. **180**: p. 22-27.

86. Mahesh, M., *The AAPM/RSNA physics tutorial for residents - Fluoroscopy: Patient radiation exposure issues.* Radiographics, 2001. **21**(4): p. 1033-1045.

87. Rehani, M.M., *Training of interventional cardiologists in radiation protection - the IAEA's initiatives.* International Journal of Cardiology, 2007. **114**(2): p. 256-260.

88. Granfors, P., D. Albagli, E.J. Tkaczyk, R. Aufrichtig, H. Netel, G. Brunst, *et al.*, *Performance of a Flat Panel Cardiac Detector.* Proc. SPIE, 2001. **4320**: p. 77-86.

89. Zorzetto, M., G. Bernardi, G. Morocutti and A. Fontanelli, *Radiation exposure to patients and operators during diagnostic catheterization and coronary angioplasty.* Catheterization and Cardiovascular Diagnosis, 1997. **40**(4): p. 348-351.

90. Hansson, B. and A. Karambatsakidou, *Relationships between entrance skin dose, effective dose and dose area product for patients in diagnostic and interventional cardiac procedures.* Radiation Protection Dosimetry, 2000. **90**(1-2): p. 141-144.

91. Vaño, E., L. Gonzalez, J.M. Fernandez and E. Guibelalde, *Patient dose values in interventional radiology.* British Journal of Radiology, 1995. **68**(815): p. 1215-1220.

92. Morrell, R.E. and A.T. Rogers, *A mathematical model for patient skin dose assessment in cardiac catheterization procedures.* British Journal of Radiology, 2006. **79**(945): p. 756-761.

93. den Boer, A., P.J. de Feijter, P.W. Serruys and J. Roelandt, *Real-time quantification and display of skin radiation during coronary angiography and intervention.* Circulation, 2001. **104**(15): p. 1779-1784.

94. Smans, K., M. Tapiovaara, M. Cannie, L. Struelens, F. Vanhavere, M. Smet, *et al.*, *Calculation of organ doses in x-ray examinations of premature babies.* Medical Physics, 2008. **35**(2): p. 556-568.

95. ICRP, *Radiological protection and safety in medicine. Publication 73.* Ann. ICRP, Oxford, UK: Pergamon Press, 1996.

96. Marshall, N.W., C.L. Chapple and C.J. Kotre, *Diagnostic reference levels in interventional radiology.* Physics in Medicine and Biology, 2000. **45**(12): p. 3833-3846.

97. Neofotistou, V., E. Vaño, R. Padovani, J. Kotre, A. Dowling, M. Toivonen, *et al.*, *Preliminary reference levels in interventional cardiology.* European Radiology, 2003. **13**(10): p. 2259-2263.

98. Vano, E. and L. Gonzalez, *Patient dosimetry and reference doses: Practical considerations.* Radiation Protection Dosimetry, 2000. **90**(1-2): p. 85-88.

99. Cousins, C. and C. Sharp, *Medical interventional procedures - reducing the radiation risks.* Clinical Radiology, 2004. **59**(6): p. 468-473.

100. Kuon, E., C. Dorn, M. Schmitt and J.B. Dahm, *Radiation dose reduction in invasive cardiology by restriction to adequate instead of optimized picture quality.* Health Physics, 2003. **84**(5): p. 626-631.

101. Kuon, E., J.B. Dahm, D.M. Robinson, K. Empen, M. Gunther and W. Wucherer, *Radiation-reducing planning of cardiac catheterisation.* Zeitschrift Fur Kardiologie, 2005. **94**(10): p. 663-673.

102. Chida, K., K. Fuda, H. Saito, Y. Takai, S. Takahashi, S. Yamada, *et al.*, *Patient skin dose in cardiac interventional procedures: Conventional fluoroscopy versus pulsed fluoroscopy.* Catheterization and Cardiovascular Interventions, 2007. **69**(1): p. 115-121.

103. Aufrichtig, R., P. Xue, C.W. Thomas, G.C. Gilmore and D.L. Wilson, *Perceptual comparison of pulsed and continuous fluoroscopy.* Medical Physics, 1994. **21**(2): p. 245-256.

104. den Boer, A., P.J. Defeyter, W.A. Hummel, D. Keane and J. Roelandt, *Reduction of radiation exposure while maintaining high-quality fluoroscopic images during interventional cardiology using novel X-ray tube technology with extra beam filtering.* Circulation, 1994. **89**(6): p. 2710-2714.

105. Nicholson, R., F. Tuffee and M.C. Uthappa, *Skin sparing in interventional radiology: the effect of copper filtration.* British Journal of Radiology, 2000. **73**(865): p. 36-42.

106. Balter, S., *X-ray image intensifier.* Catheterization and Cardiovascular Interventions, 1999. **46**(2): p. 238-244.

107. Partridge, J., G. McGahan, S. Causton, M. Bowers, M. Mason, M. Dalby, *et al.*, *Radiation dose reduction without compromise of image quality in cardiac angiography and intervention with the use of a flat panel detector without an antiscatter grid.* Heart, 2006. **92**(4): p. 507-510.

108. Tapiovaara, M.J., A. Servomaa, M. Sandborg and D.R. Dance, *Optimising the imaging conditions in paediatric fluoroscopy.* Radiation Protection Dosimetry, 2000. **90**(1-2): p. 211-216.

109. Tapiovaara, M.J., M. Sandborg and D.R. Dance, *A search for improved technique factors in paediatric fluoroscopy.* Physics in Medicine and Biology, 1999. **44**(2): p. 537-559.

110. Kuon, E., J.B. Dahm, K. Empen, D.M. Robinson, G. Reuter and M. Wucherer, *Identification of less-irradiating tube angulations in invasive cardiology.* Journal of the American College of Cardiology, 2004. **44**(7): p. 1420-1428.

111. Vaño, E., *Radiation exposure to cardiologists: how it could be reduced.* Heart, 2003. **89**(10): p. 1123-1124.

112. Ruiz, C.E., C.E. Mullins, A.P. Rochini, W.A.K. Radtke, Z.M. Hijazi, M.P. Olaughlin, *et al.*, *Core curriculum for the training of pediatric invasive/Interventional cardiologists: Report of the Society for Cardiac Angiography and Interventions Committee on Pediatric Cardiology Training Standards.* Catheterization and Cardiovascular Diagnosis, 1996. **37**(4): p. 409-424.

113. Beller, G.A., *A proposal for an advanced cardiovascular imaging training track.* Journal of the American College of Cardiology, 2006. **48**(7): p. 1299-1303.

114. Picano, E., G. Santoro and E. Vaño, *Sustainability in the cardiac cath lab.* International Journal of Cardiovascular Imaging, 2007. **23**(2): p. 143-147.

115. d'Othee, B.J. and P.J.P. Lin, *The influence of angiography table shields and height on patient and angiographer irradiation during interventional radiology procedures.* Cardiovascular and Interventional Radiology, 2007. **30**(3): p. 448-454.

116. Vano, E., L. Gonzalez, J.M. Fernandez, F. Alfonso and C. Macaya, *Occupational radiation doses in interventional cardiology: a 15-year follow-up.* British Journal of Radiology, 2006. **79**(941): p. 383-388.

117. Vaño, E. and F. Vargas, *Training in radiological protection for interventional cardiology.* Revista Espanola De Cardiologia, 2003. **56**(1): p. 111-112.

118. Busse, F., W. Rütten, B. Sandkamp, P.L. Alving, B. R. and D. T., *Design and performance of a high-quality cardiac flat detector.* Proc. SPIE, 2002. **4682**: p. 819-827.

119. Bruijns, T., R. Bastiaens, B. Hoornaert, E. von Reth, F. Busse, V. Heer, *et al.*, *Image Quality of a Large Area Dynamic Flat Detecor: Comparison with a sate-of-the-art II/TV system.* Proc. SPIE, 2002. **4682**: p. 332-343.

120. Krone, R.J., L. Johnson, T. Noto, G.W. Vetrovec, J.D. Babb, J. Chapman, *et al.*, *Five year trends in cardiac catheterization: A report from the Registry of the Society for Cardiac Angiography and Interventions.* Catheterization and Cardiovascular Diagnosis, 1996. **39**(1): p. 31-35.

121. Scanlon, P.J., D.P. Faxon, A.M. Audet, B. Carabello, G.J. Dehmer, K.A. Eagle, *et al.*, *ACC AHA guidelines for coronary angiography - A report of the American College of Cardiology American Heart Association Task Force on Practice Guidelines (Committee on Coronary Angiography).* Journal of the American College of Cardiology, 1999. **33**(6): p. 1756-1816.

122. Weber, O.M., A.J. Martin and C.B. Higgins, *Whole-heart steady-state free precession coronary artery magnetic resonance angiography.* Magnetic Resonance in Medicine, 2003. **50**(6): p. 1223-1228.

123. Kim, W.Y., P.G. Danias, M. Stuber, S.D. Flamm, S. Plein, E. Nagel, *et al.*, *Coronary magnetic resonance angiography for the detection of coronary stenoses.* New England Journal of Medicine, 2001. **345**(26): p. 1863-1869.

124. Schuijf, J.D., J.J. Bax, L.J. Shaw, A. de Roos, H.J. Lamb, E.E. van der Wall, *et al.*, *Meta-analysis of comparative diagnostic performance of magnetic resonance imaging and multislice computed tomography for noninvasive coronary angiography.* American Heart Journal, 2006. **151**(2): p. 404-411.

125. Kehl, H.G., J. Jager, N. Papazis, D. Dimitrelos, J. Gehrmann, R. Kassenbohmer, *et al.*, *3D heart modelling from biplane, rotational angiocardiographic X-ray sequences.* Computers & Graphics-Uk, 2000. **24**(5): p. 731-739.

126. Garcia, J.A., J. Chen, A. Hansgen, O. Wink, B. Movassaghi and J.C. Messenger, *Rotational angiography (RA) and three-dimensional imaging (3-DRA): an available clinical tool.* International Journal of Cardiovascular Imaging, 2007. **23**(1): p. 9-13.

127. Panzer, J., Y. Taeymans and D. De Wolf, *Three-dimensional rotational angiography of a patient with pulmonary atresia intact septum and coronary fistulas.* Pediatric Cardiology, 2008. **29**(3): p. 686-687.

128. Kuon, E., P.N. Niederst and J.B. Dahm, *Usefulness of rotational spin for coronary angiography in patients with advanced renal insufficiency.* American Journal of Cardiology, 2002. **90**(4): p. 369-373.

129. Raman, S.V., R. Morford, M. Neff, T.T. Attar, G. Kukielka, R.D. Magorien, *et al.*, *Rotational x-ray coronary angiography.* Catheterization and Cardiovascular Interventions, 2004. **63**(2): p. 201-207.

130. Akhtar, M., K.T. Vakharia, J. Mishell, A. Gera, T.A. Ports, Y. Yeghiazarians, *et al.*, *Randomized study of the safety and clinical utility of rotational vs. standard coronary angiography using a flat-panel detector.* Catheterization and Cardiovascular Interventions, 2005. **66**(1): p. 43-49.

131. Maddux, J.T., O. Wink, J.C. Messenger, B.M. Groves, R. Liao, J. Strzeiczyk, *et al.*, *Randomized study of the safety and clinical utility of rotational angiography versus standard angiography in the diagnosis of coronary artery disease.* Catheterization and Cardiovascular Interventions, 2004. **62**(2): p. 167-174.

132. Rigatelli, G., P. Cardaioli, L. Roncon, M. Giordan, E. Bedendo, L. Oliva, *et al.*, *Impact of intracardiac echocardiography on radiation exposure during adult congenital heart disease catheter-based interventions.* International Journal of Cardiovascular Imaging, 2007. **23**(2): p. 139-142.

133. Zanchetta, M., E. Onorato, G. Rigatelli, L. Pedon, M. Zennaro, A. Carrozza, *et al.*, *Intracardiac echocardiography-guided transcatheter closure of secundum atrial septal defect - A new efficient device selection method.* Journal of the American College of Cardiology, 2003. **42**(9): p. 1677-1682.

134. Zanchetta, M., G. Rigatelli, L. Pedon, M. Zennaro, E. Onorato and P. Maiolino, *Intracardiac echocardiography during catheter-based procedures: Ultrasound system, examination technique, and image presentation.* Echocardiography-a Journal of Cardiovascular Ultrasound and Allied Techniques, 2002. **19**(6): p. 501-507.

135. Flohr, T.G., U.J. Schoepf, A. Kuettner, S. Halliburton, H. Bruder, C. Suess, *et al.*, *Advances in cardiac imaging with 16-section CT systems.* Academic Radiology, 2003. **10**(4): p. 386-401.

136. Achenbach, S., S. Ulzheimer, U. Baum, M. Kachelriess, D. Ropers, T. Giesler, *et al.*, *Noninvasive coronary angiography by retrospectively ECG-gated multislice spiral CT.* Circulation, 2000. **102**(23): p. 2823-2828.

137. Achenbach, S., F. Moselewski, D. Ropers, M. Ferencik, U. Hoffmann, B. MacNeill, *et al.*, *Detection of calcified and noncalcified coronary atherosclerotic plaque by contrast-enhanced, submillimeter multidetector spiral computed tomography - A segment-based comparison with intravascular ultrasound.* Circulation, 2004. **109**(1): p. 14-17.

138. Hoffmann, U., F. Moselewski, R.C. Cury, M. Ferencik, I.K. Jang, L.J. Diaz, *et al.*, *Predictive value of 16-slice multidetector spiral computed tomography to detect significant obstructive coronary artery disease in patients at high risk for coronary artery disease - Patient-versus segment-based analysis.* Circulation, 2004. **110**(17): p. 2638-2643.

139. Romeo, G., L. Houyel, C.Y. Angel, P. Brenot, J.Y. Riou and J.F. Paul, *Coronary stenosis detection by 16-slice computed tomography in heart transplant patients - Comparison with conventional angiography and impact on clinical management.* Journal of the American College of Cardiology, 2005. **45**(11): p. 1826-1831.

140. Leber, A.W., A. Knez, F. von Ziegler, A. Becker, K. Nikolaou, S. Paul, *et al.*, *Quantification of obstructive and nonobstructive coronary lesions by 64-slice computed tomography - A comparative study with quantitative coronary angiography and intravascular ultrasound.* Journal of the American College of Cardiology, 2005. **46**(1): p. 147-154.

141. Flohr, T.G., U.J. Schoepf and B.M. Ohnesorge, *Chasing the heart - New developments for cardiac CT.* Journal of Thoracic Imaging, 2007. **22**(1): p. 4-16.

142. Raff, G.L., M.J. Gallagher, W. O'Neill and J.A. Goldstein, *Diagnostic accuracy of noninvasive coronary angiography using 64-slice spiral computed tomography.* Journal of the American College of Cardiology, 2005. **46**(3): p. 552-557.

143. Crouse, J.R., *Imaging atherosclerosis: state of the art.* Journal of Lipid Research, 2006. **47**(8): p. 1677-1699.

144. Orakzai, S.H., R.H. Orakzai, K. Nasir and M.J. Budoff, *Assessment of cardiac function using multidetector row computed tomography.* Journal of Computer Assisted Tomography, 2006. **30**(4): p. 555-563.

145. Prokop, M., *New challenges in MDCT.* European Radiology, 2005. **15**: p. E35-E45.

146. Theocharopoulos, N., J. Damilakis, K. Perisinakis and N. Gourtsoyiannis, *Energy imparted-based estimates of the effect of z*

overscanning on adult and pediatric patient effective doses from multi-slice computed tomography. Medical Physics, 2007. **34**(4): p. 1139-1152.

147. Coles, D.R., M. Smail, I. Negus, P. Wilde, M. Oberhoff, K.R. Karsch, *et al.*, *Radiation dose in coronary multislice CT: A comparison with conventional diagnostic angiography.* Heart, 2005. **91**: p. A16-A16.

148. Hausleiter, J., T. Meyer, M. Hadamitzky, E. Huber, M. Zankl, S. Martinoff, *et al.*, *Radiation dose estimates from cardiac multislice computed tomography in daily practice - Impact of different scanning protocols on effective dose estimates.* Circulation, 2006. **113**(10): p. 1305-1310.

149. Jakobs, T.F., C.R. Becker, B. Ohnesorge, T. Flohr, C. Suess, U.J. Schoepf, *et al.*, *Multislice helical CT of the heart with retrospective ECG gating: reduction of radiation exposure by ECG-controlled tube current modulation.* European Radiology, 2002. **12**(5): p. 1081-1086.

150. Abada, H.T., C. Larchez, B. Daoud, A. Sigal-Cinqualbre and J.F. Paul, *MDCT of the coronary arteries: Feasibility of low-dose CT with ECG-pulsed tube current modulation to reduce radiation dose.* American Journal of Roentgenology, 2006. **186**(6): p. S387-S390.

151. Shemesh, J., R. Evron, N. Koren-Morag, S. Apter, J. Rozenman, D. Shaham, *et al.*, *Coronary artery calcium measurement with multi-detector row CT and low radiation dose: Comparison between 55 and 165 mAs.* Radiology, 2005. **236**(3): p. 810-814.

152. Coles, D.R., M. Smail, I. Negus, P. Wilde, M. Oberhoff, K. Karsch, *et al.*, *Effective dose from multislice CT calcium scoring and coronary anglography compared with conventional diagnostic coronary angiography.* Journal of the American College of Cardiology, 2005. **45**(3): p. 267A-267A.

153. Schoenhagen, P., A.E. Stillman, S.S. Halliburton, S.A. Kuzmiak, T. Painter and R.D. White, *Non-invasive coronary angiography with multi-detector computed tomography: comparison to conventional X-ray angiography.* International Journal of Cardiovascular Imaging, 2005. **21**(1): p. 63-72.

154. Brenner, D.J., *Estimating cancer risks from pediatric CT: going from the qualitative to the quantitative.* Pediatric Radiology, 2002. **32**(4): p. 228-231.

155. Brenner, D.J., R. Doll, D.T. Goodhead, E.J. Hall, C.E. Land, J.B. Little, *et al.*, *Cancer risks attributable to low doses of ionizing radiation: Assessing what we really know.* Proceedings of the National Academy of Sciences of the United States of America, 2003. **100**(24): p. 13761-13766.

156. Frush, D.P., L.F. Donnelly and N.S. Rosen, *Computed tomography and radiation risks: What pediatric health care providers should know.* Pediatrics, 2003. **112**(4): p. 951-957.

157. Danias, P.G., A. Roussakis and J.P.A. Ioannidis, *Diagnostic performance of coronary magnetic resonance anglography as compared against conventional x-ray angiography - A meta-analysis.* Journal of the American College of Cardiology, 2004. **44**(9): p. 1867-1876.

158. Prakken, N.H.J., E. Vonken, B.K. Velthuis, P. Doevendans and M.J.M. Cramer, *3D MR coronary angiography: optimization of the technique and preliminary results.* International Journal of Cardiovascular Imaging, 2006. **22**(3-4): p. 477-487.

159. FANC, *FEDERAAL AGENTSCHAP VOOR NUCLEAIRE CONTROLE. 12 oktober 2006 - Richtlijnen van het FANC voor het gebruik van röntgenstralen voor medische doeleinden : Patiëntendosimetrie. http://www.fanc.fgov.be*. 2006.

160. Vaño, E., B. Geiger, A. Schreiner, C. Back and J. Beissel, *Dynamic flat panel detector versus image intensifier in cardiac imaging: dose and image quality.* Physics in Medicine and Biology, 2005. **50**(23): p. 5731-5742.

161. Dowset, D.J., P.A. Kenny and R.E. Johnston, *The Physics of Diagnostic Imaging*. 1998: Chapman & Hall, Londen, UK.

162. Flohr, T.G. and B.M. Ohnesorge, *Imaging of the heart with computed tomography.* Basic Research in Cardiology, 2008. **103**(2): p. 161-173.

163. Jahnke, C., I. Paetsch and E. Nagel, *3D MR coronary angiography: optimization of the technique and preliminary results.* International Journal of Cardiovascular Imaging, 2006. **22**(3-4): p. 489-491.

164. Zanzonico, P., L.N. Rothenberg and H.W. Strauss, *Radiation exposure of computed tomography and direct intracoronary angiography - Risk has its reward.* Journal of the American College of Cardiology, 2006. **47**(9): p. 1846-1849.

Catheterization of coronary arteries, heart chambers and vessels of the heart, shortly denoted by 'interventional cardiology' in medicine, is highly appreciated for its non-invasive character in comparison to surgery. Both adults and children can benefit of the technique either for diagnosis or treatment of heart and coronary specific disorders. However, as investigation is performed through dynamic x-ray imaging the radiation burden to the patient can be important.

This work deals with the incidence of short-term effects related to the skin dose and long term effects such as cancer or tumour induction for adult and paediatric populations. It also comprises a comparative study between a conventional image intensifier and a recent flat detector, being the new technology for image capture in interventional cardiology. A practical approach is emphasised in this work.